UNIVERSITY OF Southampton

University of Southampton Research Repository
ePrints Soton

Copyright © and Moral Rights for this thesis are retained by the author and/or other copyright owners. A copy can be downloaded for personal non-commercial research or study, without prior permission or charge. This thesis cannot be reproduced or quoted extensively from without first obtaining permission in writing from the copyright holder/s. The content must not be changed in any way or sold commercially in any format or medium without the formal permission of the copyright holders.

When referring to this work, full bibliographic details including the author, title, awarding institution and date of the thesis must be given e.g.

AUTHOR (year of submission) "Full thesis title", University of Southampton, name of the University School or Department, PhD Thesis, pagination

http://eprints.soton.ac.uk

UNIVERSITY OF SOUTHAMPTON

Pb-Zn mineralisation within the Limerick Basin (SW Ireland): A role for volcanism?

by

Holly A. L. Elliott

A thesis submitted in partial fulfillment for the degree of Doctor of Philosophy

in the
National Oceanography Centre, Southampton
School of Ocean and Earth Science

November 2015

Declaration of Authorship

I, Holly Elliott, declare that this thesis titled, 'Pb-Zn mineralisation within the Limerick Basin (SW Ireland): A role for volcanism?', and the work presented in it are my own and has been generated by me as the result of my own original research. I confirm that:

- This work was done wholly or mainly while in candidature for a research degree at this University.
- Where any part of this thesis has previously been submitted for a degree or any other qualification at this University or any other institution, this has been clearly stated.
- Where I have consulted the published work of others, this is always clearly attributed.
- Where I have quoted from the work of others, the source is always given. With the exception of such quotations, this thesis is entirely my own work.
- I have acknowledged all main sources of help.
- Where the thesis is based on work done by myself jointly with others, I have made clear exactly what was done by others and what I have contributed myself.
- Part of this work has been published before submission as: 'Elliott, H. A. L., Gernon, T. M., Roberts, S. and Hewson, C. (2015), 'Basaltic maar-diatreme volcanism in the Lower Carboniferous of the Limerick Basin (SW Ireland)', *Bulletin of Volcanology* **77**, 37–59'.

Signed: _____

Date: _____

Abstract

Doctor of Philosophy

by Holly A. L. Elliott

Lead-zinc exploration drilling within the Limerick Basin (SW Ireland) has revealed the deep internal architecture and extra-crater deposits of five alkali-basaltic maar-diatremes. Base metal mineralisation, appearing to be spatially and temporarily associated with these diatremes, overprints adjacent hydrothermal Black Matrix Breccia (BMB) horizons. Diatremes and extra-crater deposits were emplaced during the Carboniferous Period as part of a regional tectonomagmatic trend across NW Europe. Trace element data indicates a genetic relationship between the diatremes and sequences of the extra-crater Knockroe Formation. Field relationships and textural evidence from diatreme and Knockroe deposits, suggest eruptions occurred in a shallow submarine environment (<120 m). Eruptions were dominated by phreatomagmatic activity, however emergence above sea level and subsequent drying out led to a decline in seawater ingress, which corresponded to a late magmatic phase. This study utilises a rare opportunity to investigate both the deep architecture and extra-crater surface deposits, providing detailed volcanic lithofacies descriptions of the submarine maar-diatreme systems at Limerick.

The pyroclastic sequences are highly altered, therefore a principal objective was to analytically distinguish between primary and secondary alteration mineral phases and elemental trends. Rare earth element (REE) patterns suggest the magma was sourced by partial melting of an enriched and metasomatised mantle, which erupted in a within-plate continental rift environment. The lower diatreme is overprinted by a greenschist metamorphic assemblage of minerals, in addition to pervasive dolomitisation of the volcanic deposits. Dolomite is a key mineral in BMBs and the presence of diatreme clasts within polymict BMB horizons, combined with small concentrations of ore-forming minerals (sphalerite, galena and pyrite) in the lower diatremes, suggest that hydrothermal fluids utilised the diatremes as conduits.

The Irish Orefield is a base metal source of global importance, but evidence has not previously been documented to link the large-scale Lower Carboniferous volcanic activity to the Pb-Zn mineralisation. Sulphur isotope data indicates that diatreme formation in Limerick had a significant impact on mineralisation within the basin. Increased permeability and porosity of the diatremes, compared to the traditional Irish-type fault fluid pathways, allowed enhanced formation of BMB mineralisation hosts adjacent to the diatremes and an increased flow of metal-rich hydrothermal fluid from the basement. The presence of large volumes of volcanic material also provided additional magmatic sulphur as well as ore-forming constituents.

Acknowledgements

Thanks first goes to my supervisors, Tom Gernon and Steve Roberts for their support, advice and patience throughout this project and the paper writing process. My panel chair, Rex Taylor, is thanked for many helpful discussions of the project and geochemical data as well as many fond memories supporting Tenerife fieldtrips. I would like to thank Teck Ireland Ltd for providing financial support for this project, as well as Patrick Redmond and Chad Hewson for their enthusiasm and interest. The staff at Limerick are thanked for their helpful discussions and manual labour required to move many many heavy boxes of core! I would like to acknowledge and thank the expert staff at the SUERC isotope facility in East Kilbride, especially Adrian Boyce, for helping obtain and understand my sulphur isotope data. I would also like to acknowledge the financial support of SUERC for awarding a grant (IP-1397-1113), allowing me to work at this facility. Thanks also goes to Stuart Kearns for his help with microprobe analysis at the University of Bristol. I would like to acknowledge the help of many staff at the University of Southampton for their part in sample preparation and obtaining data including Bob Jones, John Ford, Richard Pearce, Ian Croudace and Matt Cooper. Helpful reviews were given on Chapter 3, based on Elliott et al. (2015), by Richard Brown, Pierre-Simon Ross and James White, which greatly improved the manuscript and my writing style. Finally, I would like to thank my mother, Tracey Elliott, for far too many things to list, Jon Neades for many helpful discussions on statistics and coding and Jason Friend for his unending support.

Contents

List of Figures

List of Tables

Abbreviations

BMB	**B**lack **M**atrix **B**reccia
BSE	**B**ackscattered **E**lectron Detector
HFSE	**H**igh **F**ield **S**trength **E**lement
HREE	**H**eavy **R**are **E**arth **E**lement
LILE	**L**ight **I**on **L**ithophile **E**lement
LFSE	**L**ow **F**ield **S**trength **E**lement
LREE	**L**ight **R**are **E**arth **E**lement
masl	**m**etres **a**bove **s**ea **l**evel
mbgs	**m**etres **b**elow **g**round **s**urface
mbsl	**m**etres **b**elow **s**ea **l**evel

This work is dedicated to my mother, Tracey Elliott, for being a constant rock in my life (pardon the pun). MJ, thank you for everything.

Chapter 1

Introduction

1.1 Maar-diatreme volcanism

Maar-diatremes are volcanic pipes formed through explosive processes (White and Ross, 2011). The parent magmas are typically, but not exclusively, of alkaline composition, for example, kimberlites, lamproites and alkali basalts. Diatremes typically utilise weaknesses such as faults (Kurszlaukis and Barnett, 2003; Jelsma et al., 2009), commonly forming linear trends or clusters. At the surface, diatremes are expressed as maar-craters and tephra rings, typically accumulated through a series of bedded density current and fallout deposits (Lorenz, 1975). The diatreme is a diverging depression in the country rock that can be excavated to depths of up to 2.5 km (Lorenz, 2003; Valentine, 2012), with wall angles averaging 80–85^{o} (Field and Scott Smith, 1999; Lorenz, 2003; Gernon et al., 2008). The diatreme is typically infilled by volcaniclastic deposits—largely consisting of pyroclasts, ash, crystals and country-rock lithic fragments that can not escape from the system during the waning eruptive phases (Sparks et al., 2006; Gernon et al., 2009*a*, 2013) (see Fig. 3.1). The upper diatreme tends to be filled with a well bedded, unfluidised lithofacies. These are thought to form by undercutting of the tephra ring by vent widening, causing the overlying maar deposits to subside into the vent, forming a marginal bedded facies of deformed beds or megablocks (Sparks et al., 2006; Lorenz and Kurszlaukis, 2007; Brown et al., 2008b; Valentine, 2012). Deposition by dilute density currents in the maar-crater, originating from the same or neighbouring vents, can also form a series of thin beds at the top of the diatreme (Lorenz, 1986; Lorenz and Kurszlaukis, 2007; Gernon et al., 2009*a*, 2013; Delpit et al., 2014). The base of the diatreme

typically consists of a root zone—a series of intrusions that can intermingle with the upper volcaniclastic infill and feed the magmatic eruptions.

Two key models have been proposed to explain diatreme emplacement (see Fig. 3.1). A 'magmatic model' commonly invoked for kimberlite volcanism (Sparks et al., 2006), involves the explosive expansion of volatiles propagating down ascending magmatic intrusions. This results in excavation of a deep pipe via a series of sub-Plinian to Plinian eruptions (Field and Scott Smith, 1999; Sparks et al., 2006; Porritt et al., 2008). Field and Scott Smith (1999) suggest that magma can intrude along joints by stoping and wedging, effectively creating a large zone of brecciated country rock that formed an embryonic pipe from the base to the surface. Sparks et al. (2006) suggest however, that magma travelling through fissures, transform into many explosive flows within the top few hundred metres of the surface. When pressure of the gas exsolved from the magma exceeds the confining pressure of the rock, explosive fragmentation of the overlying rock occurs (Field and Scott Smith, 1999; Sparks et al., 2006). Propagation of this explosion through the magma column results in large volumes of expanding gases ejecting juvenile and country rock clasts (Skinner and Marsh, 2004). Pyroclastic material becomes trapped in the pipe by virtue of widening of the diatreme, which decreases the gas velocity, or alternatively by a decrease in magma supply rate (Sparks et al., 2006; Brown et al., 2008a).

The 'phreatomagmatic model' involves diatreme excavation by magma propagating to the surface and encountering water either within hydraulically active faults, aquifers, sediments or surface water (Lorenz, 1985; Kurszlaukis and Lorenz, 1997; Kurszlaukis et al., 1998; Lorenz and Kurszlaukis, 2007; Brown et al., 2008b). Different styles of phreatomagmatic activity are discussed in chapter 3. The near-instant transfer of heat from magma to water causes it to flash explosively to steam, creating a shock wave that fragments the magma and surrounding country rock. This process propagates up the water column and super heated steam can be ejected at velocities up to 100 ms^{-1} (Lorenz, 1985). Early investigations into diatreme eruptive methods suggest that explosions depleted groundwater, causing the water table to drop and a cone of depression (the downward migration of the hydrostatic pressure barrier of 2–3 MPa, commonly assumed to act as a barrier for phreatomagmatic explosions, caused by the loss of groundwater (Lorenz, 1986; Lorenz and Kurszlaukis, 2007)) to form adjacent to the pipe. This would cause explosions to occur progressively deeper (Lorenz and Kurszlaukis, 2007). Valentine

(2012) and Graettinger et al. (2014) have since suggested that explosions can occur at variable depths within the diatreme, throughout its eruptive history.

Explosive magmatic and phreatomagmatic eruptions produce shock waves of sufficient force to induce radial fractures (Barnett and Lorig, 2007), causing spalling of the pipe walls. This processes creates a highly permeable network of fractures radiating out from the vent. During diatreme excavation, pressure is very low within the vent compared to the surrounding lithostatic pressure. This results in underpressures of several MPa, which are sufficient to overcome the rock tensile strength and cause implosions at depth (Field and Scott Smith, 1999; Sparks et al., 2006), forming country-rock lithic clasts. Material within the vent becomes fluidised when the drag force exerted by the interstitial gas flow exceeds the weight of the bed (Sparks et al., 2006; Walters et al., 2006; Brown et al., 2008a; Gernon et al., 2008, 2009*b*). At this stage, a convective system is established that effectively homogenises the vent material (Skinner and Marsh, 2004; Walters et al., 2006; Gernon et al., 2008). Widening of the diatreme causes a decrease in gas velocity and a narrowing of the central fluidised section, which gradually moves to the centre of the vent creating a series of nested conduits (see Fig. 3.1) (Walters et al., 2006; Gernon et al., 2008).

1.2 Regional activity and timing

NW Europe experienced a major phase of widespread extensional tectonic and magmatic activity during the Carboniferous that began with the onset of the Variscan orogeny (Woodcock and Strachan, 2000; Timmerman, 2004; Wilson et al., 2004) (see Fig. 1.1 and Fig. 3.2). Closure of the Rhenohercynian Ocean and the accretion of foreign terranes (Timmerman, 2004) is thought to have caused episodic N-S extension in the foreland of the Variscan Orogen, re-activating NE-SW Caledonian basement faults (Woodcock and Strachan, 2000). In addition, early stages of collapse in the central Variscan orogeny led to crustal thinning, wide-spread basin formation and high heat flow (Praeg, 2004), eventually establishing a rift system in the northern Variscan foreland (Wilson et al., 2004).

Lithospheric stretching during extensional regimes in the Lower Carboniferous, led to alkaline basaltic volcanism and magmatic activity across NW Europe that culminated

during the Viséan (Timmerman, 2004). The British Isles experienced high levels of magmatic activity throughout the Carboniferous (see Fig. 1.1 and Fig. 3.2). During the Tournaisian, Scotland experienced volcanism and magmatism at Orkney which occurred throughout the Carboniferous and into the Permian (Upton et al., 2004). Viséan activity in Scotland was widespread but largely concentrated around intrusions and long-lived outpourings of lava up to 1000 m thick in the Midland Valley (Upton et al., 2004). Activity in this area is separated into the Garleton Hills phase near the Tournaisian-Viséan boundary, and the Clyde Plateau Formation in the mid to late Viséan (Monaghan and Pringle, 2004). The southern Bathgate Hills in West Lothian, Scotland, erupted during a similar timescale, involving the 600 m thick episodic accumulation of basaltic lavas and tuffs (Smith et al., 1994). Similarly, East Fife has been the site of multiple eruptions during the Carboniferous including the predominantly subaerial Kinghorn Formation, which consists of up to 485 m of basaltic lavas and pyroclastic rocks (Upton et al., 2004). In addition, the Elie Ness diatreme is one of approximately 100 vents and intrusions emplaced into a rift system during the Upper Carboniferous and Early Permian (Thirlwall and Walder, 1995; Gernon et al., 2013).

Magmatism in Ireland occurred predominantly in the Lower and Mid Carboniferous during the Tournasian and Viséan (see Fig. 1.1). Croghan Hill (central Ireland) consists of a series of agglomerates, tuffs and basalts emplaced within lower Carboniferous limestones either side of the Tournasian-Viséan boundary (Timmerman, 2004). This activity overlaps with that of the Knockroe Formation basalts and tuffs at Limerick, SW Ireland (Somerville et al., 1992). There is evidence for other diatreme volcanism during the Upper Carboniferous, including the Black Ball Head eruption in County Cork dated at ∼318 Ma (Pracht and Timmerman, 2004).

Mineralisation in the Irish Orefield occurred in the Lower Carboniferous, predominantly within the Viséan. The majority of Pb-Zn deposits in Ireland occur along faults that were most active during the late Tournaisian to Arundian (Hitzman and Beaty, 1996). This corresponds to later stages of the Variscan orogeny, and is approximately coeval with a major phase of extension and rifting (see Fig. 1.1). This time frame also closely coincides with the onset of volcanic activity in the Limerick Basin, outlined by grey shading on Fig. 1.1. The timing of mineralisation at Navan has been constrained to the Chadian-Arundian (345–339 Ma) on the basis of the presence of mineralised clasts of 'Pale Beds' in the Arundian aged Boulder Conglomerate as well as cutting the matrix

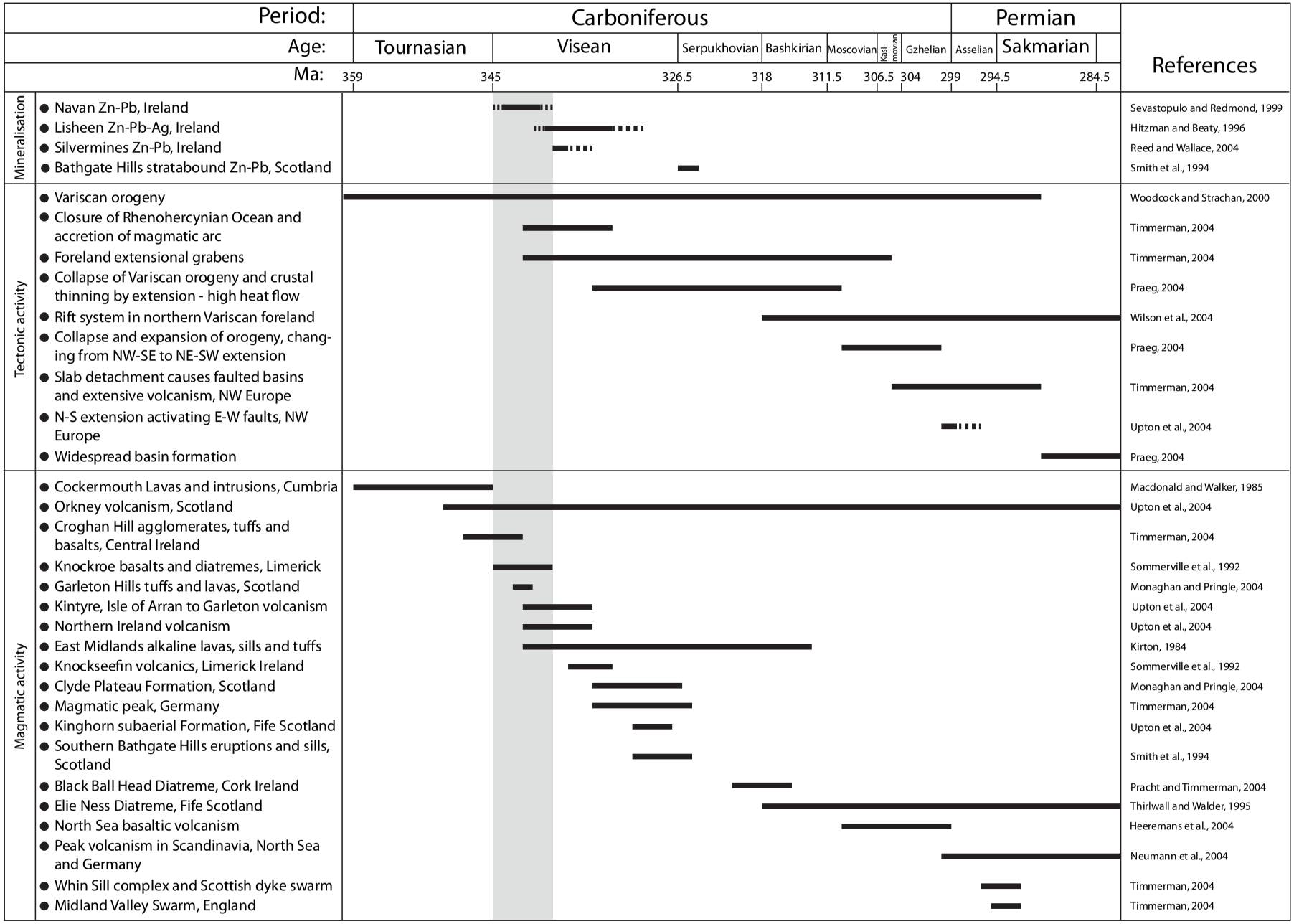
Period:
Carboniferous
Permian
Age:
Tournasian
Visean
Serpukhovian
Bashkirian
Moscovian
Kasi-movian
Gzhelian
Asselian
Sakmarian
Ma:
359
345
326.5
318
311.5
306.5
304
299
294.5
284.5
References
Mineralisation
Navan Zn-Pb, Ireland
Lisheen Zn-Pb-Ag, Ireland
Silvermines Zn-Pb, Ireland
Bathgate Hills stratabound Zn-Pb, Scotland
Sevastopulo and Redmond, 1999
Hitzman and Beaty, 1996
Reed and Wallace, 2004
Smith et al., 1994
Tectonic activity
Variscan orogeny
Closure of Rhenohercynian Ocean and accretion of magmatic arc
Foreland extensional grabens
Collapse of Variscan orogeny and crustal thinning by extension - high heat flow
Rift system in northern Variscan foreland
Collapse and expansion of orogeny, changing from NW-SE to NE-SW extension
Slab detachment causes faulted basins and extensive volcanism, NW Europe
N-S extension activating E-W faults, NW Europe
Widespread basin formation
Woodcock and Strachan, 2000
Timmerman, 2004
Timmerman, 2004
Praeg, 2004
Wilson et al., 2004
Praeg, 2004
Timmerman, 2004
Upton et al., 2004
Praeg, 2004
Magmatic activity
Cockermouth Lavas and intrusions, Cumbria
Orkney volcanism, Scotland
Croghan Hill agglomerates, tuffs and basalts, Central Ireland
Knockroe basalts and diatremes, Limerick
Garleton Hills tuffs and lavas, Scotland
Kintyre, Isle of Arran to Garleton volcanism
Northern Ireland volcanism
East Midlands alkaline lavas, sills and tuffs
Knockseefin volcanics, Limerick Ireland
Clyde Plateau Formation, Scotland
Magmatic peak, Germany
Kinghorn subaerial Formation, Fife Scotland
Southern Bathgate Hills eruptions and sills, Scotland
Black Ball Head Diatreme, Cork Ireland
Elie Ness Diatreme, Fife Scotland
North Sea basaltic volcanism
Peak volcanism in Scandinavia, North Sea and Germany
Whin Sill complex and Scottish dyke swarm
Midland Valley Swarm, England
Macdonald and Walker, 1985
Upton et al., 2004
Timmerman, 2004
Sommerville et al., 1992
Monaghan and Pringle, 2004
Upton et al., 2004
Upton et al., 2004
Kirton, 1984
Sommerville et al., 1992
Monaghan and Pringle, 2004
Timmerman, 2004
Upton et al., 2004
Smith et al., 1994
Pracht and Timmerman, 2004
Thirlwall and Walder, 1995
Heeremans et al., 2004
Neumann et al., 2004
Timmerman, 2004
Timmerman, 2004

FIGURE 1.1: Diagram showing timings of magmatic and tectonic events throughout the Carboniferous and Permian and correlations with local mineralising events. The eruption interval of the Knockroe Formation from the diatremes in Limerick is highlighted as a grey band showing the correlation in timing with other mineralising events in the region. References for the age of each event are given. (Heeremans et al., 2004; Kirton, 1984; Monaghan and Pringle, 2004; Macdonald and Walker, 1985; Neumann et al., 2004; Praeg, 2004; Thirlwall and Walder, 1995; Timmerman, 2004; Upton et al., 2004)

of the same formation (Hitzman and Beaty, 1996; Sevastopulo and Redmond, 1999). Hydrothermal dolomite and mineralisation cross-cuts regional dolostone at Lisheen and Galmoy, replacing Chadian and early Arundian sediments and indicating a minimum Arundian age for sulphide precipitation (Hitzman and Beaty, 1996). The nature of breccias hosting mineralisation in the Silvermines district of Ireland is very similar to that observed at Limerick. Reed and Wallace (2004) states that deposits formed after diagenesis but before the Variscan deformation, indicating an early to mid Viséan age of ∼347–307 Ma. The timing of mineralisation at Bathgate Hills, Scotland (∼326 Ma - Smith et al. (1994)), is later than deposits in Ireland. These stratabound Pb-Zn sulphide lenses and nodules are associated with the late-stage intrusion of doleritic sills, which experienced diagenetic recrystallisation and remobilisation during later intrusion events (Smith et al., 1994).

1.3 Irish-Type mineralisation

The Irish Midlands is classified as a major base metal orefield, hosting many significant deposits (see Fig. 1.2), prospects and the world-class Navan orebody (Hitzman and Beaty, 1996). Pb-Zn mineralisation in the Irish Midlands has been designated as its own 'type', displaying a style transitional between Mississippi valley type (MVT) and sedimentary exhalative (SEDEX) Pb-Zn deposits (Robb, 2005). The host rocks and mineral textures of Irish deposits have been compared to many MVTs, however they also contain a wider suite of metals and extensive zones of massive sulphides not observed in the latter (Hitzman and Beaty, 1996). Irish-type deposits are thought to be structurally controlled, with a very close spatial association with large-scale faults, often localised adjacent to and along extensional basement faults (Hitzman and Beaty, 1996; Wilkinson et al., 2005*b*).

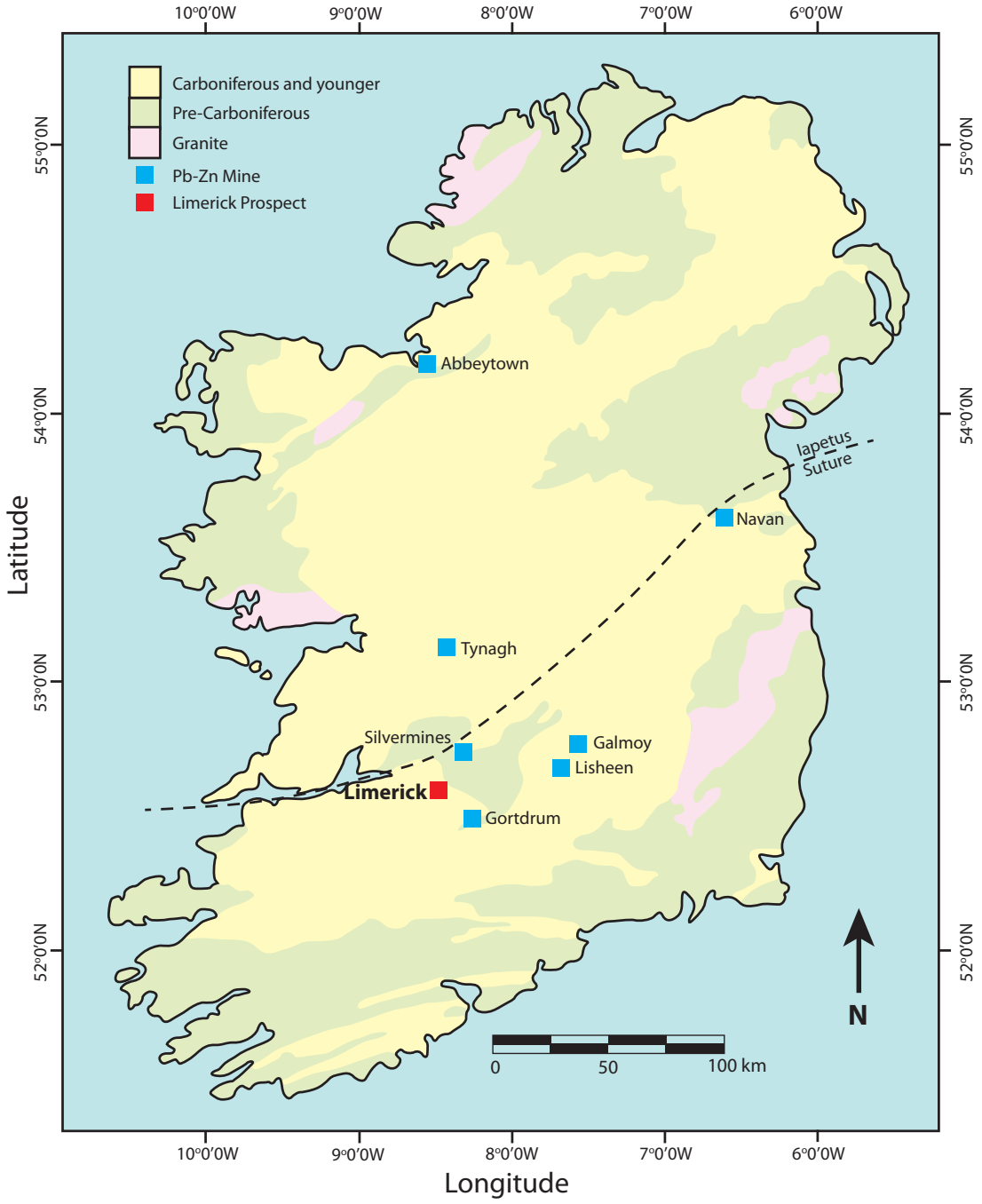

FIGURE 1.2: Map of Ireland displaying positions of currently exploited major Pb-Zn mines and age of country rock. Adapted from Hitzman (1995).

Despite extensive research into these Irish deposits, there is still much controversy as to their origin and mode of formation. There is still considerable debate as to whether faults provide pathways for syngenetic exhalation and seafloor deposition of sulphides (Boyce, 1983; Banks, 1985; Boyce et al., 2003) or epigenetic mixing of fluids and replacement of hydrothermal breccias by sulphides (LeHuray et al., 1987; Hitzman and Beaty, 1996; Hitzman et al., 2002; Wilkinson et al., 2005*b*; Redmond, 2010). Deposits such as

Silvermines and Tynagh are thought to display textures indicative of sea floor deposition, mineralised vents as well as fossilised fauna similar to both modern and ancient vent fauna (Banks, 1985; Boyce et al., 2003). Boyce (1983) states that a convective system dominated by fluids of a seawater origin was driven by heat from underlying magma and exhaled onto or near the seafloor forming a series of chimneys (Boyce et al., 2003), producing localised syngenetic sediment-hosted sulphides.

Many of the Pb-Zn deposits are associated with large-scale extensional faults such as Lisheen, Silvermines and Navan (Hitzman and Beaty, 1996; Wilkinson et al., 2005*b*), which are thought to act as pathways allowing the passage of hydrothermal fluids. Hydrothermal brecciation within the Waulsortian Limestone Formation formed the highly permeable Black Matrix Breccias (BMBs), which were later replaced by large-scale epigenetic sulphide precipitation (Wilkinson et al., 2005*b*) upon mixing of a seawater and basement derived hydrothermal fluid (Banks et al., 2002; Wilkinson et al., 2005*a*). Precipitation of sulphides within the permeable BMBs generated acid, causing dissolution of the dolomite matrix and thereby forming additional pore spaces (Wilkinson et al., 2005*b*). This dolomite replacement by sulphides involved a reduction in volume, increasing porosity by up to 25 %, allowing greater fluid flow, mixing and further precipitation of sulphides (Wilkinson et al., 2005*b*).

There is now general consensus that precipitation of massive sulphides within the Irish Orefield involved the mixing of two hydrothermal fluids with very different properties (see Fig. 1.3). However, the origin of these fluids and the depth at which mixing occurred is still controversial. Fluid inclusion studies on samples from Silvermines and Tynagh by Banks et al. (2002), have shown the first fluid to be a seawater-derived brine that evaporated to reach high salinities of up to 25 wt % NaCl. This fluid was of a lower temperature (<40 °C) and contained a high concentration of reduced bacteriogenic sulphur. The second fluid was of a higher temperature (200–280 °C), lower salinity (12–18 wt %) and contained a high concentration of metals and hydrothermal sulphur. Two fluids of similar properties were also observed by Everett et al. (1999) within samples from Navan.

Many theories exist as to the origin of these fluids. Wilkinson et al. (2005*b*) and Hitzman and Beaty (1996) suggest that the high salinity fluids are formed by evolution of basin waters, forced northward by a topography-driven hydraulic head formed by the

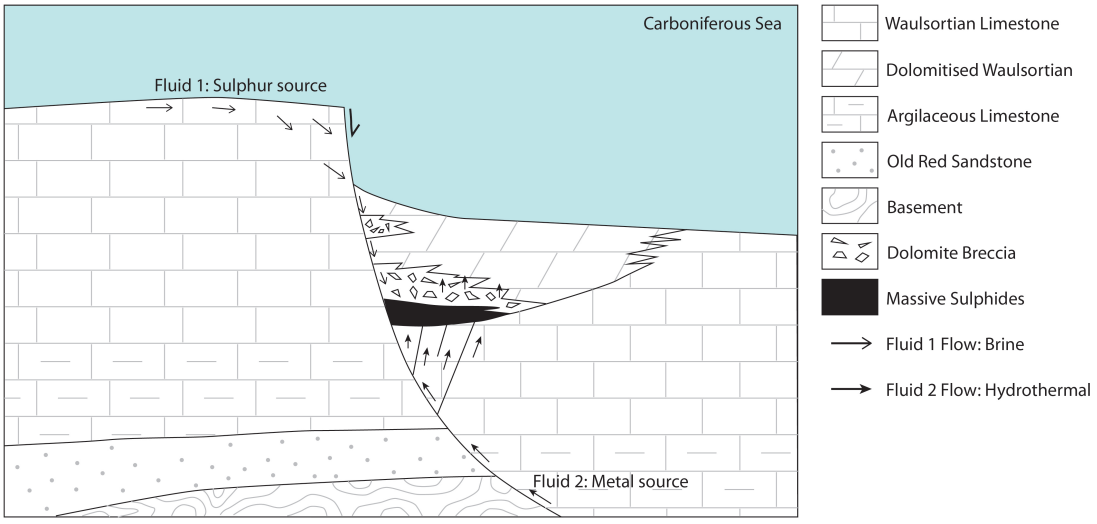

FIGURE 1.3: Schematic genetic model of Irish-type mineralisation involving the mixing of a sulphur-rich brine and metal-rich hydrothermal fluid. This causes precipitation of massive sulphide lenses replacing pre-existing hydrothermal country rock breccias. After Wilkinson et al. (2005*b*).

Variscan orogeny to the south. Hitzman and Beaty (1996) states that the fluid would have been buried along the flow path, increasing in temperature and leaching metals from the Old Red Sandstone Formation. However, Everett et al. (1999) and Wilkinson et al. (2005*a*) indicate that the fluid characteristics require the presence of deep, density-driven convection cells and is therefore inconsistent with a topographically driven flow. This model uses the Old Red Sandstone Formation as the main aquifer for transport of fluid, however Everett et al. (1999) has observed that alteration of this formation is localised around faults. The higher temperature, metal-rich fluid has also been suggested to be sea-water derived, forming brines that entered the crust via fracture zones and extensional faults. High heat flow associated with crustal extension then formed a convective system whereby they returned to the surface via deep basement faults (Hitzman and Beaty, 1996; Banks et al., 2002; Wilkinson et al., 2005*a*). This fluid has also been found to exhibit isotopic signatures consistent with high temperature equilibration with basement rocks, indicating metals may have been stripped from these rocks by the convective cells (LeHuray et al., 1987; Everett et al., 1999; Banks et al., 2002). Strontium isotope studies undertaken by Wilkinson et al. (2005*a*) indicate mixing of a crustal fluid and seawater-derived fluid with the latter penetrating as deep as several hundred metres within fracture zones. This isotopic modification indicates that fluids reached depths of 5–10 km (Wilkinson et al., 2005*a*).

The Limerick Basin has recently undergone an intense level of mineral exploration, and

borehole drilling has intersected numerous diatremes >500 m deep. Two main sites of interest have been located within the license block at Stonepark and Stonepark North, with boreholes intersecting grades up to 11.6 % Zn, 3.5 % Pb and 19.2 % Zn, 8.5 % Pb respectively. However, unlike the rest of the Irish Orefield, the Limerick Basin is associated with large-scale Lower Carboniferous volcanic activity that appears to have both a close spatial and temporal association with the mineralisation (Redmond, 2010).

1.4 Limerick geology and tectonic setting

The Limerick Basin is located in the western Irish midlands, immediately south of the Iapetus suture zone (see Fig. 1.2 and Fig. 3.2). The basin is thought to have been graben-bound, within which a sequence of transgressive Lower Carboniferous carbonate rocks were deposited within a shallow marine environment (Holland and Sanders, 2009). This carbonate sequence is underlain by a continental red sandstone of Devonian age (Hitzman and Beaty, 1996). The Lough Gur wackestones are the youngest of the carbonate sequence observed at Limerick. The thickness of this formation is controlled largely by bathymetry defined by the underlying cavity-rich Waulsortian reef limestones and carbonate mud mounds (see Fig. 1.4 for full stratigraphic column). Much of south-eastern Ireland experienced regional dolomitisation of the Waulsortian Limestone during the early Chadian (Hitzman and Beaty, 1996; Hitzman et al., 1998). However, the fluids responsible for this event did not extend as far northwest as Limerick (Hitzman et al., 1998). The marine transgression is thought to be the product of tectonic subsidence during extension and basin formation, with only a small contribution from eustatic sea level rise (Holland and Sanders, 2009). This sequence is offset by a series of NE-SW trending faults and overlies a faulted Precambrian and Lower Paleozoic basement of greenschist facies metamorphic terranes, accreted during the final closure of the Iapetus Ocean (Hitzman, 1995).

Volcanic sequences within the Shannon Trough consist of two formations, each interbedded with the diachronous transgressive carbonate sediments. The earlier volcanic material is that of the Knockroe Formation, which is interbedded with the upper section of the underlying Lough Gur wackestones (Somerville et al., 1992), and the overlying Herbertstown biosparitic grainstones (Strogen, 1988). Conodonts within wackestones interbedded with the Knockroe Formation indicate that eruptions occurred during the

Lower Viséan and Arundian ages (345–339 Ma) (Somerville et al., 1992; Holland and Sanders, 2009). These eruptions produced a variety of surtseyan-type vitric and lithic tuffs, tuff breccias and lavas 250–500 m thick (see chapter 3). This formation is also associated with clusters of diatremes and later intrusives (Strogen, 1988; Holland and Sanders, 2009) suggesting a similar Lower Viséan age for the Limerick diatremes. The Knockroe Formation comprises alkali basalts and trachytes that grade from aphyric in the early stages to plagiophyric and then phenocrysts of plagioclase + olivine ± clinopyroxene (Strogen, 1988). Pyroclastics were erupted from at least six volcanic centres in two ENE trending alignments on either limb of the Limerick Basin (Somerville et al., 1992; Holland and Sanders, 2009; Redmond, 2010). Volcanism migrated and therefore youngs and thickens from the west to the east (Strogen, 1988; Holland and Sanders, 2009), with the easternmost deposits being of Holkerian age (339–332 Ma) (Wilson et al., 2004). The latter of the two volcanic formations is the Knockseefin, of Asbian age (332–326 Ma) (Holland and Sanders, 2009). Although this formation is not observed in the Teck license area, Strogen (1988), Somerville et al. (1992), Wilson et al. (2004) and Holland and Sanders (2009) have reported it to be lithologically similar to the Knockroe Formation.

The diatremes described in this study belong to a cluster that trends in a NE-SW direction throughout the basin. The diatremes intrude through the Waulsortian Limestone and appear to have erupted diachronously with deposition of the Lough Gur wackestones (see chapter 3). The depths of these diatremes are unknown, as drilling terminated at a maximum depth of 560 m, within the massive lapilli tuff of the central diatreme facies.

The geochemistry and petrology of the Limerick volcanics indicate low degree of melting of the upper undepleted mantle as a result of moderate crustal extension (Holland and Sanders, 2009). However, Strogen (1988) suggested that the beta value of stretching required to produce the Shannon Trough would have been insufficient to cause the onset of volcanism. As such, Strogen (1988) proposed that sporadic episodes of magmatism must have been caused by transtensional opening of the basin. Crustal extension in either of these theories would promote adiabatic melting of the mantle (see section 1.5), generating small volumes of magma that would have utilised tectonic weaknesses to reach the surface (Holland and Sanders, 2009). Rapid basin subsidence throughout the Viséan kept pace with the high volcanic input, preventing the formation of either deep sea conditions or widespread subaerial deposits (Lees and Miller, 1985).

Mineralisation within the Limerick Basin is stratigraphically and structurally controlled, found in very close spatial and temporal association with the diatremes. These deposits consist of Pb-Zn sulphides within Waulsortian Limestone hosted stratiform lenses or hydrothermal breccia bodies (BMBs) (Wilkinson et al., 2005*b*; Redmond, 2010). At Limerick, these breccias have a dolomite-rich matrix and can become completely replaced by base metal sulphides, such as sphalerite, galena and pyrite. Throughout the Irish Midlands, these hydrothermal dolomite breccias are found cross-cutting regional dolomite at such deposits as Silvermines, Lisheen and Galymoy (Hitzman and Beaty, 1996; Hitzman et al., 1998), indicating that localised BMB formation post-dates fluid flow in southeast Ireland.

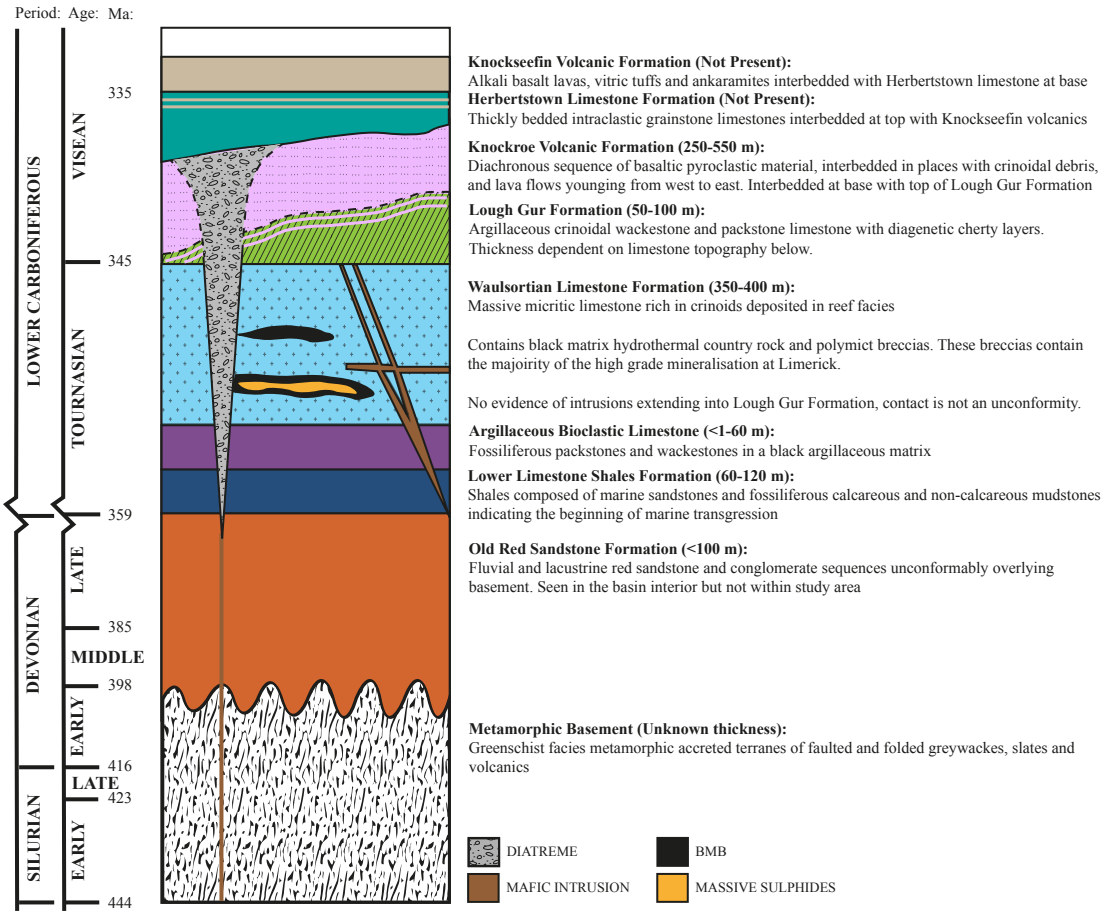

FIGURE 1.4: Stratigraphic column showing timescales of deposition and brief lithological descriptions. Knockseefin and Herbertstown Formation not observed at Limerick and boreholes do not drill deep enough to intersect Old Red Sandstone Formation or the metamorphic basement. Thicknesses are estimated based on borehole data provided by Teck Ireland Ltd. Timescale of deposition adapted from Strogen (1988) and Somerville et al. (1992). Note scale change at start of Tournasian.

1.5 Continental rifting

Many tectonic features within the Limerick area are indicative of extension and continental rifting, such as graben bound and pull apart basins, associated with the regional stage of tectonic activity described in section 1.2. Although volcanic rocks in continental rifts exhibit a wide range of compositions, alkali basalts are perhaps the most common in intra-continental settings, for example the Cameroon line, West Africa (Fitton and Dunlop, 1985), Clyde Plateau, Scotland (Young and Caldwell, 2011) and the Beara Peninsula, Ireland (Pracht and Kinnaird, 1997). Extension and basin formation results in lithospheric thinning, decompressing the mantle rocks beneath and causing adiabatic melting. Decompression causes the rocks to cross the P-T conditions of the solidus and melt the mantle (Ganguly, 2005) (see Fig. 1.5). Melt fractions during adiabatic melting of the mantle are thought to be on the order of a few percent (McKenzie, 1984; Nicolas, 1986; Vernieres et al., 1997). During melting, incompatible elements such as the light rare earth elements (LREE) become enriched in the melt and depleted in the solid residue (Norry and Fitton, 1983; Best, 2003).

Partial melting of the mantle commonly occurs through one of two processes which represent end member models. Batch melting describes the process by which a partial melt

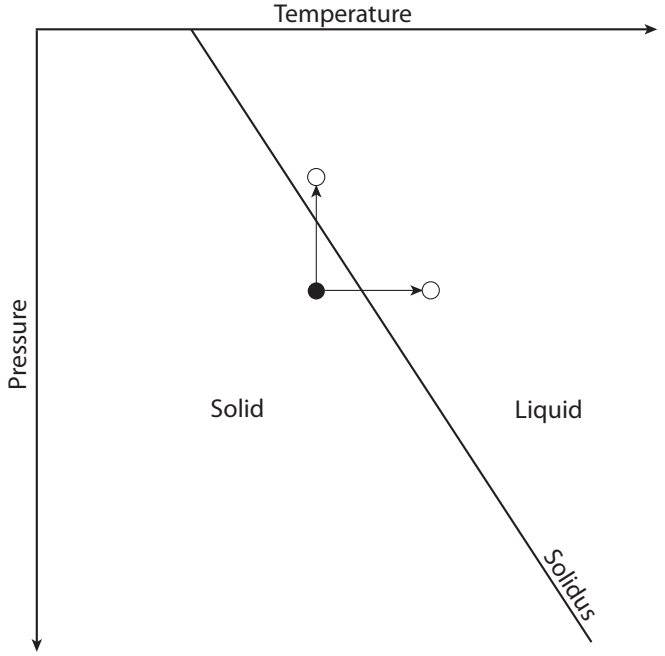

FIGURE 1.5: Schematic graph showing how changes in temperature and / or pressure can cause conditions to move across the solidus and cause mantle melting

increment remains in-situ, continuously equilibrating with the solid residue. During fractional (Rayleigh) melting, the melt increment is instantly segregated and removed from the solid residue (Rollinson, 1993; Karato and Jung, 1998). The process that occurs is dependent on many factors including the porosity and permeability of the source region, as well as the physical properties of the melt such as viscosity (McKenzie, 1985; Rollinson, 1993). The chemical composition of the magma will be affected by the melting process. Increments removed during fractional melting retain the original element concentrations, for example incompatible enrichment within early melts or depletion during later melt formation. However, during batch melting, any element enrichment during early melting phases will be diluted by later, less enriched increments.

The assimilation of continental crust as magma rises through the lithosphere is common. Due to the diverse range in rock types present in the lithosphere, this can have a variety of effects on the magma chemical composition. These can include Pb anomalies such as those in the southern Kenya Rift basalts (Roex et al., 2001), high concentrations of Th (Pearce, 1983), or high light ion lithophile element (LILE) to high field strength element (HFSE) ratios e.g. K/La and Sr/Y (Bouvier et al., 2010).

1.6 Project rationale

The Irish Midlands is a globally important source of base metals, with many deposits currently being exploited (see Fig. 1.2). The Limerick Basin has been the focus of intense exploration activity since 2005, with important discoveries by Xstrata-Minco at Pallas Green and Teck-Connemara at Stonepark (Redmond, 2010). Alkali diatremes within the Teck-Connemara Limerick license area appear to be spatially and temporally associated with breccia-hosted Pb-Zn mineralisation. The presence of these diatremes challenges previously accepted theories that the Irish-Type Pb-Zn deposits were not related to Carboniferous magmatic activity. Volcanism-mineralisation links have been suggested by Redmond (2010) and McCusker and Reed (2013), but evidence has not previously been documented to confirm this link. The geology and tectonic setting of the Limerick Basin has previously been described by Geikie (1897) and Ashby (1939). Strogen (1983, 1988) provides an extensive study of volcanism in the basin, however a full investigation into the diatremes or their association to the mineralisation is not undertaken. Therefore, the principal aims of this project are:

- To characterise the structure and lithofacies of the diatremes to determine their eruptive history and evolution, as well as any association with other volcaniclastic deposits. Drill core extending >500 m below ground surface has provided a rare and unique opportunity to study both the diatreme and volcaniclastic deposits to enhance our understanding of processes and explosive eruptions within a shallow marine environment.

- To identify alteration phases and element alteration trends in order to determine how late stage fluid flow has altered the deposit chemistry. Both diatreme and Knockroe Formation deposits are altered to various degrees, obscuring the original magma petrology and geochemistry. Therefore, elements immobile during hydrothermal alteration are used to characterise the magma. This will allow any genetic relationship between the diatremes, pyroclastic deposits and intrusions to be determined.

- To understand any processes that the magma may have experienced during ascent such as fractional crystallisation or assimilation of continental crust, that may have

affected the chemical composition. Study of the magma evolution will be achieved through analysis of both relatively immobile major and trace elements.

- To understand the nature of any relationship existing between the diatremes and adjacent mineralisation, the relative timing of both, and how the diatremes may have affected the surrounding Pb-Zn mineralisation. Initial studies of the Limerick mineralisation have shown an apparent temporal and spatial relationship with the diatremes. Current Irish-type mineralisation models do not include a genetic relationship with the large volumes of Carboniferous volcanism that occurred in the Irish Midlands. In order to better understand processes at Limerick, the nature, setting and isotopic composition of the mineralisation must be compared to other well-studied deposits in the Irish Orefield.

The subsequent chapters are outlined as follows:

Chapter 2: Methodology

This chapter outlines the methods used for recording fieldwork and brief descriptions of data acquisition. This chapter also indicates the precision and accuracy associated with these data sets.

Chapter 3: Basaltic maar-diatreme volcanism in the Lower Carboniferous of the Limerick Basin

This chapter has been published as Elliott et al. (2015) and takes advantage of >500 m of drill core to describe both the diatreme and extra-crater volcaniclastic lithofacies, as well as a comprehensive vesicle distribution study on both deposits. This paper provides unique insights into both shallow and deep processes, deposits and architecture of diatremes, particularly the evolution of those that erupted into a shallow marine environment. In addition, understanding of diatreme-related processes within the Limerick Basin may shed light on any genetic relationship between their eruption and the emplacement of base metal deposits.

Chapter 4: Geochemistry of diatremes and associated deposits: insights into the origin and evolution of their parent magmas

Direct analysis of deposit composition can be used to improve our understanding of the origin and evolution of magma and any processes undergone, such as fractional crystallisation or the assimilation of continental crust. However due to the various states of

alteration observed within these deposits, major element magma classification methods cannot be used. This chapter focuses on the classification of diatreme and Knockroe Formation deposits, in terms of chemistry and magmatic origin, using immobile elements which are not affected by later hydrothermal alteration.

Chapter 5: Post emplacement alteration of basaltic diatremes in Limerick, Ireland: Implications of 'Irish-Type' Pb-Zn emplacement

Pyroclastic deposits confined to diatremes are characteristically porous, permeable and in many cases metastable, therefore making them susceptible to strong alteration, obscuring the original magma geochemistry. The identification of element alteration trends can help in determining the primary composition of the magma. This chapter aims to understand how the deposits have been altered from their primary composition, and as such, investigate the processes that have occurred post-diatreme emplacement. In addition, studying the deposit alteration allows us to understand the relationship between diatremes and fluid flow including BMB and mineralising fluids.

Chapter 6: A role for diatremes in formation of Pb-Zn mineralisation of the Limerick District of the Irish Orefield: The sulphur isotope evidence

Previous chapters present evidence for a clear genetic relationship between the diatremes and Pb-Zn mineralisation. As evidence has not previously been documented associating the Irish Orefield deposits with large volumes of Lower Carboniferous volcanic activity, this link is controversial. This chapter integrates all the evidence for this genetic link and compares the Limerick mineralisation system to other comparatively well understood systems such as Navan and Lisheen, to determine whether the diatremes have played a similar role to the 'traditional' extensional faults, or whether they have played a more active role in mineralisation. Sulphur isotope data are presented in this chapter to determine how the mineralising system differs from other Irish Orefield deposits. Finally, a model is proposed suggesting the diatremes provided a fluid pathway similar to an extensional fault, but more porous and permeable, as well as providing heat and elements required for mineralisation.

Chapter 7: Conclusions and potential future work

This chapter draws together the main results from each chapter and provides conclusions for the diatreme-mineralisation system as a whole. Potential future work on the Limerick diatremes and sulphide samples is also discussed.

Chapter 2

Methodology

2.1 Geological fieldwork

Approximately nine weeks of fieldwork was undertaken within Teck's license area in Co. Limerick (see Fig. 3.2), over the course of three visits to Ireland between 2011–2014. Exposure was very poor over the license area and access to private property limited; therefore most of the study was concentrated on drill core obtained by Teck Ireland Ltd during their exploration. Local topographic highs occasionally exposed more resistive lithologies such as dykes, basalt flows and reef limestones. Exposures and structural information was recorded on 1:10,000 maps of the area. The locations of known (drilled) diatremes were visited but they were not exposed at the surface.

Over 230 rock samples were collected over the study period, including diatreme, intrusion, extrusive pyroclastics, lava flows and black matrix breccia (BMB) samples. The objective of the first fieldwork visit was to log, characterise and sample the diatreme-related drill cores. The subsequent visit aimed to log, correlate and sample the extrusive Knockroe Formation. The purpose of the last visit was to collect mineralised samples from a variety of different environments for sulphur isotope analysis, including replaced BMBs, layered sediments within Waulsortian Limestone cavities (internal sediments), intrusions, diatremes, veins and breccias.

2.2 Available datasets

Teck Ireland Ltd provided trace and major elemental datasets upon commencing fieldwork. These were obtained by both powdering bulk samples and by taking a groove out of a length of core (u-channeling). Powders were sent away to a commercial lab for analysis and therefore their exact method of preparation is unknown. These data were only used to determine geochemical patterns and have been separated from other analyses. Another sulphur isotope data set obtained by Nick Kerr for a Masters dissertation at the Colorado School of Mines, was plotted alongside the data from this study for comparison purposes. To obtain this data set, ninety-five sulphide samples were powdered using a micro drill and combusted at 1050°C using a Eurovector 3000 elemental analyser. The sulphur dioxide gas produced was analysed in a Micromass Isoprime mass spectrometer in a helium carrier gas at the Colorado School of Mines, USA (Kerr, 2014).

2.3 Core logging

Clast composition and size were systematically measured by recording the maximum diameter of the clast crossing the central line of the core at 10 cm intervals. Prior to logging, clast sizes of the same 5 m of core (borehole 28, 477.4–482.4 mbgs) were logged continuously (every clast) and at 5 cm, 10 cm and 20 cm intervals, in order to determine how the interval of data changed the clast size distribution. The results of this study can be seen in supplementary material 2.1. Clast size distributions differed little between intervals of 5 cm and 10 cm, whereas 20 cm intervals did not represent more subtle changes. Therefore a measuring interval of 10 cm was determined to be the most appropriate compromise between time and detail. Where changes occurred at a scale less than this, smaller intervals were adopted. Significant gradual and sudden changes in the characteristics of the volcanics were noted and used to identify lithofacies. These characteristics included colour, angularity, matrix proportion, support, size, composition, sorting, lapilli vesicularity, alteration and textures. Clast characteristics were described based on criteria outlined in White and Houghton (2006). Angularity, matrix proportion, sorting, clast vesicularity and ash size were all visually estimated in the field using reference charts. Lithofacies were grouped into associations based on similar characteristics and inferred formation processes.

2.4 Sample preparation

Samples selected for whole rock analysis tended to be representative of the lithofacies at a given depth. Preparing samples for major and minor elemental analysis involved coarsely crushing the sample using a flypress. The required parts of the sample, for example juvenile lapilli, were picked, separated from surrounding matrix (e.g. carbonates) and washed to remove dust produced by crushing and potential contamination. Samples were placed in clean sample bags between sheets of paper during crushing to minimise the risk of contamination. An agate mortar and pestle were used to create a fine powder from the crushed samples before preparation more specific to the analysis method was undertaken (see sections 2.6–2.8 and supplementary material 2.2 for more information). Acetone was used to clean all equipment before preparation of the next sample.

2.5 Scanning electron microscopy

Polished thin sections of representative lithofacies from the diatreme, Knockroe Formation and polymict BMB were made and coated with 20 nm of carbon in a vacuum chamber. Samples were linked to the metal stage using carbon tape to create a better contact. Each point sampled with the PGT energy dispersive X-ray microanalysis system at the University of Southampton, consists of a 2 μm^2 circular area. Where mineral phases of interest were smaller than this, surrounding minerals were also ablated. This gave less accurate elemental percentages but in most cases still allowed mineral identification. The scanning electron microscope (SEM) contains an internal calibration, automatically converting counts per second into an elemental percentage. The working distance of the stage from the electron emitter was kept consistently at 19 $\pm$ 0.2 mm and each sample run for 120 seconds to ensure maximum consistency within the data. All SEM images displayed are captured using a backscattered electron detector (BSE).

2.6 X-ray diffraction

Fine-grained clay phases were often too small to identify individually using the SEM, whole rock samples were therefore analysed using X-ray diffraction (XRD) to identify these minerals. Samples taken at regular intervals down the diatremes and from polymict

BMBs were crushed and passed through a 500 μm sieve. 1.5 g of sample was added to 0.5 g of corundum and added with isopropanol to a vessel containing corundum beads for micronising. Weights were measured to an accuracy of $\pm$ 0.001 g and beads were placed in the vessel using a stencil to ensure they were positioned correctly. Micronising ensures a homogenised sample and consistent powder size to prevent X-rays from diffracting differently over the sample area. The sample was placed on a hot plate at 66 ^{o}C in a fume cupboard overnight to dry. Unstable clay phases start to alter at higher temperatures. Dried samples were poured into a glass fronted mount to create a smooth surface and prevent X-ray scattering. The XRD machine used was a Panalytical Xpert Pro diffractor. Radiation was obtained from copper tubing at 1.54 $\mathring{A}$ wavelength. A scan speed of 1.2 ^{o}/min was used with data recorded every 0.02 $^{o}\Theta$.

2.7 Inductively coupled plasma mass spectrometry

Trace elements were analysed using inductively coupled plasma mass spectrometry (ICP-MS) at the University of Southampton. After coarse crushing, the juvenile volcaniclastic material was picked out for analysis, ensuring no secondary porosity infill (that might have a different chemical signature) was incorporated. Samples were repeatedly digested with HF and HCl, until no residue was visible, to ensure sample was completely dissolved. Solutions made for trace element analysis were of a dilution factor of 4,000, for major element analysis samples were diluted to a factor of approximately 80,000. Data quality was checked using three standards and blanks run at the beginning and end of each sample set. Where ICP-MS data is normalised, chondrite C1 values were obtained from McDonough and Sun (1995) and primitive mantle values from Sun and McDonough (1989). Multi-element graph anomalies are calculated and quantified using the method described in Taylor and McLennan (1985) and Rollinson (1993).

To determine the quality of this ICP-MS data, the accuracy and precision of three standards (BAS206, JA-2 and BRR-1) run with the samples were recorded and are displayed in Tables 2.1–2.3. Precision (%RSD) was calculated using the following formula:

Eq 2.1: $\%\ \mathrm{RSD} = 100 \times \sigma_{\mathrm{X}} \ / \ \bar{x}$

σ_X = standard deviation of element from mean over all runs; $\bar{x}$ = mean value of element over all runs

Jenner (1996) and Piercey (2014) define degree of precision as follows: 0–3 %RSD: excellent precision; 3–7 %RSD: very good precision; 7–10 %RSD: good precision; >10 %RSD: poor precision

Accuracy (%RD) was calculated using the following formula:

Eq 2.2: % RD = 100× ($\bar{x}$ - STD) / STD

$\bar{x}$ = mean value of element over all runs; STD = compiled or published known value of element in standard material

Jenner (1996) and Piercey (2014) define degree of accuracy as follows: ± 0–3 %RD: excellent accuracy; ± 3–7 %RD: very good accuracy; ± 7–10 %RD: good accuracy; >± 10 %RD: poor accuracy

Standards BAS206 and JA-2 display excellent to very good accuracy and precision. One of the BRR-1 standard samples for both major and minor analysis shows lower than expected results. This has changed the average and standard deviation for BRR-1 giving poor accuracy and precision. Zn values are consistently poor quality and are therefore considered to be unreliable. Figures 2.1 and 2.2 show data for samples measured by both ICP-MS and X-ray fluorescence spectrometry (XRF) analysis. Correlation of the two datasets is precise for all major and minor elements except Cr, Pb and Cu which all show rotational bias (see Piercey, 2014) and may reflect incomplete digestion of these metals. V displays translational bias, indicating that ICP-MS analysis was detecting lower concentrations of the element than XRF analysis. Correlation is better at higher concentrations of elements due to increased accuracy of data above the machines detection limits.

	$\bar{x}$	**STD**	$\sigma_{\mathbf{X}}$	**%RSD**	**%RD**
Na	19980	20055	342.2	1.71	-0.37
Mg	39873	40166	570.1	1.43	-0.73
Al	72477	72623	1360.6	1.88	-0.20
K	1323	1501	145.1	10.97	-11.88
Ca	65027	68708	4152.4	6.39	-5.36
Ti	11783	12060	312.1	2.65	-2.29
V	442	455	10.8	2.45	-2.81
Cr	83	83	4.3	5.25	0.08
Mn	1884	1913	19.0	1.01	-1.53
Fe	101037	100444	2601.3	2.57	0.59
Co	54	54	1.22	2.24	0.90
Ni	49	49	1.2	2.43	-0.41
Cu	72	71	0.9	1.22	0.86
Zn	-148	130	228.1	-153.82	-213.81
Sc	49.74	50.08	1.24	2.49	-0.68
Rb	1.97	1.98	0.03	1.29	-0.52
Sr	105.13	101.24	1.15	1.09	3.85
Y	47.92	48.81	0.37	0.77	-1.82
Zr	127.27	128.56	0.76	0.59	-1.01
Nb	4.33	4.32	0.00	0.04	0.17
Cs	0.08	0.06	0.00	2.00	1.17
Ba	42.40	42.53	0.15	0.35	-0.31
La	4.61	4.67	0.03	0.63	-1.24
Ce	13.85	13.97	0.04	0.29	-0.88
Pr	2.40	2.43	0.01	0.60	-1.17
Nd	12.99	13.15	0.06	0.47	-1.22
Sm	4.67	4.73	0.06	1.24	-1.21
Eu	1.62	1.66	0.01	0.31	-2.25
Gd	6.65	6.67	0.03	0.41	-0.37
Tb	1.20	1.21	0.01	0.46	-0.88
Dy	7.86	8.00	0.01	0.12	-1.73
Er	4.92	5.00	0.01	0.24	-1.70
Yb	4.80	4.86	0.04	0.76	-1.21
Lu	0.71	0.73	0.01	0.70	-2.47
Pb	0.56	0.54	0.02	3.81	4.01
Th	0.29	0.31	0.01	2.22	-5.59
U	0.32	32	0.00	1.32	-1.35

TABLE 2.1: Accuracy and precision values for major and trace ICP-MS data for standard BAS206, measured in ppm. The standard was run three times. $\bar{x}$ = sample mean, STD = compiled standard value, σ_{X} = sample standard deviation, %RSD = precision (percent relative standard deviation), %RD = accuracy (percent relative difference).

	$\bar{x}$	**STD**	$\sigma_{\mathbf{X}}$	**%RSD**	**%RD**
Na	12282	14590	5210.2	42.42	-15.82
Mg	42023	52353	16838.5	40.01	-19.73
Al	61877	75833	25152.0	40.65	-18.40
K	214	442	122.9	57.54	-51.68
Ca	67033	85630	25325.8	37.78	-21.72
Ti	4848	6197	1903.7	39.27	-21.77
V	247	308	94.7	38.34	-19.74
Cr	295	371	118.9	40.36	-20.58
Mn	1128	1431	444.5	39.40	-21.14
Fe	67997	83085	27140.0	39.91	-18.16
Co	40	48	15.8	39.54	-17.13
Ni	105	127	42.6	40.62	-17.32
Cu	72	87	29.0	40.08	-16.98
Zn	-192	87	194.8	-101.50	-320.07
Sc	35.75	43.85	13.29	37.18	-18.48
Rb	0.49	0.55	0.18	35.59	-10.48
Sr	59.26	68.41	22.67	38.25	-13.38
Y	22.65	27.76	8.51	37.56	-18.42
Zr	45.27	56.67	16.91	37.36	-20.11
Nb	0.90	1.08	0.34	38.21	-16.48
Cs	0.01	0.01	0.00	48.22	-3.38
Ba	5.74	7.11	2.22	38.71	-19.23
La	1.28	1.54	0.49	38.15	-16.67
Ce	4.28	5.13	1.62	37.90	-16.61
Pr	0.81	0.98	0.30	37.78	-17.82
Nd	4.69	5.7	1.78	37.95	-17.78
Sm	1.86	2.25	0.72	38.49	-17.23
Eu	0.71	0.85	0.27	38.68	-16.67
Gd	2.84	3.4	1.06	-37.35	-16.58
Tb	0.53	0.64	0.20	38.55	-17.50
Dy	3.59	4.36	1.37	38.07	-17.61
Er	2.36	2.87	0.89	37.85	-17.62
Yb	2.41	2.91	0.92	38.39	-17.23
Lu	0.37	0.44	0.14	37.10	-16.52
Pb	0.28	0.30	0.12	43.81	-7.67
Th	0.06	0.08	0.02	41.10	-28.57
U	0.04	0.04	0.02	40.05	-9.30

TABLE 2.2: Accuracy and precision values for major and trace ICP-MS data for standard BRR-1, measured in ppm. The standard was run three times. $\bar{x}$ = sample mean, STD = compiled standard value, σ_{X} = sample standard deviation, %RSD = precision (percent relative standard deviation), %RD = accuracy (percent relative difference).

	$\bar{x}$	**STD**	$\sigma_{\mathbf{X}}$	**%RSD**	**%RD**
Na	23143	23733	180.1	0.78	-2.48
Mg	43287	43839	372.3	0.86	-1.26
Al	82380	83245	440.0	0.53	-1.04
K	13300	12876	2030.4	15.27	3.29
Ca	39780	44523	3785.8	9.52	-10.65
Ti	3848	3962	135.4	3.52	-2.87
V	112	111	4.3	3.83	1.14
Cr	371	383	8.7	2.33	-3.17
Mn	778	794	19.8	2.55	-2.05
Fe	42950	42891	311.9	0.73	0.14
Co	28	28	0.6	2.20	2.15
Ni	126	126	4.3	3.40	-0.26
Cu	30	31	0.6	1.84	-2.20
Zn	-220	63	239.6	-108.72	-452.08
Sc	17.70	18.04	0.58	3.29	-1.87
Rb	75.80	76.74	1.33	1.76	-1.23
Sr	257.27	246.60	1.43	0.56	4.33
Y	17.32	17.62	0.16	0.91	-1.70
Zr	118.17	120.76	1.11	0.94	-2.15
Nb	8.87	9.11	0.12	1.32	-2.61
Cs	5.15	5.17	0.04	0.80	-0.37
Ba	318.77	321.92	1.51	0.48	-0.98
La	15.98	16.11	0.10	0.60	-0.81
Ce	33.56	33.80	0.14	0.40	-0.72
Pr	3.81	3.84	0.01	0.15	-0.73
Nd	14.45	14.59	0.12	0.80	-0.94
Sm	3.12	3.12	0.02	0.73	-0.16
Eu	0.90	0.91	0.00	0.36	-1.50
Gd	3.04	3.07	0.03	0.93	-0.86
Tb	0.48	0.48	0.00	0.55	0.42
Dy	2.91	2.93	0.02	0.62	-0.56
Er	1.71	1.72	0.01	0.29	-0.72
Yb	1.69	1.70	0.01	0.74	-0.80
Lu	0.71	0.73	0.01	0.70	-2.47
Pb	21.81	21.92	0.17	0.80	-0.50
Th	4.94	4.92	0.09	1.89	0.37
U	2.28	2.27	0.05	2.31	0.56

TABLE 2.3: Accuracy and precision values for major and trace ICP-MS data for standard JA-2, measured in ppm. Each standard was run three times. One BRR-1 standard run provided element compositions of nearly half the other two runs for BRR-1, skewing the accuracy and precision for this standard. $\bar{x}$ = sample mean, STD = compiled standard value, σ_{X} = sample standard deviation, %RSD = precision (percent relative standard deviation), %RD = accuracy (percent relative difference).

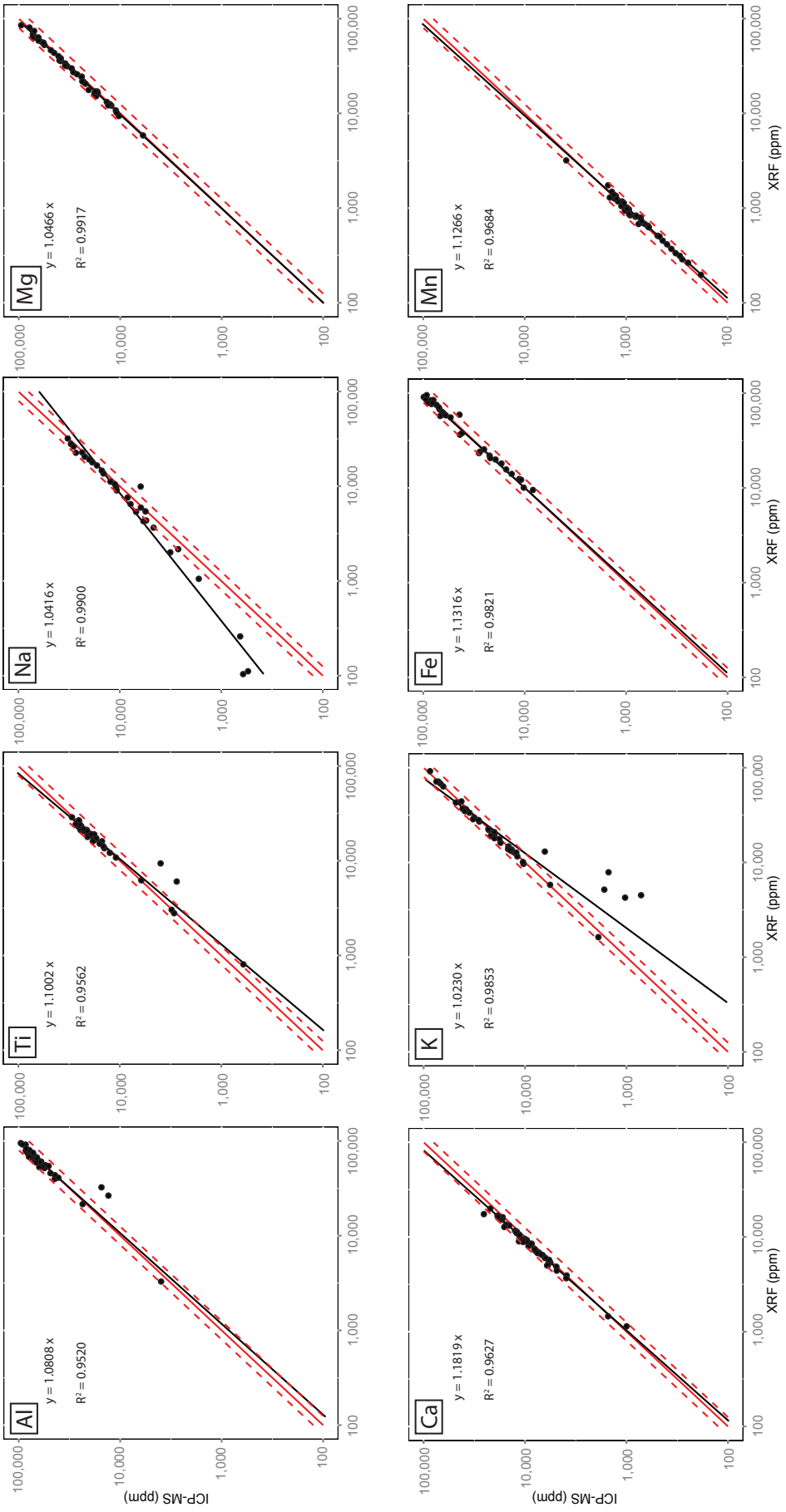

FIGURE 2.1: Correlation between major XRF and ICP-MS data for the same samples. Solid red line indicates perfect 1:1 correlation, dashed red lines indicate ± 25 %. Black line indicates best fit linear trend of the data. Data sets show a good correlation between XRF and ICP-MS analysis.

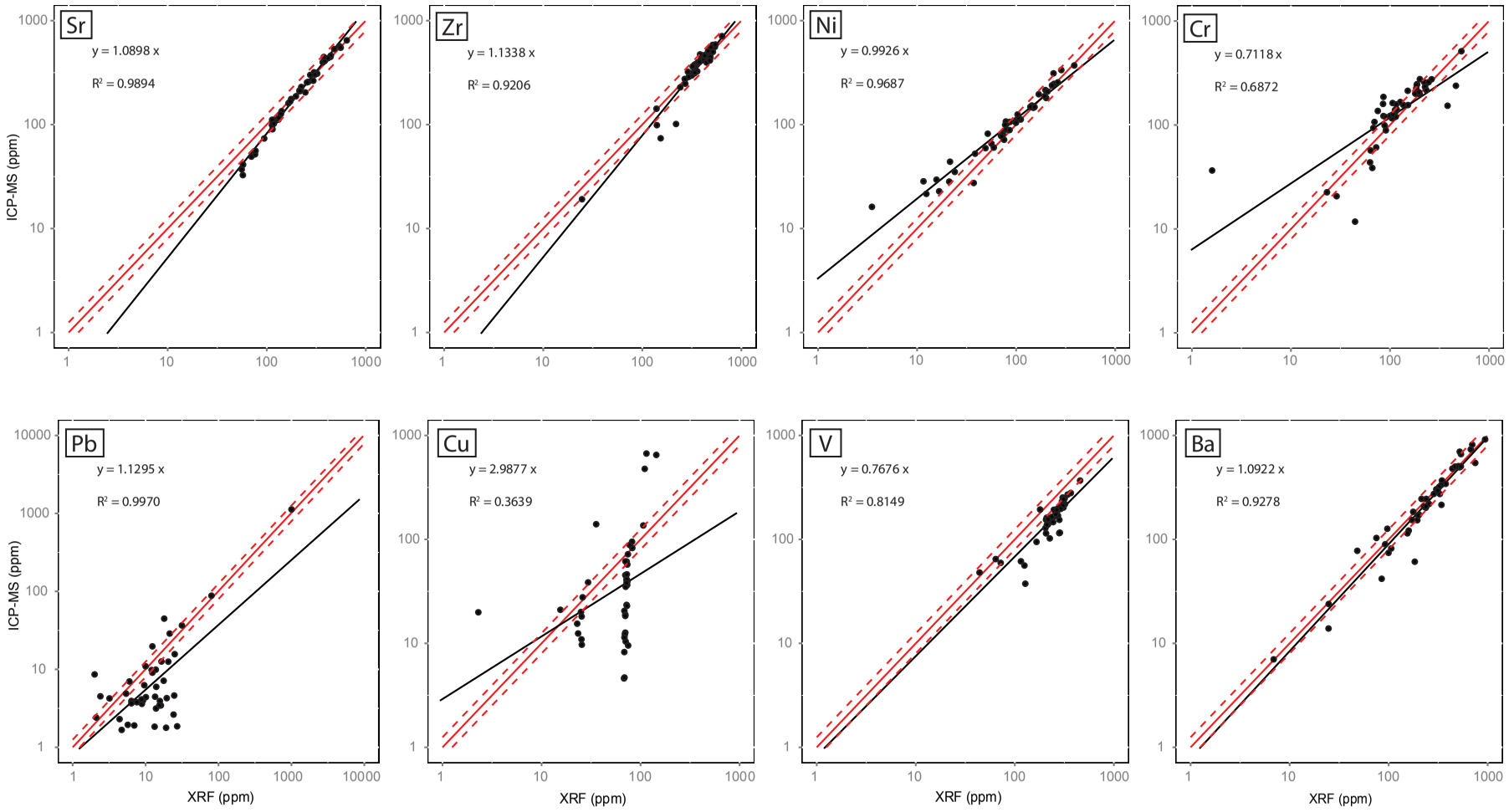

FIGURE 2.2: Correlation between minor XRF and ICP-MS data for the same samples. Solid red line indicates perfect 1:1 correlation, dashed red lines indicate ± 25 %. Black line indicates best fit linear trend of the data. Data correlation tends to be highest at higher element concentrations due to increased accuracy above detection limits. Data sets show a good correlation between XRF and ICP-MS analysis for all elements except Cr, Pb and Cu. This may be reflect incomplete digestion of these metals.

2.8 X-ray fluorescence spectrometry and loss on ignition

Major elemental analysis was obtained at the University of Southampton by XRF analysis of glass beads. Before preparation of the beads, LOI was determined on the powdered samples by drying in ceramic crucibles at 450 °C for four hours. Samples were cooled in a desiccator to prevent reabsorption of water before re-weighing and calculating LOI via the following calculation:

$$\textbf{Eq 2.3: } \text{LOI (wt\%)} = 100 \times (\text{wt}_2 - \text{wt}_1) \,/\, \text{wt}_1$$

wt_1 = raw sample weight; wt_2 = sample weight after ignition

LOI was determined as an approximate alteration index for juvenile material due to their hydrothermally altered nature. The presence of sulphides within the samples may also have had an adverse affected on the heated Pt-Au crucibles used for bead preparation. Temperature trials were undertaken for LOI at 110 °C, 450 °C and 1050 °C on the same samples (see supplementary material 2.5). Drying to 100 °C will remove atmospheric water, 400 °C will remove water from clays and 1000 °C will burn away carbonates and will produce a sample more comparable to the original, unaltered rock.

A homogenised mixture of powdered sample and di-lithium tetraborate flux at a ratio of 1:10 (∼0.5 g sample and ∼5 g flux) was heated to form glass beads. The molten liquid was poured on to a Pt-Au stencil dish to cool into a bead. If solids are present within the glass bead or it cracks upon cooling, then the bead is re-melted and produced again. Analysis of these glass beads was undertaken in a Panalytical Magix-Pro WD-XRF fitted with a 4 kW Rh X-ray tube calibrated using over twenty international geochemical reference samples.

Precision and accuracy of XRF was determined using four runs of the internal standard BRR-1 at the beginning and end of the samples. Major element compounds all exhibit excellent precision and accuracy, except MnO which exhibits very good accuracy. XRF analysis does not appear to be very accurate in determining the concentration of trace elements.

Compound	**1**	**2**	**59**	**60**	$\bar{x}$	**STD**	$\sigma_{\mathbf{X}}$	**%RSD**	**%RD**
SiO_2	49.59	49.32	49.28	49.28	49.37	49.82	0.15	0.30	-0.91
TiO_2	1.02	1.03	1.02	1.02	1.02	1.03	0.00	0.30	-0.54
Al_2O_3	14.38	14.27	14.37	14.33	14.34	14.37	0.05	0.37	-0.22
Fe_2O_3	11.70	11.75	11.67	11.66	11.69	11.88	0.04	0.33	-1.56
MnO	0.19	0.19	0.19	0.19	0.19	0.18	0.00	1.28	4.89
MgO	8.50	8.45	8.49	8.48	8.48	8.57	0.02	0.28	-1.03
CaO	11.76	11.81	11.74	11.75	11.76	11.95	0.03	0.26	-1.56
K_2O	0.05	0.05	0.05	0.05	0.05	0.05	0.00	2.77	2.00
Na_2O	1.92	1.90	1.92	1.90	1.91	1.97	0.01	0.57	-2.96
P_2O_5	0.08	0.08	0.08	0.08	0.08	0.09	0.00	1.19	-10.83
Element									
Sr	85.5	90.7	92.6	88.9	89.40	71.20	3.02	3.38	25.56
Zr	60.3	61.6	56.7	59.4	59.50	54.91	2.07	3.49	8.36
Ni	125.9	120.9	119.1	118.6	121.13	133.23	3.33	2.75	-9.08
Cr	354.3	352.7	354.0	342.6	350.90	384.48	5.58	1.59	-8.73
Pb	5.6	17.3	9.5	6.3	9.68	0.38	5.36	55.39	2446.05
Zn	84.1	84.6	83.1	85.6	84.35	85.20	1.04	1.23	-1.00
Cu	64.6	64.8	66.4	61.5	64.30	86.10	2.05	3.18	-25.29
Co	32.2	44.0	12.7	35.9	31.20	47.75	13.28	42.57	-34.66
V	248.9	253.9	250.3	251.6	251.18	323.25	2.13	0.85	-22.30
Ba	1.4	441.9	5.3	12.5	115.28	6.55	217.80	188.94	1659.92

TABLE 2.4: Accuracy and precision of XRF data based on analysis of internal standard BRR-1. Compound measurements are in wt% and elements in ppm. BRR-1 STD values are compiled averages from the University of Southampton. $\bar{x}$ = sample mean, STD = compiled standard value, σ_X = sample standard deviation, %RSD = precision (percent relative standard deviation), %RD = accuracy (percent relative difference).

2.9 Sulphur isotope mass spectrometry

Samples, in which sulphides were visible and easy to separate, were coarsely crushed using a flypress and then mortar and pestle. Sulphides including galena, sphalerite and pyrite were separated from the gangue minerals using a binocular microscope and separated in glass vials. These sulphides were analysed by standard techniques (see Robinson and Kusakabe, 1975) by which 4–5 mg of sample was combusted with excess Cu_2O at 900 °C in a vacuum for 20 minutes, to liberate SO_2 gas. Liberated gases were analysed by a VG Isotech SIRA II mass spectrometer at the stable isotope laboratory, SUERC (East Kilbride), providing a raw $\delta^{66}SO_2$, to which standard corrections were applied to produce a true $\delta^{34}S$ value.

Samples including complicated intergrown textures of sulphides were made into resin mounted polished blocks. These were combusted in-situ by a laser in an oxygen-rich vacuum chamber (Fallick et al., 1992). The minimum spot size of the laser was ∼100 μm, producing a minimum volume of 0.05–0.10 μmol SO_2 gas required for analysis. The laser used was a spectron laser 920Q CW Nd:YAG (1W power) operating in TEM_{00}

mode. The SO_2 gas produced was purified in a glass extraction line, using an acetone trap to remove water and a n-pentane trap to separate CO_2. Analysis of the sulphur isotope composition was carried out on-line by a VG SIRA II gas mass spectrometer. Laser extraction results in sulphur isotope fractionation between the host mineral and the SO_2 gas produced via combustion. A mineral-specific correction was therefore applied to each data value (see Wagner et al., 2002). Sphalerite that experienced difficulties burning under the laser, was powdered using a micro-drill then analysed using conventional methods.

All data are reported in $\delta^{34}S$ notation as per mil ($‰$) variations from the Vienna Canyon Diablo Troilite (V-CDT) standard. Data obtained using conventional methods was corrected using internal gas standard BG MAC, as well as international standards, CP-1 (chalcopyrite), NBS-123 (sphalerite) and IAEA-S3 (silver sulphide). The internal standard gas was itself calibrate regularly throughout analysis by running the same suite of international standards. The standard values, accuracy (%RD) and precision (%RSD) can be seen in Table 2.5. Precision is predominantly excellent, although CP-1 lies at -3.46, within the very good precision range. Negative precision values within Table 2.5

Run	**BG MAC**	**CP-1**	**NBS-123**	**S3**
1	-22.41	-4.6	16.2	-31.4
2	-22.42	-4.38	16.2	-31.58
3	-22.295		17.00	
4	-22.38			
5	-22.36			
6	-21.21			
7	-22.11			
8	-21.75			
9	-22.37			
10	-22.36			
11	-22.37			
12	-22.39			
13	-22.42			
14	-22.38			
15	-22.38			
Published	-22.38	-4.58	17.44	-31.55
Mean	-22.24	-4.49	16.47	-31.49
SD	0.33	0.16	0.46	0.13
%RSD	-1.50	-3.46	2.79	-0.40
%RD	-0.62	-1.97	-5.59	-0.19

TABLE 2.5: Accuracy and precision of sulphur isotope data (per mil) based on analysis of internal gas standard BG MAC, and international standards CP-1 (value published by SUERC), NBS-123 (Sharp, 2006) and S3 (value published by IAEA).

are due to negative sulphur isotope data. Accuracy again is predominantly excellent, although NBS-123 has a value of -5.59, placing it within the very good accuracy category.

2.10 Electron microprobe

More targeted major elemental analyses were undertaken on five samples from the Knockroe Formation and diatreme deposits using a Cameca SX100 microprobe at the School of Earth Science, University of Bristol. The study focused on juvenile material on which a 10 μm beam was used to obtain a homogenised analysis of intergrown alteration products. The detector was run for 10 seconds for all elements except Mg and Al, for which the detector was run for 30 seconds.

Amphibole standard KK1 (USNM 143965) is a kaersutite from Kakanui, New Zealand and was used as an internal standard during microprobe analysis. Published composition of KK1 can be found in Jarosewich et al. (1980), however this is a natural mineral standard and therefore prone to heterogeneity. This standard is known to contain inclusions of FeTi oxide crystals. Discrepancies are therefore present between the published and average measured values obtained from analyses on the University of Bristol's Cameca EPMA, both of which are displayed in Table 2.6. As such, the average measured values

Sample	**SiO_2**	**TiO_2**	**Al_2O_3**	**Fe(Tot)**	**MnO**	**MgO**	**CaO**	**Na_2O**	**K_2O**
kk1-34	40.63	5.68	14.36	9.96	0.07	12.98	9.98	2.60	1.99
kk1-35	40.46	5.55	14.30	10.25	0.16	13.10	9.89	2.74	2.01
kk1-36	40.77	5.62	14.13	10.19	0.10	12.80	9.83	2.57	1.98
kk1-37	40.47	5.57	14.22	10.15	0.09	12.95	10.00	2.57	2.01
kk1-38	40.88	5.62	14.14	9.84	0.09	12.97	9.93	2.49	2.05
kk1-159	40.64	5.65	14.01	10.17	0.07	12.55	9.78	2.49	2.01
kk1-160	40.87	5.73	14.18	9.95	0.14	12.37	9.86	2.65	2.10
kk1-164	41.03	5.85	14.25	9.96	0.07	12.87	9.91	2.69	1.91
kk1-165	40.99	5.78	14.02	9.80	0.08	12.61	9.97	2.66	1.94
kk1-166	40.86	5.77	14.02	9.76	0.08	12.71	9.89	2.58	2.09
Published	40.37	4.72	14.90	11.25	0.09	12.80	10.30	2.60	2.05
Measured Average	40.27	5.63	14.47	9.38	0.09	12.98	10.30	2.60	1.95
Mean	40.76	5.68	14.16	10.00	0.09	12.79	9.90	2.60	2.01
SD	0.20	0.10	0.12	0.18	0.03	0.23	0.07	0.08	0.06
%RSD	0.49	1.75	0.87	1.77	30.87	1.79	0.71	3.12	3.02
%RD	1.22	0.91	-2.12	6.65	5.30	-1.46	-3.84	0.19	3.03

TABLE 2.6: Accuracy and precision of microprobe data (oxide wt %) based on analysis of internal standard kk1, published values from Jarosewich et al. (1980) and measured average values obtained from analyses on University of Bristol's Cameca EPMA.

are considered to be more representative of the overall standard and are therefore used to measure accuracy and precision in Table 2.6. Based on the general rule proposed by Jenner (1996), all elements except MnO and Na_2O have excellent precision. All elements have excellent accuracy except Fe(Tot), MnO, CaO and K_2O, which have very good accuracy.

2.11 Sample locations

Borehole locations for the Teck license area are illustrated in Figure 2.3 to give the reader an idea of the spatial relationship between samples. The majority of boreholes were sampled during the duration of the fieldwork, however not all were chosen to be geochemically analysed. The type of sample analysed from each borehole and the method by which it was analysed is outlined in supplementary material 2.6.

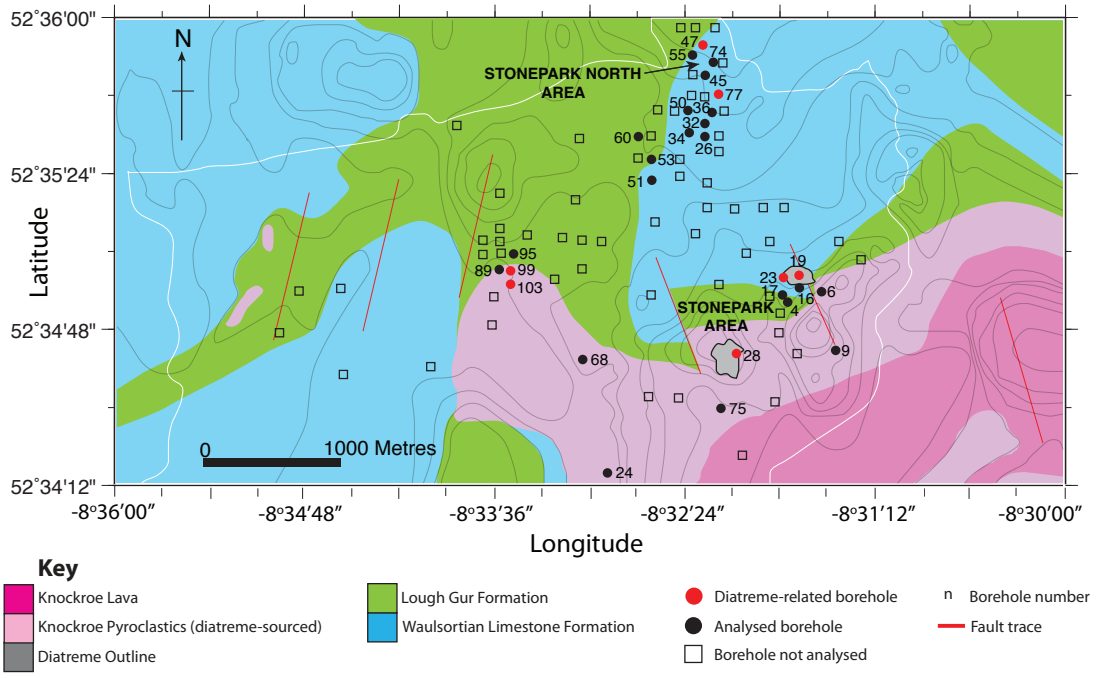

FIGURE 2.3: Map of the Limerick license area indicating the distribution of exploration boreholes which were analysed using a variety of techniques. For details of the type of sample analysed from each borehole and the method by which it was analysed, please refer to supplementary material 2.6.

Chapter 3

Basaltic maar-diatreme volcanism in the Lower Carboniferous of the Limerick Basin (SW Ireland)

3.1 Abstract

Lead-zinc exploration drilling within the Limerick Basin (SW Ireland) has revealed the deep internal architecture and extra-crater deposits of five alkali-basaltic maar-diatremes. These were emplaced as part of a regional north-east south-west tectonomagmatic trend during the Lower Carboniferous Period. Field relationships and textural observations suggest that the diatremes erupted into a shallow submarine environment. Limerick trace element data indicates a genetic relationship between the diatremes and extra-crater successions of the Knockroe Formation, which records multiple diatreme filling and emptying cycles. Deposition was controlled largely by bathymetry defined by the surrounding Waulsortian carbonate mounds. An initial non-diatreme forming eruption stage occurred at the water-sediment interface, with magma-water interaction prevented by high magma ascent rates. This was followed by seawater incursion and the onset of phreatomagmatic activity. Magma-water interaction generated poorly vesicular blocky clasts, although the co-occurrence of plastically deformed and highly vesicular clasts indicate that phreatomagmatic and magmatic processes were not mutually exclusive. At a later stage, the diatreme filled with a slurry of juvenile lapilli and country

rock lithic clasts, homogenised by the action of debris jets. The resulting extra-crater deposits eventually emerged above sea level, so that water ingress significantly declined, and late-stage magmatic processes became dominant. These deposits, largely confined to the deep vents, incorporate high concentrations of partially sintered globular and large "raggy" lapilli showing evidence for heat retention. Our study provides new insights into the dynamics and evolution of basaltic diatremes erupting into a shallow water (20–120 m) submarine environment.

3.2 Introduction

Maar-diatremes are formed during explosive eruptions, and are pre-dominantly associated with alkaline magmas including kimberlites, lamproites and alkali basalts. Our knowledge of the behaviour of these systems is based mainly on the study of either extra-crater maar or eroded diatreme deposits. Due to their association with diamonds, kimberlites are well studied, contributing a large amount to our understanding of diatreme eruptions and their associated deposits (Mitchell, 1990; Sparks et al., 2006; Walters et al., 2006; Brown et al., 2008a). In addition, maar-diatremes, although the second most common type of volcano (Lorenz, 1985; Cas and Wright, 1988; Lorenz, 2007), tend to be eroded and poorly preserved in older sequences. In rare cases, exposures of the lower diatreme zone enables detailed investigation of the internal architecture and structure of the system (e.g. Francis, 1970; Hawthorne, 1975; Kurszlaukis and Lorenz, 1997; Davies et al., 2008; Gernon et al., 2013; Lefebvre et al., 2013; Mundula et al., 2013) or preservation of extra-crater tephra deposits allow a detailed insight into depositional processes (e.g. Fisher and Waters, 1970; Aranda-Gómez and Luhr, 1996; Sohn, 1996; Gernon et al., 2009*a*; Calvari and Tanner, 2011; Lefebvre et al., 2013). Rarely can the maar-crater and diatreme facies be studied at a single site.

Diatremes are irregular, cone shaped pipes up to 2.5 km deep, that erupt through country rock stratigraphy (Lorenz, 2003; Valentine, 2012). Different volcaniclastic lithofacies characteristically form at different levels in the diatreme (see Fig. 3.1); for example the root zone consists of a series of intrusions 'feeding' diatreme eruptions. Typically the central zone (Fig. 3.1) is characterised by a massive volcaniclastic infill consisting of accumulated pyroclasts, crystals and country-rock lithic debris trapped in the pipe (Sparks et al., 2006). Diatremes are expressed at the surface as maar-craters and tephra

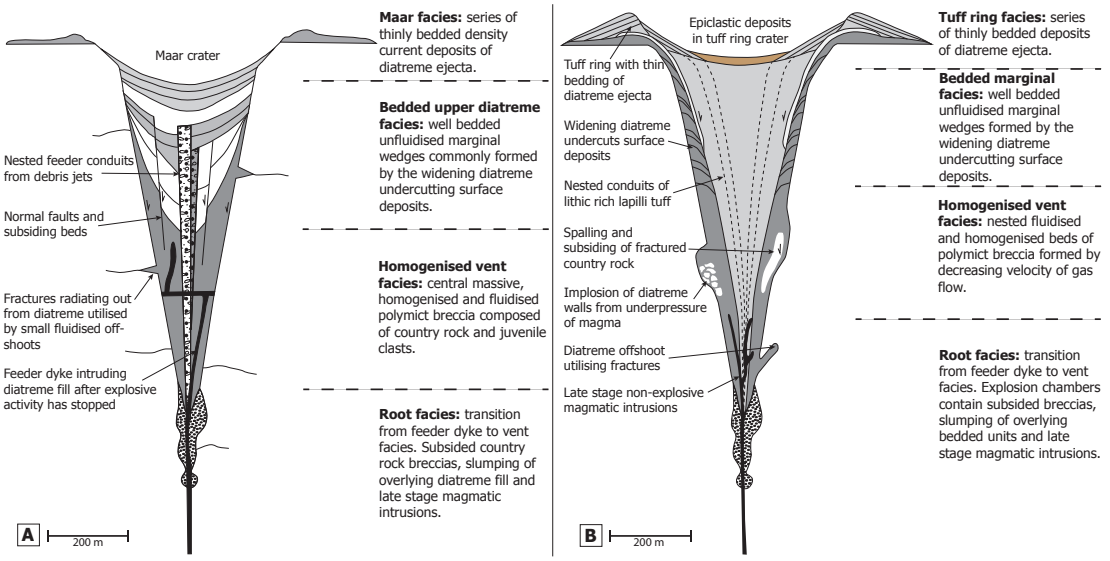

FIGURE 3.1: **A**: Schematic diagram showing the root, diatreme and maar-crater zones of a typical phreatomagmatic diatreme (modified after Lorenz and Kurszlaukis, 2007). **B**: Schematic diagram showing the structure of a diatreme dominated by magmatic processes, which typically involve multiple events of waning gas velocity due to progressive diatreme widening and/or decline in magma discharge rates (modified after Brown et al., 2008b).

rings, typically comprising bedded dilute pyroclastic density current (PDC) and fallout deposits (Lorenz, 1975). There are two plausible methods for the presence of bedding in the upper diatreme. Firstly, undercutting of the tephra ring by vent widening and subsequent subsiding, can form a marginal bedded facies, commonly comprising megablocks (Sparks et al., 2006; Lorenz and Kurszlaukis, 2007; Brown et al., 2008b; Valentine and White, 2012). Alternatively, the upper thinly bedded diatreme facies may have been deposited by dilute density currents in the base of the maar-crater, originating from the same or neighbouring vents (Lorenz, 1986; Lorenz and Kurszlaukis, 2007; Gernon et al., 2009*a*, 2013; Delpit et al., 2014).

Two key models have been proposed to explain the emplacement of diatremes. The first, common in kimberlitic diatreme models, involves the explosive expansion of volatiles propagating down rising intrusions. This creates a deep pipe resulting from a series of sub-Plinian to Plinian eruptions (Field and Scott Smith, 1999; Sparks et al., 2006; Porritt et al., 2008). The second model involves diatreme excavation during phreatomagmatic eruptions as magma propagating to the surface encounters water (Lorenz, 1985; Kurszlaukis and Lorenz, 1997; Kurszlaukis et al., 1998; Lorenz and Kurszlaukis, 2007; Brown et al., 2008a).

Phreatomagmatic activity can cover a range of eruption styles with varying water/ magma ratios. The two main end members are briefly described here but many eruptions lie somewhere along this scale. The first consists of eruptions that involve magma explosively interacting with groundwater or wet sediment, with a low water/magma ratio of <0.3 (Wohletz and McQueen, 1984; Moore, 1985; Kokelaar, 1986), producing gas-supported jets of debris (cf. Lorenz et al., 2002; McClintock and White, 2006). These are often referred to as 'Taalian' (Kokelaar, 1986; Sohn, 1996) and tend to be continental eruptions that form deep diatremes filled with volcaniclastic debris, brecciating the surrounding country rock and incorporating these lithics into their maar deposits at the surface (White, 1991; Lorenz et al., 2002; Valentine, 2012). These maars can reach up to 5 km in diameter with craters several hundred metres deep. Maar deposits tend to be of shallow gradient and consist of well developed beds and stratification with a high proportion of country rock clasts (Lorenz, 1975, 2007; White and Ross, 2011).

Surtseyan eruptions are at the other end of the spectrum, involving a high water/ magma ratio of ∼0.3-50 (Wohletz and McQueen, 1984; Kokelaar, 1986). This tends to produce a funnel-shaped vent containing a partially fluidised and highly mobile mix of juvenile material, water and steam termed a 'slurry' (Kokelaar, 1983; Moore, 1985; Ross and White, 2006). Phreatomagmatic eruptions in these conditions consist of shallow short-lived pulses of tephra jets and continuous eruptions that form due to injection of magma into this water-saturated and fluidised slurry, which is rapidly flashed-heated to steam (cf. Kokelaar, 1983; Moore, 1985). Surtseyan eruptions tend to form weakly bedded tuff cones with steep flanks (White, 1996; Mattsson et al., 2005; White and Ross, 2011) and less than a few percent of non-juvenile clasts (White and Ross, 2011). These tuff cones tend to sit on a shallowly dipping platform of volcaniclastic material, commonly composed of non-explosive deposits such as pillow lavas and hyaloclastites (Moore, 1985) or a combination of fallout and density current deposits from both magmatic and phreatomagmatic processes (Brand and Clarke, 2009).

A suite of alkali basaltic diatremes occurs within the Limerick Basin, part of the Irish Orefield, host to world-class lead-zinc deposits (Banks et al., 2002; Redmond, 2010; McCusker and Reed, 2013). The Limerick Basin has recently undergone extensive mineral exploration, and borehole drilling has intersected several alkali basaltic diatremes. The drill cores, some extending to >500 metres below ground surface (mbgs), provide a unique opportunity to study deposits and the eruptive processes of basaltic diatremes.

This paper describes the volcaniclastic lithofacies, as observed in drill core, of two of the five identified alkali basaltic maar-diatremes from Limerick, and interprets these observations in the context of the magmatic and phreatomagmatic models outlined above. A model depicting a clear relationship between the diatremes and a thick sequence (up to 150 m) of extra-crater volcaniclastic deposits is proposed. This is a type locality for studying the deep internal structure of basaltic diatremes, with the potential to enhance our understanding of processes and interactions during explosive eruptions within a submarine environment.

3.2.1 Geological and geotectonic setting

The Limerick diatreme cluster is located in the western midlands of Ireland, immediately south of the trace of the Iapetus suture zone (Fig. 3.2a)—a series of major NE-SW trending faults, known to have exerted a strong influence on later tectonomagmatic activity. The diatremes erupted through a sequence of Lower Carboniferous limestones,

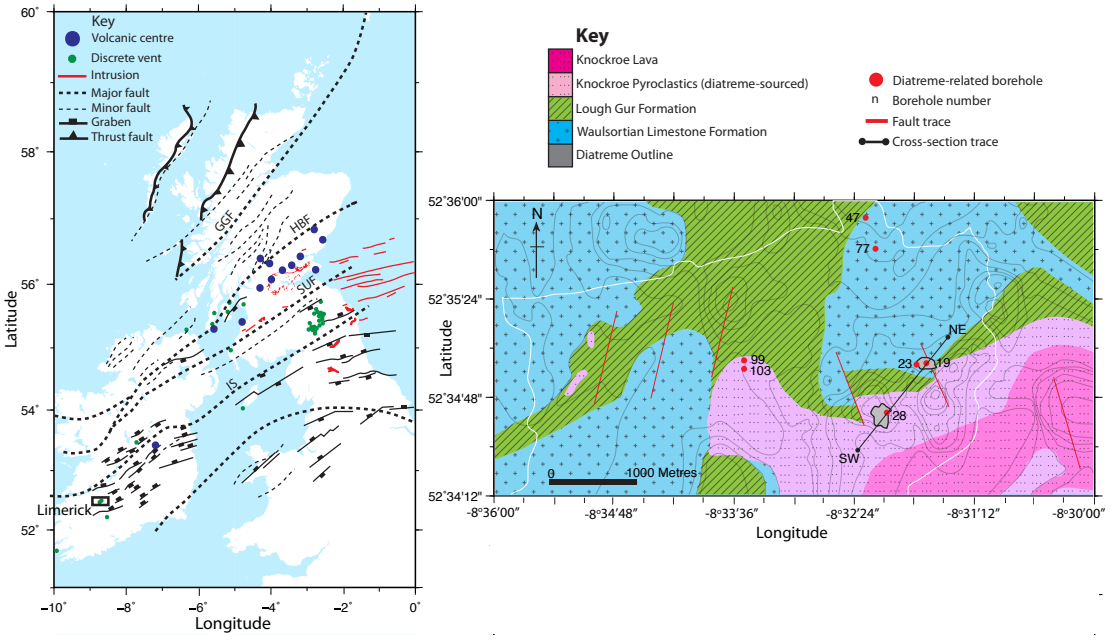

FIGURE 3.2: **A**: Regional map of the British Isles showing major NE-SW trending faults and significant volcanic centres. This tectonic and magmatic trend reflects reactivation of Caledonian basement faults by episodic N-S back arc extension related to the Variscan subduction zone to the south. GGF = Great Glen Fault, HBF = Highland Boundary Fault, SUF = Southern Uplands Fault and IS = Iapetus Suture. **B**: Summary geological map of the study area outlined by rectangle in Figure 3.2A, showing diatreme-related boreholes and outline of diatremes as resolved by magnetic surveys. Contours represent topography of study area.

later overlain by pyroclastic deposits of Viséan age (Somerville et al., 1992). These deposits form part of the Limerick Syncline, and are offset by a series of NE-SW-trending faults. This igneous activity is part of a major phase of NE-SW trending regional rifting across Europe during the Carboniferous Period (Woodcock and Strachan, 2000; Wilson et al., 2004). Volcanism in Limerick was similar in style and timing to magmatic and volcanic activity in Scotland and Northern England, including East Fife (see Gernon et al., 2013) and the Whin Sill Complex (Timmerman, 2004) (Fig. 3.2a). The extensional regime resulted from episodic N-S back arc extension in response to a Variscan subduction zone to the south, which reactivated NE-SW trending Caledonian basement faults (Woodcock and Strachan, 2000). As a result of crustal extension, small volumes of basaltic magma ascended and fractionated extensively within the upper crust before exploiting tectonic weaknesses to reach the surface (Holland and Sanders, 2009).

The Limerick Basin is dominated by transgressive carbonates (Holland and Sanders, 2009). The oldest country rock observed in the boreholes is the Lower Argillaceous Bioclastic Limestone (LABL), which occurs as lithic clasts within the diatreme fill. The LABL is overlain by the Waulsortian Limestone, a reef carbonate containing large cavities, with the latter thought to comprise over half the formation volume (Lees and Miller, 1985; Hitzman, 1995; Hitzman and Beaty, 1996). Overlying the reef carbonate are the Lough Gur wackestones and cherts, the uppermost of which are interbedded with the Knockroe Formation, a series of lava flows and pyroclastic deposits (see Fig. 3.3) that migrate and therefore young from the west to the east (Strogen, 1988; Holland and Sanders, 2009). The earliest phases of Knockroe Formation eruption are thought to be Surtseyan, initally within a submarine environment before tuff rings built up into a subaerial environment and were partially buried by subaerial basaltic lavas (Holland and Sanders, 2009). Using microfauna, Somerville et al. (1992) assigned a Lower Viséan to Chadian-Arundian age (345–339 Ma) to the Knockroe Formation. Irish Waulsortian-hosted Pb-Zn deposits are precipitated in hydrothermal breccia bodies (Wilkinson et al., 2005*b*), termed Black Matrix Breccias (BMB), which appear to have a close spatial and temporal relationship with the diatremes in Limerick. The nature of this relationship remains unclear and highly controversial. The Irish Orefield has not previously been linked to high levels of magmatic activity during the Carboniferous (Redmond, 2010; McCusker and Reed, 2013).

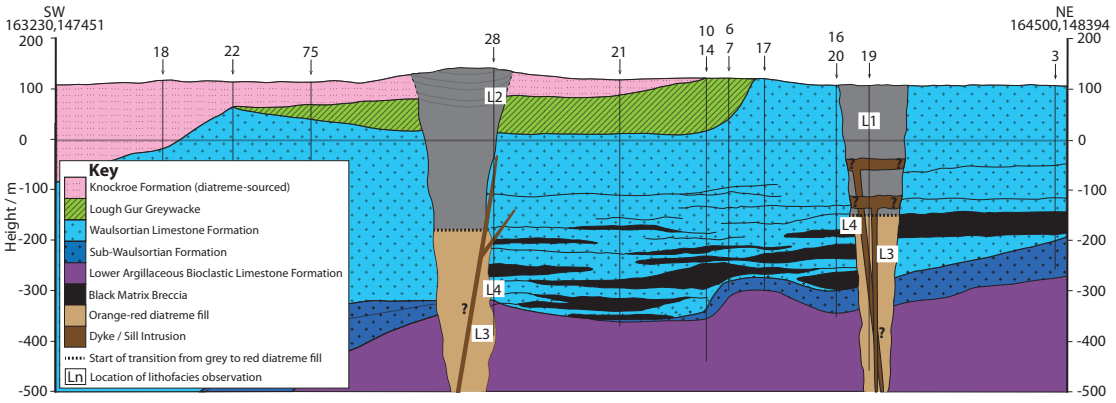

FIGURE 3.3: Cross-section showing the relationships between diatremes and the country rock sequence. The cross-section shows the levels of BMB within the Waulsortian Formation and the level of major sills within the diatreme. Diatreme 28 does not intrude through the Knockroe Formation, but infills accommodation space created by the maar-crater. The lower section of the diatremes overprinted by dolomitisation are indicated. Boxed numbers indicate where LFAs described in Table 3.2 have been observed. Numbers indicate the locations of boreholes drilled through the sequence (borehole data courtesy of Teck Ireland).

3.2.2 Previous studies

The first detailed description of the Limerick Basin was provided by Geikie (1897) and Ashby (1939) who correlated the diatremes they termed 'vent-agglomerates' to a younger Knockseefin Formation, which was deposited during the Early Asbian (Somerville et al., 1992). However, textural and geochemical evidence now suggests a strong relationship with the Knockroe Formation (see Fig. 3.5). Somerville et al. (1992) found that the Knockroe Formation volcaniclastic rocks are interbedded with shallow water ooids and bioclastic carbonates, suggesting deposition in a shallow marine environment (Strogen et al., 1996). Strogen (1983, 1988) determined that the Knockroe Formation pyroclastic rocks generally young from west to east, and identified seven breccia-filled vents across the Limerick Basin. Strogen (1983) showed that these vents were filled with coarse vitric-lithic tuff-breccias containing clasts mainly of phreatomagmatic appearance (described as vitric incipiently vesicular lapilli and ash with curvi-planar surfaces and containing feldspar microphenocrysts) and lacking substantial quantities of vesicular tephra. Strogen (1983) attributed the homogeneity of the deposits, lack of bedding and presence of marginal layering to fluidisation processes during emplacement.

3.3 Methods and terminology

3.3.1 Fieldwork

Although there is little surface exposure of diatremes in the studied area of Ballyneety, Limerick (Fig. 3.2b), six exploration drill cores intercepted diatremes, and another six intercepted volcaniclastic rocks of the Knockroe Formation. Graphic logging recorded the characteristics of the volcaniclastic rocks including maximum clast length, clast composition, vesicularity, colour, angularity, degree of sorting, proportion of ash-grade matrix, alteration and textures. These characteristics were used to correlate lithofacies between logs, particularly for the Knockroe Formation where beds are more laterally continuous.

3.3.2 Laboratory work

Representative samples were taken from each lithofacies and thin sections investigated using transmitted light and scanning electron microscopy (SEM). A study of vesicle size distribution was performed on the different lithofacies.

Variations in vesicle proportions within a deposit or multiple vesicle populations within a juvenile clast can be used to elucidate magma evolution over the timescale of the eruption (Shea et al., 2010), and help determine the eruptive style (Houghton and Wilson, 1989; Ross and White, 2012). Vesicularity estimates were made by manually digitising vesicles both in scaled photographs of thin sections and drill core. Vesicle measurements were obtained using image analysis software ImageJ and the protocols of Sahagian and Proussevitch (1998) and Shea et al. (2010). Non-vesicular lapilli are defined as 0–5 % and incipiently vesicular as 5–20 % vesicles, poorly vesicular ranges between 20-40 %, moderately vesicular 40–60 %, highly vesicular ranges between 60–80 % and >80 % vesicles is termed extremely vesicular (Houghton and Wilson, 1989).

Trace element analysis was undertaken by solution ICP-MS on volcanic material repeatedly digested with HF and HCl and cross-referenced using several international standards (including BAS206, JA-2 and BRR-1).

3.3.3 Terminology

Clast types and sizes were described using the protocols outlined in Fisher (1961) and White and Houghton (2006). Terms used to describe diatreme deposits follow the procedure of Branney and Kokelaar (2002) and Lorenz and Kurszlaukis (2007). The term 'autolith' is used to describe clasts of pre-existing partially lithified diatreme fill, lapilli tuff or tuff, that have been incorporated into later deposits of similar composition (Cas et al., 2008). 'Pelletal lapilli' is a term used to describe a core of material, for example an autolith, phenocryst or lithic clast, that was coated in single or multiple layers of juvenile magma (Gernon et al., 2012). We follow the terminology proposed by Ingram (1964) in describing bed thickness, grain size classification after White and Houghton (2006) and degree of vesicularity of volcanic rocks after Houghton and Wilson (1989). Lithofacies associations are named and abbreviated based on the non-genetic scheme proposed by Branney and Kokelaar (2002).

3.4 Drillcore observations and interpretations

3.4.1 Diatremes

Boreholes drilled down the margins and centres of five diatremes in the study area provide insights into diatreme architecture. The diatremes lack surface expression because the landscape has been modified by glacial and fluvial erosion during the Quaternary Period. The diatremes appear to have experienced late-stage fluid flow, forming a range of alteration products. Based on a magnetic survey, diatreme 19 (named from intersecting borehole number) has a minimum diameter of ∼170 m and a surface area of ∼1.3 × 10^4 m^2, and diatreme 28 has a minimum diameter of ∼240 m and a surface area of 2.6 × 10^4 m^2 (see Fig. 3.2b). Measured wall angles vary between 42–83°, similar to the commonly observed range of 60–85° for diatremes emplaced in hard rock (Hawthorne, 1975; Lorenz, 2007). Assuming a maximum wall angle of 83° gives an estimated minimum volume of 5.2 × 10^6 and 7.4 × 10^6 m^3 for diatremes 19 and 28 respectively. Borehole drilling ceased at <600 m, therefore this volume is a minimum estimate.

Figure 3.3 shows diatreme 28 with adjacent rocks of the Knockroe Formation ∼40 m thick. We attribute the Knockroe Formation to diatreme eruptions, based on their

textural, petrological and geochemical similarities (see Fig. 3.5). The upper bedded lithofacies at the top of the diatremes, adjacent to the extra-crater Knockroe Formation deposits (see Fig. 3.3), has most likely formed by debris currents, remobilisation of maar material and fallout from the water column, gradually filling up accommodation space within the maar-crater. Analogous crater deposition has been described by Lorenz (1986), Lorenz and Kurszlaukis (2007), Gernon et al. (2009*a*), Gernon et al. (2013) and Delpit et al. (2014). Diatreme 28 has experienced partial erosion of the extra-crater sequences, however the entirety of the maar deposits surrounding diatreme 19 have been removed. If the same upper bedded deposits observed at the top of diatreme 28 were also originally deposited in diatreme 19, a minimum of between 80-100 m has been eroded from the upper diatreme, excluding the height of the surrounding tephra ring.

The volcaniclastic diatreme infill has been categorised into eight lithofacies that have been grouped into five lithofacies associations (LFA). LFAs 1–4 are described in Tables 3.1–3.2 and Figure 3.4, LFA 5 is a post-eruption lithofacies and described in section 5.4. These distinctions are based on differences in composition and textural characteristics. The diatremes appear to have a central massive section with localised country rock breccias toward the base. The upper parts of the diatremes and margins consist of bedded lapilli tuff. Intrusions of variable thickness occur within the diatremes, and to a lesser extent in the adjacent country rock. Juvenile lapilli lack macroscopic phenocrysts and are characterised by a low proportion of vesicles (typically 2–25 %). The majority of volcaniclastic material has been altered to clay, overprinting most primary textures and micro-phenocrysts. Ore-forming minerals such as sphalerite and galena occur within the lower diatremes in small quantities, visible under the SEM. This study focused on diatremes 19 and 28 as these preserve the most complete records and are covered by magnetic surveys and drill cores intersecting the central and marginal facies down to 560 m. In contrast, diatremes 47 and 77 were only sampled intermittently, as the drill core alternates been limestone and volcaniclastic material which has been brecciated and remobilised by later hydrothermal fluids forming polymict BMBs.

LFA	Lithofacies	Description	Interpretation
1	Massive lapilli tuffs (mLT)	Predominantly massive, well-sorted lithofacies with high proportion of juvenile fine ash matrix altered to chlorite and locally infilled by carbonates.	Mass wasting of maar-diatreme walls and deposition by gravity flows in an open crater; possible elutriation of ash from lower in the system.
1	Lapillistones (Lf)	Structureless and clast supported with small lapilli and a low proportion of matrix; juvenile bombs and large lithic clasts present. Localised "raggy" juvenile lapilli, preferred vertical orientation of clasts and apparent welding.	Fluidisation of hot lapilli in the central diatreme and transportation of outsized lithic clasts from lower in the stratigraphy
2	Bedded lapilli tuffs (bLT)	Highly heterogeneous lithofacies consisting of both massive and normally graded beds containing a high proportion of juvenile lapilli and highly variable proportion of fine ash matrix. Locally pockets of fine ash, pyrite and secondary calcite occur.	Subsided maar strata deposited near-vent as dilute density currents and later undercut by diatreme widening, leading to downward slumping along margins.
3	Massive lithic-rich lapilli tuffs (mlLT)	Structureless lithofacies locally with abundant lithic clasts and blocks, pervasive red-brown discolouration and fines-rich pockets and pipes.	Homogenous and structureless nature and degassing structures indicate fluidisation of diatreme fill.
3	Lithic-rich graded lapilli tuffs (l(n)LT)	Very poorly sorted, containing a high proportion of ash matrix and abundant juvenile lapilli and lithic blocks. Graded bedding with clast alignment, fines pockets and localised red-brown discolouration.	Accumulation through collapses of the country rock walls and overlying maar.
4	Lapilli tuffs (LTf)	Well-sorted highly altered lithofacies with a large proportion of matrix and lithic clasts. Localised small-scale grading, alignment of clasts, orange-red discolouration and localised injection of the tuffs into cracks in the country rock.	Deposited by a high pressure fluidised flow capable of dilating cracks in country rock.

TABLE 3.1: Summary of lithofacies characteristics, context and interpretation for each lithofacies association in the diatremes

3.4.2 Lithofacies characteristics

3.4.2.1 LFA 1: massive lapilli tuffs (mLT) and lapillistones (Lf)

This lithofacies association is exemplified within the upper 130 m of the centre of diatreme 19, consisting of two key lithofacies, massive lapilli tuffs and lapillistones that grade into each other with no visible bedding. The massive lapilli tuffs (mLT) consist of well sorted fine to coarse ash, lack structure and grade downwards into a more

lapilli-rich tuff. The proportion of juvenile material is high at approximately 95–100 % with only 0–3 vol. % country rock limestone fragments (see Table 3.2) and <5 % pelletal lapilli (see Fig. 3.4A). These predominantly subspherical pelletal lapilli consist of as many as three rims of incipiently vesicular juvenile material surrounding lapilli of volcaniclastic material, carbonate country rock or highly crystalline metamorphic lithic fragments. The rocks contain 40-72 % lapilli and 1-4 % blocks, with matrix proportion varying between 30-70 % but averaging around 60 vol. %, consisting mainly of fine ash. Clasts are sub-angular to sub-rounded and vary between 2–11 mm. Juvenile lapilli tend to be blocky and incipiently to poorly vesicular (8–23 %, Table 3.2). The lithofacies has a pervasive green colouration due to extensive alteration of ash and lapilli to chlorite. Localised areas (decimetre to metre scales) have experienced Fe stained carbonate replacement of the ash matrix.

The lapillistones (Lf) are similar in composition and structure to the more lapilli-rich mLT but contain 75-81 % lapilli, <1–4 % blocks and only 15-25 vol. % matrix, which predominantly consists of fine ash altered to chlorite. Although the average juvenile lapillus is ∼4 mm, the occasional limestone clast reaches 48 mm. The juvenile lapilli have a measured vesicularity of 12–24 % (Table 3.2) similar to the mLT, and a low proportion of feldspar micro-phenocrysts (see Fig. 3.4H). Within the lithofacies, larger "raggy" juvenile lapilli (see Ross and White, 2012) occur in addition to a localised sub-vertical clast orientation and partial welding.

3.4.2.2 Interpretation of LFA 1

The lapilli tuffs and lapillistones may have accumulated through a combination of progressive mass-wasting of the maar-crater walls (Gernon et al., 2009*a*) and preferential transport of fine ash to the upper part of the diatreme via gas-particle dispersions (Gernon et al., 2009*b*). Winnowing of fine ash from areas of LFA1, formed a large proportion of secondary pore space and high permeability allowing precipitation of a carbonate infill surrounding the lapilli (Davies et al., 2008). The blocky nature and incipient vesicularity suggests the lapilli were formed by fragmentation as a result of magma-water interaction (Houghton and Wilson, 1989; Mattsson, 2010).

The pelletal lapilli most likely formed when a dyke or sill intruded earlier water saturated volcaniclastic infill. Intense magma degassing combined with vaporisation of the

diatreme fill produced powerful gas jets in which globules of melt coated clasts scavenged from the adjacent deposits (cf. Gernon et al., 2012). Another theory suggests agglutination of small melt droplets to a core in the deep magma plumbing system (Lloyd and Stoppa, 2003). These lapilli were likely transported from depth to the top of the diatreme by debris jets (Ross et al., 2008*b*; Valentine, 2012) as evidenced by the vertical orientation of clasts (cf. White, 1991) and partial welding.

3.4.2.3 LFA 2: Bedded lapilli tuffs (bLT)

Bedded lapilli tuffs occur near the margins in the upper ∼80 m of diatreme 28. Bed thickness varies considerably, averaging between 2–8 cm, but reaching up to several metres thick and generally increasing with depth. Transitions between beds are either sharp or diffuse, with normal and inverse grading observed, typically towards the base of beds. Bedding angles vary between 4–52°. On average, beds contain 50–60 % ash matrix, pervasively altered to chlorite with pockets of secondary calcite and pyrite, decreasing to <15 % in clast supported beds. Lapilli proportions vary from 40 to extremes of 85 % and blocks <1 %. The degree of sorting decreases with depth, with uppermost beds well sorted and the lowest moderately sorted. Clasts are predominantly rounded and consist of 80–95 % juvenile material, 1–4 % limestone clasts and 3–20 % dark and blocky lapilli of low average vesicularity and possible juvenile origin. Clast sizes vary from 2–40 mm but most juvenile particles are small, averaging between 2–4 mm. Juvenile lapilli are non to incipiently vesicular (2–25 % vesicles), typically altered to chlorite and many have a dark green outer rim.

3.4.2.4 Interpretation of LFA 2

The sequence of thin beds is characteristic of frequent, small-scale phreatomagmatic eruptions (Lorenz, 1986; Sohn, 1996; McClintock and White, 2006). The nature of bedding, high degree of sorting, grading and rounded nature of clasts within this lithofacies suggests they were deposited in the maar crater from a series of dilute density currents (Cas and Wright, 1991; White, 2000). Very thin beds of tuff may be attributed to fallout of ash from suspension in the water column (White, 2000). The rounded nature of the clasts suggests mechanical alteration of their shape by collisions and abrasion during

transport in currents and debris jets (Calvari and Tanner, 2011) or by recycling of juvenile material by later eruptions (Houghton and Smith, 1993; Leahy, 1997). Alternatively, mass wasting of the maar-diatreme walls and introduction of water-supported gravity currents could have introduced this material into the open crater (cf. Gernon et al., 2009*a*). The dark green rims to juvenile lapilli are interpreted as altered glass, thought to represent quenched margins that formed during ejection of hot pyroclasts into the water column. These quenched margins suggest that the lapilli were ejected molten and therefore capable of plastically deforming during the expansion stage of magma-water interaction, providing another possible explanation for their round shapes (Kokelaar, 1986). Progressive deepening of the diatreme would have caused widening and undercutting of the maar and slumping along the diatreme margins (Lorenz and Kurszlaukis, 2007). These wedges of pyroclastic material and their associated bedforms (Fig. 3.1) are commonly preserved along the margins of diatremes and may result from fluidisation of a central region, which effectively destabilises the marginal deposits causing them to slump downwards (Gernon et al., 2008). The dark non-vesicular lapilli that comprise up to 20 % of this lithofacies are similar to "blocky" clasts described by Fisher and Schmincke (1984), Houghton et al. (1999) and Ross and White (2012). These are interpreted as cognate clasts of either fragmented dykes intruded into the diatreme-fill (cf. Gernon et al., 2013) or poorly vesicular magma that experienced brittle fragmentation (cf. Ross and White, 2012).

3.4.2.5 LFA 3: Massive lithic-rich lapilli tuffs (mlLT) and lithic-rich graded lapilli tuff (l(n)LT)

The central part of the diatremes (e.g. diatreme 19) consist largely of massive lithic-rich lapilli tuffs with localised lithic-rich graded lapilli tuffs, penetrated by many late-stage vesicle and phenocryst poor intrusions, commonly exhibiting undulating contacts. Intrusions vary in thickness from tens of centimetres to 45 m, averaging at 2.5 m thick. However intrusion angles vary between 2-69^{o} from the horizontal, averaging 37^{o}. Changes within the mlLT lithofacies are gradual with no visible beds and an increasing proportion of matrix with depth from 15–70 % and 30–85 % lapilli and no blocks between ∼110-330 mbgs with localised variations. The lower part of diatreme 19 (c. 390–560 mbgs) contains a high proportion of clasts and only ∼35 % matrix consisting of varying proportions of medium grained ash, limestone lithic clasts and localised patches of

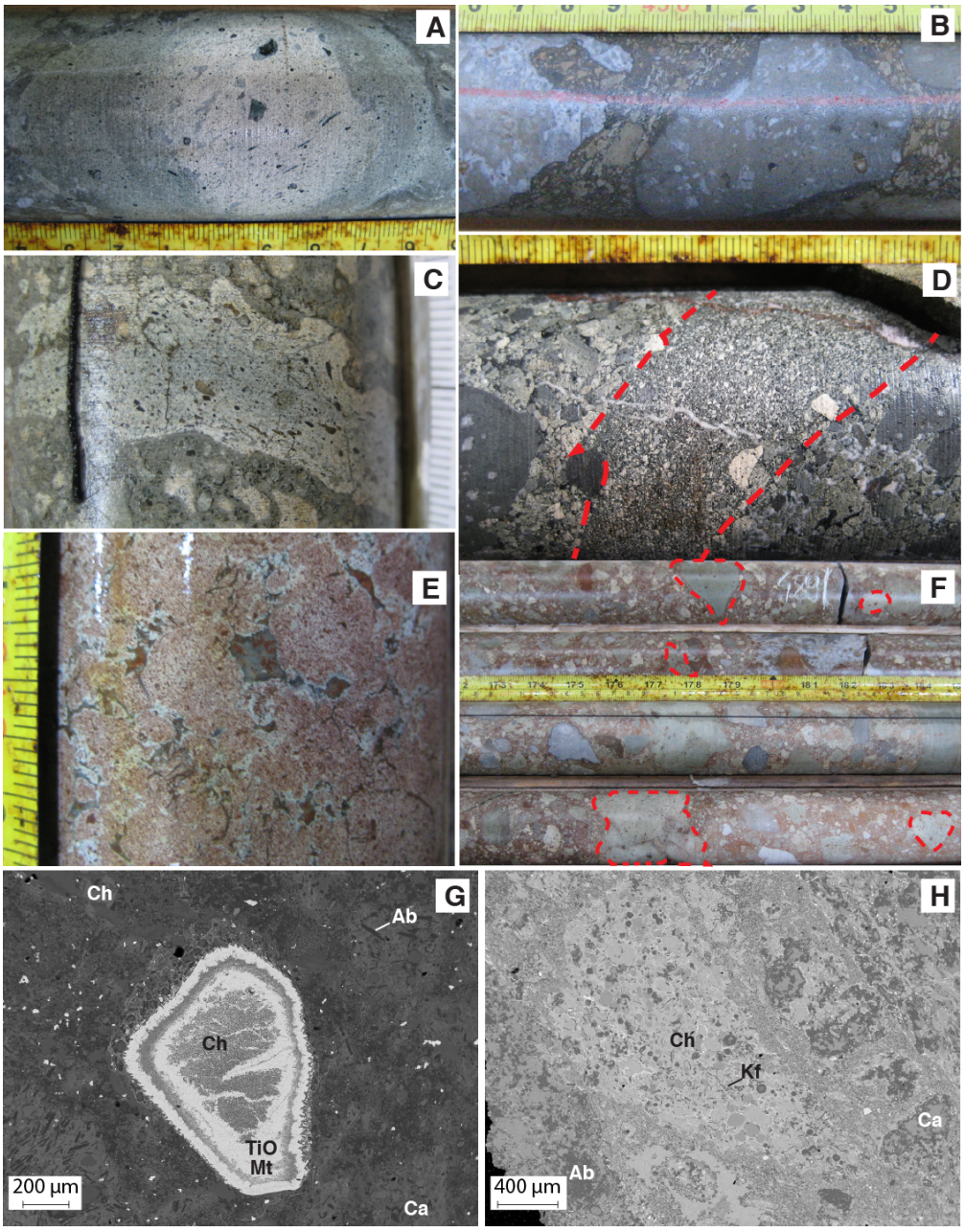

FIGURE 3.4: **A:** Photograph of pelletal lapillus with multiple basalt coatings within mlLT (Borehole 28, 139.6 m) **B:** Large Waulsortian Limestone clasts with alignment of smaller clasts around embayed edges in mLT (Borehole 28, 514.5 m) **C:** "Raggy" juvenile lapillus with flattened, irregular shape (Borehole 19, 54.9 m) **D:** Well sorted fines-rich pipe intruding into bLT lapillistone, outlined in dashed red lines (Borehole 28 , 26.7 m) **E:** Equal sized globular juvenile lapilli with no interstitial ash matrix and slight welding within mlLT (Borehole 19, 553.0 m) **F:** Lithic-rich poorly sorted massive lapilli tuff with Waulsortian Limestone, intrusion and blocky juvenile lapilli (examples outlined in dashed red lines). Pervasive red discolouration is attributed to dolomitisation of mlLT (Borehole 19, 491.7 m) **G:** BSE SEM image of a deep crustal xenolith comprising titanium oxide and magnetite coated with vesicular basalt (Borehole 19, 274 m) **H:** BSE SEM image of vesicular lapillus in the upper diatreme containing feldspar micro-phenocrysts and vesicles filled with chlorite (Borehole 19, 50 m). Ab: Albite, Ca: Calcite, Ch: Chamosite, Mt: Magnetite, Kf: K-feldspar, TiO: Rutile.

pyrite disseminated within the matrix. Clasts have angular shapes towards the top of the lithofacies but become rounded with depth, with 26-73 % lapilli and 3-7 % blocks at the diatreme base. Juvenile lapilli remain dominant (65–90 %), with higher proportions of limestone country rock clasts (up to 17 %) and <1 % lower crustal xenoliths coated with juvenile material (Fig. 3.4G). Limestone clasts frequently exhibit embayed edges and a thin dark rim, possibly consisting of a mud coating (Houghton et al., 1999; Brown et al., 2008a). The average juvenile lapilli size is larger (6–13 mm) than within the upper diatreme, with local variations in sorting and maximum clast size reaching 76 mm. The proportion of dark incipiently vesicular material varies considerably between <5–90 % of the clast population and includes small lapilli to large blocks. The upper lithofacies is lacking in fine ash while the lower section contains isolated pockets and pipes rich in ash sized particles. Juvenile lapilli exhibit vesicularity ranging between 4–58 % and show a wide diversity in habit throughout the lithofacies. These include blocky with fracture-defined edges, areas of equigranular lapilli with little or no interstitial ash matrix and large "raggy" lapilli. Pelletal lapilli commonly display multiple coatings of pale and dark magmatic material. Thin lapilli-rich and fines-rich pipes (1–4 cm wide) and partial welding are visible within the sequence. These partially welded areas are usually found adjacent to boundaries such as dykes, veins or fractures and involve elongation parallel to the boundary and partial merging of juvenile particles.

An orange-red colouration, initially related to alteration of juvenile lapilli, starts at ∼288 mbgs in borehole 19, locally at 182 mbgs in borehole 28 and intermittently at 295 mbgs in borehole 23. Towards the lower diatremes the alteration and discolouration of both clasts and matrix becomes more persistent and juvenile lapilli appear bleached (e.g. Fig. 3.4F). XRD analysis has shown this alteration is the result of increasing dolomitisation with depth (see chapter 5).

The l(n)LT units have sharp contacts with the surrounding mlLT and are characterised by a high concentration (up to 23 %) of blocks up to 1.7 m in diameter (79-100 % of which are country rock clasts) and 57–79 % lapilli. These units are poorly sorted with clast sizes averaging 11 mm, and a large range in angularity from sub-angular to well rounded. The units are lithic-rich with 4–30 % limestone clasts and approximately 3 % dark LABL clasts and between 65–95 % juvenile lapilli, including up to 10 % dark, blocky incipiently vesicular clasts. Beds are typically graded with alignment of smaller clasts around larger clasts, and fines-rich pockets are also observed (Fig. 3.4D).

3.4.2.6 Interpretation of LFA 3

The massive nature of mlLT is consistent with the homogenisation of a large part of the diatreme fill, partly through the action of debris jets (Lorenz, 1975; Valentine, 2012; Delpit et al., 2014) and gas-fluidisation (Walters et al., 2006; Gernon et al., 2008).

The majority of lapilli found within this lithofacies are blocky with fractured boundaries, and likely result from phreatomagmatic fragmentation (Fisher and Schmincke, 1984; Houghton et al., 1999; Ross and White, 2012). "Raggy" clasts retain enough heat to remain in a hot plastic state (Ross and White, 2012) as evidenced by their elongate shape and uneven edges, effectively moulding around adjacent clasts during transport (Fig. 3.4C). Globular lapilli are considered to result from gas streaming through magma, fragmenting and depositing hot lapilli and welding grain boundaries (Fig. 3.4E). This process is similar to that described by Gernon et al. (2012) for the formation of pelletal lapilli and is consistent with the high degree of sorting and paucity of fines.

The localised lithic-rich graded lapilli tuffs within the mlLT are thought to be lenses of material resulting from episodic diatreme wall collapses or formed from explosions near the diatreme-country rock margin (Ross and White, 2006). The proportion of country rock is higher toward the base of the mlLT (>250 mbgs), possibly because the limestone clasts are larger and denser and cannot easily be propelled by fluidising gases or debris jets (Valentine, 2012). The undulating nature of intrusion margins indicates that they were emplaced prior to consolidation of the diatreme fill (Valentine, 2012).

3.4.2.7 LFA 4: Lapilli tuffs (LTf)

This lithofacies is closely associated with the brecciated country rock-diatreme contact, either as undulations in the diatreme walls or injected into fractures in the country rock. This lapilli tuff commonly grades downwards into a polymict black matrix hydrothermal breccia, not discussed in this paper. Defining characteristics include a high proportion of fine juvenile ash and limestone matrix (60–70 %), large clasts (Fig. 3.4B) and alignment of small juvenile lapilli around the country rock contacts. Proportions of clasts are variable with ∼70–90 % juvenile lapilli and a high proportion of limestone (∼10–30 %). Both juvenile and lithic clasts are sub-angular to well rounded and limestone clasts frequently show embayed edges (see Fig. 3.4B). Clast sizes range from 2–86 mm

LFA	Lithofacies	Juv. %	Juv. size (mm)	Lithic %	Lithic size (mm)	Matrix %	Ves. %	Ves. Av %	Ves. size (μm)
1	mLT	95–100	2–11	0–3	3–7	50–60	8–23	15	30–3000
1	Lf	98–100	2–48	0–2	5–16	15–25	12–24	19	12–2000
2	bLT	80–99	2–18	1–4	10–39	15–60	2–33	13	119–23500
3	mlLT	65–90	2–52	10–17	3–71	15–70	4–58	17	6–11300
3	l(n)LT	65–95	2–76	4–35	5–1670	20–30	4–8	15	134–3200
4	LTf	71–87	2–8	11–29	5–25	60–70	–	5–25	–

TABLE 3.2: Summary of measured characteristics of juvenile lapilli and lithics clasts, and vesicle size and percentage for each lithofacies association in the diatremes.

with a low degree of vesicularity (5–25 %). This unit is highly altered with red-brown dolomitisation increasing with depth and proximity to country wall contact.

3.4.2.8 Interpretation of LFA 4

Brecciation of the diatreme walls may be due to late-stage mass wasting (Gernon et al., 2009*a*), wall rock collapses during pipe excavation (Sparks et al., 2006), or alternatively by phreatomagmatic explosions when rising magma interacts with water-saturated diatreme fill (Lorenz et al., 2002; Lorenz and Kurszlaukis, 2007). These processes would create a highly permeable network of fractures, exploitable by fluidised lapilli tuff and magmatic intrusions. Smaller-scale features of ash and lapilli injected into cracks suggest that the lapilli tuff was fluidised and under sufficient pressure to further fragment the country rock. Irregular, embayed edges of larger limestone clasts suggest they have encountered acidic hydrothermal fluids after brecciation (Hitzman et al., 2002; Redmond, 2010). The increased evidence for fluid interaction in this lithofacies suggests these fluids preferentially flowed along the limestone-diatreme contact.

3.4.3 Knockroe Formation

The Knockroe Formation within the Limerick study area is a 5–155 m-thick suite of alkali basaltic pyroclastic strata and lavas (Fig. 3.7). Several boreholes <1 km from the diatremes containing Knockroe Formation pyroclastic rocks were sampled at a range of depths between 6-178 m and analysed for trace element concentrations by solution ICP-MS. Our data, which is discussed in greater detail in chapter 4, shows the Knockroe Formation to exhibit very similar trace and REE patterns to that of the diatremes (Fig. 3.5a). The Knockroe Formation average lies consistently below that of the diatremes,

which may represent dilution by the uptake of Mg and other elements during alteration in seawater (Humphris and Thompson, 1978; Seyfried Jr and Mottl, 1982; Utzmann et al., 2002). Zr is plotted against Nb (Fig. 3.5b) as Zr is considered relatively immobile under hydrothermal conditions (MacLean, 1980; Rollinson, 1993; Zhou et al., 2000), and Nb is highly incompatible and will therefore be enriched in early mantle melts. The Knockroe Formation samples clearly follow the same linear pattern and Nb/Zr gradient as the diatreme samples, indicating that they follow a similar fractionation trend. These data show a clear genetic link between the diatreme and Knockroe Formation, suggesting the latter formed predominantly by diatreme sourced material.

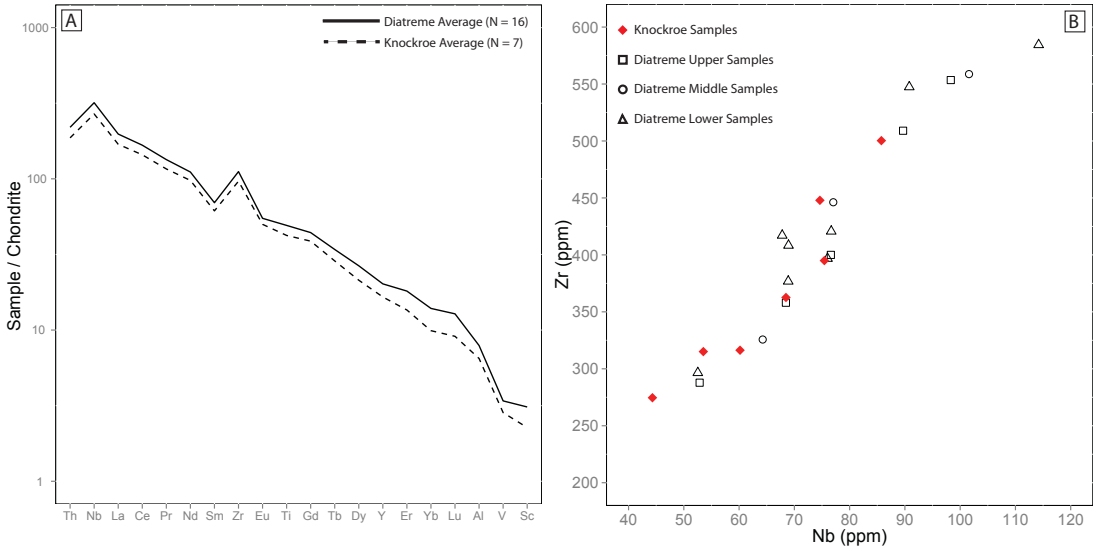

FIGURE 3.5: Trace element data obtained by ICP-MS for diatremes (19 and 28) and the Knockroe Formation. **A:** Multi-element plot shows two very similar trace element patterns for the two deposits. The Knockroe Formation average data are consistently slightly more diluted than that of the diatreme for all elements, most likely due to alteration in seawater e.g. uptake of Mg. **B:** Nb vs Zr plot showing very similar trends and trace element data for diatremes and the Knockroe Formation. Majority of error bars smaller than symbols on plot, full range of error values shown in supplementary material 2.4.

Various parts of the sequence are interbedded with cherty wackestones of the Lough Gur Formation. The Knockroe Formation is divided into five different lithofacies based on their textural characteristics and depositional processes and numbered in depositional order (Fig. 3.6). The fine-grained lithofacies 1 occurs at the base of three of the boreholes but thins out toward the SE, exhibiting normal grading and commonly fine laminations in beds that vary from <0.1–1 m thick. Typically these beds are overlain by dark lapilli-rich lapilli tuff (lithofacies 2). Lithofacies 2 grades upwards into a fines-poor unit (lithofacies 3) with larger rounded lapilli with clay or ash matrix near the base

and small lapilli with ash matrix near the top. The overlying lithofacies 4 is typically interbedded with fines-poor material. Here lapilli are sparse within the wackestones or are interbedded with crinoidal debris in more concentrated, thin beds and contain occasional volcaniclastic autoliths. At the top is lithofacies 5, a matrix-supported and poorly sorted massive unit, which predominantly contains altered volcaniclastic material and limestone clasts, texturally and compositionally resembling deposits of the upper diatreme. This lithofacies increases in thickness toward the SE from 1 m in borehole 24 to 25 m in borehole 6 (Fig. 3.7) with beds typically dipping between 3–50°, averaging ~30°.

3.4.3.1 Interpretation of the Knockroe Formation

To the SW, the thickened Knockroe Formation truncates the carbonate formations, infilling a pre-existing topography most likely formed by carbonate mounds of the Waulsortian Limestone. Greywacke beds within the Knockroe Formation were deposited during the Lower Viséan (345–399 Ma) (Somerville et al., 1992) in a shallow water submarine environment (Lees and Miller, 1985; Holland and Sanders, 2009). Deposition of these greywackes at Limerick is estimated to have occurred at water depths between 20-120 m. This upper limit is based on the depth ranges proposed by Wood (1957), Riding (1975) and Gallagher and Somerville (2003) for foram and algae (taxa *Draffania* and *Girvanella*) observed in the Lough Gur beds by Somerville et al. (1992). The lower depth limit is based on the lack of ooids in the Limerick upper Waulsortian that have been observed in other areas where this Formation has reached depths <120 m (Lees and Miller, 1985), and also reflects the underlying carbonate bathymetry seen in Figure 3.7.

The thin to medium cross-laminated tuff beds of lithofacies 1 were most likely deposited from dilute turbidity currents linked to density flows. The thin discrete beds likely formed by ash fall from suspension in the water column after Surtseyan-type pulses of activity (White, 2000). The lithic content is negligible at <1 % indicating that any magma-water interaction was not diatreme-forming, due to the lack of country rock fragmentation. Any explosive magma-water interaction therefore most likely occurred at the water-sediment interface, rather than being confined within solid rock (Kokelaar, 1986). Magma fragmentation within the submarine environment would also most likely

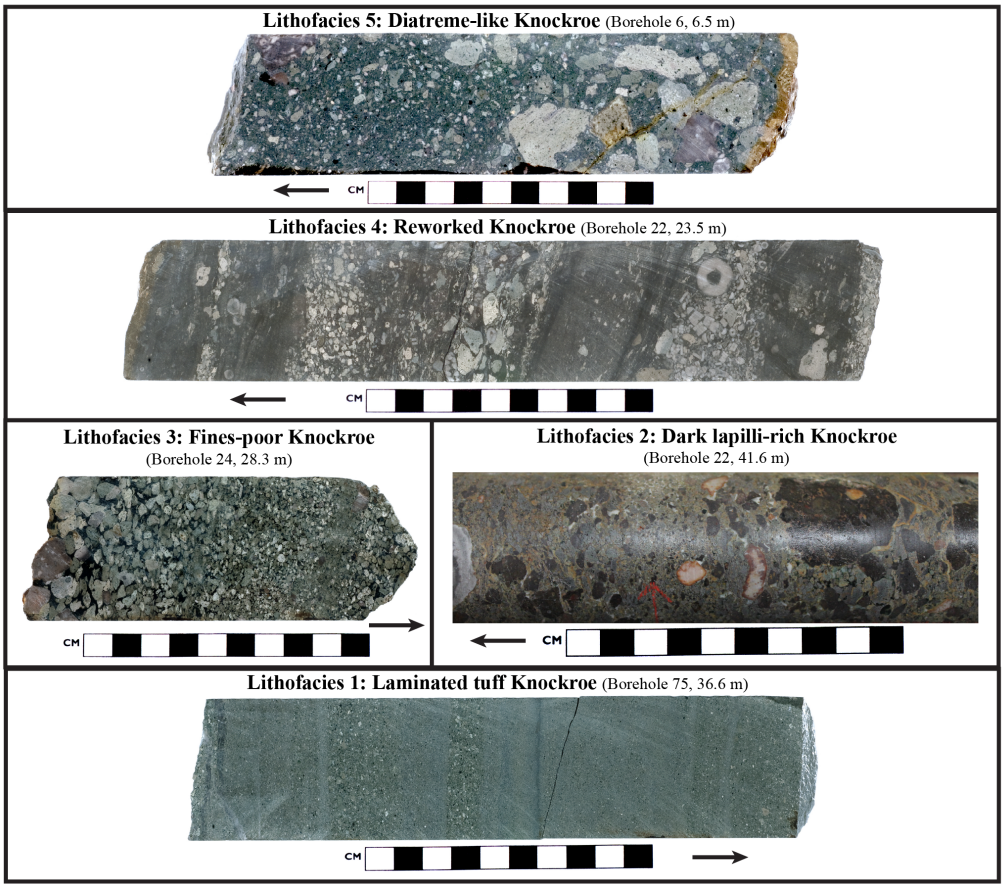

FIGURE 3.6: Photographs of the Knockroe Formation volcaniclastic formation divided into five lithofacies. Arrows indicate sample orientation, pointing toward the top of the borehole. **L5:** Upper Knockroe Formation, surrounding the diatreme, consisting of poorly sorted lapilli tuff with an altered green ash matrix. Lapilli are subrounded and incipiently vesicular, containing aligned feldspar phenocrysts. Clasts consist primarily of juvenile lapilli, dark blocky lapilli and Waulsortian Limestone. Beds tend to be very thick varying between 0.5–25 m. **L4:** Greywacke beds with thin layers of volcaniclastic material. Beds vary greatly in thickness between 0.1–7 m and are matrix supported, containing 0-50 % lapilli and crinoidal debris. Lapilli are altered, incipiently vesicular and sub-rounded to rounded. Some beds contain rounded autoliths. **L3:** Clast supported and normally graded beds usually 0.5–2 m thick, predominantly juvenile lapilli with occasional limestone or crinoidal clasts. Clasts are sub- to well-rounded and range from pebble sizes at the base to sand grades of ash at the top. Spaces between the lapilli are filled with dark clays or calcite. Lithofacies may grade vertically into sections with an ash matrix. **L2:** Typically occurs above the laminated tuff: packages of lapilli tuff between 5-10 m thick containing high proportions of blocky non to incipiently vesicular dark clasts. Other clasts include rounded chloritised juvenile lapilli and Waulsortian limestone; occasionally altered orange and containing diatreme autoliths. **L1:** Thin to medium beds (0.1–1 m thick) of often laminated and normally graded ash interbedded with lithofacies 2. Ash is moderately to poorly sorted and consists of non-vesicular juvenile material and blocky dark fragments.

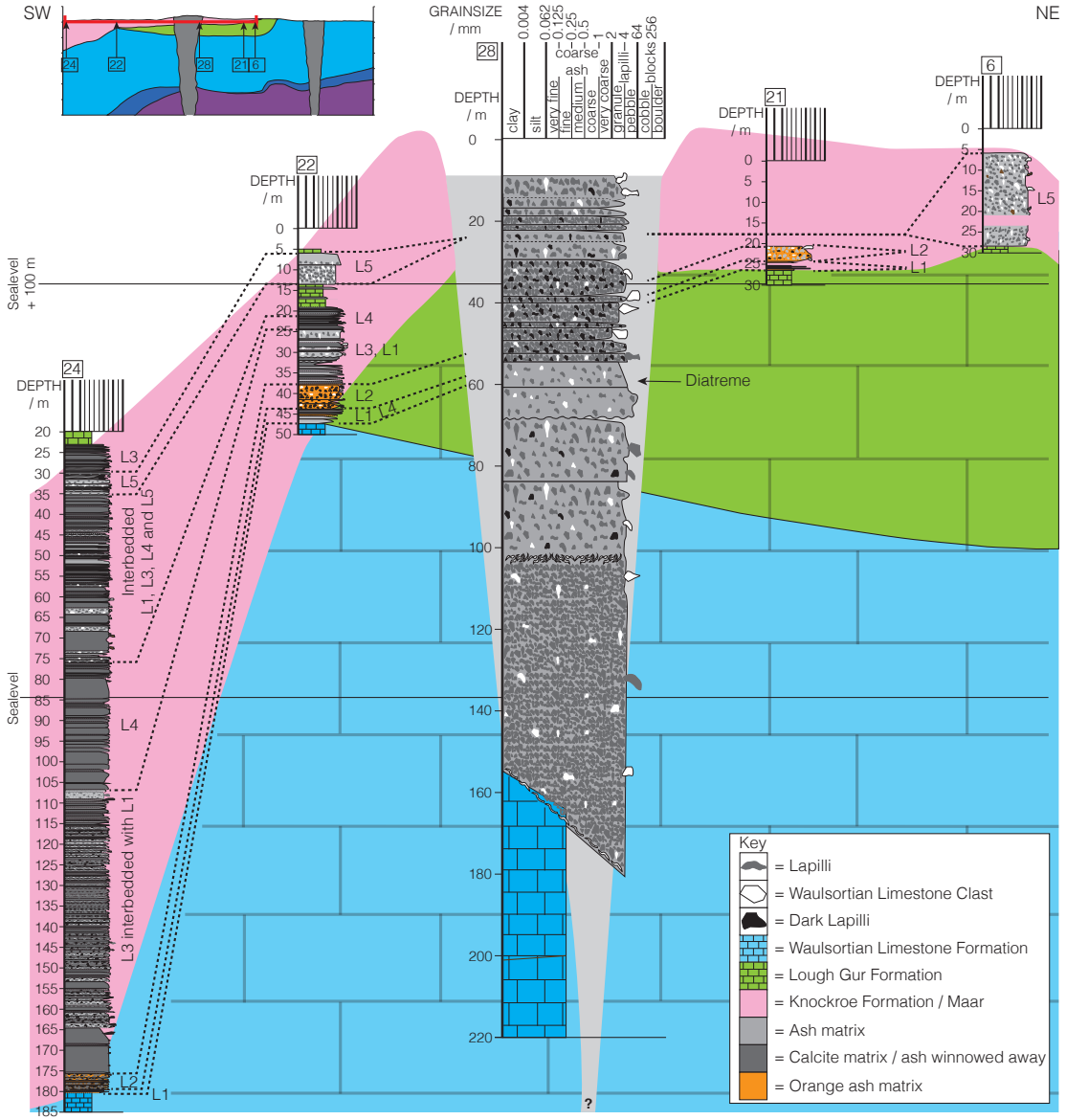

FIGURE 3.7: Cross-section from SW to NE, showing 4 logs of drillcore of the Knockroe Formation and their spatial relationship to a diatreme (shown in centre). The lateral extent of the diagram is indicated by the red line on the cross-section (inset). Numbers in boxes at the top of the logs indicate the borehole number. Dotted lines indicate where packages of beds have been correlated between the logs. Ln indicates the lithofacies package and relates to the lithofacies described in Figure 3.5.

involve cooling-contraction granulation processes (Kokelaar, 1986), explaining the fine-grained lapilli and ash within this lithofacies.

Lithofacies 2 contains a high proportion of dark, blocky, non- to incipiently vesicular clasts that appear fresh compared to the surrounding juvenile material and contain small proportions of microcrystalline feldspar. These could represent country rock lava fragments (Kurszlaukis et al., 1998; Gernon et al., 2013), disrupted sills (Nemeth et al.,

2001) or fragmentation of a rapidly cooled melt (Ross and White, 2012). The appearance of limestone clasts possibly indicates the onset of country rock fragmentation and diatreme-forming phreatomagmatic activity (Lorenz et al., 2002; Ross and White, 2006).

The normally graded beds of lithofacies 3 most likely formed in debris currents related to eruption column collapse in water, that may or may not have breached the water surface (Fiske et al., 1998). In this submarine environment, these density currents would have been water-supported (White, 2000). These currents can be eruption-fed, formed by rising tephra jets expanding and ingesting water (White, 2000), subsiding and flowing outward from the volcanic centre. Alternatively, where the eruption column breaches the water surface, tephra and particles can be deposited subaerially. High concentrations of particles in the water column can lead to gravitational instabilities, forming vertical density currents (Fiske et al., 1998) that would be hard to distinguish from other deposits. These water-supported currents deposit Bouma-type sequences with concentrated basal flows depositing massive unsorted units, grading up into stratified ash beds deposited by the more dilute particle current above (Mueller and White, 1992; White, 2000). The bases of such sequences are not observed at Limerick, due to direct injection of tephra jets into the water column. This created multiple pulses of more dilute eruption-fed flows depositing a series of unwelded and graded beds (Kneller and Branney, 1995; White, 2000), similar to the typical upper sequence.

Isolated beds of lithofacies 4, interbedded with fossiliferous debris, indicate a submarine eruption environment. The lithofacies is attributed to re-working of pre-existing pyroclastic deposits, which were saturated, highly mobile and liable to slump (Fiske et al., 1998; White, 2000; Pittari et al., 2008). The Knockroe Formation lithofacies are broadly comparable to the deposits of Bridge Point, New Zealand, where pauses in the Surtseyan-type eruption sequence are recorded by gradual resumption of normal sedimentation and re-working of abraded clasts and fossils (White, 2000).

Beds of lithofacies 5 typically show normal grading at the top and inverse to non-graded bases, indicative of deposits of subaqueous debris flows (Nemec and Steel, 1984) similar to those observed at the Costa Giardini diatreme, southern Italy (Calvari and Tanner, 2011). The presence of Waulsortian Limestone clasts indicate brecciation of country rock at least 80 m below the seabed. This can occur during phreatomagmatic explosions

(Lorenz et al., 2002; Lorenz and Kurszlaukis, 2007), and/or diatreme expansion by implosion, spalling or undercutting (Sparks et al., 2006). Juvenile lapilli reveal incipiently vesicular blocky shards (Fig. 3.6) suggesting magma fragmentation by explosion rather than intense vesiculation (Heiken, 1972; Houghton and Wilson, 1989; Ross and White, 2012). All these features suggest the uppermost lithofacies resulted from high-density debris currents sourced from the diatremes.

3.5 Vesicle distributions

In general, the vesicularity within both diatreme 19 and Knockroe Formation juvenile clasts is low. Vesicularity within the Knockroe Formation ranges between 6–50 %, averaging ∼17 %, and in the diatremes varies between 2–63 %, averaging ∼30 % (Fig. 3.8). Although, vesicularity is slightly lower in the Limerick samples, values are comparable to the emergent Surtseyan-type phreatomagmatic eruptions at Capelas, Azores (18–58 vol. %) and the phreatomagmatic deposits of Miyakejima, Japan containing 20–70 vol. % (Shimano and Nakada, 2006; Mattsson, 2010). The higher Limerick values lie within the range required for explosive magmatic activity (50–80 %; Houghton and Wilson, 1989), and tend to be found at the base of the Knockroe Formation and in the lower parts of the diatremes (∼350–520 m) (Fig. 3.10). The magma fragmenting to form these lapilli at the base of diatreme 19 was likely more mature, having undergone a higher degree of coalescence.

Image analysis has captured a total of $\sim 0.0135 \times 10^6$ vesicles (Fig. 3.9a), using the method described in section 3.3.2. Figure 3.9b plots L, the equivalent vesicle length, against the natural log of n, the vesicle number density for vesicle lengths placed into the same categories used in Figure 3.9a. The multiple modal values can be seen by the two changes in gradient for the Knockroe Formation and three for the diatreme, and indicate multiple nucleation events took place before magma fragmentation (Shea et al., 2010).

Clasts of the Knockroe Formation contain a population of smaller vesicles relative to diatreme 19 (Fig. 3.9) and exhibit two nucleation events, most likely material ejected at an early eruptive stage. Diatreme deposits record a third population of larger vesicles which may reflect an additional nucleation event or inflation of vesicles due to later outgassing

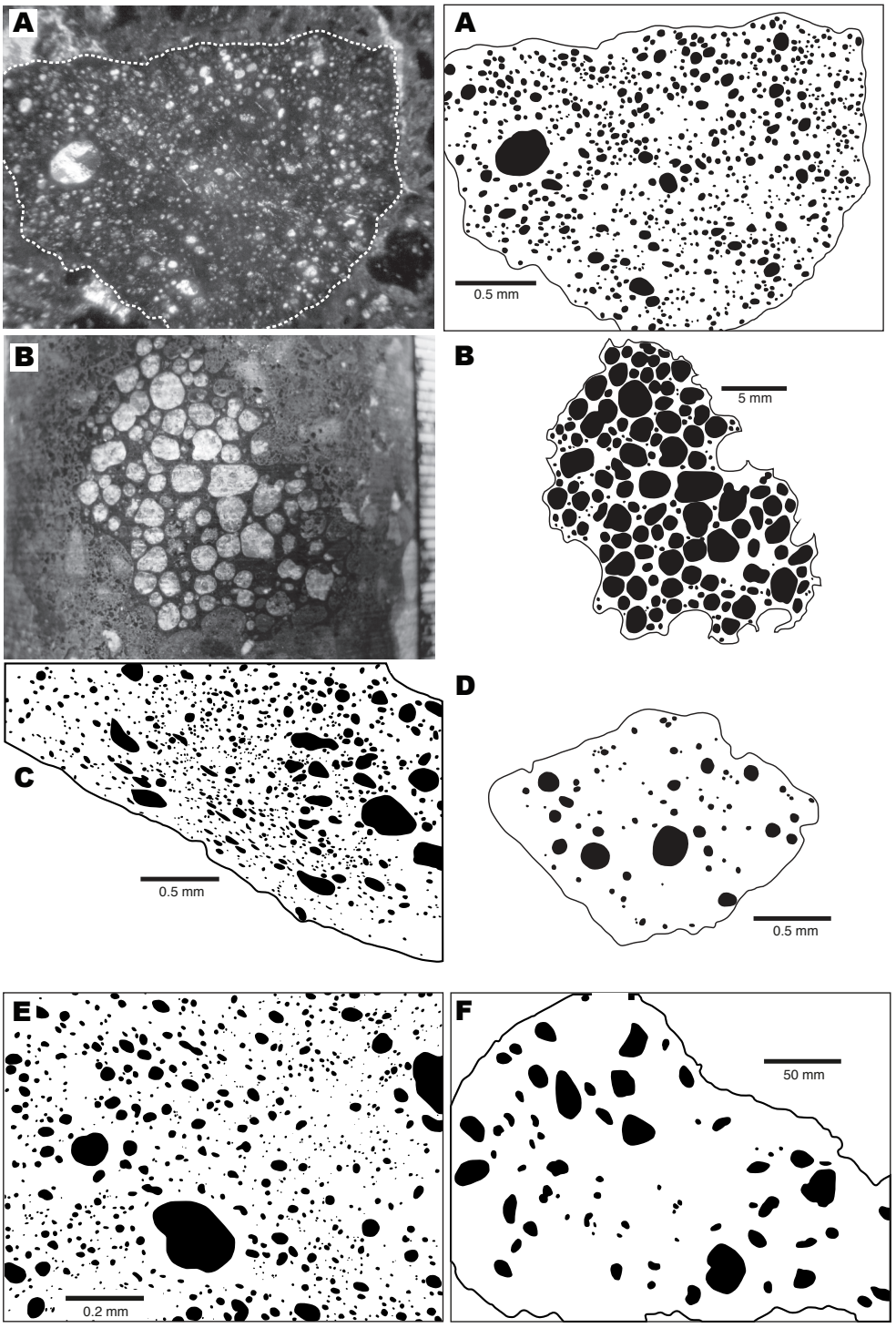

FIGURE 3.8: Examples of typical lapilli and digitised vesicles used in image analysis (vesicularity values shown in brackets). **A:** Lower diatreme lapillus (11 %) in an ash and disseminated limestone matrix (Borehole 19, 274 m) **B:** Upper diatreme lapillus (64 %) infilled with calcite (Borehole 28, 33.7 m) **C:** Middle diatreme lapillus (21 %) with calcite infilling elongated vesicles (Borehole 19, 102 m) **D:** Lower diatreme lapillus (21 %) with a high number density of small vesicles (Borehole 19, 274 m) **E:** Knockroe Formation lapillus (17 %) (Borehole 24, 86.7 m) **F:** Knockroe Formation lapillus (12 %) (Borehole 24, 28.2 m).

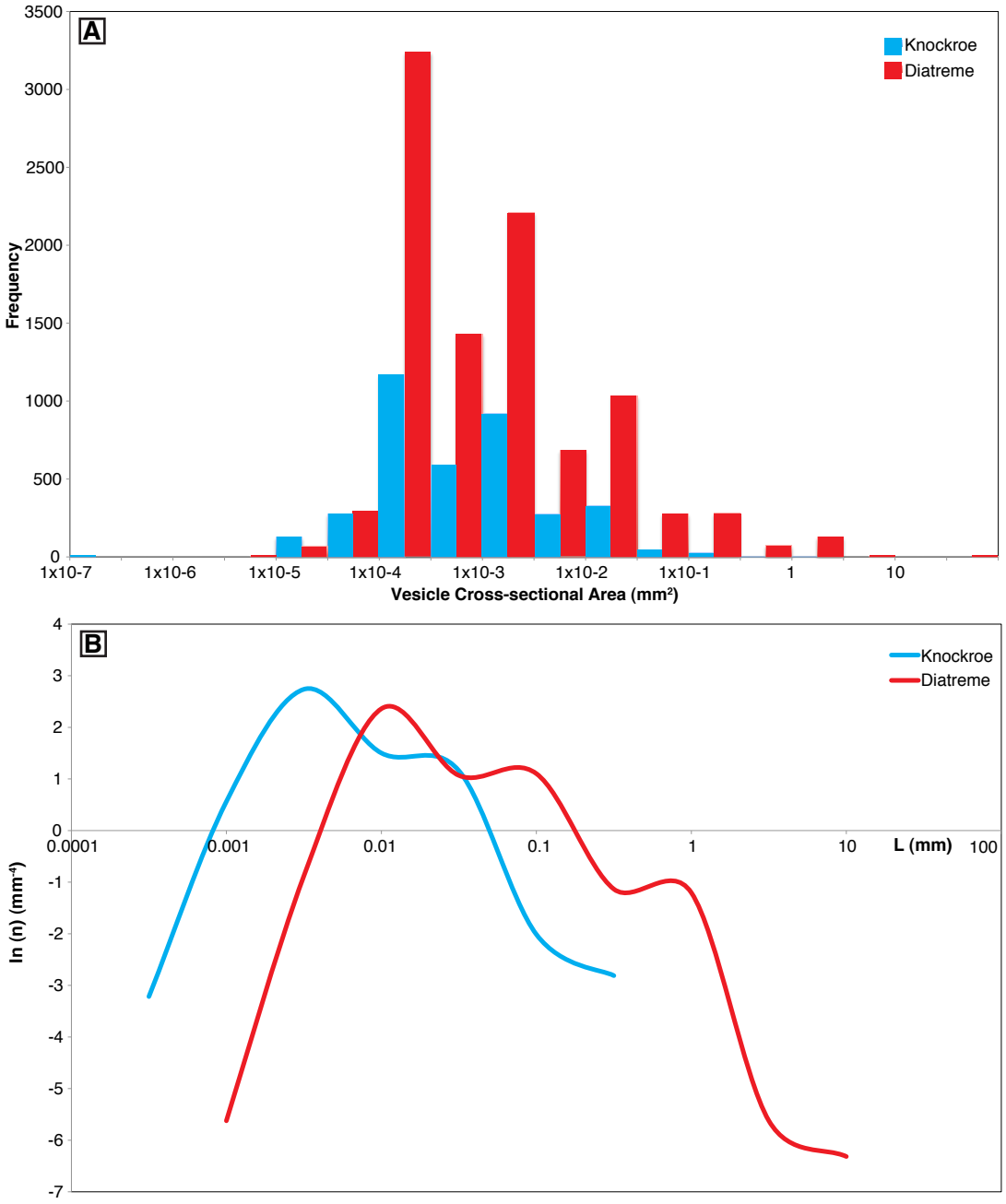

FIGURE 3.9: **a:** Histogram of vesicle cross-sectional area versus frequency for juvenile lapilli from both the Knockroe Formation and diatreme deposits. Three modal categories are observed for the diatreme samples and two for the Knockroe Formation samples, indicating separate nucleation events. **b:** Plot of equivalent length against the natural log of the vesicle number density. The same nucleation events can be seen as modal values of the equivalent length and upturning at the end of the lines are interpreted as due to vesicle coalescence.

as diatreme lapilli are insulated and capable of sustained plastic deformation. Both a positive and a negative gradient are shown (Fig. 3.9b), suggesting the vesicles were in the early stages of ripening (Shea et al., 2010)—the process by which volatiles diffuse

from high pressures present in smaller bubbles to regions of low pressure in larger bubbles (Mangan and Cashman, 1996). Alternatively, these larger vesicles may have formed by maturing from nucleation to coalescence before eventual bubble wall relaxation. An upturning of the trend line (Fig. 3.9b) is interpreted as due to bubble coalescence (Shea et al., 2010). Figure 3.9a shows the majority of vesicles are smaller than 1.5×10^{-2} mm^2 cross-sectional area. Tsukui and Suzuki (1995) suggested that vesicles smaller than 2×10^{-1} mm^2 are the result of super-cooling related nucleation resulting from quenching during phreatomagmatic eruptions (Mattsson, 2010). However, Shimano and Nakada (2006) suggest that smaller bubble fractions are unrelated to fragmentation method and solely represent the high rate of magma decompression and eruption (Mattsson, 2010).

In general, vesicularity increases with depth within diatreme 19 (Fig. 3.10) indicating an increasing importance of exsolving gas in the eruption processes. However, the majority of lapilli within the central diatreme and Knockroe Formation exhibit incipient to poor vesicularity (averaging 14–21 %), well below that required for fragmentation by rapid bubble growth, suggesting fragmentation by an external water source. The Knockroe Formation only record two nucleation events, whereas diatreme 19 record three events (Fig. 3.9); this is attributed to more rapid quenching of ejecta in the water column, relative to thermally insulated pyroclasts in the diatreme, which are capable of more sustained degassing and vesiculation.

3.6 Discussion

On the basis of the observed structural, compositional and textural characteristics of these lithofacies associations (Table 3.1), we propose a multi-stage phreatomagmatic and magmatic model for the eruption of diatremes within the Limerick cluster (Fig. 3.10).

3.6.1 Initial eruption stage

The thin, well-sorted and graded beds deposited near the base of the the Knockroe Formation by dilute density currents (see Fig. 3.8), show similarities with well-documented subaqueous and submarine eruptions such as those of Iblean, Southern Italy (Calvari

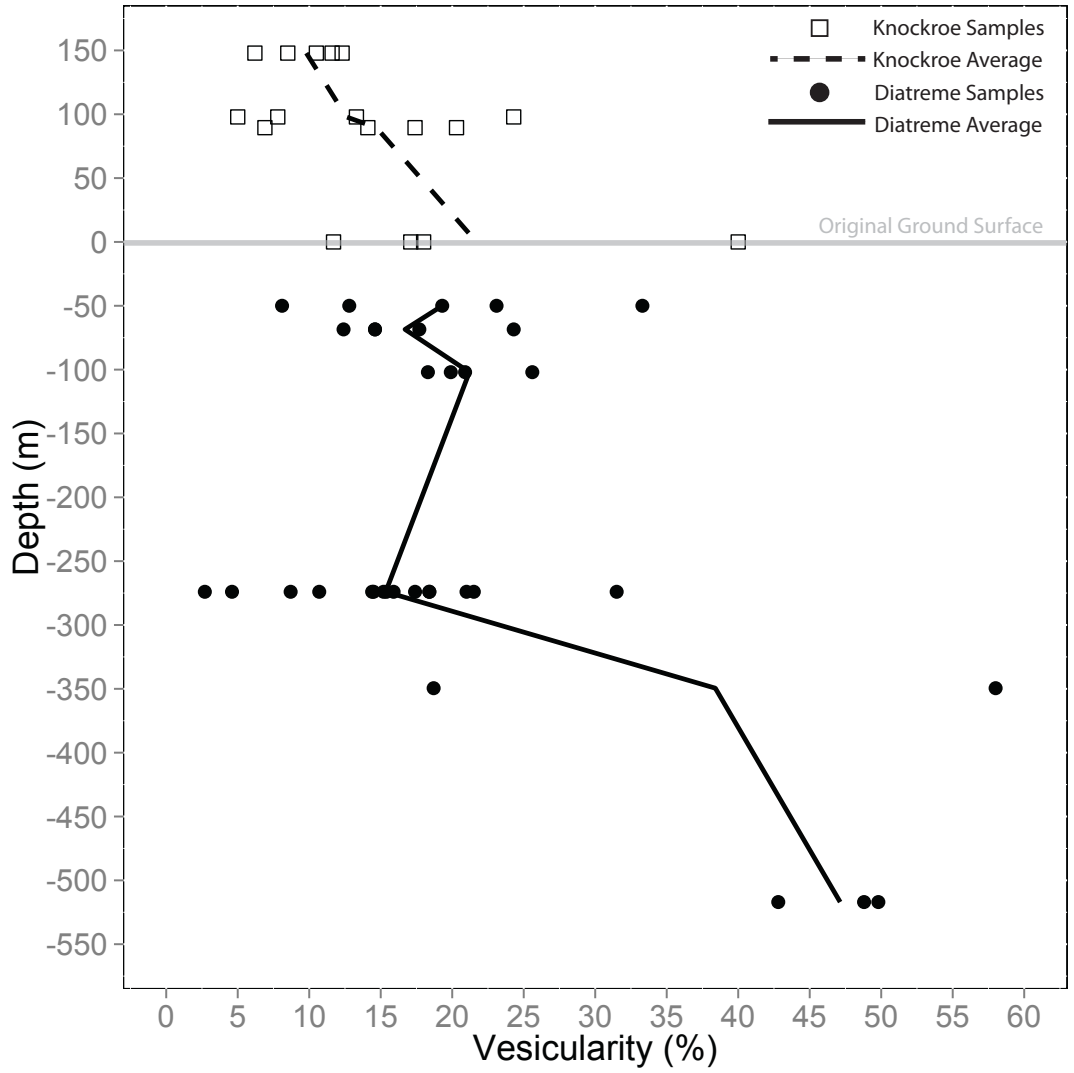

FIGURE 3.10: Graph showing ranges and mean values of clast vesicularity in both Knockroe Formation and diatreme deposits. Knockroe Formation borehole 24 and diatreme borehole 19 have been used for this graph as they contain the most complete records of volcaniclastic material. Note that vesicularity generally increases with depth in both environments. The zero line represents the original ground surface upon which the Knockroe Formation extra-crater material would have been deposited, creating positive topography. Diatreme sample depths are indicated by negative numbers.

and Tanner, 2011) and Pahvant Butte, Utah (White, 1996), resulting from Surtseyan-type eruptions (White, 2000; White and Houghton, 2006; Calvari and Tanner, 2011). The paucity of lithic clasts in lithofacies 1 indicates initial eruptions did not involve significant country rock brecciation and were not diatreme forming.

Diatreme juvenile lapilli contain very low concentrations of feldspar micro-phenocrysts (Fig. 3.4H). This paucity of phenocrysts might suggest that the parent magmas experienced rapid volatile driven ascent from lower crustal levels, as evidenced by the presence

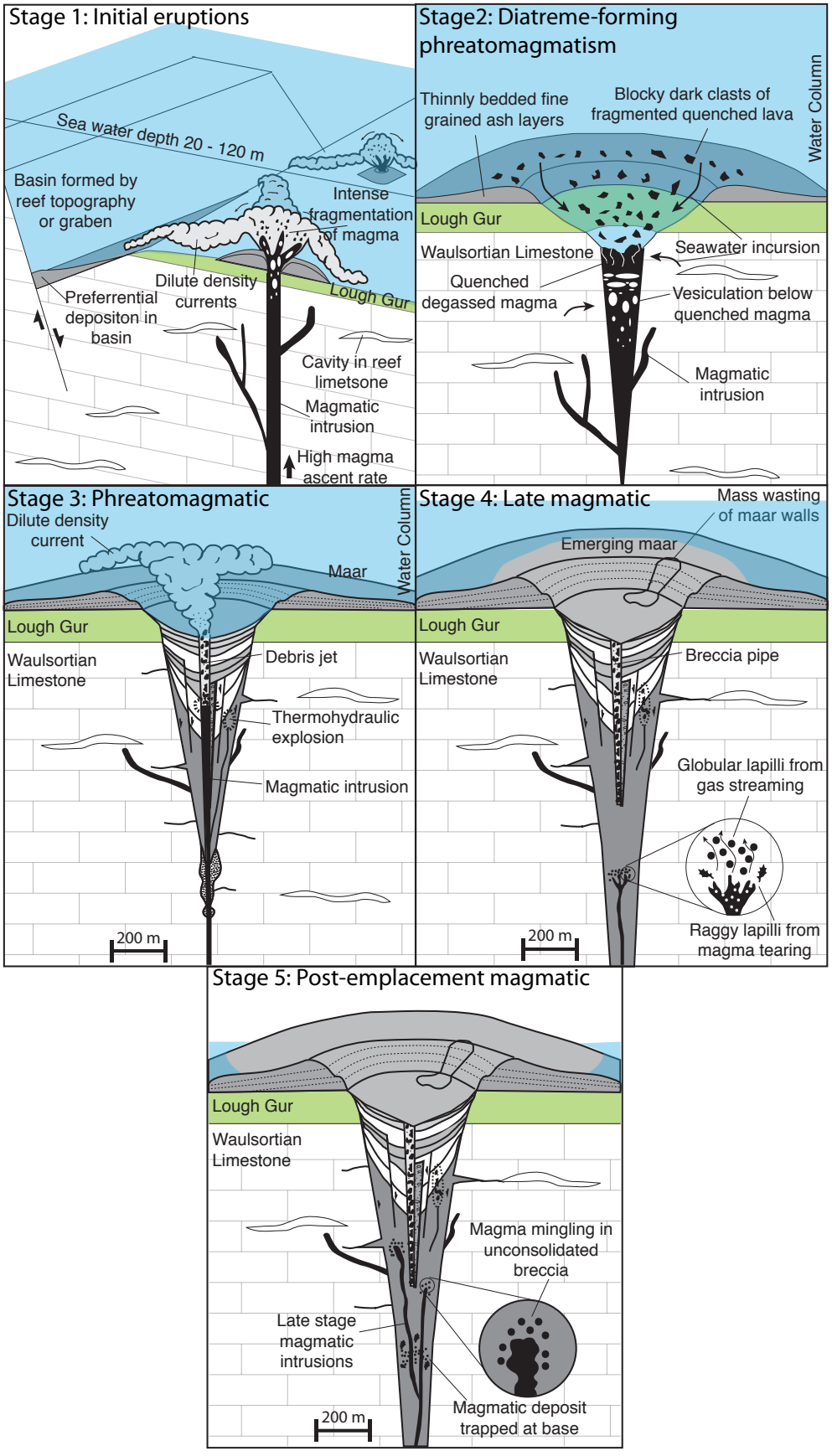
Stage 1: Initial eruptions
Sea water depth 20 - 120 m
Basin formed by reef topography or graben
Intense fragmentation of magma
Dilute density currents
Preferrential depositon in basin
Lough Gur
Cavity in reef limetsone
Magmatic intrusion
High magma ascent rate
Stage2: Diatreme-forming phreatomagmatism
Thinnly bedded fine grained ash layers
Blocky dark clasts of fragmented quenched lava
Water Column
Lough Gur
Waulsortian Limestone
Seawater incursion
Quenched degassed magma
Vesiculation below quenched magma
Magmatic intrusion
Stage 3: Phreatomagmatic
Dilute density current
Maar
Water Column
Lough Gur
Waulsortian Limestone
Debris jet
Thermohydraulic explosion
Magmatic intrusion
200 m
Stage 4: Late magmatic
Mass wasting of maar walls
Emerging maar
Lough Gur
Waulsortian Limestone
Breccia pipe
Globular lapilli from gas streaming
Raggy lapilli from magma tearing
200 m
Stage 5: Post-emplacement magmatic
Lough Gur
Waulsortian Limestone
Magma mingling in unconsolidated breccia
Late stage magmatic intrusions
Magmatic deposit trapped at base
200 m

FIGURE 3.11: Schematic cartoon illustrating the five stages of diatreme emplacement (see discussion). Stage 1 shows eruption sites shedding pyroclastic material via dilute density currents into the adjacent basin. Stage 2 depicts the onset of phreatomagmatic activity. Sea water incursion through the vent and fractured country rock forms a quenched non vesicular body of magma which is fragmented and ejected by initial phreatomagmatic explosions. Stage 3 shows phreatomagmatic explosions producing debris jets that homogenised the central diatreme facies and widened the diatreme, undercutting overlying maar deposits. Stage 4 illustrates the late stage magmatic activity forming globular and "raggy" lapilli, trapped at the base of the diatreme. Stage 5 involves post diatreme emplacement and non-explosive intrusion of magma into unconsolidated diatreme fill.

of deep crustal xenoliths in the diatreme fill (Fig. 3.4G) and in the Knockroe Formation (Redmond, 2010). Rapid magma ascent rates would prevent both extensive crystallisation and interaction with water (Valentine, 2012), preventing country rock brecciation (cf. Gernon et al., 2013) (Fig. 3.11). Explosive magma-water interaction at the sediment-water interface as well as cooling-contraction granulation (Kokelaar, 1986) fragmenting the hot clasts, most likely accounts for the fine-grained nature of the basal Knockroe Formation lithofacies.

3.6.2 Transition to diatreme-forming phreatomagmatic stage

Within the Knockroe Formation, beds of lithofacies 2 contain up to 40 % less-intensely altered vesicular dark lapilli and up to 10 % limestone lithic clasts. The co-occurrence of abundant juvenile clasts and country rock lithic clasts are attributed to an onset of diatreme excavation by explosive magma-water interaction. After an initially high magma flux, water incursion into the vent within a submarine environment would likely have led to rapid cooling and fragmentation of magma, degassed during initial eruptions. Further water incursion may have caused phreatomagmatic explosions, brecciating the surrounding country rock (Lorenz et al., 2002; Lorenz and Kurszlaukis, 2007; Ross and White, 2006; Sparks et al., 2006) and ejecting both limestone clasts and basalt in pulsatory explosions (Fig. 3.11).

3.6.3 Phreatomagmatic stage

Below the upper bLT, diatremes 19 and 28 consist of massive lithic-rich lapilli tuffs (mlLT) with localised lithic-rich graded lapilli tuffs (l(n)LT). Homogenisation of this deposit is considered to be the result of fluidisation by volatiles sourced from outgassing

magma (Sparks et al., 2006; Walters et al., 2006; Gernon et al., 2009*b*) or alternatively by conversion of water to steam (White, 1991; Lorenz and Kurszlaukis, 2007), creating debris jets. The blocky, fracture bound and incipiently vesicular clasts, combined with high concentrations of lithic clasts (10–35 %) suggest eruptions were caused by magma-water interactions (Lorenz et al., 2002; Ross and White, 2006).

After the initial high magma flux, seawater incursion into the vent likely formed a mobile water-rich slurry into which magma intruded (Kokelaar, 1983). The rising magma would have flash heated water within this slurry to steam, creating gas propelled jets of debris and localised fluidisation of the diatreme fill (Kokelaar, 1983; White, 1991; Gernon et al., 2009*b*). Upward transport of material by these two processes and subsequent subsidence would have led to vertical mixing and large-scale homogenisation of the water-rich mix (McClintock and White, 2006; Gernon et al., 2009*b*; Valentine, 2012). Such processes and creation of debris jets could explain the elutriated fines-rich pockets and pipes observed at Limerick and many other diatreme sites (cf. McClintock and White, 2006; Ross and White, 2006; Brown et al., 2008a; Gernon et al., 2008, 2013).

Vesicularity studies support this interpretation, as vesicle sizes and percentages are similar to Surtseyan-type emergent phreatomagmatic eruption deposits at Capelas, Azores and Miyakejima, Japan (Tsukui and Suzuki, 1995; Shimano and Nakada, 2006; Mattsson, 2010). This stage is recorded by multiple pulses of debris flows (Nemec and Steel, 1984) recorded in lithofacies 3 of the Knockroe Formation, which contains large country rock lithic clasts and a paucity of fines due to elutriation by turbulent flows. Similar repetitive sequences are observed within maars in both subaerial settings, e.g. the Joya Honda maar, Mexico (Aranda-Gómez and Luhr, 1996), and the Colli Albani maars, Italy (Sottili et al., 2009), and in submarine settings, e.g. Iblean, Southern Italy (Calvari and Tanner, 2011). Pauses in pyroclast deposition are marked by the resumption of greywacke sedimentation and may represent periods of inactivity or alternatively phreatomagmatic activity that was too deep for debris jets to breach the surface and eject material (Ross and White, 2006; Ross et al., 2008*a*; Valentine, 2012; Graettinger et al., 2014). Regional deposition of the Lough Gur greywacke Formation occurred in water depths of 20-120 m, indicating these diatremes initially erupted into a significant body of water. The presence of greywacke beds within the Knockroe Formation is thought to indicate that basinal subsidence continued at rates comparable to volcanic accumulation (Strogen, 1988).

The large "raggy" clasts were emplaced whilst still in a hot plastic state (Ross and White, 2012), after limited interaction with water. Although the majority of juvenile clasts are incipiently vesicular, a small proportion of larger clasts exhibit up to ∼60 % vesiculation. Magma-water interaction can form a large range in vesicularity depending on the degree of magmatic gas exsolution at the time of fragmentation (Houghton and Wilson, 1989). Although this prolonged stage is dominated by phreatomagmatic activity, the greater vesicularity of these lapilli indicates that magmatic processes were still important.

3.6.4 Late magmatic stage

At the lowest observed levels in diatreme 19, the mlLT contains a higher ratio of juvenile to lithic clasts. Juvenile lapilli have undergone a higher degree of vesiculation (∼50–60 %) and coalescence creating 'frothy' lapilli also observed in the Joya Honda maar, Mexico (Aranda-Gómez and Luhr, 1996). Here, this texture is attributed to low confining pressure exerted on the magma during vent excavation, allowing more advanced vesiculation before groundwater interaction (Aranda-Gómez and Luhr, 1996). Proportions of 'raggy' and pelletal lapilli also increase, indicating a lower degree of magma-water interaction toward the base of the diatreme. These lapilli exhibit evidence for heat retention, including fluid, plastically deformed shapes and partial sintering with adjacent lapilli. A basaltic lava flow directly overlies volcaniclastic deposits of the Knockroe Formation less than 500 m to the south-west of diatreme borehole 28. The flow has not formed hyaloclastites or pillows and does not exhibit an extensive chilled margin, indicating eruption into a subaerial environment (Griffiths, 1992; Gregg and Fink, 1995; White, 2000). This observation is consistent with the inferred decline in magma-water interaction, and collectively are best explained by emergence of the system (Fig. 3.11) as suggested by Holland and Sanders (2009), explaining the lack of submarine fossiliferous debris in the upper Knockroe Formation (lithofacies 5). Emergence and subsequent drying out of the diatreme may have caused a downward migration of explosion depths (Mattsson et al., 2005), prior to or during this late magmatic stage.

3.6.5 Post-emplacement magmatic stage

Late-stage intrusion of magma into unconsolidated diatreme-fill, is a common feature of diatremes (Valentine, 2012), as observed in the Gibeon Kimberlite Field, Namibia

(Kurszlaukis et al., 1998), Iblean, Italy (Calvari and Tanner, 2011) and Elie Ness, Scotland (Gernon et al., 2013). They represent late stage upwelling of magma soon after the cessation of explosive volcanic activity (Kurszlaukis and Barnett, 2003; Lorenz and Kurszlaukis, 2007; Valentine, 2012). Dense dark clasts are closely associated with a ∼1 m thick intrusion, and thought to result from magma fragmentation upon contact with unconsolidated diatreme fill, causing magma mingling and disintegration into blocky clasts (White, 2000; Calvari and Tanner, 2011).

3.7 Conclusions

The Knockroe Formation records an initial eruption stage of the Limerick diatremes, involving rapid magma ascent from lower crustal levels. High ascent rates allowed magma to reach the sediment-water interface before any appreciable crystallisation or magma-water interaction occurred, resulting initially in small (non-diatreme forming) phreatomagmatic eruptions. An extended period of phreatomagmatic activity formed diatremes of greater than 500 m depth filled with massive deposits homogenised by fluidisation and debris jet action. Evidence for this stage is recorded in the ∼150 m thick Knockroe Formation with interludes of sediment deposition (i.e., Lough Gur greywackes). These interludes may have been periods of inactivity or alternatively when phreatomagmatic activity was too deep for debris jets to breach the surface and eject material. The occurrence of lithic clasts within this deposit marks the onset of country rock brecciation and diatreme-forming phreatomagmatic activity.

A minor late phase of magmatic activity, largely affecting the lower parts of the diatremes, was most likely associated with emergence and subsequent drying out of the maar-diatreme system. Here, the presence of lapilli of apparent magmatic or low water/-magma origin (e.g. “raggy” and globular lapilli) suggests the diatremes lie somewhere between the two end members of magmatic and phreatomagmatic activity.

Our observations of diatreme architecture coupled with their extra-crater deposits, reveal a complicated eruption chronology of maar-diatremes initially in a submarine environment, which will have implications for the study of other volcanic systems. The detailed lithofacies observations and interpretations in this study can be used to compare and identify features and processes in similar diatreme systems.

Chapter 4

Geochemistry of diatremes and associated deposits: insights into the origin and evolution of their parent magmas

4.1 Summary

The geochemical compositions of igneous rocks are often used to constrain the origin and evolution of their parent magmas, and specifically can be used to investigate the occurrence of fractionation or contamination caused by crustal melting. Due to the highly altered nature of the volcaniclastic rocks (due to their age, depositional environment, physical properties and composition), traditional magma classification methods are of limited use. This chapter disentangles primary elemental trends from those produced by post-emplacement alteration, to show how the Limerick maar-diatreme systems evolved throughout their eruptive history. Incompatible element geochemistry suggests that magma formed from the partial melting of a metasomatised mantle, similar to that experienced below Scotland during the Carboniferous. The Knockroe Formation appears to be genetically related to the diatreme-fill, most likely forming extra-crater maar deposits from diatreme ejecta. Volcanic clasts within polymict BMB horizons also follow very similar trends to that of the Knockroe Formation and diatreme deposits,

again suggesting a common genetic source. However a small percentage of dark clast samples do not follow the same elemental trends as other deposits, suggesting that they may have been externally sourced. Immobile trace elemental trends for diatreme and Knockroe Formation samples indicate they are of alkali-basaltic composition, emplaced in a 'within-plate' environment, through crustal thinning and opening of graben basins resulting from back arc extension during the Lower Carboniferous.

4.2 Introduction

A detailed field investigation of maar-diatreme volcanism in the Limerick Basin, including the diatreme and extra-crater sequences of the Knockroe Formation, is outlined in chapter 3. Here, we present geochemical analyses of juvenile material from these volcaniclastic deposits, in order to better understand the origin and magmatic evolution (e.g. degree of melting and fractionation) of the parent magmas. During the Carboniferous, Europe experienced large-scale faulting, basin formation and continental rifting as a result of episodic N-S back arc extension related to the Variscan subduction zone to the south (Woodcock and Strachan, 2000). Sporadic episodes of strike-slip motion along these faults (Strogen, 1988) led to the opening of many graben-bound basins across the Irish Midlands (Woodcock and Strachan, 2000). Crustal thinning as a result of this extension led to volcanic centres and intrusions across Ireland, Scotland and the English Midlands (see Fig. 1.1 and 3.2).

Volcanic rocks in continental rifts typically exhibit a wide compositional array, generally ranging from basaltic (i.e. primitive MORB) toward rhyolitic (Fitton and Dunlop, 1985; Best, 2003). The complex chemistry of intra-continental magmas are thought to result from numerous parameters including partial melting, mantle temperature, lithosphere thickness, source composition, crystal fractionation and contamination through the assimilation of continental crust (Fitton and Dunlop, 1985; Xu et al., 2001). Alkali basalts are perhaps the more common rock composition in intra-continental settings, for example the Cameroon line, West Africa (Fitton and Dunlop, 1985), Clyde Plateau, Scotland (Young and Caldwell, 2011) and the Beara Peninsula, Ireland (Pracht and Kinnaird, 1997). The parent magmas tend to be rich in incompatible elements such as LILEs and LREEs (Smedley, 1986; Best, 2003; Young and Caldwell, 2011).

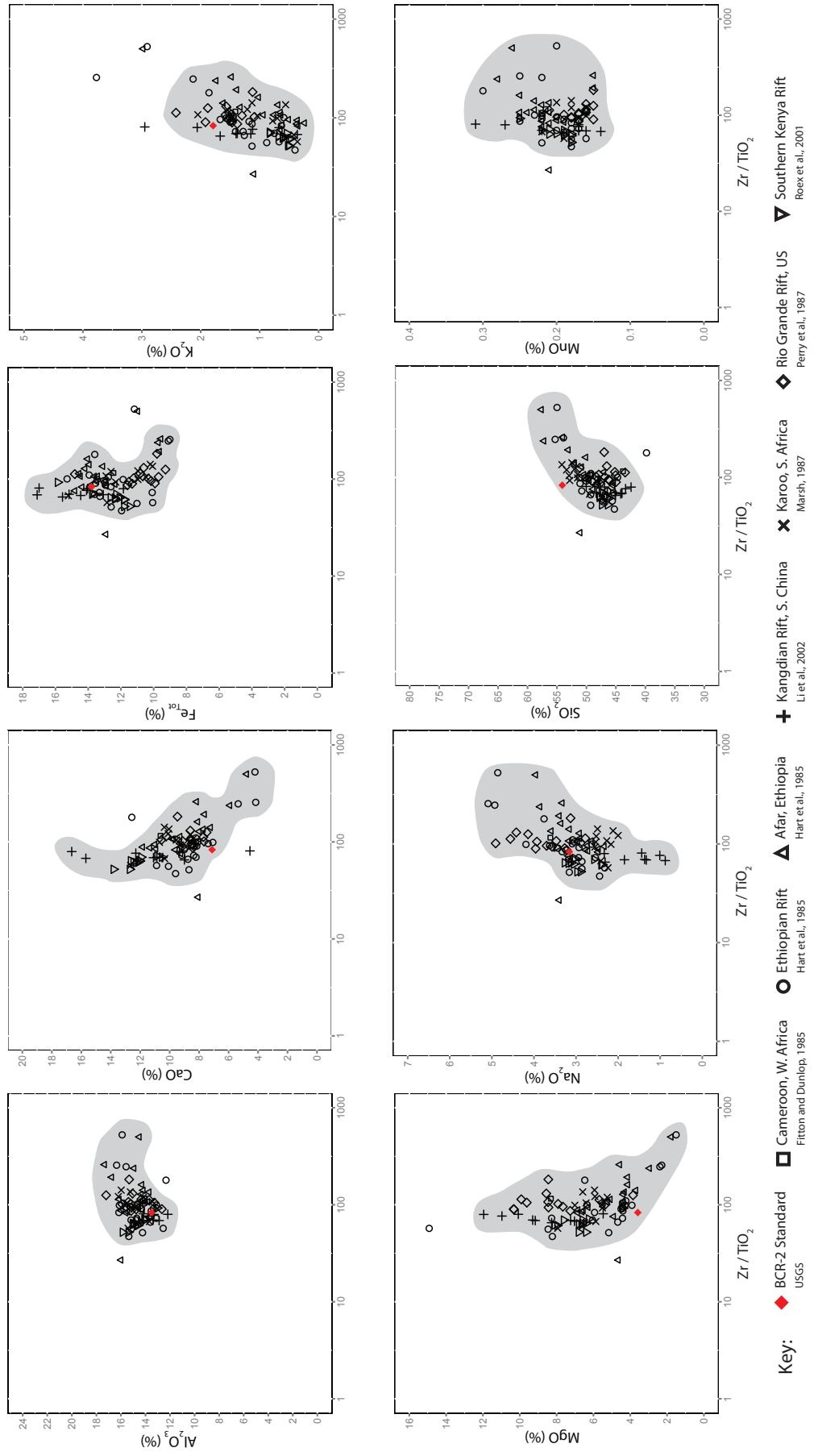
Al2O3 (%)
CaO (%)
Fetot (%)
K2O (%)
MgO (%)
Na2O (%)
SiO2 (%)
MnO (%)
Zr / TiO2
Key:
BCR-2 Standard
USGS
Cameroon, W. Africa
Fitton and Dunlop, 1985
Ethiopian Rift
Hart et al., 1985
Afar, Ethiopia
Hart et al., 1985
Kangdian Rift, S. China
Li et al., 2002
Karoo, S. Africa
Marsh, 1987
Rio Grande Rift, US
Perry et al., 1987
Southern Kenya Rift
Roex et al., 2001

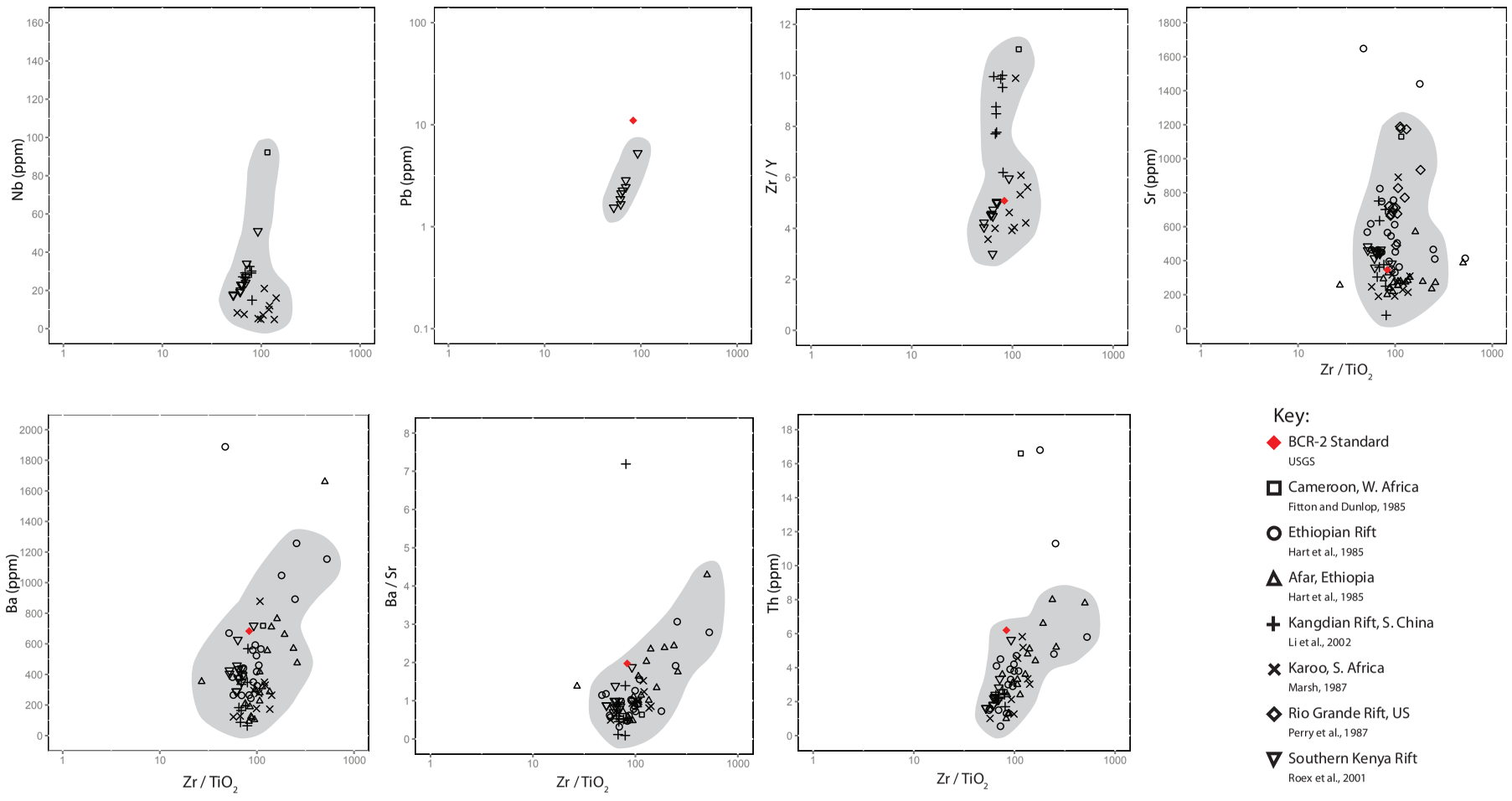

FIGURE 4.1: Graphs illustrating major and minor element data from a universal standard (BCR-2) and seven relatively fresh continental alkali basalts. Data values are obtained from Fitton and Dunlop (1985); Hart et al. (1989); Marsh (1987); Perry et al. (1987); Roex et al. (2001); Li et al. (2002) and data distributions indicated by grey area drawn manually, not including anomalous results.

Volcanic alteration can obscure primary elemental trends resulting from magma fractionation (Winchester and Floyd, 1976; Humphris and Thompson, 1978; MacLean, 1980; Gibson, 1991). Figure 4.1 illustrates elemental distributions for seven relatively fresh continental alkali basalts and a universal standard, BCR-2. Data distributions obtained from these samples are compared to the Limerick data, allowing discrimination between expected concentrations and discrepancies caused by alteration in chapter 5 (Fig. 5.9). Primary elemental trends occur as a result of their compatibility during partial fractional melting of the mantle (Rollinson, 1993). Incompatible elements become enriched in initial melt fractions, whereas compatible elements are retained in the mantle and concentrated in later melts (Campbell and Gorton, 1980; Rollinson, 1993). Fractional crystallisation of the magma can also affect elemental concentrations and trends, with compatible elements becoming depleted in the melt (Rollinson, 1993). Major elements can also become segregated during this process, for example, crystallisation of pyroxene or plagioclase at depth could remove elements such as Ca and Mg from the melt (Peterson and Moore, 1987; Rollinson, 1993). Deviations from expected element concentrations can result from contamination (Fitton and Dunlop, 1985) or alteration. Magmas that have undergone crustal assimilation are often enriched in Th relative to Nb (Pearce, 1983). As a general rule, incompatible elements of the low field strength (LFSE) group are mobile, whereas high field strength elements (HFSE) are considered immobile during hydrothermal alteration (Rollinson, 1993).

This chapter describes major and trace element geochemical data. Major element classification and AFM diagrams have limited uses for altered volcanic rocks due to the mobility of most major elements such as Na and K during alteration (Ross and Bédard, 2009). Large-scale remobilisation of Si and Ca within the diatreme can also render magma classification based on Si concentrations ineffective. Although trace element abundances will be affected by the loss/gain of elements during alteration, immobile element ratios are unaffected (Gifkins et al., 2005; Ross and Bédard, 2009) and can be usefully applied to understanding ancient volcanic successions. This chapter discusses the major and trace element data obtained by ICP-MS, XRF and microprobe from both diatreme and extra-crater Knockroe Formation samples, to better understand the origin and evolution of their parent magma and tectonic environment. Due to pervasive alteration, this chapter focusses on trace and immobile element data to classify the magma type and tectonic setting.

4.3 Methodology and terminology

Full methods for the preparation of samples and for each analysis technique, can be found in chapter 2 and supplementary material 2.2. Trace elements were analysed using solution ICP-MS on juvenile volcanic material repeatedly digested with HF and HCl, and cross-referenced using internal and international standards including BAS206, JA-2 and BRR-1. Major elements were obtained via calibrated XRF analysis of glass beads formed from the same juvenile samples. The major elemental composition of a select few samples were analysed at greater detail to characterise the deposit type using a Cameca SX100 electron microprobe at the School of Earth Sciences, University of Bristol. This study focused both on juvenile material and micro-phenocrysts. 53 samples were chosen from diatreme 19, and 31 were taken from diatreme 28.

Diatreme samples are classified and referred to using the following depths: upper diatreme = 0–100 m, middle diatreme = 100–300 m, lower diatreme = >300 m. The lower diatreme starts at the approximate depth of orange-red discolouration within boreholes 19 and 28 (see Fig. 3.3). Boreholes sampling the diatreme margins are classified as those that alternate between carbonate country rock and volcaniclastic material due to undulations in the diatreme wall. Diatreme brecciated samples are classified as those from boreholes that have undergone passage of BMB hydrothermal fluids and exhibit brecciation of diatreme material with dark matrix in between. Normalised elemental values and ratios are depicted using the notation of a subscript N, for example $(La/Sm)_N$ or $(La/Sm)_{CN}$ which indicates that the ratio utilises the chondrite normalised values of both La and Sm. Anomalies identified within descriptions of multi-element graphs in Fig. 4.4 and 4.5 are defined and quantified using the method of Taylor and McLennan (1985), that applies the geometric mean. For example (Rollinson, 1993):

$$\textbf{Eq. 4.1: } Eu/Eu* = Eu_N/\sqrt{[(Sm_N).(Gd_N)]}$$

Equation 4.1 predicts what the element concentration or ratio value should be based on the element either side. The anomaly is then quantified by calculating the difference between the actual and predicted value for a given element. A value >1.0 indicates a positive anomaly, whereas a value <1.0 indicates a negative anomaly (Rollinson, 1993).

4.4 Major element geochemistry

Major element concentrations can be significantly affected by alteration and diagenesis due to their mobility under hydrothermal conditions. As such, variations in major element concentrations are primarily attributed to both degree of alteration and products of alteration, discussed in section 5.7. Si and Al concentrations within Limerick samples differ the least from the continental basalt data distributions (see Fig. 5.9), and therefore any primary chemical differences between lapilli types or diatreme deposits, not caused by alteration, will be most easily identified using these elements. Each element is plotted against a ratio of Zr/TiO_2 as both of these elements are considered relatively immobile under hydrothermal conditions (MacLean, 1980; Rollinson, 1993; Zhou et al., 2000). Therefore, any variations in the ratio between the two elements is considered to be a measure of alkalinity (Winchester and Floyd, 1977), and the result of magma fractionation, as opposed to alteration.

4.4.1 Lapilli type

Two main types of juvenile lapilli are described within the diatremes and Knockroe Formation (see chapter 3). The first are green, altered and low vesicularity lapilli with blocky shapes. The second type are dark, relatively unaltered with a range of vesicularity from low to high and edges ranging from blocky to fragmented vesicles.

In general, dark clasts contain lower concentrations and a smaller range of SiO_2 (22–42 %) compared to green lapilli (14–68 %). This may suggest that darker clasts are less fractionated, possibly derived from an earlier melt. Both Fig. 4.2A and 4.2B show two main groups of dark clasts, the first shows similar elemental proportions to the green lapilli and consists of both diatreme and Knockroe Formation clasts. The second contains a higher Zr/TiO_2 ratio than other lapilli (>1,000 – highlighted by dashed ellipse on Fig. 5.9), consisting almost entirely of dark lapilli found within the upper diatremes (see Fig. 4.2). SiO_2 concentrations within the Knockroe samples appear to follow a general linear trend up to ∼50 % (see Fig. 4.2A). More fractionated (Si-rich) lapilli within the Knockroe Formation suggests clasts were ejected even during later stages of diatreme eruption, supporting the occurrence of magma-water interaction at a variety of depths (Valentine, 2012).

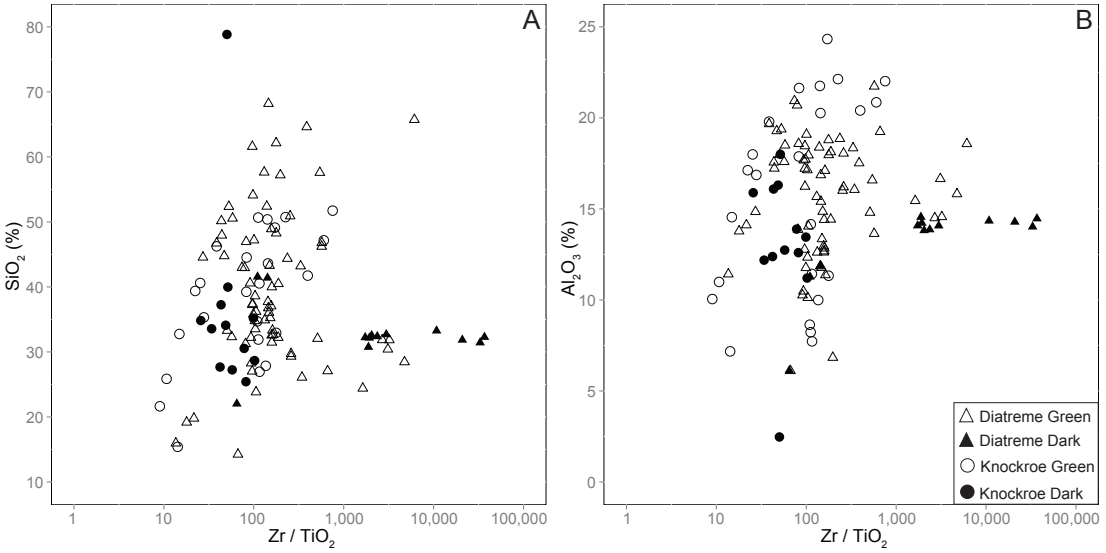

FIGURE 4.2: Graphs illustrating combined microprobe and XRF data showing the difference between green and dark lapilli in both the diatreme deposits and Knockroe Formation. Majority of error bars smaller than symbols on plot, full range of error values shown in supplementary material 2.4. **A:** SiO_2 concentrations indicate that the majority of dark clasts contain similar SiO_2 proportions as green clasts, except a smaller secondary trend consisting entirely of diatreme samples. **B:** The same trends visible for SiO_2 can also be seen for Al_2O_3 concentrations, with the smaller secondary trend more clearly exhibited by diatreme dark clasts.

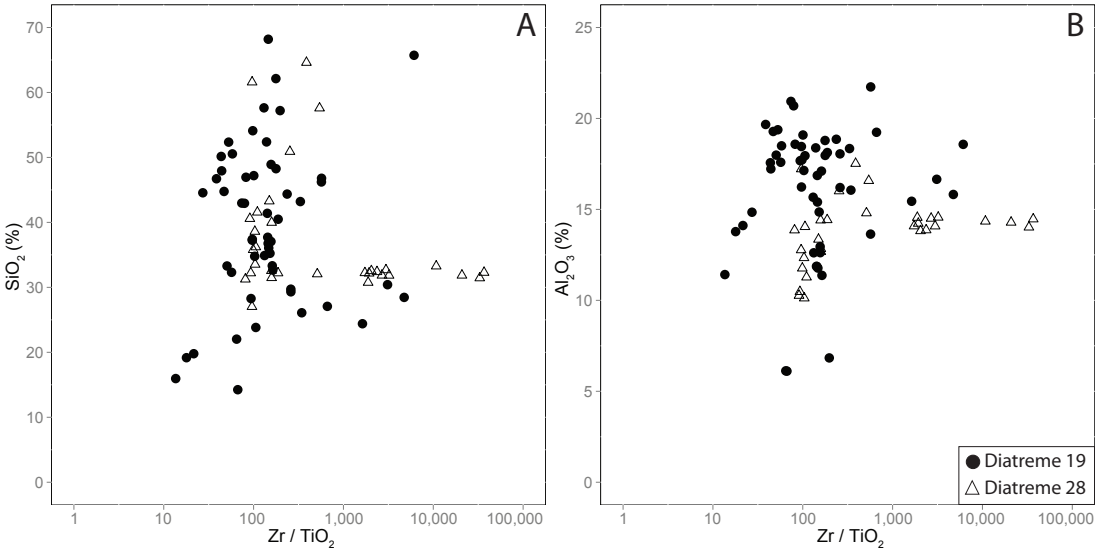

FIGURE 4.3: Graphs illustrating combined microprobe and XRF data showing the difference between diatreme 19 and diatreme 28 deposits. Majority of error bars smaller than symbols on plot, full range of error values shown in supplementary material 2.4. **A:** SiO_2 concentrations indicate that the majority of dark clasts contain similar SiO_2 proportions as green clasts, except a smaller secondary trend consisting entirely of diatreme samples. **B:** The same trends visible for SiO_2 can also be seen for Al_2O_3 concentrations, with the smaller secondary trend more clearly portrayed by diatreme dark clasts.

Dark clasts with higher ratios of Zr/TiO_2 are primarily found within the upper section of diatreme 28 (group also contains 4 green clasts from diatreme 19). The average TiO_2 concentration for volcaniclastic material at Limerick is 6.83 %, whereas lapilli with Zr/TiO_2 values >1000 contain <0.33 % TiO_2. These dark lapilli also have consistently higher concentrations of Fe, averaging at 20.3 %, compared to the overall Limerick average of 12.5 %. Mg concentrations are also high in the majority of these clasts, averaging 19.55 %, compared to the overall Limerick average of 6.16 % (see Fig. 5.9). Ti is considered relatively immobile during alteration (Humphris and Thompson, 1978; Zhou et al., 2000; Utzmann et al., 2002), therefore it is likely that this Ti deficiency is a primary feature of the parent magma. These darker lapilli appear relatively unaltered, therefore the Fe-enrichment is unlikely to be the result of pyrite or iron oxide accumulations, and therefore is also likely to be a property of the parent magma. The most plausible explanation is that these lapilli were incorporated into the deposit from a different eruption centre, depositing material into the open crater (Gernon et al., 2009*a*). Dark clasts with similar chemical compositions to that of the green clasts, are most likely derived from a similar source. Possible explanations for differences in appearance are suggested in chapter 3 and include fragmentation of early intrusions (White, 2000; Calvari and Tanner, 2011) or degassed/rapidly cooled magma (Ross and White, 2012).

4.4.2 Diatreme comparison

Diatreme 28 lies approximately 600 m to the SW of diatreme 19 (see Fig. 3.2). Juvenile lapilli samples from both diatremes were analysed by XRF and microprobe to determine if the magma sources were related. Excluding the dark clasts, lapilli from diatremes 19 and 28 appear to follow very similar trends for both SiO_2 and Al_2O_3 concentrations (see Fig. 4.3). This suggests the same or similar magma source for both diatremes. As there appears to be no major discrepancies in degree of magma fractionation between the two diatremes, this also suggests that the two erupted at similar times. Diatreme 19 lapilli appear to show a little more variation in Zr/TiO_2 values, however this may be due to concentrations of rutile observed in areas of higher alteration (see Fig. 5.4). The higher concentrations of Al within diatreme 19 most likely reflect the apparent enhanced state of alteration within this diatreme.

4.5 Multi-element observations

Environment	Element	Observation	Interpretation
All	Multiple	Diatremes, intrusions and Knockroe Formation exhibit very similar profiles and anomaly magnitudes.	Juvenile magma shares a common source.
	REE	All display steep REE profile gradients with $(La/Yb)_{CN}$ values ranging between 11.8 and 21.8 and $(La/Sm)_{CN}$ 1.7 and 3.6.	Enriched LREE indicating enriched mantle source or low degree of partial melting.
	Nb	All display positive anomaly of 1.2–1.8.	Increased LREE concentrations during partial melting or apparent increase due to removal of mobile elements.
	Zr	All profiles display similar values (88.8–114.6) except dark diatreme clasts.	Potential skewing of average by one sample containing low Zr concentrations.
	Eu	Negative anomalies are present but minimal at 0.92–1.0.	Crystallisation and removal of feldspars or pyroxene.
	Ba, Sr	Negative anomalies of various magnitudes, Sr anomalies are of a greater magnitude.	Elements are mobile under hydrothermal conditions. Sr depletion may be higher due to partition into plagioclase.
	K	Concentrations vary considerably between environments.	Most likely reflects varying proportions of illite, which is a proxy for alteration.
BMB	Multiple	Clasts display almost identical chondrite normalised profiles to other juvenile material. BMB matrix mirrors clast profile except negative immobile element anomalies for Nb, Zr and Ti of 0.5, 0.9 and 0.3 respectively.	Juvenile magma shares a common source. Matrix mirrors clast profile due to leaching of elements except those immobile under hydrothermal conditions which would be retained by clasts.
	K	Contain greater concentrations compared to other profiles.	Greater levels of illite, therefore enhanced alteration.
	Pb	Large positive anomaly of 103.0 within matrix.	Host to metal-bearing sulphides.
	REE	Matrix mirrors that of clasts.	Hydrothermal fluids would leach elements from clasts in addition to matrix containing ash sized clasts.
Intrusions	K	Greater concentrations compared to other profiles.	Higher illite concentrations due to enhanced alteration.
Diatreme	Multiple	Lower, middle and upper samples follow similar profiles but slight differences in REE gradients.	Same magma source throughout eruption history. REE gradient changes due to magma fractionation.
	Pb	Lower diatreme contains large positive anomaly of 2.0 compared to negative anomalies of 0.4 in upper and middle diatreme.	Leaching by hydrothermal fluids in the upper diatremes and precipitation lower in the system.
	U	Brecciated samples contain small negative anomaly.	High mobility of U under hydrothermal conditions.
Knockroe Formation	Multiple	Very similar profiles to that of the diatreme samples.	Majority of Knockroe Formation sourced from diatreme ejecta.

Environment	Element	Observation	Interpretation
Dark Clasts - Diatreme	Multiple	Clasts exhibit lower LREE and HREE concentrations.	Melting of an already depleted mantle or melting of a larger mantle proportion.
	LILE	Lower concentrations of these incompatible elements - Rb, Ba and Th.	Melting of a mantle already depleted of these elements by previous melt increments.
	Zr	Positive Zr anomaly observed in all other profiles is not present.	Potential skewing of average by one sample containing low Zr concentrations.
	Ti	Negative anomaly of 0.6.	Suggests a higher $(Zr/Ti)_{CN}$ and therefore greater alkalinity and magma fractionation.
Dark Clasts - Knockroe	LREE	Highly elevated concentrations.	Represent an earlier melt enriched in incompatible elements.
	Ti	Larger negative anomaly of 0.4	Increased differentiation of magma
	U	Small negative anomaly	High mobility of U under hydrothermal conditions

TABLE 4.1: Observations and interpretation summary of multi-element ICP-MS data plots (see Fig. 4.4 and 4.5) for lithofacies associations at Limerick

The low proportion of phenocrysts (only feldspars) observed within juvenile material, indicates that crystallisation would have had limited effects on magma geochemistry. Therefore element concentrations in the Limerick deposits would have been affected predominantly by melting of the magma source and post emplacement processes. Figure 4.4 and 4.5 illustrate the average normalised concentration of elements for each environment, obtained by ICP-MS analysis and described in Table 4.2.

4.6 Multi-element interpretations

Clear geochemical similarities between polymict BMB volcanic clasts, Knockroe Formation, diatreme clasts and intrusion geochemical profiles (see Fig. 4.4 and 4.5) indicate that juvenile material from each environment shares a common source. In addition, Zr concentrations are consistent between samples, suggesting that degree of alkalinity was originally very similar for all samples (Winchester and Floyd, 1977).

LREEs are more incompatible than HREEs and therefore have a higher affinity for the melt component rather than the crystal component of a magmatic system (Norry and Fitton, 1983; Best, 2003). Juvenile material are enriched in LREEs, suggesting that the magma was either generated from an enriched mantle source or from low degree

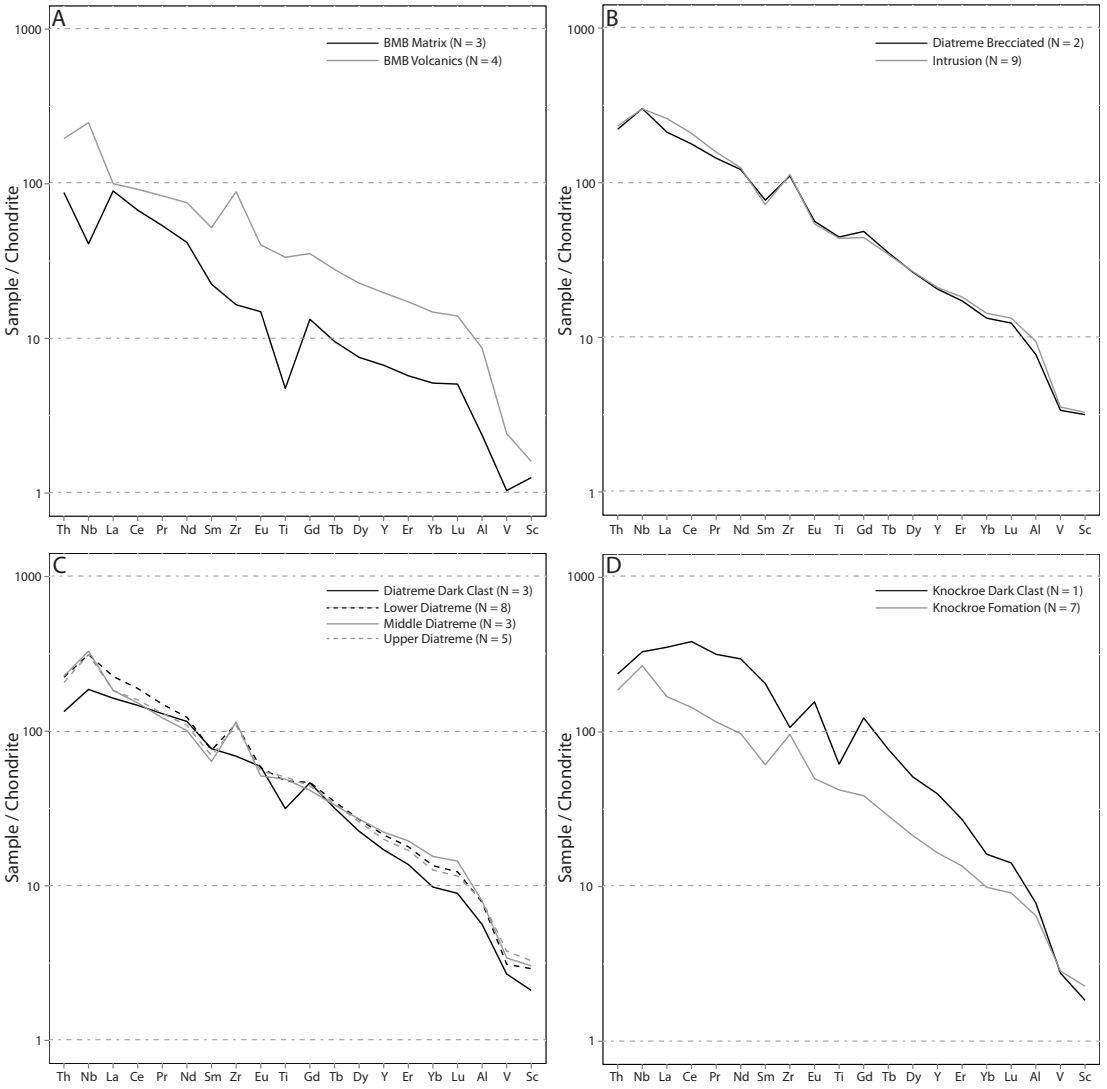

FIGURE 4.4: Multi-element ICP-MS data illustrating chondrite normalised concentrations of elements for Limerick samples using values from McDonough and Sun (1995). Lines depict averages for each environment and elements are organised in order of incompatibility. **A:** BMB matrix and volcanic clasts **B:** Diatreme brecciated and intrusion samples **C:** Diatreme related environments including upper, middle and lower diatreme (see terminology for definition of depths) and diatreme dark clasts **D:** Extra-crater Knockroe Formation volcaniclastic and dark clast samples.

partial melting (Campbell and Gorton, 1980; King et al., 1993; Sobolev and Shimizu, 1993; Best, 2003). The mantle beneath Scotland is thought to have been REE enriched to a magnitude greater than 4000 x C1 during the Carboniferous-Permian age, producing non-normalised La/Yb ratios of 40-80 (Upton et al., 1999). Limerick values range between 10-148 indicating enrichment of the mantle below Ireland may be of a similar degree to that of Scotland, likely the result of partial melting of metasomatised mantle (Upton et al., 1999). Melt fractions produced during adiabatic mantle melting are thought to be on the order of a few percent (McKenzie, 1984; Nicolas, 1986; Vernieres

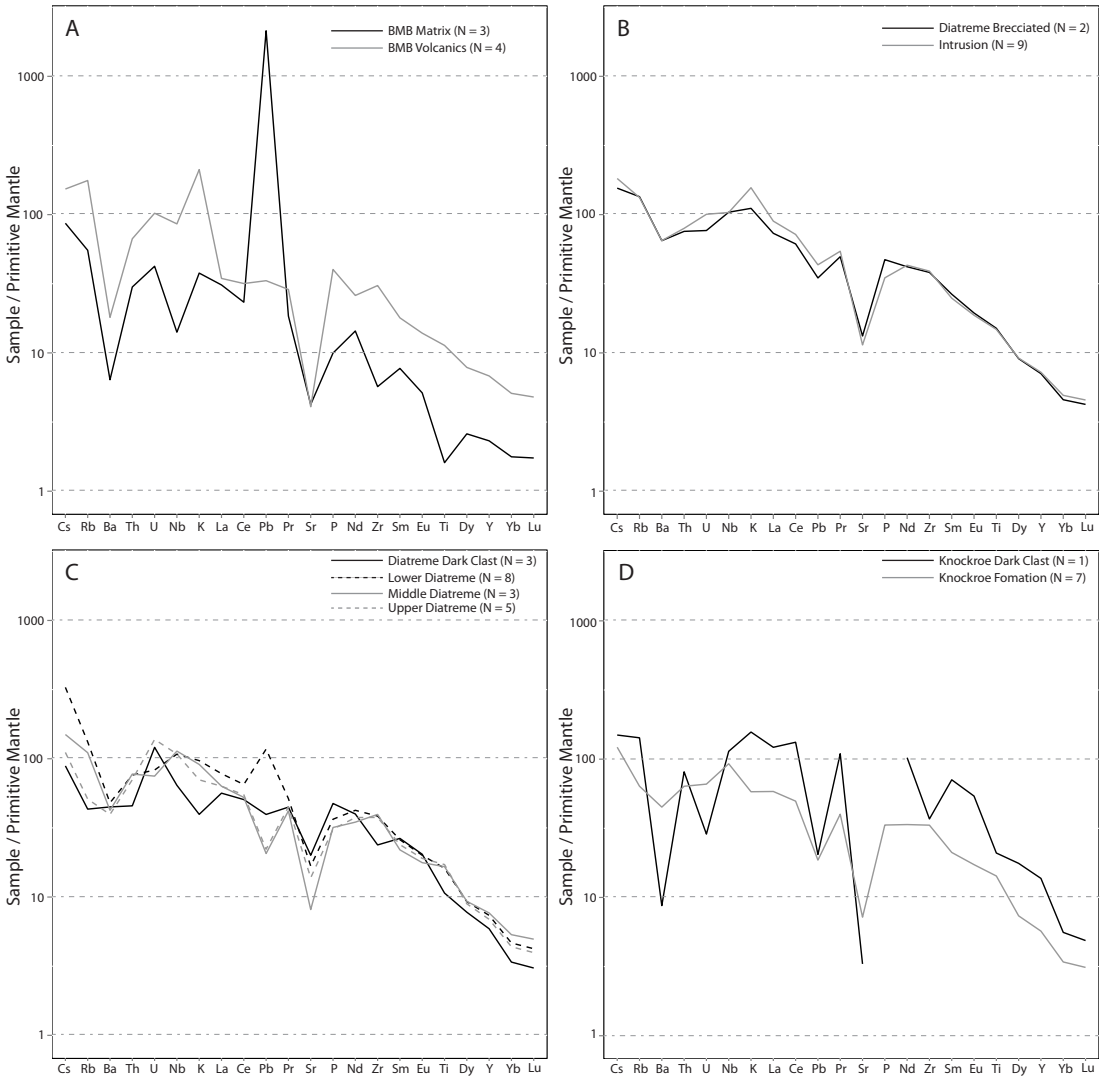

FIGURE 4.5: Multi-element ICP-MS data illustrating primitive mantle normalised concentrations of elements for Limerick samples using values from Sun and McDonough (1989). Lines depict averages for each environment and elements are organised in order of incompatibility. **A:** BMB matrix and volcanic clasts **B:** Diatreme brecciated and intrusion samples **C:** Diatreme related environments including upper, middle and lower diatreme (see terminology for definition of depths) and diatreme dark clasts **D:** Extra-crater Knockroe Formation volcaniclastic and dark clast samples.

et al., 1997). The Knockroe Formation dark clast sample contained a greater enrichment of LREEs than other juvenile material (see Fig. 4.4D). These clasts tend to be found toward the base of the Knockroe Formation sequence and most likely represent an earlier melt more enriched in incompatible elements. These less vesicular dark lapilli may be degassed magma cooled and fragmented by seawater incursion of the vent during initial eruption stages (see chapter 3).

Small negative Eu anomalies may result from crystallisation and removal of low proportions of plagioclase observed within juvenile lapilli matrix (see section 5.5). Melt can become depleted in Eu due to its compatibility in plagioclase and potassium feldspar (Mahood and Stimac, 1990; Rollinson, 1993; Best, 2003). Alternatively this effect could be caused by the mobility of Eu during hydrothermal alteration (Jenner, 1996) or the removal of pyroxene (Shearer and Papike, 1989). Much evidence exists suggesting hydrothermal alteration has had a major effect on deposit chemistry (see chapter 5), therefore it is likely that this has had the greatest effect on Eu concentrations. Positive Nb anomalies of a similar magnitude may result from increased LREE concentrations during partial melting (King et al., 1993; Wilson and Head III, 2007). However the anomaly may also result from palagonitisation, an alteration process common in basaltic glass and maar-diatreme deposits (White and Ross, 2011), removing mobile elements such as Si, Na, K, Ca, Mg and Fe (MacLean, 1980; Thorseth et al., 1991), causing an apparent increase in Nb concentration.

Dark clasts from diatremes 19 and 28 occur in greater concentrations within the upper and lower sections, and show anomalous geochemical results, notably lower concentrations of LREEs (see Fig. 4.4 and 4.5). This may have resulted from melting of a mantle that had already undergone partial melting and removal of incompatible elements, or mantle melting of more than a few percent. In addition, the negative Ti anomaly (see Fig. 4.4C) suggests a higher $(Zr/Ti)_{CN}$ and therefore higher alkalinity (Winchester and Floyd, 1977). Sample 7221-B is a dark clast analysed from the lower section (371 m) of diatreme 19, which contains significantly lower concentrations of all trace elements than other dark diatreme clasts, except for Sr, Pb and U. This sample may therefore be skewing the average slightly, lowering concentrations of both LREEs and HREEs. Possible explanations for the presence of these dark clasts in the upper diatreme have been suggested in chapter 3, and include water incursion and fragmentation of degassed magma or sourced from a different eruption centre. However, these explanations cannot explain the lower diatreme accumulations of dark clasts. Late-stage magma intrusion is common in diatremes due to passive upwelling of magma soon after the cessation of explosive activity (Kurszlaukis and Barnett, 2003; Lorenz and Kurszlaukis, 2007; Valentine, 2012). Upon contact with unconsolidated diatreme fill, the magma mingles and disintegrates in-situ forming blocky clasts (White, 2000; Calvari and Tanner, 2011). These later melts would have already experienced partial melting, explaining the lower concentrations of

LREEs observed.

BMB matrix samples mirror the profile of the volcanic clasts. This is not entirely unexpected as the matrix would inevitably contain ash-sized particles of diatreme material and would leach mobile elements from the clasts. Negative Nb, Zr and Ti anomalies are observed as these are considered relatively immobile under hydrothermal conditions (MacLean, 1980; Rollinson, 1993; Zhou et al., 2000) and are therefore more likely to be retained by the clasts.

Negative Ba and Sr anomalies of various magnitudes are observed in all environments. These elements are considered mobile under hydrothermal conditions (Humphris and Thompson, 1978; Jacobsen and Wasserburg, 1979; MacLean, 1980), and are therefore most likely to have been leached from the juvenile material. Sr anomalies are of a greater magnitude than Ba and may be explained by its strong partition into plagioclase feldspar (Blundy and Wood, 1990; Mahood and Stimac, 1990).

BMB volcanic clasts are highly altered, consisting of approximately 30 % illite, possibly explaining the high magnitude of the K anomaly. K concentrations are also greater within the lower and middle diatreme compared to the upper diatreme and relatively fresh dark diatreme clasts. K therefore provides a rough proxy for alteration, indicating enhanced alteration and fluid flow within the lower diatreme.

BMB horizons within the Irish Orefield are host to Pb-Zn deposits precipitated by the mixing of a seawater-derived brine and metal-bearing hydrothermal fluid (Fallick et al., 2001; Banks et al., 2002; Wilkinson et al., 2005*b*; Redmond, 2010), causing the large Pb anomaly within the BMB matrix (refer to chapter 6 for a full discussion). These fluids are believed to have utilised the diatremes as permeable conduits, precipitating sphalerite and galena observed within the lower diatreme (see chapter 5). Negative Pb anomalies observed in the upper and middle diatremes (see Fig. 4.5C) may be the result of leaching during the interaction of hot juvenile material with convecting seawater (Finkel et al., 1980; Barton and Johnson, 2000).

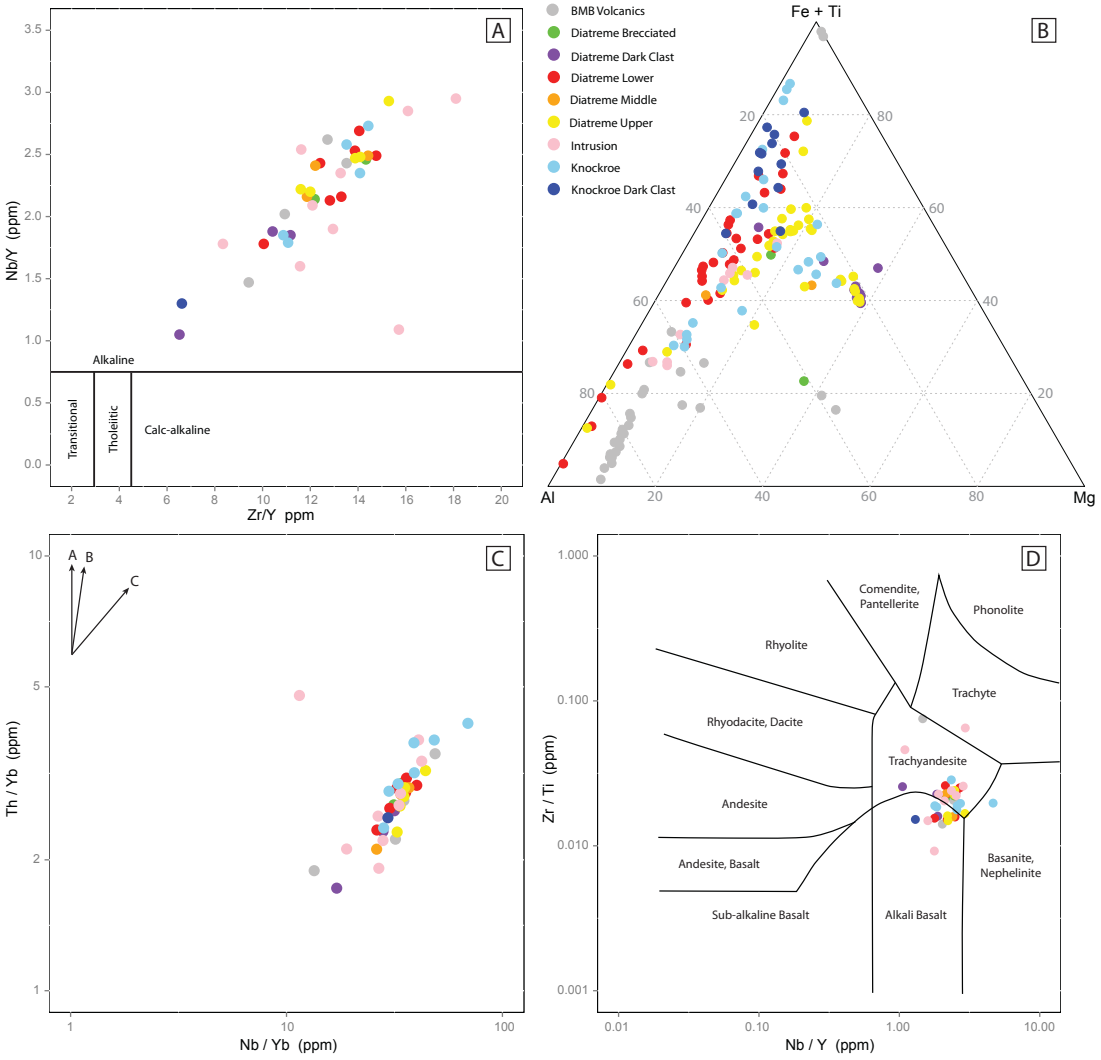

FIGURE 4.6: Graphs depict chemical trends and classification of magma. **A:** Compatible/incompatible ratios of elements analysed by ICP-MS classifying the Limerick samples as an alkali basalt. Adapted by Hollis (2013) from Ross and Bédard (2009) **B:** Jensen cation plot of major elements analysed by ICP-MS and Microprobe, classification fields removed to show variation in data. Sourced from Jensen (1976) **C:** Compatible/incompatible ratios of elements obtained by ICP-MS analysis, gradient of samples indicate magma is classified as 'within-plate enrichment'. Vector A: subduction zone enrichment, B: crustal contamination, C: within-plate enrichment and fractional crystallisation. Sourced from Pearce (1983) **D:** Classification of magma based on compatible/incompatible elements analysed by ICP-MS, diagram sourced from Winchester and Floyd (1977).

4.7 Magma classification

4.7.1 Chemical classification

The Jensen cation plot uses ratios of Al, Mg and Fe + Ti, which are considered to be relatively immobile under low grades of metamorphism and metasomatic loss of alkalis

(Rollinson, 1993). The classification fields have been removed from the diagram to show data variation. Samples exhibit similarly low ratios of Mg but differing Fe + Ti and Al proportions. Large variations in Al are most likely due to differences in degree of illite alteration, Fe due to preferential leaching and pyrite accumulations, whereas Ti concentrations are unusually high for a continental basalt due to rutile concentrations in altered samples. The previously identified high Zr/TiO_2, Mg-rich samples contain <60 % Fe + Ti and 40 % Mg, and appear to follow a different tholeiitic trend outlined in Jensen (1976).

Broad classification of the Limerick samples according to Ross and Bédard (2009) and Hollis (2013) (Fig. 4.6A) indicates that the magma lies within the alkali basalt series, on the basis of their high Nb/Y and Zr/Y. According to Winchester and Floyd (1977) samples lie across the alkali basalt and trachyandesite boundary (Fig. 4.6D), on the basis of higher Zr/Ti ratios than expected for an alkali basalt. Zr/Ti acts as a differentiation index reflecting a drop in Ti with increasing differentiation (Winchester and Floyd, 1977). This is the preferred classification method for the Limerick deposits, using elements considered to be immobile under hydrothermal conditions. This diagram developed by Winchester and Floyd (1977) also confirms observations from Fig. 4.4 that samples contain higher than expected Zr concentrations. Cross-cutting intrusions tend to represent late stage magmatic events (Lorenz et al., 2002; Lorenz and Kurszlaukis, 2007) and appear to be the most evolved of all the samples, located within the higher alkalinity fields of Fig. 4.6D.

Dark clasts of the Knockroe Formation all lie above 50 % Fe + Ti, and follow the same linear trend as the other juvenile material (Fig. 4.6B). Dark diatreme clasts contain unusually high Mg concentrations due to intense palagonitisation and dolomitisation by hydrothermal fluids, than the Knockroe Formation dark clasts. The lower diatreme and Knockroe Formation lapilli lie primarily within the upper half of Fig. 4.6B, containing low proportions of Mg but varying considerably in both Al and Fe + Ti values. Knockroe Formation lapilli contain ∼5–90 % Fe + Ti, and show consistently low proportions of Mg (<20 %). This large variation is most likely a combination of both preferential leaching or precipitation in areas of higher fluid flow as well as mixing and homogenisation of the diatreme fill. BMB clasts lie primarily in the high Al concentration section of Fig. 4.6B (>60 %), most likely resulting from ∼30 % illite, which is an Al-rich alteration product. The low Fe and Ti content of BMB volcanic clasts and diatreme brecciated

samples most likely represents leaching by the passage of BMB-related moderately acidic hydrothermal fluids up to temperatures of <280 °C (Banks et al., 2002; Wilkinson et al., 2005*b*).

Yb is the least incompatible of the trace elements and therefore undergoes negligible enrichment during mantle melting, eliminating variations due to partial melting and fractional crystallisation (Pearce, 1983). Th will become enriched in magmas contaminated by crustal assimilation relative to Nb (Pearce, 1983). The gradient of the samples in Fig. 4.6C correlates with the illustrated 'within-plate enrichment' vector from Pearce (1983), providing no evidence of significant contamination of the magma by crustal assimilation. Th and Nb concentrations are high in relation to the more compatible Yb, indicating contribution from an upper mantle source enriched in incompatible elements (Pearce, 1983). Th and Nb, both highly incompatible elements, would become more enriched in earlier melts, explaining the higher ratios in the early Knockroe Formation samples and lower ratios in the later lower diatreme and intrusion samples.

4.7.2 Tectonic environment

Magma Nb concentration can reflect mantle-related enrichment or depletion (Meschede, 1986), or alternatively the degree of mantle melting (Pearce, 1996). All samples display high concentrations of Nb and very low concentrations of Y (Fig. 4.7C and 4.7D). As a result, the Limerick volcanic samples lie within the continental/within-plate basalt fields (Fig. 4.7A-D). Ti clast concentrations tend to be higher than expected for the within-plate magma fields of both Pearce (1979) (Fig. 4.7B) and Pearce (1982). The darker clasts exhibit a slightly lower Nb/Y ratio than other clasts, plotting within the transitional within-plate magma field of Pearce (1982) (Fig. 4.7A) and the tholeiitic within-plate magma field of Meschede (1986) (Fig. 4.7D). Concentrations of Th within the magma increases with crustal contamination (Pearce, 1983). The lower concentrations of Th and gradient of data points within Fig. 4.6C indicates that the chemistry of the Limerick samples originates from partial melting of the mantle, rather than contamination of the magma by assimilation of continental crust (Pearce, 1983). Crustal thinning resulting from back arc extension and opening of graben basins (Woodcock and Strachan, 2000), would have generated magma of a few percent from the mantle by adiabatic melting (McKenzie, 1984; Nicolas, 1986; Vernieres et al., 1997).

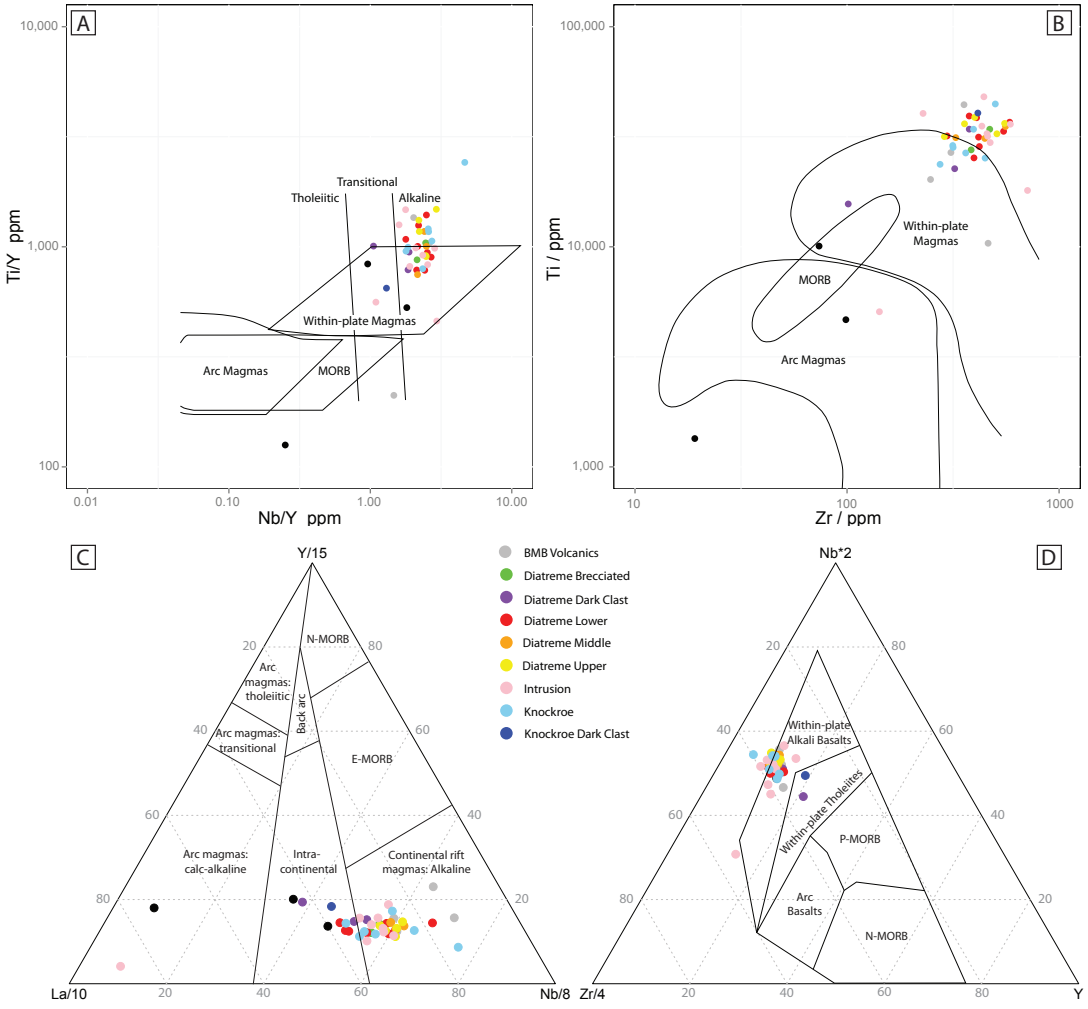

FIGURE 4.7: Graphs classify magma tectonic settings and chemistry. **A:** Compatible/incompatible ratios of elements classifying the magma chemistry and tectonic setting. Sourced from Pearce (1982). **B:** Plot outlining tectonic setting fields of basalt, using Zr as a measure of alkalinity. Sourced from Pearce (1979). **C:** Ternary plot of trace elements classifying the tectonic setting and chemistry of magmas, defining the Limerick samples as continental. Sourced from Cabanis and Lecolle (1989). **D:** Ternary plot of trace elements classifying tectonic environment of basalts, using Zr as a measure of alkalinity and Nb as a measure of mantle enrichment. Sourced from Meschede (1986).

4.8 Discussion

4.8.1 Diatreme eruptive history

Lapilli from the diatremes (19 and 28) and Knockroe Formation follow very similar trends and ranges for Si and Al concentrations. This suggests that material was ejected into the surrounding extra-crater deposits during the majority of the diatreme's eruptive history, most likely throughout pre-emergence stages (see chapter 3). The majority of Knockroe Formation values lie below 50 % SiO_2, however the presence of Si-rich material within

the extra-crater deposits is consistent with diatreme explosions occurring at a variety of depths (Valentine, 2012).

A less significant secondary trend consisting primarily of upper diatreme, dark diatreme and a smaller number of Knockroe Formation clasts is also clear (e.g. Fig. 4.2, 4.3, and 4.6B). This more tholeiitic trend (Jensen, 1976) indicates that these clasts are more fractionated and may not have originated from the same magma source as the diatreme material, or alternatively may have been segregated and allowed to fractionate separately. These clasts may have been externally sourced material, entering the diatreme in two main ways. Debris currents from distal eruptions may have flowed into the diatreme crater, depositing material within the upper diatreme. Similar deposits formed across the Elie Ness diatreme in Scotland, by eruptions in neighbouring vents (Gernon et al., 2013). Accidental clasts could also have been entrained by debris currents and deposited within the surrounding maar, slumping into the vent to be incorporated into upper diatreme deposits (Lorenz and Kurszlaukis, 2007). Alternatively, dark clasts within the lower diatreme may have formed due to magma disintegration and mixing upon intrusion into the unconsolidated fill of the diatreme (White, 2000; Calvari and Tanner, 2011). This tends to be a late-stage phenomenon, after cessation of explosive activity (Kurszlaukis and Barnett, 2003; Lorenz and Kurszlaukis, 2007; Valentine, 2012), and consequently intrusions consist of more fractionated magma.

4.9 Conclusions

Diatremes in the Limerick Basin are of alkali-basaltic composition, emplaced in a within-plate continental rift environment, and show no significant evidence for crustal contamination. Partial melting of only a few percent, most likely of an enriched and metasomatised mantle, resulted in diatreme volcanism (cf. Carboniferous Scotland; Upton et al., 1999). Graphs show almost identical trace and REE trends for both the diatreme and Knockroe Formation samples, indicating a common source and/or magmatic processes. Continued ejection of more evolved pyroclasts into the extra-crater Knockroe Formation sequence suggests that explosions occurred at a variety of levels in the diatreme throughout the eruptive history, consistent with other maar-diatreme systems. More fractionated dykes and sills intruded the diatreme-fill, soon after cessation of explosive

activity. Polymict BMB volcanic clasts appear to follow very similar immobile trace element trends to that of the diatreme juvenile material, also indicating a similar genetic source. However, prolonged exposure to hydrothermal fluids have substantially altered their major element geochemistry, and as such is discussed in chapter 5.

Chapter 5

Post-emplacement alteration of alkali-basaltic diatremes in Limerick, Ireland: Implications for 'Irish-Type' Pb-Zn emplacement

5.1 Summary

Maar-diatreme volcanism at Limerick initially involved the emplacement of hot volcanic deposits within a shallow marine environment. Consequently, the extra-crater and diatreme deposits are pervasively altered, obscuring the original magma geochemistry. Identification of alteration phases and element trends allow the primary composition of the magma to be inferred. This chapter presents SEM and XRD data to further understand post-emplacement alteration processes and mechanisms. Due to the spatial and temporal relationship between diatremes, BMB horizons and mineralisation, these data can also provide insights into the composition and characteristics of late stage fluids, and the relationship between diatremes and mineralisation. Volcaniclastic rocks in the lower diatremes have been overprinted by a greenschist metamorphic mineral assemblage combined with dolomitisation and small-scale precipitation of ore-forming minerals. The

high concentration of dolomite within BMB matrix, coupled with the presence of diatreme clasts within BMB horizons, suggests that hydrothermal fluids responsible for the formation of these breccias utilised the diatremes as conduits. This evidence indicates that the diatremes acted as inert conduits for the fluids, broadly analogous to an extensional fault, as opposed to playing an active role in promoting BMB formation and mineralisation.

5.2 Introduction

Pyroclastic deposits confined to diatremes are characteristically porous, permeable and in many cases metastable, making them susceptible to strong alteration, typically replacement by hydrous mineral phases and carbonates (see Afanasyev et al., 2014, and references therein). Commonly, fresh basaltic glass will be altered to fine grained clays such as chlorite and smectite (Seyfried Jr and Bischoff, 1979; Seyfried Jr and Mottl, 1982; Bednarz et al., 1991; Utzmann et al., 2002), as well as palagonite (Bednarz et al., 1991; Utzmann et al., 2002), during low temperature alteration processes. As a result, interstitial pore spaces and vesicles are often filled with secondary precipitates such as zeolites and oxides (Utzmann et al., 2002).

Explosive diatreme eruptions produce thermohydraulic shockwaves that brecciate the surrounding country rock (Lorenz et al., 2002; Lorenz and Kurszlaukis, 2007), creating a highly permeable network of fractures. These fractures greatly enhance fluid flow both into and out of the diatreme. Diatreme formation is not only caused by phreatomagmatic explosions resulting from interactions between magma and ground or surface water, but can also occur due to exsolving and condensing volatiles (Lorenz, 1985; Kurszlaukis and Lorenz, 1997; Kurszlaukis et al., 1998; Lorenz and Kurszlaukis, 2007; Brown et al., 2008b). The presence of accumulated hot volcaniclastics cooling within the diatreme over long timescales (10^2–10^4 years) (Afanasyev et al., 2014), has many implications for the onset of a hydrothermal system, affecting alteration patterns and products.

Afanasyev et al. (2014) proposed a model for the alteration of a kimberlite, which is also applicable to other diatreme compositions. Large pressure gradients between the country rock and porous pipe cause influxes of water, aided by the surrounding fracture network. Fluids are heated and ascend upwards in the centre of the pipe. Alteration

and the formation of hydrous minerals, as well as precipitation of carbonates, reduces the pipe porosity and permeability, suppressing fluid flow and effectively sealing off unaltered sections of the diatreme. This can increase the cooling timescale of a diatreme from 10^2 to 10^3 years. Localised high intensity alteration can be caused by features such as bedding and steep internal structures, which would act as a focus for fluid flow within a diatreme.

Diatremes at the Limerick site erupted into a shallow marine environment (see chapter 3), forming deposits of the Knockroe Formation. Interaction between seawater and ejected pyroclasts can occur at a variety of temperatures depending on the depth and speed of submarine eruption, ranging from 11–99 °C with increasing depth and speed for a moderately volatile magma (Head III and Wilson, 2003). Interaction at temperatures as low as 70 °C can cause glass to remove Mg, Na and K from the seawater (see Fig. 5.1), whilst elements such as Ca and Si are leached into the seawater (Seyfried Jr and Bischoff, 1979). However, other studies have reported a loss of Mg during the initial stages of the low temperature transformation of glass to palagonite, before the process of unstable palagonite crystallising to form smectite causes an uptake of Si, Al, Mg and K from surrounding fluid (Stroncik and Schminke, 2001; Utzmann et al., 2002). At higher temperatures of 150–300 °C, Mg and SO_4 are quickly removed from the seawater and Ca, Si, Na, K, Fe, Mn and Ba are leached from the glass (Seyfried Jr and Bischoff, 1979; Seyfried Jr and Mottl, 1982; Utzmann et al., 2002). This process also lowers the pH of the fluid, liberating heavy metals such as Cu, Zn, Ti and Fe from the glass (Seyfried Jr and Mottl, 1982; Utzmann et al., 2002).

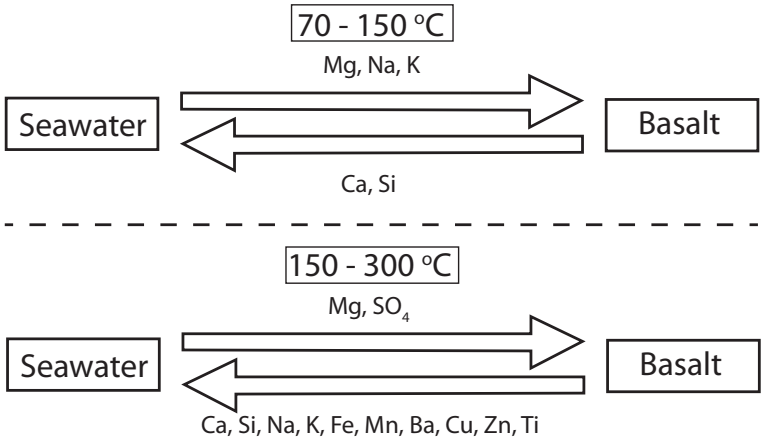

FIGURE 5.1: Summary of element exchange between seawater and basalt during alteration at different temperatures

Diatremes are also associated with other resources such as epithermal gold, for example the Kelian Mine, Indonesia (Davies et al., 2008). Analogous to Limerick, the diatreme breccias themselves are weakly mineralised whereas strong mineralisation has been found within country rock hydrothermal breccias adjacent to the diatremes. It is believed that the breccias acted as aquicludes, focusing fluids into the country rock rather than the diatremes. In contrast, the United States Cripple Creek gold deposit is confined to a large diatreme complex (Thompson et al., 1985; Jensen, 2003; Davies et al., 2008). The contrast in mineral deposit characteristics between two apparently similar diatreme systems, indicates the complexity of the relationship between diatremes, fluid flow and country rock.

Pb-Zn sulphide mineralisation within the Irish Orefield is classified as 'Irish-type' (Hitzman and Beaty, 1996), consisting of carbonate-hosted stratiform hydrothermal breccia bodies (Wilkinson et al., 2005*b*), termed Black Matrix Breccias (BMB). Within the Limerick Basin there is a close spatial and temporal relationship between the diatremes and mineralised BMB horizons (Redmond, 2010; McCusker and Reed, 2013). Evidence has not previously been documented to link the extensive volcanism within this region to the Pb-Zn mineralisation.

Pervasive alteration has obscured the original geochemistry of the magma. The identification of alteration mineral phases and elemental trends can help in understanding how the deposits have been altered and determining the primary composition of the magma. This chapter presents SEM and XRD data to further our understanding of post-diatreme emplacement alteration processes. In addition, study of the BMB horizons and diatreme alteration will further understanding of the relationship between fluid flow and diatremes, including both BMB and mineralising fluids.

5.3 Methodology and terminology

A large proportion of the Limerick volcanic deposits are altered to a mix of fine-grained clays that are unidentifiable via optical microscopy. SEM analysis was required to identify the mineral assemblage of each lithofacies, the clay phases of which differ depending on the initial chemistry of the material and post-emplacement fluids. Alteration phases

are often inter-grown and physically smaller than the SEM spot beam, hence irresolvable. Therefore samples were also analysed by XRD to identify clay mineral phases replacing the original volcanic glass and mineral assemblages.

5.4 Post-eruption lithofacies

Observations of the primary volcaniclastic lithofacies are outlined in chapter 3. LFA 5, described below, was intersected by two boreholes (47 and 77) within the Stonepark North district of the license area (see Fig. 2.3). Boreholes between the two do not intersect any similar material, suggesting that these two features are unconnected to each other. The formation of BMBs is believed to have occurred post diatreme emplacement, due to the presence of volcanic clasts within the BMB matrix.

5.4.1 LFA 5: Black matrix polymict breccia (BPBr) and volcaniclastic tuffisitic dykes (mTd)

These lithofacies are observed in boreholes 47 and 77, both drilled along diatreme walls. The black matrix polymict breccia consists of poorly sorted thinly to thickly bedded clast- and matrix-supported units containing a very wide variety of clast and matrix compositions (Fig. 5.2). Beds dip between 1–89^{o} and average 40^{o}. The beds consist of 20–80% very angular to rounded clasts between 2–147 mm in length (mean: 19 mm). Clast compositions include those of the Lough Gur Formation, Waulsortian Limestone, Lower Argilaceous Bioclastic Limestone (LABL), juvenile lapilli and lapilli tuff autoliths. Some tuff clasts contain ripples (Fig. 5.2A) and well-defined layering. Large limestone clasts have embayed edges and one type of non-diatreme igneous clast is phenocryst-rich and not observed in-situ. The matrix is dark grey to black and contains ash, pyrite and disseminated fine lithic clasts. These units commonly exhibit grading in clast composition with juvenile lapilli trapped at the base, and normal or inverse grading of grain size.

BPBr sections are commonly separated by thin layers of coherent well-sorted, bedded tuff and fine lapillistone (bLT, chapter 3). Contacts and bedding range from horizontal to sub-vertical, commonly with flame and sag structures. Gradation from this lithofacies to BPBr is also common. Beds contain a variety of features including massive, well

laminated, graded, brecciated with jigsaw-fit clasts (Fig. 5.2B), pockets of fines and clast alignment.

Volcaniclastic tuffisitic dykes consist of well sorted tuff or matrix-supported lapilli tuff which intrude at sub-vertical angles into the BPBr, but are not observed intruding into the bLT. Contacts are highly irregular and truncate clasts, occasionally appearing to cause thermal metamorphism of the host rock. These dykes contain between 30–60% ash matrix and 40–70 % small poorly vesiculated lapilli and <1 % country rock clasts, both of which tend to have their long axes vertically aligned.

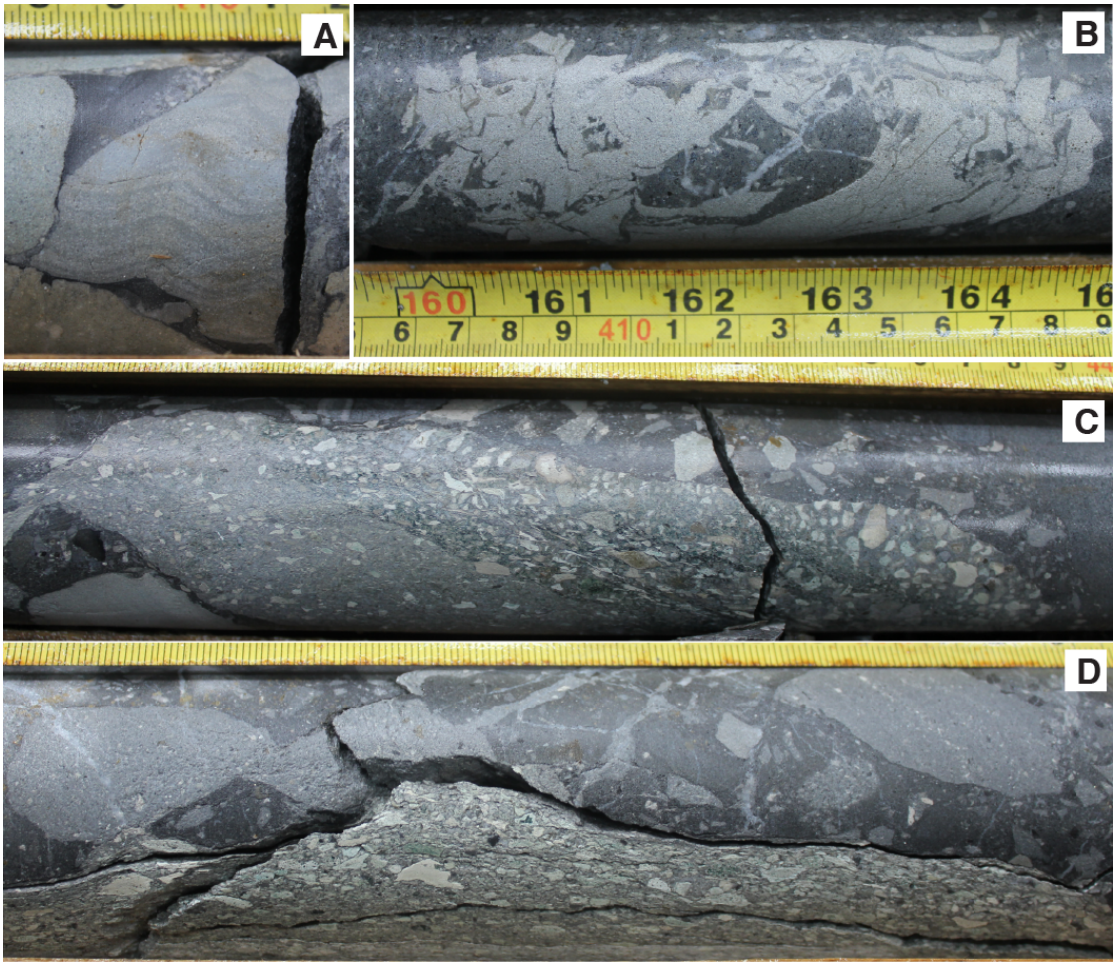

FIGURE 5.2: Photos illustrating features described in LFA 5. **A:** Tuff clast incorporated into lithofacies BPBr showing thin laminations and ripples, indicating that this clast originated at the surface within the maar and was subject to reworking of ash grains (Borehole 77 - 135.4 m) **B:** Tuff that has undergone brecciation but remained in-situ forming a jigsaw texture (Borehole 47 - 86.1 m) **C:** Large diatreme autolith within lithofacies BPBr containing three thin beds, irregular boundaries and truncation of clasts. This smaller clast is an analogue for larger bedded megablocks within the diatreme (Borehole 47 - 58.9 m) **D:** Well sorted lapilli tuff dyke (lithofacies mTd) intruding at sub-vertical angles into BPBr (Borehole 47 - 59.7 m)

5.4.1.1 Interpretation of LFA 5

Autoliths share similarities with the mLT and bLT lithofacies. A small proportion of clasts display ripples similar to those observed in Knockroe Formation ash beds, and are observed downhole to 135 mbgs. The large variety in bed characteristics and contact angles suggests these are autolith blocks (<1–2 m minimum width), which are analogous (albeit on a smaller-scale) to those observed at Venetia kimberlite pipes, Africa (Walters et al., 2006), Jwaneng Centre, Botswana (Brown et al., 2008a) and the Elie Ness diatreme, Scotland (Gernon et al., 2013). These reworked clasts suggest that diatreme and Knockroe Formation deposits predate breccia formation with sufficient time to allow at least partial lithification. Irregular, embayed edges of larger limestone clasts suggest they have encountered acidic hydrothermal fluids after brecciation (Hitzman et al., 2002; Redmond, 2010).

The high angle, discordant intrusion of tuffisitic dykes into the polymict breccias indicates that they are a late stage feature, occurring after both BMB fluid flow and diatreme emplacement. Tuffisitic dykes elsewhere have been attributed to debris jets (Ross et al., 2008*a*; Gernon et al., 2013) and aggressive fluidisation (Kurszlaukis and Barnett, 2003; Davies et al., 2008) during the waning stages of eruption. The intrusion of these tuffisitic dykes into BPBr therefore suggests that BMB formation occurred during late stage magmatic activity in diatremes 47 and 77.

5.5 SEM observations and interpretations

The occurrence of each mineral phase for each environment is summarised in Table 5.1.

	Upper Diatreme	Lower Diatreme	Polymict BMB	Knockroe
Albite	✓	✓		
Calcite	✓	✓	✓	✓
Apatite			✓	
Chamosite	✓	✓		
Clinochlore				✓
Dolomite		✓	✓	
Fe Oxides		✓		✓
Galena		✓		
Illite		✓	✓	✓
Pyrite	✓	✓	✓	✓
Rutile	✓	✓	✓	✓
Sanidine	✓	✓		✓
Silica	✓	✓	✓	✓
Smectite		✓		
Sphalerite		✓		
Spinels		✓		✓

TABLE 5.1: Comparisons of summarised mineralogy between different volcanic-related environments obtained by XRD and SEM analysis

5.5.1 Upper diatreme observations

Lapilli and ash matrix in the upper diatremes have been almost entirely replaced by chamosite, a Fe-rich chlorite (see Fig. 5.3B and 5.3C). The clay tends to be very fine-grained and bladed, often seen with zonation in either habit or Fe-Mg ratio. Chamosite also tends to fill vesicles within lapilli, partially and completely filling the voids with concentric zones of fine-grained clay. Chlorite is closely associated with irregular masses of albite, calcite and silica, appearing to overprint primary juvenile material (see Fig. 5.3C). Albite is observed surrounding vesicle rims, pore spaces and replacing the outer rims of small lapilli.

Thin sections reveal small prismatic crystals of feldspar, often exhibiting simple twinning, typical of sanidine (MacKenzie and Adams, 2011) (see Fig. 5.3B). These and rare larger crystals of multiple twinned plagioclase feldspar are the only phenocryst phases observed in the juvenile lapilli. Bladed sanidine often exhibits a preferred alignment and (unusually for K-feldspars) contains 0.28-0.72 % Fe_2O_3 (see supplementary material 5.1). Many phenocrysts also contain dark spots of very pure albite and TiO_2.

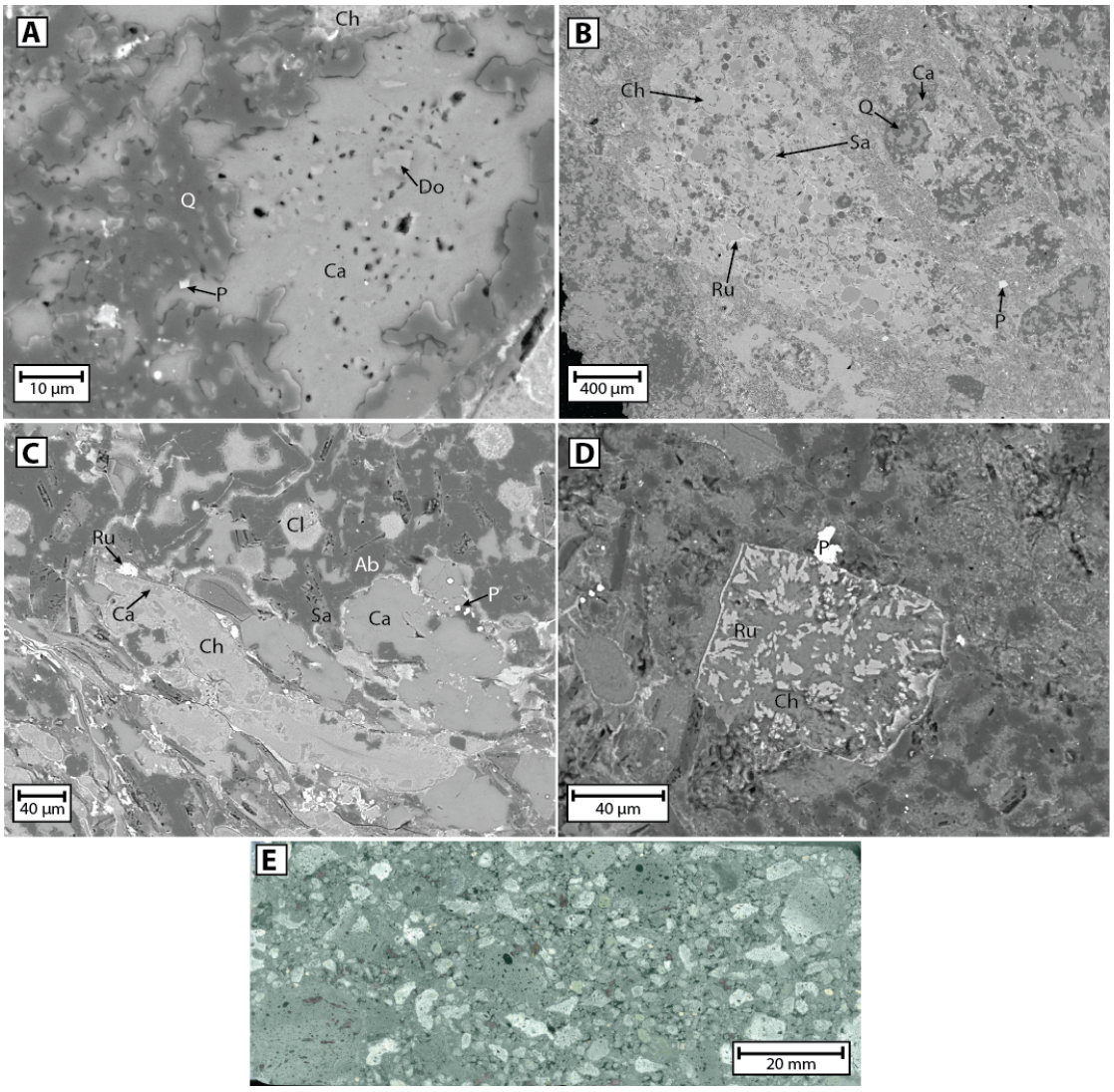

FIGURE 5.3: SEM BSE images of upper diatreme sample S1 (borehole 19, 49.95 m). **A:** Intergrowing silica and calcite replacing clast matrix. **B:** Common texture of juvenile lapilli in breccia matrix. Sanidine phenocrysts can be seen with a random orientation around vesicles filled with chamosite. Disseminated rutile crystals are highly concentrated around vesicle and ash grain boundaries. Juvenile lapilli and breccia matrix is being replaced by secondary silica and calcite. **C:** The primary minerals present are the sanidine and plagioclase phenocrysts that exhibit extensive alteration. Irregular albite masses can be seen overprinting pre-existing lapilli. Calcite xenoliths are rounded with irregular boundaries due to abrasion and dissolution. Remobilisation of Ca has allowed the crystallisation of secondary calcite during alteration of ash grains. **D:** Replacement of altered clast in breccia by rutile and chamosite. **E:** Sample S1, tuff from upper diatreme, borehole 19, 49.95 m **Ab:** Albite **Ca:** Calcite **Ch:** Chamosite **Cl:** Clinochlore **Do:** Dolomite **P:** Pyrite **Q:** Silica **Sa:** Sanidine **Ru:** Rutile

Metallic phases within the upper diatreme include both pyrite and rutile. Pyrite is visible within lapilli and the breccia matrix, often as fine-grained euhedral to anhedral crystals often but not exclusively associated with secondary silica and the edges of ash particles. Rutile is often observed replacing clasts and around the periphery of ash

particles. Small crystals are often associated with chlorite (see Fig. 5.3D), but are also visible as fine-grained disseminated rutile within albite and irregular masses of calcite.

5.5.2 Upper diatreme interpretations

Feldspars within the upper diatreme often exhibit a preferred orientation, indicating flow-parallel alignment during magma transport or alignment upon eruption of magma. The unusually high Fe content within the K-feldspar and dark Fe-rich spots, most likely represents iron exsolution upon cooling (Deer et al., 1996). Dark spots of very pure albite also contained within many phenocrysts indicate that the K-feldspar has undergone albitization (Kaur et al., 2012). This is consistent with irregular patches of $Albite_{95\text{-}100}$ observed replacing lapilli and filling pore spaces (see supplementary material 5.1).

Sanidine is the common form of alkali feldspar in volcanic rocks, but the potassium component rarely exceeds 75 % (Deer et al., 1996). The diatreme erupted into a shallow marine environment, creating a water-rich slurry in the upper diatreme (Kokelaar, 1983; Moore, 1985) and creating dilute density flow deposits in the surrounding maar. Hot juvenile material would have interacted with (K-rich) seawater. This mechanism of K-metasomatism may explain the presence of alkali feldspars with potassium components of 70-90 % in the upper diatreme and Knockroe Formation (Schoen and White, 1967; Requia and Fontbote, 1999).

Within the upper diatreme, chlorite has a large variation in Fe:Mg ratio but chamosite, the Fe-rich end member is much more abundant than clinochlore, the Mg-rich end member (Deer et al., 1996). Variations in habit and chemistry of chlorite may represent multiple generations of alteration products (Afanasyev et al., 2014). Assemblages of chlorite with irregular masses of calcite and silica is commonly associated with greenschist grade metamorphism (Deer et al., 1996). Chlorite is a typical low temperature alteration product of many minerals including micas, tending to contain a very similar Mg content to the parent mineral (Parry and Downey, 1982). Pyroxenes are often altered to chlorite, for example augite (Deer et al., 1996) and diopside due to reactions with volatiles such as CO_2 and H_2O (McGetchin et al., 1973; Fagan and Day, 1997). Alteration has obliterated or modified all primary phenocryst phases. The presence of chlorite in both the ash and breccia matrix however, indicates that it is the product

of glass alteration in fine-grained ash (as opposed to phenocryst alteration). Glass alteration tends to form chamosite with a high Fe:Mg ratio (Sturesson, 1992; Sturesson et al., 2000). Chlorite formed in vesicles most likely resulted from the mobilisation of elements upon dissolution of volcanic glass (Sturesson, 1992), recrystallising in available pore spaces.

Metallic phases in the upper diatreme are primarily associated with areas of albite and silica replacing juvenile material or surrounding edges of lapilli. This association with minerals replacing primary material suggests that the metallic phases are secondary minerals, precipitating in the same event as the albite and silica, after formation of the diatreme breccia.

5.5.3 Lower diatreme observations

Extensive albite crystallisation has formed small subhedral to euhedral crystals reaching a maximum of 0.1 mm in the breccia matrix and juvenile lapilli (see Fig. 5.4A and 5.4B). The crystals tend to be randomly orientated, appear relatively fresh, contain inclusions of rutile and silica, and occasionally overprint sanidine crystals. At depths greater than 500 m there is a distinct paucity of phenocrysts within juvenile lapilli.

Patches of juvenile material and breccia matrix have been replaced by irregular intergrown patches of albite, calcite (commonly pockmarked), silica and clay minerals including chamosite, illite and smectite associated with a variety of metallic phases (see Fig. 5.4C). The proportion of juvenile material replaced by this mineral assemblage increases with depth from 10-20 % at 274 m to 80-100 % at 517 m. Zeolites such as analcime, also occur as acicular crystals radiating out from the centre of vesicles in juvenile lapilli. Small euhedral hexagonal crystals of apatite have formed within the lapilli matrix and also overprinting albite crystals.

Many spinels found in the lower diatreme are coated with juvenile material and zoned, appearing dark and mottled in the centre with a brighter, paler outer zone (see Fig. 5.4D). The centres are heavily substituted with a typical composition of $Fe_{1.89}Al_{0.46}Ti_{0.4}Cr_{0.27}Zn_{0.23}O_4$. The outer rim has a composition varying from titanomagnetite to almost pure magnetite (see supplementary material 5.1).

The lower diatreme exhibits a large increase in metalliferous phases as well as patches of secondary silica and calcite. A large patch of monazite is associated with these secondary minerals. At depths >500 m, ore-forming minerals are present, dominated by sphalerite (see Fig. 5.4C), pyrite and rutile with lesser amounts of galena, plattnerite and chalcopyrite. These Zn, Pb and Fe phases are similar to those occurring in the Limerick BMB horizons and characteristic of regional mineralisation (Hitzman and Beaty, 1996; Redmond, 2010). Metallic phases are highly concentrated within magma-coated xenoliths (see Fig. 5.4B), often associated with chamosite and calcite.

5.5.4 Lower diatreme interpretations

Albite crystallisation is extensive within both the juvenile lapilli and breccia matrix and may represent phenocrysts liberated from a porphyritic magma upon fragmentation (Yasui and Koyaguchi, 2004; Carracedo Sánchez et al., 2009). However, much of the albite within the lower diatremes appear to be amorphous masses overprinting pre-existing material, relatively fresh and contain inclusions of rutile and silica. The synthesis of both these minerals and the albite are typically associated with hydrothermal processes (Deer et al., 1996). Albite overprinting pre-existing sanidine is abundant and most likely due to albite being less resistant to hydrothermal alteration than K-feldspar (Lagat, 2009), and therefore more likely to be altered and re-precipitated by hydrothermal fluids. Illite and smectite are common alteration products of K-feldspar (Deer et al., 1996; Lagat, 2009) and their presence may explain the paucity of phenocrysts within juvenile lapilli below 500 m.

Spinels within the lower diatreme often exhibit a coating of juvenile material, suggesting that they are xenoliths incorporated into the ascending magma. Crystals contain a highly substituted centre and magnetite or titanomagnetite rim. This trend is very similar to that observed by Tracy (1980) and Wang et al. (2012), with the central Cr-Al spinel representing the primary composition. The outer titanomagnetite rim is thought to represent a secondary spinel resulting from reaction with the host magma after its entrainment. This indicates that the primary spinels originally crystallised deeper in the magmatic system, either within the lower crust or upper mantle (Wang et al., 2012).

Zeolites such as analcime commonly form through alteration and dissolution of volcanic glass (Best, 2003). The process is relatively rapid, with the release of Si and Al from

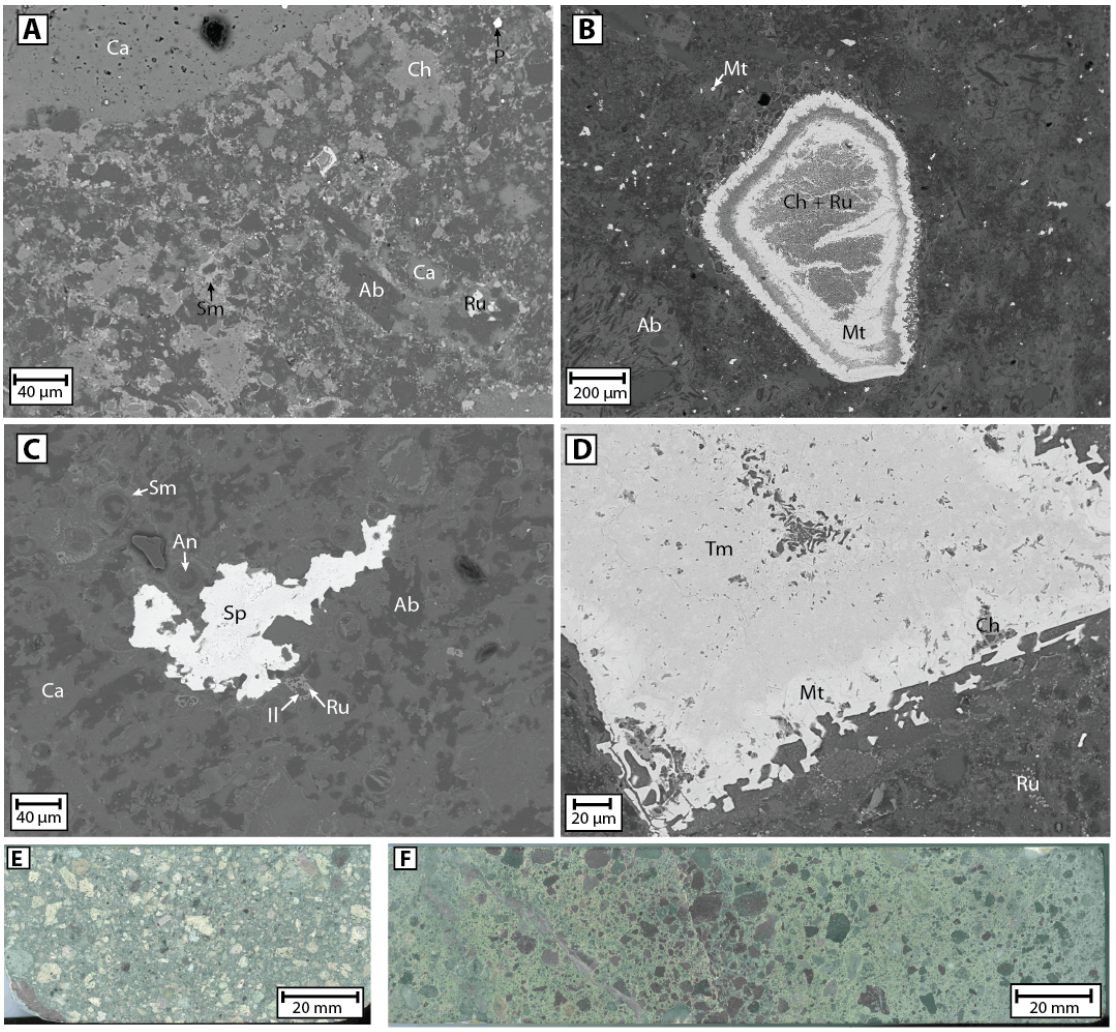

FIGURE 5.4: SEM BSE images from the lower diatreme samples. **A:** Heavily altered breccia matrix with secondary minerals including chamosite, smectite, albite and rutile with in-fillings of calcite. A large rounded calcite xenolith can be seen in the top left corner. **B:** Magma coated zoned xenolith of magnetite altered to chamosite and rutile. Smaller magnetite crystals can be seen within the breccia matrix. Vesicles are filled with calcite and albite crystals can be seen within juvenile lapilli. **C:** Sphalerite mineralisation within juvenile lapilli matrix. The matrix has been heavily altered to clay phases within secondary albite and calcite infills. Bladed analcime crystals can be seen filling vesicles. **D:** Part of large zoned spinel xenolith within the breccia matrix. The inner zone consists of titanomagnetite with substitutions of Zn, Cr and Al. The breccia matrix consists of chamosite and disseminated rutile crystals. **E:** Sample S17 (A & C), lapilli tuff from lower diatreme, borehole 19, 517 m. **F:** Sample S9b (B & D, heavily altered lapilli tuff from lower diatreme, borehole 19, 274 m. **Ab:** Albite **An:** Analcime **Ca:** Calcite **Ch:** Chamosite **Il:** Illite **Mt:** Magnetite **P:** Pyrite **Q:** Silica **Ru:** Rutile **Sm:** Smectite **Sp:** Sphalerite **Tm:** Titanomagnetite

vitric tuff typically occurring over timescales on the order of 10^3 years, but is dependent on particle size and temperature (Utzmann et al., 2002). The presence of analcime within lapilli vesicles suggests that the alteration fluids were of moderate salinity (Deer et al., 1996).

Increases in abundance of metallic phases are accompanied by an abundance of secondary minerals such as albite, calcite and silica, suggesting the metallic phases precipitated as a result of hydrothermal alteration (Deer et al., 1996). Hydrothermal fluids >300 °C leach large amounts of Fe, Cu and reduced sulphur from basalt (Mottl et al., 1979). This creates an oxide-sulphide assemblage including pyrite, chalcopyrite, hematite and magnetite, very similar to that seen within the diatreme.

Xenoliths are observed in both juvenile lapilli and the breccia matrix, the latter of which sometimes exhibit a thin magma coating. This suggests that they are transported by the magma from considerable depth or sprayed by magma globules during degassing of the source dyke (Gernon et al., 2012). Many of the carbonate country rock xenoliths are rounded and exhibit irregular and embayed edges, demonstrating abrasion during repeated ejection and collapse back into the vent (Aranda-Gómez and Luhr, 1996; Brown et al., 2008a). Dissolution and embayment of carbonate clast edges would have occurred in a weakly acidic environment. These conditions may have occurred as a result of magma volatiles combining with abundant water (Aranda-Gómez and Luhr, 1996) during phreatomagmatic eruptions, or by later hydrothermal fluids. The presence of limestone and sandstone xenoliths would also provide sources of Si and Ca (Afanasyev et al., 2014), remobilised and re-precipitated by the passage of fluids.

5.5.5 Polymict BMB (LFA 5) observations

Juvenile lapilli within the BMB contain larger and more irregularly shaped vesicles (see Fig. 5.5C and 5.5E) than those of the diatreme lithofacies. The matrix to lapilli consists primarily of granular apatite crystals with fine-grained illite filling the interstices (see Fig. 5.5D). Large areas of lapilli have also been replaced by small irregular patches of calcite and silica as well as large angular patches of dolomite (see Fig. 5.5C). Vesicles in the lapilli are filled with a similar mix of carbonate and silica.

The matrix to the breccia consists of varying proportions of the same minerals that have replaced the juvenile lapilli (see Fig. 5.7). Silica appears to constitute a large proportion of the matrix at about 20–50 area %, containing small isolated patches of calcite and disseminated metallic phases. Dolomite is another abundant mineral in the matrix, forming large, tabular and angular crystals often with a pockmarked surface containing

small patches or inclusions of calcite and pyrite (see Fig. 5.5A). Apatite crystals in the matrix are small, rounded and are often associated with illite and rutile.

Pyrite within the juvenile lapilli range from subhedral masses to large euhedral and tabular clumps of crystals within the lapilli and vesicles. Smaller disseminated crystals are also observed in the breccia matrix and tend to be more concentrated around the periphery of clasts. Large concentrations of rutile (10–20 %) are observed within lapilli matrix. Smaller proportions of rutile have crystallised as subhedral to euhedral tabular crystals clumped in association with illite.

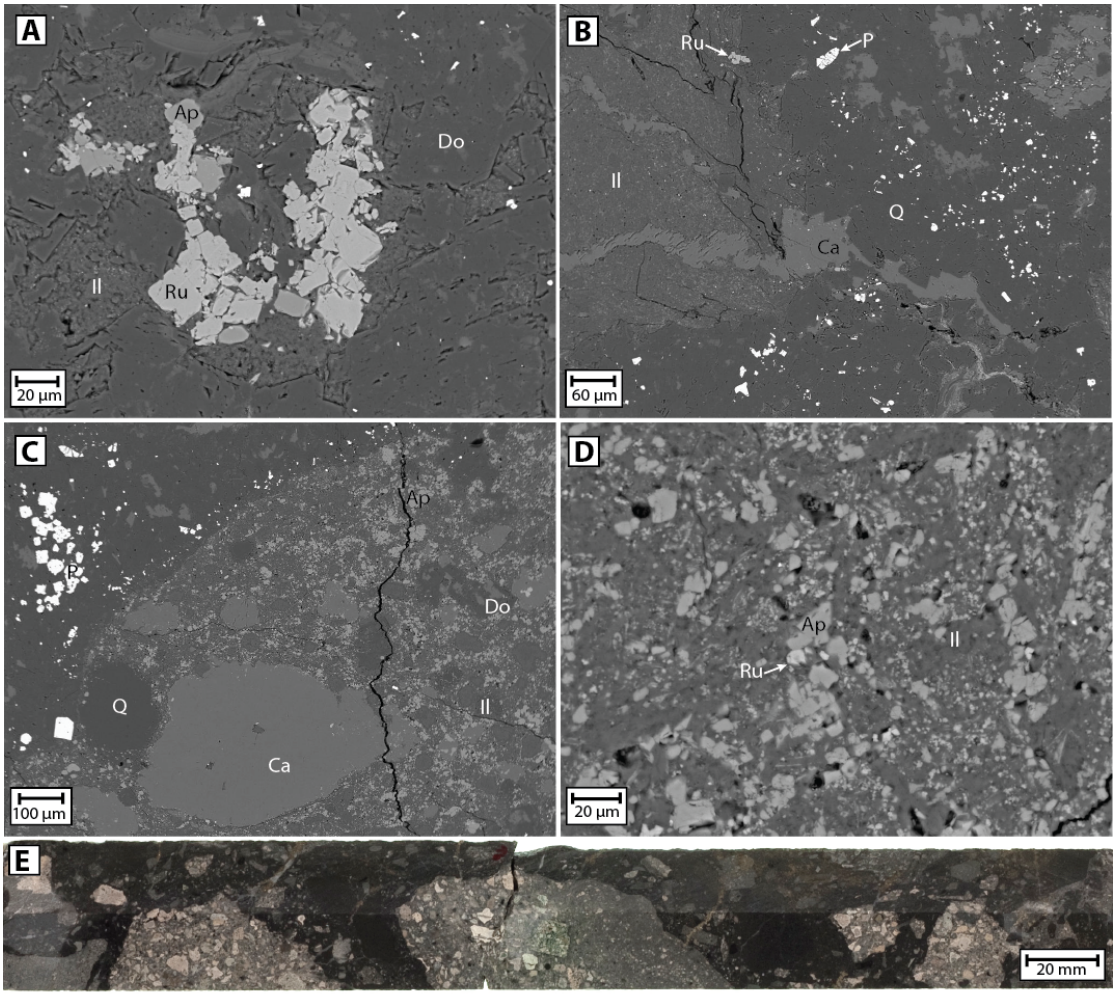

FIGURE 5.5: SEM BSE images from sample LS9 (borehole 47, 53.22 m). **A:** BMB matrix including large crystals of dolomite with interstitial illite and crystals of apatite and rutile. **B:** Typical BMB matrix consisting of intergrown illite, calcite and silica with crystals of rutile and pyrite. **C:** Volcanic agglomerate clast completely replaced by BMB minerals. The clast matrix consists primarily of apatite and illite with patches of silica, calcite and dolomite. Large crystals of pyrite can be seen in the BMB matrix. **D:** Typical replaced matrix of agglomerate clast consisting of illite with crystals of apatite and rutile. **E:** Sample LS9, polymict BMB from borehole 47, 53.22 m. **Ap:** Apatite **Ca:** Calcite **Do:** Dolomite **Il:** Illite **P:** Pyrite **Q:** Silica **Ru:** Rutile

5.5.6 Polymict BMB (LFA 5) interpretations

The primary constituents of the volcanogenic clasts have been completely destroyed by prolonged exposure to BMB hydrothermal fluids. The two fluids considered to have flowed through and mineralised these breccias are <140 °C and 200-280 °C (Banks et al., 2002; Wilkinson et al., 2005*b*). The higher temperatures of the second fluid would have been sufficient to completely replace the primary mineral assemblage. The current mineralogical constituents are very similar to the assemblage observed at the base of diatremes 19 and 28 (see Fig. 5.7). Although the BMB sample contains greater concentrations of apatite and lacks chlorite and albite, the signature minerals of the BMB (apatite, calcite, dolomite, illite and silica - see Fig. 5.7 and 5.8) all occur within the lower diatreme, but in smaller concentrations. Mineralogical evidence and the presence of polymict BMB in diatremes 47 and 77, indicates that the diatremes have been subject to the passage of BMB forming fluids. Therefore the simplest explanation is that the volcanogenic clasts within the BMB originated from the diatremes. The larger and irregular vesicles observed in the BMB lapilli were possibly enlarged by the passage of acidic hydrothermal fluids, leading to dissolution of juvenile material around the edges of pre-existing vesicles (Sruoga and Rubinstein, 2007).

The lack of smectite and abundance of illite within the BMB suggests that the smectite present in the diatreme-related material may have been converted to illite. This chemical reaction occurs with increasing temperature (Deer et al., 1996) and suggests that the BMB lapilli experienced higher temperatures or a prolonged heating time (Roaldset et al., 1998), compared to the diatreme material during hydrothermal alteration.

5.5.7 Knockroe Formation volcaniclastics observations

Two main types of mineral assemblages occur within different lithofacies of the Knockroe Formation. The first consists of lapilli matrix completely replaced by secondary minerals (see Fig. 5.6D and 5.6F). Small bladed crystals of clinochlore and illite completely replace small ash grains, lapilli and vesicle-fills. Irregular silica and calcite patches completely overprint the primary mineralogy, and are often associated with high concentrations of metallic phases. These lapilli also have a low proportion of phenocrysts of small dark, blades of sanidine. Feldspars often exhibit a preferred alignment and mottled alteration.

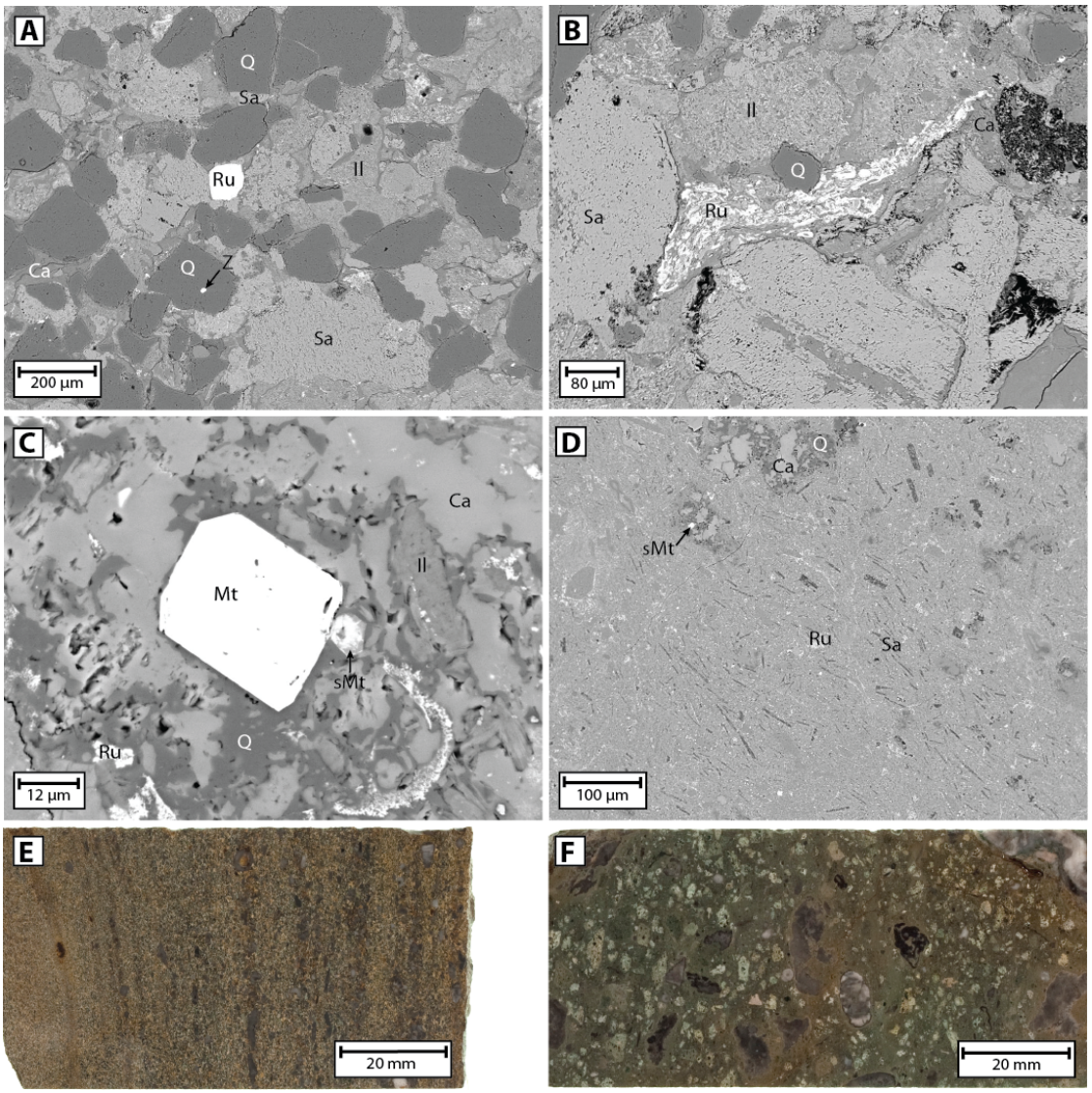

FIGURE 5.6: SEM BSE images from two Knockroe Formation pyroclastic lithofacies. **A:** Large liberated rutile grain amongst juvenile lapilli. The lapilli are being replaced by silica as can be seen by the partially replaced grain at the top. The juvenile lapilli appear to consist of fine grained sanidine. The interstitial matrix consists of illite and calcite. **B:** Large concentration of deformed rutile crystals in matrix between juvenile lapilli. The lack of vesiculation is clearly evident. **C:** Magnetite crystal within secondary silica and calcite. Illite and rutile are associated with this secondary mineralisation. The small zoned crystal is magnetite substituted with Cr and Al. **D:** Aligned and highly altered sanidine crystals within juvenile lapilli matrix. Secondary calcite, silica and rutile can be seen associated with a substituted magnetite grain. **E:** Sample S22 (A & B), fine-grained laminated Knockroe Formation tuff interbedded with crinoidal debris from borehole 89, 46.81 m. **F:** Sample S12 (C & D), Knockroe Formation lapilli tuff with limestone xenoliths and crinoidal debris from borehole 89, 34.23 m. **Ca:** Calcite **Cl:** Clinochlore **Il:** Illite **Mt:** Magnetite **P:** Pyrite **Sa:** Sanidine **Q:** Silica **Ru:** Rutile **sMt:** Substituted magnetite including Cr, Ti, Al, Zn **Z:** Zircon

Matrix surrounding the lapilli consists primarily of irregular intergrown patches of silica and calcite (see Fig. 5.6C), often associated with apatite crystals. Fine-grained bladed clinochlore crystals are common in areas not overprinted by silica.

The second mineral assemblage occurs in a fine-grained laminated tuff lithofacies that lacks any phenocryst phases (L1 - see Fig. 3.6). Beds are clast-supported with rounded and mostly equigranular lapilli that lack vesicles (see Fig. 5.6A and 5.6E). They consist almost entirely of small bladed euhedral crystals of sanidine with random orientations. Other lapilli within this lithofacies appear to consist partially of sanidine-rich material and partially amorphous silica. Fine-grained bladed crystals of illite constitute the majority of the external matrix, infilling the small interstices between juvenile lapilli. Calcite is also seen in higher concentrations along grain boundaries.

Disseminated rutile occurs in high concentrations surrounding the edges of features such as grain boundaries, vesicles and clasts in both lithofacies. Lower concentrations of rutile are observed within the matrix surrounding lapilli (see Fig. 5.6B). Many other metallic phases are observed within the lapilli matrix including subhedral hexagonal crystals of pyrite, iron oxide and magnetite. The observed magnetite tend to be small octagonal crystals with an outer darker substituted zone or complete substitution by elements such as Al, Si, Ti, Cr and Zn (see Fig. 5.6C). Metallic phases are seen in greater concentrations within lapilli that have been partially replaced by silica. However, large concentrations of iron oxide are observed within the external matrix of the clast-supported Knockroe Formation lithofacies, following a wavy fabric.

5.5.8 Knockroe Formation volcaniclastics interpretations

The texture, mineralogy and alteration of the clast-supported Knockroe Formation lithofacies is very similar to that of the upper diatreme. The chlorite observed in the Knockroe Formation is Mg-rich (clinochlore) in contrast to the Fe-rich chamosite within the diatreme. Knockroe Formation pyroclastic material is interbedded with crinoidal limestone (see Fig. 5.6E and 5.6F) (Somerville et al., 1992), indicating deposition in a shallow marine environment. Interactions between basalt and seawater at temperatures >150 ^{o}C cause a net uptake of MgO and H_2O, whilst SiO_2 and CaO are leached from the basalt (Humphris and Thompson, 1978; Mottl et al., 1979; Seyfried Jr and Bischoff, 1979; Seyfried Jr and Mottl, 1982; Utzmann et al., 2002). CaO and SiO_2 would have

been remobilised from the basalt into the heated seawater, re-precipitating as secondary calcite and silica within the lapilli and matrix.

Magnetite within the Knockroe Formation is associated with secondary silica and exhibits a different zoning substitution pattern to the diatreme spinels, which have an inner core of substituted spinel with an outer zone of pure magnetite (see section 5.4.3). However, the reversed pattern within the Knockroe Formation may be the result of trace amounts of Cr, Ti and Zn leached from the basalt (Mottl et al., 1979) being concentrated in hydrothermal spinels formed by the reduction of hydrated ferric oxides (Deer et al., 1996) present in the juvenile material.

5.6 XRD observations and interpretations

5.6.1 XRD observations

The primary XRD observations are summarised in Table 5.2. The main clay alteration products observed within central diatreme 19 consist of chlorite and kaolinite, which changes to be replaced by illite with depth. Both calcite and silica apparently overprint a large proportion of the lower diatreme samples (Fig. 5.4), which is not clear from the XRD analysis. The western margin of diatreme 19 (borehole 23) appears to be more altered than the centre, and exhibits a different assemblage of alteration products. The upper 285 m of this borehole consists primarily of partially dolomitised country rock (66 wt.% dolomite and 25 wt.% calcite) with intermittent horizons or sections of volcaniclastic material.

Sample	Observation	Interpretation
Diatreme Upper	Calcite proportions up to 20 wt.%.	Local Ca leaching and re-precipitation.
	Silica proportions up to 12 wt.%	Local Si leaching and re-precipitation.
	Background dolomite proportions of 0.2–0.4 wt.%.	Low dolomite proportions formed by Mg uptake from seawater.
Diatreme Middle	Alteration phases predominantly chlorite (av. 5.4 wt.%), kaolinite (av. 7.3 wt.%).	Smectite becomes unstable at higher temperatures.
	K-feldspar $\sim$ 9 wt.% above 380 m.	Potential metasomatisation of feldspars.
	Plagioclase relatively constant throughout diatreme at $\sim$ 16 wt.%.	Albite predominantly hydrothermal, small concentrations may be primary.
Diatreme Lower	>380 m, chlorite and kaolinite almost completely replaced by <31 wt.% illite.	Illite formed from consumption of K-feldspar and kaolinite, low chlorite due to leaching of Mg and Fe.
	>380 m, K-feldspar <1 wt.%.	Predominantly altered to illite.
	Calcite increases from 12 to 20 wt.% below 45 m thick intrusion (146.5–191.5m).	Increased alteration and replacement by greenschist metamorphic minerals below intrusion which acted as a fluid barrier.
	Silica increases from 3 to 10 wt.% below same intrusion.	Intrusions trap fluids, increasing alteration and replacement by silica below.
	Anomalous silica concentration of 15 wt.% directly below intrusion.	Intrusion margin appears brecciated with dark Si-rich matrix between clasts.
	Dolomite increases to 12 wt.% below intrusion.	Intrusions trap fluids, increasing alteration and replacement by dolomite below.
	Dolomite increases with depth to a maximum of 22 wt.% at 515 m.	Increased hydrothermal fluid flow and therefore dolomitisation with depth.
Diatreme Margin	B-23 more altered with different alteration products.	Increased fluid flow and alteration along diatreme margin.
	Glass mainly altered to illite (36–76 wt.%).	Moderately acid hydrothermal fluids.
	Small proportions of chlorite and kaolinite.	Illite formed from K-feldspar and kaolinite, low chlorite due Mg, Fe leaching.
	Matrix consists of 13–36 wt.% calcite and 1–13 wt.% silica.	Increased fluid flow allows increased precipitation of these two minerals.
	B-28 >183 m primarily 42–61 wt.% illite.	Highly altered diatreme margin.
	B-28, <1 wt.% kaolinite.	Majority consumed to form illite.
	B-28 chlorite is 7 wt.% at 10 m depth, decreasing to <1 wt.% by 183 m.	Due to increased leaching at depth of Mg and Fe by hydrothermal fluids.
	Upper B-28 consist of high concentrations of smectite (37–48 wt.%).	Commonly found as product of low temperature hydrothermal alteration.
	B-28 contains low feldspar: <5 wt.% K-feldspar and 0.5–16 wt.% plagioclase.	Predominately altered to illite
	High pyrite concentrations in B-28: av. 0.1–3 wt.%, max. 8 wt.% at 430 m.	Greater fluid flow along margin, allowing greater pyrite precipitation.
	Upper B-28 dolomite increases from 0.3–0.4 wt.% to 11 wt.% at 330 m.	B-28 lacks thick intrusion to trap fluids and increase dolomitisation.
BMB Matrix	Primarily dolomite (<79 wt.%).	Key BMB mineral, Mg potentially leached from lower diatremes.
	Small proportions of calcite, silica and pyrite, all <10 wt.%.	Precipitation from hydrothermal fluids

BMB Clasts	Altered to 30–53 wt.% illite.	Alteration under high temperature, moderately acidic conditions.
	Matrix replaced by 9–14 wt.% calcite, 6–7 wt.% silica, 1–2 wt.% pyrite.	Clast matrix replaced by proportions of BMB matrix minerals.
	Trace of <1 wt.% plagioclase within one clast sample.	Remaining from primary volcaniclastic mineralogy.
Knockroe Formation	Primarily altered to illite (40–48 wt.%).	Potentially altered within diatremes, ejected by later eruptions.
	Silica and calcite increase with depth. 34 m: 10 wt.% silica, 8 wt.% calcite. 47 m: 23 wt.% silica, 31 wt.% calcite.	Potential increase in greywacke matrix or percolating seawater interacting with volcaniclastic material.

TABLE 5.2: Summary of XRD data observations and brief interpretations for each environment. B-n indicates borehole number, please refer to Figure 3.2 for borehole locations.

5.6.2 XRD interpretations

The distinctive orange-red colouration of the lower diatremes was initially attributed to high concentrations of oxidised disseminated pyrite. However, XRD analysis shows proportions remain consistently <1 wt.% down the centre and a maximum of only 8 wt.% down the margin of the diatremes. Therefore, the discolouration is more likely due to the partial dolomitisation and subsequent hematisation of the diatreme fill. Results showed dolomite to be a key mineral of the BMB matrix, reaching up to 78 wt.% in some samples. The agglomerate clasts within the BMB samples exhibit the same alteration phases as the lower discoloured diatreme section, consisting predominately of illite, dolomite, calcite and silica (see Fig. 5.8B). The centre and margins of the diatremes show increasing proportions of dolomite with depth from the approximate level that the orange-red discolouration starts and BMB levels become prominent adjacent to the diatremes (see Fig. 5.7). *Dolomite is a key mineral of the BMB matrix assemblage (see Table 5.2, Fig. 5.7 and Fig. 5.8b), suggesting that the dolomitising BMB fluids passed through the vent, entraining clasts of diatreme material.* Diatremes tend to be filled with coarse volcaniclastic deposits characterised by initial porosities of up to 20-30 % (Stripp et al., 2006), facilitating late-stage fluid flow.

The large increase in dolomite concentration observed in diatreme 19 is likely due to the presence of thick intrusions, which would have acted as an impenetrable barrier to the BMB fluid. Trapped fluid would have allowed greater dolomitisation, perhaps forming a convection cell below (see Afanasyev et al., 2014, for further details on diatreme alteration models). Diatreme 28 shows a more gradual increase of dolomite with depth,

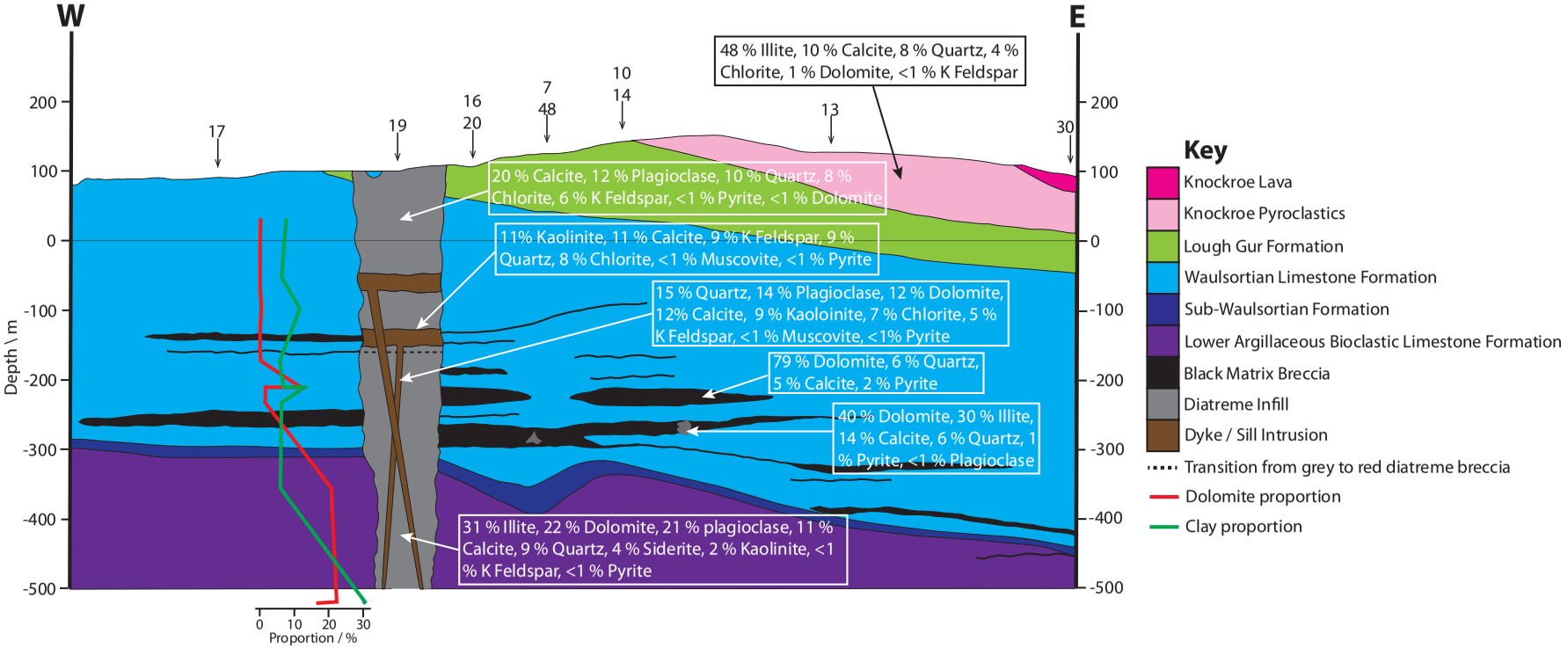

FIGURE 5.7: Cross-section from west to east through diatreme 19 summarising the mineralogy of sample each environment. The diagram shows the levels of BMB within the Waulsortian Formation and its relation to the level of sills within the diatreme. Numbers indicate the locations of boreholes drilled through the sequence from which the cross-section is constructed. The thickness and depths of each BMB layer is known at each borehole, however they have been interpreted in between. Boxes contain mineral assemblages of the different lithofacies determined by XRD analysis and the overlain graph indicates variations of dolomite and total clay proportion with depth down borehole 19.

in contrast to the large increase observed in diatreme 19. This is most likely due to the lack of an intrusion acting as a barrier within this diatreme. Surrounding country rock contains large cavities in addition to intense fracturing from explosive eruptions. This enhanced permeability would have allowed BMB fluid to pass into the country rock, explaining the high incidence of BMB horizons adjacent to the diatremes. This situation is analogous to the Kelian Gold Mine Indonesia, where diatreme breccias focussed fluid flow into the country rock adjacent to the diatremes (Davies et al., 2008).

Smectite is only observed at the very top of diatreme 28, probably because it alters very easily to kaolinite and illite (di-octahedral smectite) or chlorite (tri-octahedral smectite) with increasing depth and temperature (Deer et al., 1996). Smectite is common in low temperature hydrothermal alteration <170 °C (Bednarz et al., 1991), conditions that might be maintained within the upper diatreme (Gernon et al., 2009*a*; Fontana et al., 2011). Kaolinite is seen in low proportions, <10 %, throughout the diatreme boreholes, suggesting that they have been subjected to a moderately acidic fluid, as smectite converts to kaolinite instead of illite under acidic conditions (Deer et al., 1996).

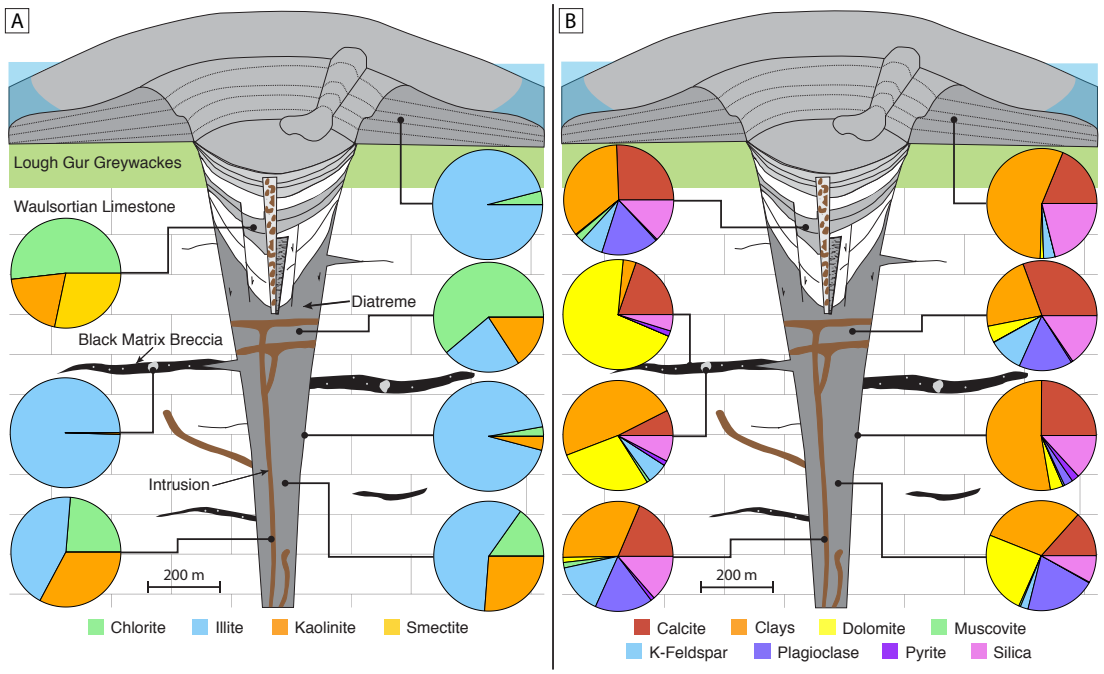

FIGURE 5.8: Cross-section through a stylised model of a Limerick diatreme. **A:** Pie charts illustrate average proportions of clay alteration products obtained by XRD in different diatreme-related and BMB environments. **B:** Pie charts illustrate average proportions of minerals and clay obtained by XRD in different diatreme-related and BMB environments. Environments left side: Upper diatreme, BMB matrix, BMB clasts, intrusions. Environments right side: Knockroe Formation extra-crater deposits, middle diatreme, diatreme margins, lower diatreme.

The original source of the illite is most likely the alteration of K-feldspar (Deer et al., 1996; Lagat, 2009), that decreases in proportion from 16 wt.% at 255 m to <1 wt.% at 515 m. Illite can form via consumption of K-feldspar and kaolinite, using feldspar as a source of potassium according to the following equation 5.1 (Thyne et al., 2001):

Eq 5.1: $(KNa)AlSi_3O_8 + Al_2Si_2O_5(OH)_4 \rightarrow KAl_2AlSi_3O_{10}(OH)_2 + 2\,SiO_2 + H_2O + Na^+$

$$\text{Sanidine} + \text{Kaolinite} \rightarrow \text{Illite} + \text{Quartz} + H_2O$$

Levels of illite are much higher within the marginal diatreme boreholes (23 and 28) compared to the centre (borehole 19). This is most likely due to increased fluid flow and alteration down the margins, consistent with the presence of up to 17 wt.% K-feldspar in diatreme 19, and the noteable absence of any within the marginal boreholes.

Chlorite proportions are minor within the marginal diatreme boreholes and lower diatreme (0–6 % - see supplementary materials 5.2), which both show an increase in illite proportions. Chlorite contains both Mg and Fe (Deer et al., 1996), however there is no increase in another mineral containing these elements to suggest a phase transition. This indicates that the BMB fluids within the lower diatreme have leached the Mg and Fe out of the juvenile material, perhaps explaining the elevated levels of pyrite within the BMB compared to the diatremes. Illite (as opposed to kaolinite) is the primary clay phase of the BMB agglomerate clasts, suggesting that the BMB-forming fluids were of moderate acidity (Deer et al., 1996).

5.7 Major and trace element geochemistry

5.7.1 Major and trace element observations

Figure 5.9 illustrates elemental data distributions of the altered Limerick volcanic samples compared to those of the relatively fresh continental basalts (see Fig. 4.1), described in Table 5.3. Major element ICP-MS and microprobe data distributions exhibit scatter (Fig. 5.9), most likely reflecting major element mobility as a result of alteration. All sample types exhibit higher than expected concentrations of Zr, as evidenced by high Zr/Y values and Fig. 4.6D.

Environment	Element	Observation	Interpretation
Knockroe Formation	Al_2O_3	Highly variable (2–25 %).	Illite is predominant alteration phase, degree of alteration varies.
	K_2O	Variable but majority above continental basalt distribution.	Enrichment during low temperature seawater-basalt interaction.
	MgO	Highly variable (0–23 %), one group containing anomalously high concentrations.	Net uptake of MgO upon interaction between hot basalt and seawater forming clinochlore.
	Na_2O	Negligible concentrations.	Na released during low temperature basalt-seawater interactions.
	Nb	Linear trend, increasing with increase Zr/TiO_2.	Magma fractionation trend.
	Ba, Sr	Low concentrations of both, slightly higher loss of Sr.	Alteration and leaching by hydrothermal fluids.
Polymict BMB clasts	SiO_2	More Si-rich and smaller range (38–54 %).	Precipitation from Si-rich hydrothermal fluid.
	Al_2O_3	Consistently high between 23–30 %.	Illite-rich alteration products (up to 65 %).
	K_2O	Consistently high, above continental basalt distribution, predominantly >8 %.	Enrichment during illitisation.
	CaO	Large range between 0 and >45 %.	Leaching and subsequent precipitation and replacement by CaO.
	Fe_2O_3	Concentrations negligible at <5 %.	Mobilised by hydrothermal fluids.
Upper Diatreme	Al_2O_3	Values concentrated in group ∼11-19 %.	Similar to continental basalt values in Fig. 4.1 (∼12–18 %) due to relative immobility of Al <300 °C.
	Fe_2O_3	Lie predominantly above the continental basalt distribution.	Most likely Fe uptake by smectite.
	MgO	16 samples contain anomalously high values >20 % and 100-37,000 Zr/TiO_2.	Ejected into water column hot, causing uptake of MgO. Deposition in maar-crater before being undercut.
	Na_2O	Low to negligible Na.	Leached under low temperature palagonitisation.
Lower Diatreme	Al_2O_3	Contain up to 22 % Al.	Variations in degree of illite alteration.
	CaO	High values in the mid-lower diatreme (10–30 %).	Partial replacement by calcite and dolomite.
	Fe_2O_3	Large variation in concentration between 0–37 %.	Hydrothermal leaching from some areas and subsequent re-precipitation in others.
	MgO	Concentrations lower, averaging 2.9 % compared to 12.3 % for upper diatreme.	Leaching by hydrothermal fluids and concentration in secondary dolomite.
	Na_2O	High concentrations up to 9.5 %.	Enrichment during high temperature alteration e.g. albitisation.
	Pb	Large variation of values up to 100 ppm.	Small-scale mineralisation by galena.

Table 5.3: Observations and interpretation summary of major and trace elemental data (see Fig. 5.9)

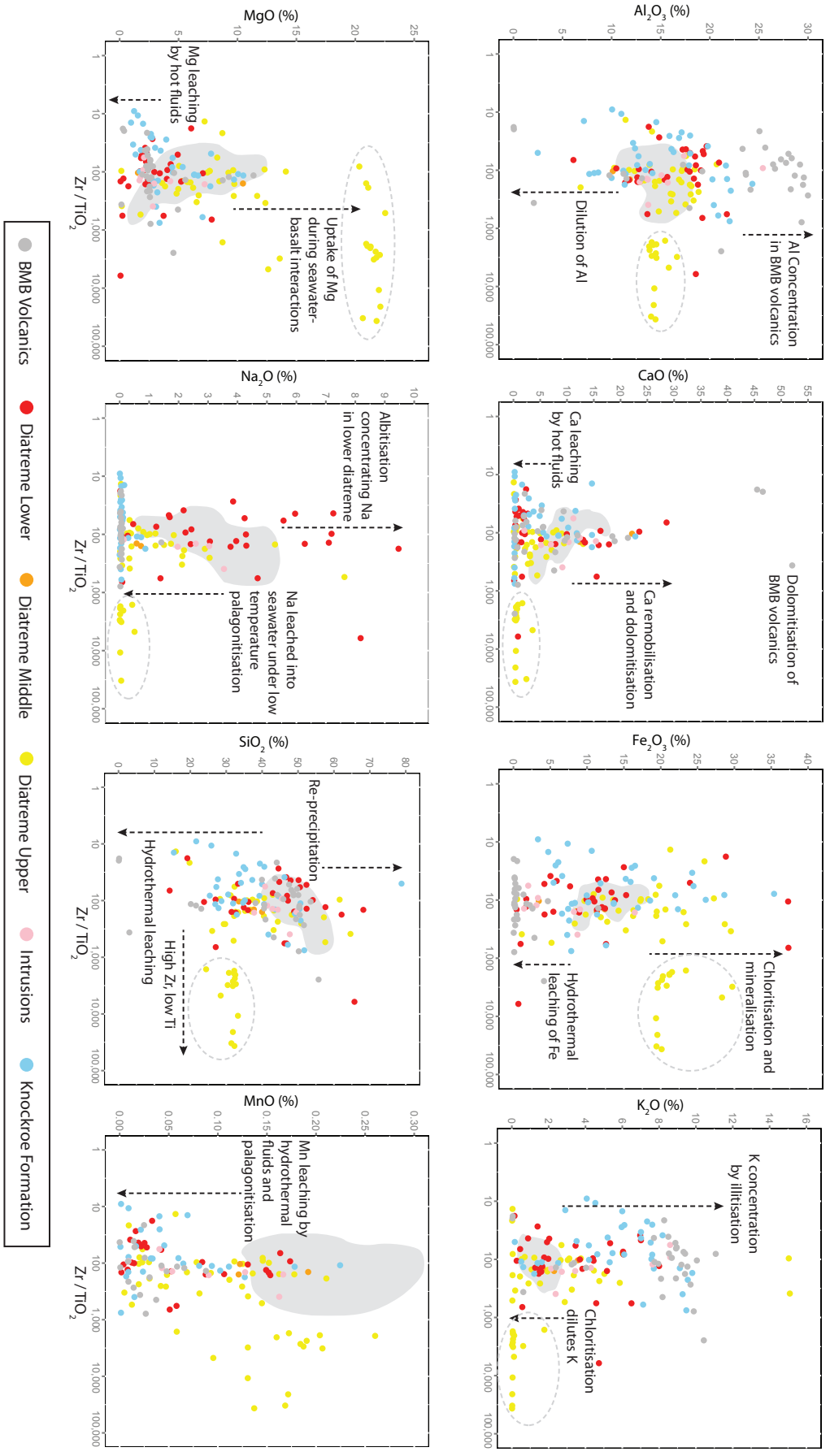
Al2O3 (%)
Al Concentration in BMB volcanics
Dilution of Al
CaO (%)
Dolomitisation of BMB volcanics
Ca leaching by hot fluids
Ca remobilisation and dolomitisation
Fe2O3 (%)
Chloritisation and mineralisation
Hydrothermal leaching of Fe
K2O (%)
K concentration by illitisation
Chloritisation dilutes K
MgO (%)
Mg leaching by hot fluids
Uptake of Mg during seawater-basalt interactions
Na2O (%)
Albitisation concentrating Na in lower diatreme
Na leached into seawater under low temperature palagonitisation
SiO2 (%)
Re-precipitation
Hydrothermal leaching
High Zr, low Ti
MnO (%)
Mn leaching by hydrothermal fluids and palagonitisation
Zr / TiO2
BMB Volcanics
Diatreme Lower
Diatreme Middle
Diatreme Upper
Intrusions
Knockroe Formation

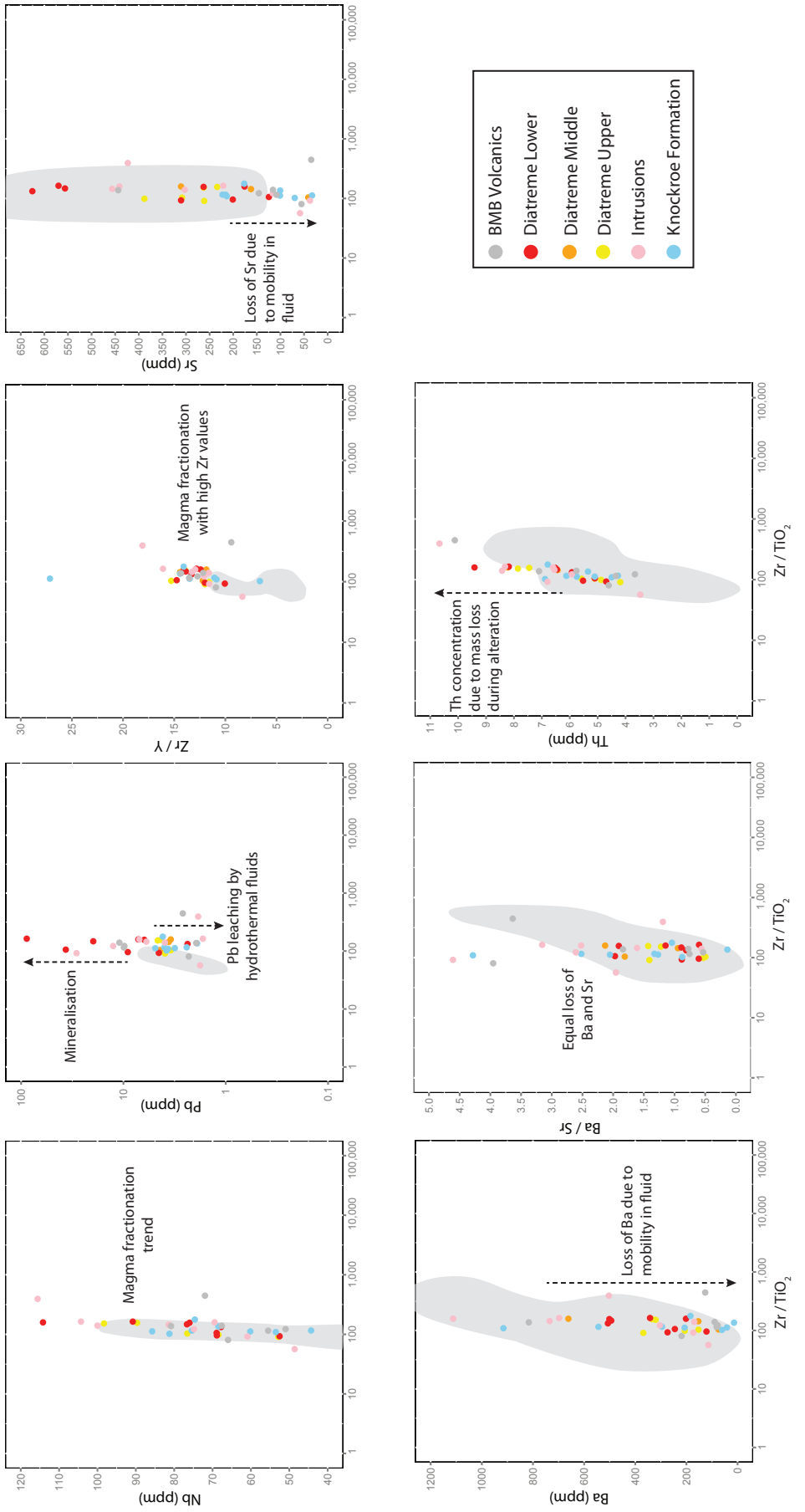

FIGURE 5.9: Panel of graphs depicting major and minor element concentrations of volcanic-related samples from Limerick, plotted with relation to Zr/TiO_2. As a comparison, grey solid arrows indicate elemental trends obtained from relatively unaltered continental basalts, the data of which can be seen in Figure 4.1. Dotted black arrows illustrate elemental trends resulting from alteration of the Limerick volcanic samples with the most likely explanation of that trend stated. Dashed ellipses indicate anomalously high Zr/TiO_2 samples discussed in section 4.4. Majority of error bars smaller than symbols on plot, a full range of error values can be found in supplementary material 2.4.

5.7.2 Major and trace element interpretations

On each of the major element graphs of Fig. 5.9, a group of upper diatreme samples have an anomalously high Zr/TiO_2 value, outlined by dashed ellipses and discussed in section 4.4. Rutile is visible on SEM images throughout the Limerick volcaniclastic deposits, in the form of small granular rutile crystals and intergrown with ore-forming minerals, such as sphalerite and galena, within xenoliths toward the base of the diatreme. On average, middle and lower diatreme samples contain 4–9 % rutile with accumulations reaching as high as 34 % (see Fig. 5.4), compared to an average of 2.5 % for the upper diatreme. However, it is a combination of high Zr values with low Ti that makes the upper diatreme distinctive.

Most samples show a higher Al content relative to a general continental basalt data distribution (see Fig. 4.1 and Fig. 5.9), with the BMB volcanic samples containing the highest concentrations. In general, the upper diatreme samples contain a consistently low proportion of Al, with the majority of points lying between 11–19 %, similar to the range for continental basalts in Fig. 4.1. Al is considered relatively immobile during hydrothermal alteration below 300 °C (Humphris and Thompson, 1978; Seyfried Jr and Mottl, 1982), and data most likely reflect primary concentrations. A large proportion of upper diatreme material would have been ejected into extra-crater deposits before being undercut and slumping into the diatreme. Head III and Wilson (2003) have determined that submarine density current temperatures generally vary between 11–99 °C, temperatures below that required for Al mobility. The lower diatreme samples contain up to 22 % Al, Knockroe Formation samples up to 24 % and the BMB volcanic clasts up to 30 %. The higher concentrations of Al in the BMB clasts are most likely due to their higher proportion of illite as an alteration phase, which can reach up to 65 % in BMB-related volcanic material (see Fig. 5.8A). This is also reflected in the concentration of K_2O in BMB volcanics, Knockroe Formation deposits and the lower diatreme, the majority of which lie above the continental basalt data distribution, ranging between 4–11 %. Enrichment of K_2O is common during seawater alteration of basalt at low temperatures, with a very high seawater to rock ratio (Bednarz et al., 1991) – conditions pertinent during the deposition of the Knockroe Formation extra-crater deposits.

Ca content varies considerably between samples, with the highest values of >45 % occurring within BMB volcanic clasts. High values of 10–30 % CaO occur within the mid and

lower diatreme as well as intrusion samples and other BMB volcanic clasts, most likely due to partial replacement by dolomite and calcite (see Fig. 5.4A and 5.4C). Samples that lie below the continental basalt data distribution have most likely been leached of CaO during interactions of basalt with seawater (Humphris and Thompson, 1978).

Iron concentrations are extremely variable throughout the samples, most likely due to leaching of Fe and local precipitation as pyrite and Fe oxides (Utzmann et al., 2002). Upper diatreme samples lie predominantly above the continental basalt data distribution. Clay alteration phases consist primarily of Mg-rich chlorite (52 %) and smectite (28 %) (Fig. 5.8A), therefore high Fe concentrations are most likely due to its uptake by smectite in the slightly acidic and relatively low temperature environment (200 °C; Mottl et al., 1979). BMB volcanics contain negligible Fe, most likely due to leaching by hydrothermal fluids. The lower diatreme and intrusion samples exhibiting <5 % Fe, have most likely experienced similar leaching by these fluids. Mn follows a very similar trend to that of Fe. The majority of samples appear to be leached of Mn, as expected in a water-rich environment (Mottl et al., 1979; Seyfried Jr and Mottl, 1982). However, Mn appears to be concentrated in a group of the upper diatreme samples, most likely due to its uptake during alteration to smectite (Mottl et al., 1979) and formation of other precipitates (Utzmann et al., 2002).

Samples containing >7 % Mg are most commonly from the upper diatreme and Knockroe Formation samples, with an upper diatreme group containing an anomalously high concentration between 20–25 %. This is most likely due to removal of Mg from seawater during its interaction with host basaltic material and incorporation into secondary clays (Humphris and Thompson, 1978; Seyfried Jr and Mottl, 1982; Utzmann et al., 2002), in this instance the Mg-rich chlorite observed in the Knockroe Formation and upper diatreme deposits. Concentrations of MgO in lower diatreme samples is lower (2.9 %) than that of the upper (12.3 %) and middle diatreme (5.8 %). This observation is consistent with the lack of a Mg-bearing clay phase in the lower diatreme (see Fig. 5.8A). The passage of hydrothermal fluids may therefore have leached Mg from the lower diatreme and BMB volcanic clasts, contributing to the precipitation of secondary dolomite in these environments.

A small proportion of diatreme and intrusion samples lie within Na continental basalt data distribution. However, a large number of BMB volcanic, Knockroe Formation and

upper diatreme samples contain negligible Na. Lower diatreme samples contain higher concentrations of Na, up to 9.5 %. Na is often released during low temperature (>4 °C) alteration processes (Seyfried Jr and Mottl, 1982; Bednarz et al., 1991; Utzmann et al., 2002), however the lower diatreme would have cooled over longer timescales, retaining or perhaps becoming slightly enriched in Na during alteration at higher temperatures (Bednarz et al., 1991; Utzmann et al., 2002).This coincides with large-scale overprinting of primary mineralogy in the lower diatreme by a greenschist metamorphic assemblage including Na-rich albite (see Fig. 5.4A and 5.4C). The higher temperature alteration due to hydrothermal fluid flow would have caused a net uptake of Na_2O (Bednarz et al., 1991) during alteration of the lower diatreme samples.

Most samples lie within or below the continental basalt data distribution for SiO_2. A small proportion of lower and upper diatreme samples exhibit higher concentrations of SiO_2, up to 70 %, most likely the result of leaching and re-precipitation of silica during interaction of seawater and hydrothermal fluids with the basaltic material (Humphris and Thompson, 1978; Seyfried Jr and Mottl, 1982). This is consistent with large-scale overprinting of primary volcanic minerals and textures by amorphous silica observed in SEM images (see Fig. 5.3A).

Nb data are consistent with that of the continental basalt data distribution, indicating that variations most likely result from magma fractionation. Pb concentrations however, appear to lie below the continental basalt data. The exception to this is the four lower diatreme and two intrusion samples which likely have undergone small-scale precipitation of ore-forming minerals, including galena, during the passage of hydrothermal fluids. Samples containing lower Pb concentrations have most likely been leached to various degrees by hydrothermal fluids. Zr/Y ratios appear to follow a similar gradient to the continental basalt data, but positively translated to slightly higher values. This most likely reflects higher concentrations of Zr in relation to Y, as evidenced by positive Zr anomalies observed in both diatreme and Knockroe Formation samples in Fig. 4.4. Ba and Sr are considered to be the least mobile of the alkali earth metals (Aiuppa et al., 2000), however the Limerick data for both elements lie within the lower section of the continental basalt data distribution. This and the Ba/Sr ratio suggests some loss of both elements, most likely due to alteration and leaching by hydrothermal fluids. Th is a relatively immobile trace element, usually retained by basalt during alteration

processes (Aiuppa et al., 2000); enrichment is therefore most likely due to mass loss during alteration.

5.8 Alteration index

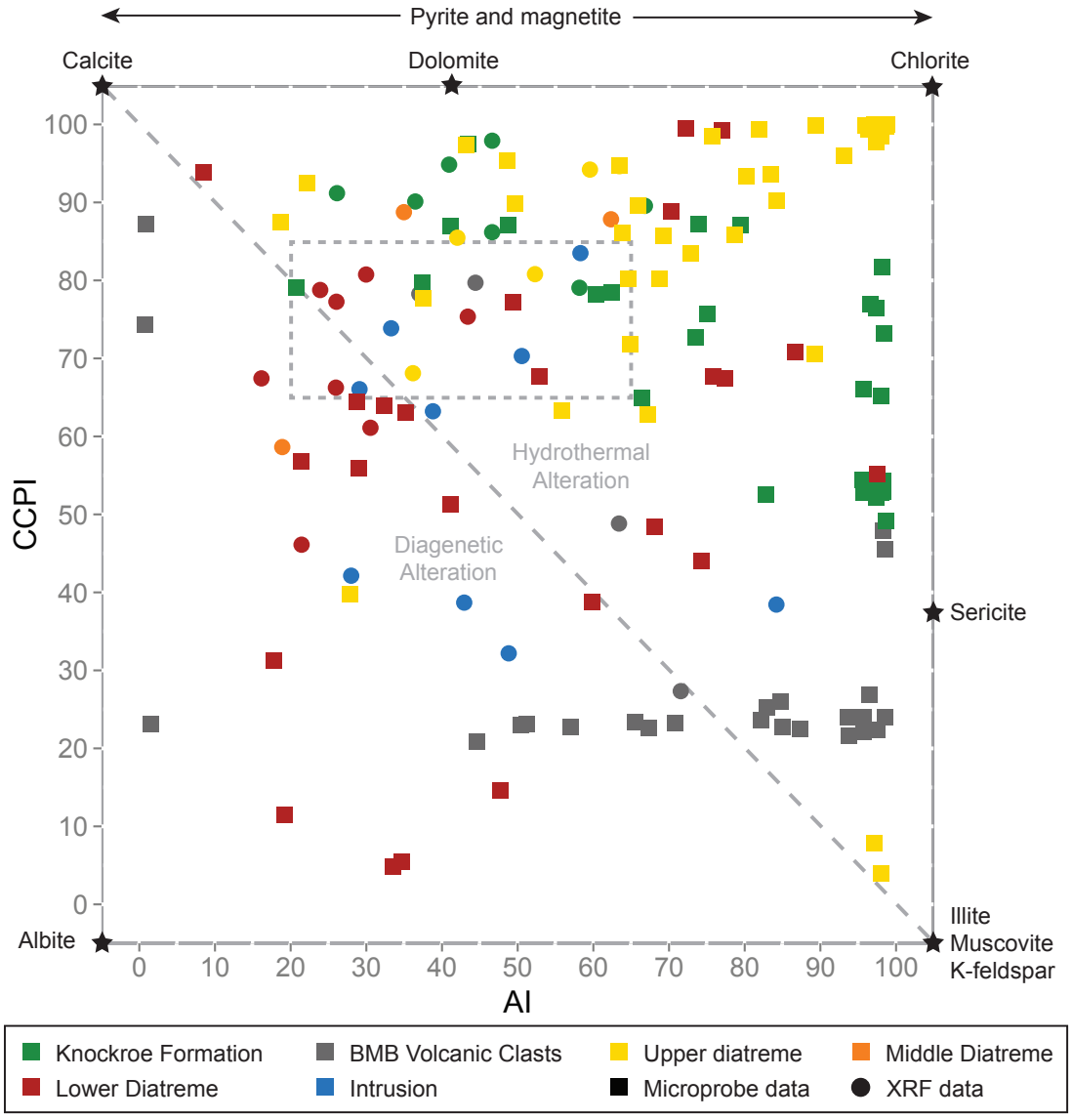

FIGURE 5.10: Graph plotting CCPI (chlorite-carbonate-pyrite-index) on the y axis against AI (Ishikawa alteration index) on the x axis, modified after Large et al. (2001). Black stars indicate where certain secondary minerals pertaining to the Limerick system lie on the index. The dashed box indicates the expected range of relatively unaltered andesite/basalt samples as determined by Large et al. (2001). Dashed line joining calcite and illite represents a generalised separation between diagenetic and hydrothermal alteration fields. Changes in colour represent different sample environments, symbols represent method of data analysis.

The Alteration Index (AI) was developed by Ishikawa et al. (1976) to represent the elements gained (Mg, K) and lost (Na, Ca) during the breakdown of Na-plagioclase and volcanic glass by chlorite and sericite alteration (Large et al., 2001; Gifkins et al., 2005). High values (>60) represent high proportions of MgO and K_2O in relation to CaO and Na_2O, resulting from intense hydrothermal alteration. Low AI values (<30) may be due to intense albite or calcite diagenetic alteration (Gifkins et al., 2005). AI values of ∼100 represent complete replacement of feldspars and glass by chlorite and/or sericite (Large et al., 2001). The AI equation (Eq. 5.2) ratios elements gained during chlorite alteration over elements lost and gained (Large et al., 2001).

Eq. 5.2: $AI = 100 * [MgO + K_2O] / [MgO + K_2O + CaO + Na_2O]$

The chlorite-carbonate-pyrite index (CCPI) was developed to quantify the gains of MgO and FeO and the losses of Na_2O and K_2O (Eq. 5.3), during the replacement of feldspars or sericite with Mg-Fe chlorite (Large et al., 2001; Gifkins et al., 2005). High CCPI values reflect high proportions of MgO and FeO which may be caused by alteration to chlorite, or Fe-Mg-rich carbonates such as dolomite, in addition to enrichment in pyrite magnetite or hematite (Large et al., 2001; Gifkins et al., 2005).

Eq. 5.3: $CCPI = 100 * [MgO + FeO] / [MgO + FeO + Na_2O + K_2O]$

Each of these two indices has limitations. The AI does not take into account carbonate alteration, which is common during hydrothermal alteration and can cause a decrease in AI value (Large et al., 2001; Gifkins et al., 2005). Magma fractionation strongly affects the CCPI index. Mafic rocks that contain high proportions of primary FeO and MgO display high CCPI values, reaching as high as 70–90 in some unaltered basalts (Large et al., 2001). The alteration box plot shown in Fig. 5.10 combines these two indices in order to over come their limitations, effectively discriminating between sericite, chlorite and carbonate alteration in addition to discriminating between hydrothermal and diagenetic assemblages (for full discussion please refer to Large et al., 2001; Gifkins et al., 2005).

Values for these two indices based on Limerick XRF and microprobe data are displayed on Fig. 5.10. The upper diatreme samples have high CCPI values, the majority >65,

but a range of AI values between 15–98. These values are consistent with a hydrothermal chlorite-carbonate trend, most likely resulting from enrichment of Mg within the volcanic clasts and mobilisation of Ca during seawater-basalt interactions (Seyfried Jr and Bischoff, 1979; Seyfried Jr and Mottl, 1982; Utzmann et al., 2002). This is also true of the Knockroe Formation samples, although these have a greater range in CCPI values between 50–97, possibly representing a small proportion of samples replaced by sericite. Relatively unaltered volcanics plot within the middle of the two axes, within the centre of the graph. However, this is not the case for the lower diatreme samples that lie within the central field. The lower diatreme has been overprinted by a greenschist metamorphic assemblage, including albite, calcite, chlorite, dolomite, illite and pyrite. Therefore it is much more likely that these samples lie within the central field due to the combination of minerals they contain. Polymict BMB volcanic clasts cross the hydrothermal and diagenetic fields at the higher end of the AI index (45–100) and the lower end of the CCPI index (majority between 20–28). This most likely reflects the high degree of replacement by illite, concentrations of which vary between 20–65 % (see Fig. 5.7 and supplementary material 5.2). Approximately half the intrusion samples lie with the box representing ranges for relatively unaltered basalts.

5.9 Discussion

5.9.1 Mineralogical clues to diatreme history

Pervasive alteration of the diatreme-fill has obscured the primary mineralogy, forming an assemblage of secondary minerals summarised in Fig. 5.7. Juvenile lapilli and glass shards in the upper diatreme and extra-crater deposits have been altered and overprinted by an assemblage of albite, calcite, silica and various clay and metallic phases. This mineralogical assemblage is a common feature of the greenschist facies (Deer et al., 1996) resulting from contact or thermal metamorphism (Meldrum et al., 1994).

The fluid most commonly associated with this mineralogical assemblage is aqueous (Miyashiro et al., 1971; Wood and Graham, 1986), most likely derived from the infiltration of seawater through the diatreme infill and its subsequent heating. The presence of analcime within vesicles to lapilli suggests the fluid was of moderate salinity (Deer et al., 1996). The large-scale over-printing by albite, calcite and silica suggests the fluid

must have been rich in Na, Ca, and Si. The remobilisation of Ca, Na and Si occurs during the interaction of hot basalt and seawater at temperatures >150 °C (see Fig. 5.1) (Humphris and Thompson, 1978), however the high Na concentration may also have been an original property of the saline fluid (see section 1.3).

The presence of illite and greater concentrations of metallic phases suggests that the lower orange-red diatreme section was exposed to different fluids than the upper diatreme. Localised dissolution and re-precipitation of calcite and silica overprinting pre-existing mineralogy is observed in the lower diatreme. This is a similar mineral assemblage to that of the upper diatreme but with what appears to be more pervasive greenschist metamorphism. The decline in chlorite proportions suggests that hydrothermal fluids have leached both Mg and Fe (Deer et al., 1996) from the juvenile volcaniclastic material, most likely becoming concentrated within secondary dolomite within the lower diatreme and BMB matrix. The presence of illite as opposed to kaolinite as the predominant alteration product within the lower diatreme, indicates that these fluids were of moderate acidity (Deer et al., 1996). As such, these hydrothermal fluids are unlikely to have been seawater-derived fluids similar to those responsible for upper diatreme alteration.

The mineralogy and texture of the upper Knockroe Formation pyroclastic lithofacies (Fig. 5.6D) is very similar to that of the uppermost diatreme. They both exhibit sanidine crystals and an Mg-rich variety of chlorite, which is most likely due to the uptake of MgO by the basalt from seawater at temperatures >70 °C (Humphris and Thompson, 1978; Mottl et al., 1979; Seyfried Jr and Bischoff, 1979; Utzmann et al., 2002). These common characteristics suggest that this Knockroe Formation lithofacies most likely originated from within the diatreme and were ejected, becoming interbedded with crinoidal limestone in a shallow marine environment (Somerville et al., 1992). However, the fine-grained laminated tuff lithofacies exhibits entirely different characteristics to the upper Knockroe Formation, and could originate from an initial stage of high magma flux and explosive magma-water interaction (see chapter 3).

5.9.2 Relation of BMB to diatremes

An important question is whether the volcanogenic agglomerate clasts within the polymict BMB originated from within the diatreme. If so, this would provide circumstantial evidence that the diatreme was emplaced prior to BMB formation and that the dolomitising fluids responsible for its precipitation utilised the diatreme for fluid flow. Unfortunately, the clasts have been completely altered by the BMB fluids and have acquired the mineralogy of the BMB matrix, exhibiting no evidence of primary mineralogy.

BMB clasts exhibit the same large-scale inter-grown precipitation of dolomite, calcite and silica seen within the lower sections of the diatremes, albeit in higher concentrations. The diatreme samples also contain apatite and illite, which are present in large quantities within the BMB clasts. Therefore the diatremes have experienced very similar alteration and mineral precipitation to the BMB clasts, although to a lesser degree. The sulphide phases within the lower diatreme, chalcopyrite, galena, pyrite and sphalerite, are also the common metallic phases reported within mineralised sections of the BMB (Hitzman and Beaty, 1996; Hitzman et al., 2002; Redmond, 2010). Consequently, the diatreme must have been exposed to the passage of BMB-forming and mineralising fluids. In addition, Fig. 4.4 shows very similar REE patterns for the diatreme and BMB clasts, therefore it is highly likely that these agglomerate clasts originated from within the diatreme.

Chapter 3, summarising physical volcanological processes that occurred at Limerick, shows the relationship between the diatremes and incidences of BMB horizons within surrounding boreholes (Fig. 3.3). This shows that the shallowest BMB horizons are of equal or greater depth than the thick intrusion at 146.5–191.5 mbgs. Incidences of BMB (documented in drill-cores) are also greater proximal to the diatreme and pinch out with distance from this centre. Dolomite, a key mineral within the BMB assemblage, increases in proportion just below this intrusion down to 22 % at 515 m. Diatreme dolomitisation, in addition to the presence of diatreme clasts within BMB horizons, suggests that hydrothermal dolomitising fluids, often associated with large-scale faults within the Irish Midlands (Hitzman and Beaty, 1996), utilised the diatreme as a conduit. Hydrothermal fluids would have flowed upwards within the diatreme, driven by vertical pressure gradients (Afanasyev et al., 2014); however, within diatreme 19, these would have been unable to penetrate the thick intrusions. As a result, the fluid would have most likely exploited fractures radiating out from diatreme 19 within the surrounding country

rock. The orange-red colouration seen within diatremes 19 and 28, below the dashed line in Fig. 3.3, is therefore resulting from the complete hematisation of glass within juvenile material, reported elsewhere by Aranda-Gómez and Luhr (1996), coupled with the presence of disseminated iron phases. The intrusion would have acted as a barrier to rising acidic hydrothermal fluids responsible for BMB formation, explaining why this colouration is restricted to greater depths within diatreme 19 (as compared to 28).

5.9.3 Spinel comparison

Two types of spinels have been observed within the diatreme samples. The first type are associated with hydrothermal silica, calcite or altered xenoliths, and the second type are larger zoned spinel crystals, thought to be xenoliths observed within the lapilli tuff matrix or within the juvenile lapilli.

The first type of spinel is associated with, and often inter-grown with, secondary minerals in fibrous masses and are assumed to be hydrothermal in origin. These spinels are unzoned and often composed of pure magnetite, occasionally with small substitutions of Zn, Cr, Ti and Al throughout the entire crystal. The conditions required for these to form include high temperatures up to 350 ^{o}C, high pH and a saline solution containing NaCl (Gainsford et al., 1975). These conditions are attributed to mixing of the two different hydrothermal solutions that were thought to have reached a maximum of 280 ^{o}C, and would have contained large amounts of NaCl originating from the percolating seawater (Banks et al., 2002; Wilkinson et al., 2005*b*).

Zoned spinels have an inner core of Cr, Al and Zn-rich spinel surrounded by almost pure magnetite or titanomagnetite. The inner core is thought to represent the primary spinel that crystallised deep within the magmatic system. The secondary outer spinel is thought to have formed as a result of reaction with the host magma in which it became entrained (Tracy, 1980; Wang et al., 2012). The enrichment of Fe and Ti in the secondary spinels suggests that the magma they crystallised from was fractionated (Tracy, 1980) with a TiO_2 concentration greater than 4 wt.% and FeO/MgO ratio >2.7 (Thy, 1983).

5.10 Conclusions

Volcaniclastic deposits at Limerick have been pervasively altered and replaced by a number of fine-grained clay phases, albite, silica and calcite. The lower section of the diatreme has been overprinted with a greenschist metamorphic assemblage and experienced various degrees of dolomitisation and local, small-scale precipitation of ore-forming minerals. Metamorphism in the upper diatremes most likely resulted from heated seawater percolating through the breccia and fractured country rocks, whereas the lower diatreme appears to have been altered by hydrothermal fluids. This evidence, combined with the entrainment of diatreme agglomerate clasts into polymict BMB, indicates that the diatremes acted as conduits, utilised by the same hot hydrothermal fluids that formed the BMB horizons. These fluids were unable to penetrate the thick crosscutting intrusions of diatreme 19; therefore under hydraulic pressure, the fluid most likely exploited the extensive network of fractures and resulting permeable breccias radiating out from the diatreme, entraining clasts of volcanic material.

Although evidence indicates mineralising fluids passed through the diatremes, this does not prove that the diatremes had an active role in forming or contributed to the mineralisation of BMB horizons. The diatremes may have acted solely as inert highly permeable conduits for the fluids, similar to a fault in the 'traditional' Irish-type mineralisation model. Alternatively, the diatremes may have actively contributed to mineral formation, for example providing heat required for the hydrothermal system or important ore-forming elements. However, analysis of the clay phases at the top and base of the diatremes have indicated that iron and magnesium have been leached from juvenile lapilli within the lower diatremes, and may provide the first clue to answering this question.

Chapter 6

A role for diatremes in the formation of Pb-Zn mineralisation of the Limerick District of the Irish Orefield: The sulphur isotope evidence

6.1 Summary

The Irish Orefield is a source of base metals of global importance. The Irish-type mineralisation model involves large-scale extensional faults acting as fluid pathways for two hydrothermal fluids; a shallower, cooler sulphur-rich brine and a deeper, hotter metal-rich fluid thought to be of basement origin. Select mineral deposits within the Irish Orefield have been hypothesised to be linked to large-scale Carboniferous volcanism, but evidence has not previously been documented to confirm this relationship. Exploration drilling within the Limerick Basin discovered five diatreme-related areas in close spatial and temporal association with black matrix breccia (BMB) horizons replaced by Pb-Zn mineralisation. Thus a link between volcanism and mineralisation is credible, and a hypothesis to be tested in this chapter. Field relationships, petrology and sulphur isotope data are combined in this study to explore the genetic relationship between the

BMB horizons and diatreme emplacement. BMB formation appears to post date diatreme emplacement on the basis of diatreme clasts incorporated within polymict BMB horizons. Further, dolomite, which forms the majority of the BMB matrix, overprints the lower half of the diatreme-fill, suggesting a compositional link. The small concentrations of ore minerals replacing the lower diatremes, suggests that both BMB and mineralising fluids utilised the diatremes as conduits, in a similar manner to that of a fault zone or other structural discontinuity. However, relative to other Irish deposits, the heavier sulphur isotope values observed at Limerick suggest that the diatremes exerted an appreciable impact on mineralisation. We suggest that the maar-diatremes provided a higher porosity and permeability, creating a greater capacity for fluid flow. Large volumes of volcanic material also provided a third magmatic sulphur source as well as important ore-forming constituents such as heat and leached elements.

6.2 Introduction

The Irish Orefield is an important and historical global source of lead and zinc, hosting many large hydrothermal base metal deposits and prospects (see Fig. 1.2), with three mines producing 2.3 % and 0.7 % of the world's supply of Zn and Pb, respectively, in 2014 (USGS 2015 Mineral Commodity Report). The largest of these three mines is at Navan, which dominated European Zn productions for more than 20 years (Ashton et al., 2015). There is still controversy as to whether the Irish-type deposits are the result of syngenetic exhalation and seafloor deposition (Banks, 1985; Boyce et al., 2003) and/or epigenetic replacement of hydrothermal breccias (LeHuray et al., 1987; Hitzman and Beaty, 1996; Anderson et al., 1997; Hitzman et al., 2002; Wilkinson et al., 2005*b*; Redmond, 2010). The age and timing of mineralisation varies across the orefield, between the early Tournaisian and the end of the Visean (359–326 Ma) (Boyce, 1983; Smith et al., 1994; Hitzman and Beaty, 1996; Sevastopulo and Redmond, 1999; Blakeman et al., 2002; Reed and Wallace, 2004; Wilkinson et al., 2003; Hnatyshin et al., 2015).

The genetic model for Irish-type ore deposits, involves large-scale extensional faults acting as fluid pathways, allowing the mixing of two hydrothermal fluids (Wilkinson et al., 2005*b*; Davidheiser-Kroll et al., 2014). Fluid inclusion studies have shown that one of the fluids was relatively shallow, and thought to be a seawater derived brine at $<140\,^{\circ}C$ with 25 wt % NaCl equivalent salinity, and a high concentration of bacteriogenic sulphide

(Everett et al., 1999; Banks et al., 2002; McKillen and Tyler, 2003). The bacterial reduction of sulphate to sulphide causes depletion in ^{34}S, producing in some open system environments, δ^{34}S values as low as -48 ‰ (Rollinson, 1993). A deeper fluid, thought to be metal-rich, was of a higher temperature (200-280 ^{o}C) and more moderate salinity (12–18 wt % NaCl equivalent) (Everett et al., 1999; Banks et al., 2002; McKillen and Tyler, 2003). The fractionation of ^{34}S at the higher temperatures present within hydrothermal fluids, causes enrichment in ^{34}S, leading to positive δ^{34}S values of up to +26 ‰ (although this fractionation is also dependent on other factors such as pH, oxygen and cation activity) (Rollinson, 1993). Large-scale sulphide precipitation occurred during mixing of these two fluids, epigentically replacing dolomite BMBs (Wilkinson et al., 2005*b*). Mantle-derived sulphur tends to have a δ^{34}S value of 0 $\pm$ 3 ‰, considered to be a primitive mantle value (Rollinson, 1993).

The Limerick Basin lies within the south-western Irish Midlands, in a highly faulted area to the south of the Iapetus Suture Zone (see Fig. 1.2 and 3.2). Mineralisation at Limerick is unusual, in the Irish context, due to the presence of a cluster of Viséan aged basaltic diatremes that erupted into a shallow marine environment, and which are spatially and temporally associated with mineralisation (see Redmond, 2010; McCusker and Reed, 2013; Elliott et al., 2015). Diatremes are irregular cone shaped pipes up to 2.5 km deep that erupt through country rock stratigraphy (Lorenz, 2003; Valentine, 2012) and are expressed at the surface as maar craters or tephra rings (Lorenz, 1975). The diatreme eruptions in the Limerick district were largely phreatomagmatic in nature, creating an extensive network of fractures in the surrounding country rock and containing accumulations of volcaniclastic and lithic fragments (see chapters 3 and 5). The high heat flow arising from volcanism, and surplus of water in a shallow marine environment and cavity-rich limestone, have potential implications for the development of hydrothermal systems early in the eruptive history of the diatreme cluster.

The presence of these diatremes offers an alternative hypothesis that the carbonate-hosted Pb-Zn deposits were directly related to Lower Carboniferous magmatic activity (Redmond, 2010; McCusker and Reed, 2013). In this chapter, we describe sulphur isotope data to elucidate the role of the diatremes in the Limerick Basin mineralisation system.

6.3 Geotectonic setting and terminology

The Limerick Basin has been explored since 2005, resulting in two discoveries at Pallas Green and Stonepark (Tyler, 2007; Redmond, 2010). Here, Pb-Zn mineralisation replaces hydrothermal Black Matrix Breccias (BMBs) or internal sediments formed within the reef carbonates of the Waulsortian Formation (Hitzman et al., 2002; Wilkinson et al., 2005*b*; Redmond, 2010).

Within the Limerick license area five diatremes have been identified, intersected by seven exploration boreholes. Two of the diatremes (19 and 28) have been imaged by magnetic surveys, and have minimum diameters of $\sim$ 170 m and $\sim$ 240 m respectively (see section 3.4.1 for more dimensions). Diatremes in Limerick are locally related to faulting, emplaced during the Carboniferous when Ireland and NW Europe experienced a major phase of NE-SW trending regional rifting that caused large-scale faulting and magmatism (Woodcock and Strachan, 2000; Wilson et al., 2004). This extensional regime was the product of episodic N-S back arc extension in response to reactivation of NE-SW trending Caledonian basement faults by the Variscan subduction zone (Woodcock and Strachan, 2000). Crustal extension allowed small volumes of basaltic magma to ascend and fractionate, exploiting weaknesses in the crust to reach the surface. Volcanism in Limerick is very similar in style and timing to activity elsewhere in the British Isles (see Fig. 1.1), e.g. Croghan Hill, Central Ireland (see Timmerman, 2004); Garleton Hills, Scotland (see Monaghan and Pringle, 2004) and the Beara Peninsula, Southern Ireland (see Pracht and Kinnaird, 1997; Pracht and Timmerman, 2004).

In the Limerick area, a series of Viséan aged (Somerville et al., 1992) extra-crater basaltic lava flows and pyroclastic deposits (Knockroe Formation), commonly interbedded with shallow marine greywackes and crinoidal limestones (Lough Gur Formation) (Strogen, 1988; Somerville et al., 1992; Holland and Sanders, 2009), were deposited adjacent to the diatremes (Fig. 6.2 and Fig. 1.4). Trace element analysis of juvenile material from the extra-crater and diatreme facies has confirmed that the two are likely related, with the Knockroe Formation sequence predominantly sourced from diatreme eruptions (see chapters 3 and 4). The greywackes overly and are part of a transgressive series of carbonates that dominate the Limerick basin (Holland and Sanders, 2009).

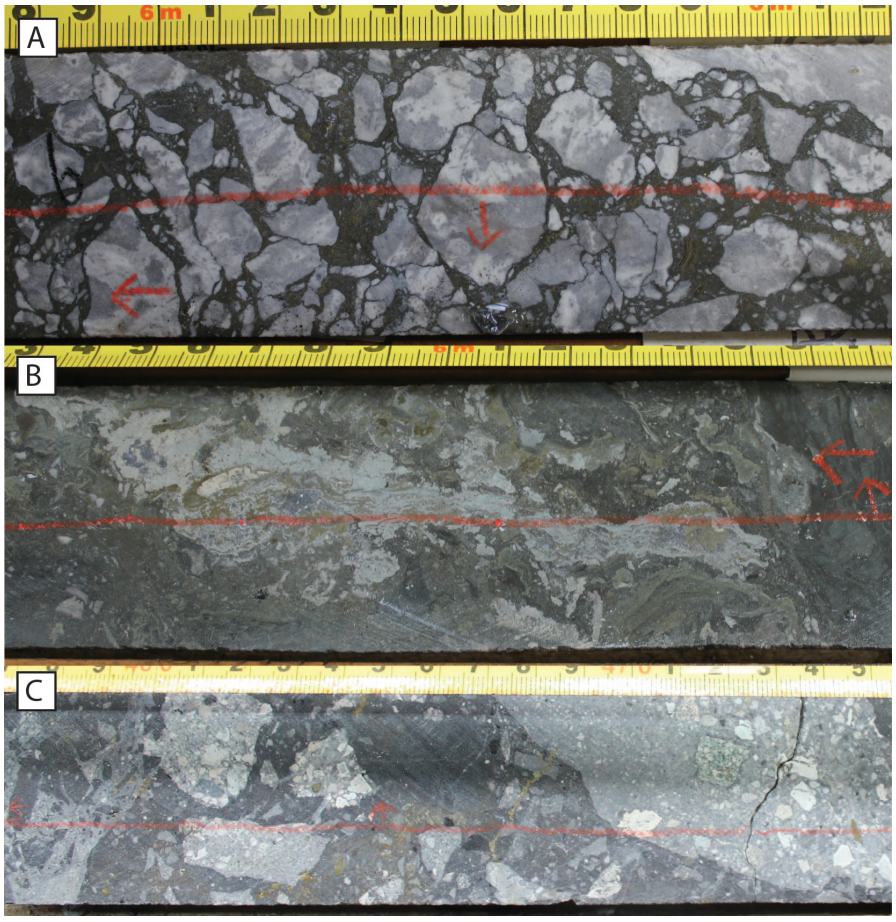

FIGURE 6.1: Photos of each BMB type sampled at Limerick. **A:** Country rock BMB. Clasts of Waulsortian Limestone country rock displaying embayed edges and often jigsaw or float textures between clasts. Matrix is relatively unmineralised, exhibiting pyrite replacement. Borehole TC-2638-036, 292.4 mbgs. **B:** Replaced BMB. Matrix and clasts of this breccia have been completely replaced by ore-forming minerals sphalerite, galena and pyrite. Traces of pre-existing clasts can be determined in the bottom left corner. Borehole TC-2638-055, 196.6 mbgs. **C:** Polymict BMB. Breccia containing clasts texturally and compositionally similar to diatreme-fill, and immobile trace elemental trends indicate are most likely sourced from the diatremes. Matrix exhibits partial replacement by pyrite, in addition to pyrite veins cross-cutting both matrix and clasts. Borehole TC-2638-047, 59.1 mbgs.

Country rock BMBs are defined as containing carbonate clasts, commonly with embayed edges in dark relatively unmineralised matrix, exhibiting minimal pyrite replacement (see Fig. 6.1A). Replacement of BMBs can be complete or partial, with a range of sulphide-host rock textures ranging from layered to intergrown. Ore-forming minerals consist of sphalerite, galena and pyrite with very minor quantities of chalcopyrite and arsenopyrite. However those termed 'replaced BMBs' contain both clasts and matrix completely replaced by ore minerals (see Fig. 6.1B). Polymict BMBs contain a range of clast types including volcanic, crystalline igneous and country rock clasts in a relatively unmineralised dark matrix (see Fig. 6.1C). Neither ore clasts or BMB clasts are observed

within the diatremes or BMB horizons, clearly indicating that diatreme emplacement pre-dated BMB formation, which is in turn post-dated by mineralisation.

The majority of BMB horizons lie below the level of dolomitisation in the lower diatremes (Fig. 6.2). They are more concentrated adjacent to the diatremes, pinching out with distance. Zn and Pb concentrations are also high in close proximity to the diatremes with concentrations of 27 % Zn and 12 % Pb ∼ 150 m southwest of diatreme 19 (see Fig. 6.2).

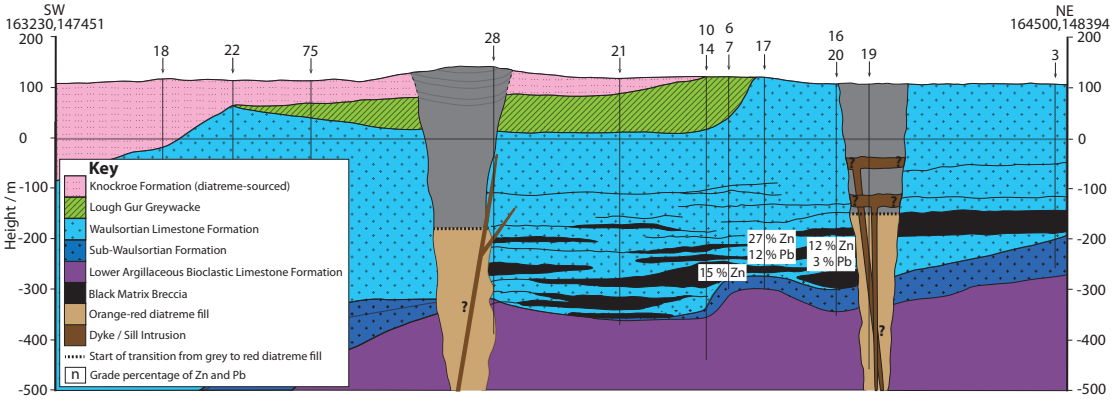

FIGURE 6.2: Cross-section depicting diatremes 19 and 28 (named from intersecting boreholes) and adjacent mineralisation grades courtesy of Teck Ireland Ltd. Grades are positioned over boreholes from which they were sourced and at the corresponding depth. Level of dolomitisation indicated by dotted line and change in diatreme colour. Horizontal scale = vertical scale, no exaggeration.

XRD and SEM analysis (chapter 5) identified dolomite overprinting the lower diatreme, increasing from 12 % to 22 % with depth (260–516 m). Dolomite is also a key mineral of the BMB, comprising ∼ 80 % of the matrix (see Fig. 5.7, 5.8 and supplementary material 5.3). A greenschist metamorphic assemblage of minerals overprints the diatremes, including albite, calcite, silica, pyrite, chlorite and various other clay and metal oxide phases, in addition to dolomite. Polymict BMB horizons contain diatreme clasts that exhibit a very similar mineralogy to that of the lower diatreme.

6.4 Sulphur isotope analysis

Samples from a variety of mineral environments including country rock, polymict and replaced BMBs at varying distances from the diatremes were analysed, in addition to Knockroe Formation pyroclastics, diatremes, dykes, xenoliths from the diatremes and sulphide-bearing veins in the Waulsortian Limestone. Sphalerite, galena and pyrite were

sampled from each environment in which they were present. High-grade mineralisation (>10 % Zn and 2 % Pb) was crushed, and sulphides separated from the host gangue by picking. Sulphides too small (or intergrown) for this technique were cut and prepared as polished blocks.

Crushed sulphide concentrates were analysed by conventional techniques (see Robinson and Kusakabe, 1975), in which SO_2 gas was liberated by combusting sulphides with excess Cu_2O at 900 °C in a vacuum. Liberated gases were analysed on a VG Isotech SIRA II mass spectrometer in the stable isotope laboratory at SUERC (East Kilbride), and standard corrections applied to raw $\delta^{66}SO_2$ values to produce true $\delta^{34}S$. Polished sulphide blocks were combusted in-situ by a laser in a vacuum chamber pumped with oxygen gas (Fallick et al., 1992). The SO_2 gas produced was purified in a glass extraction line to remove water and CO_2 then condensed into the mass spectrometer. $\delta^{34}S$ values were corrected for mineral-specific sulphur isotope fractionation, as discussed in Wagner et al. (2002). Samples were run with internal gas standard BG MAC and international standards CP-1, NBS-123 and IAEA-S3, repeat samples of which provided an average %RSD of -0.64 and %RD of -2.09. For the full methodology of conventional and laser sulphur isotope mass spectrometry procedures, please refer to Robinson and Kusakabe (1975); Fallick et al. (1992) and Wagner et al. (2002), section 2.9 and supplementary material 2.2.

6.5 Limerick isotope data

All samples analysed during this study were homogenous, except two which displayed colloform layering. Therefore the sulphur isotope values displayed in Fig. 6.3 and described in this section are not the result of sampling of sulphur from different phases or layers.

The unmineralised country rock BMBs contain pyrite with negative sulphur isotope values between -15 and -35 ‰ (Fig. 6.3A). Mineralisation within polymict BMBs varies from none, to solely pyrite to small concentrations of ore minerals. Sulphides are fine-grained, often occurring in small concentrations within the lapilli and breccia matrix. This variation in polymict BMB sulphides is reflected by the large range of isotopic values, between -45 ‰ and +10 ‰. Ore mineral isotopic values within the completely

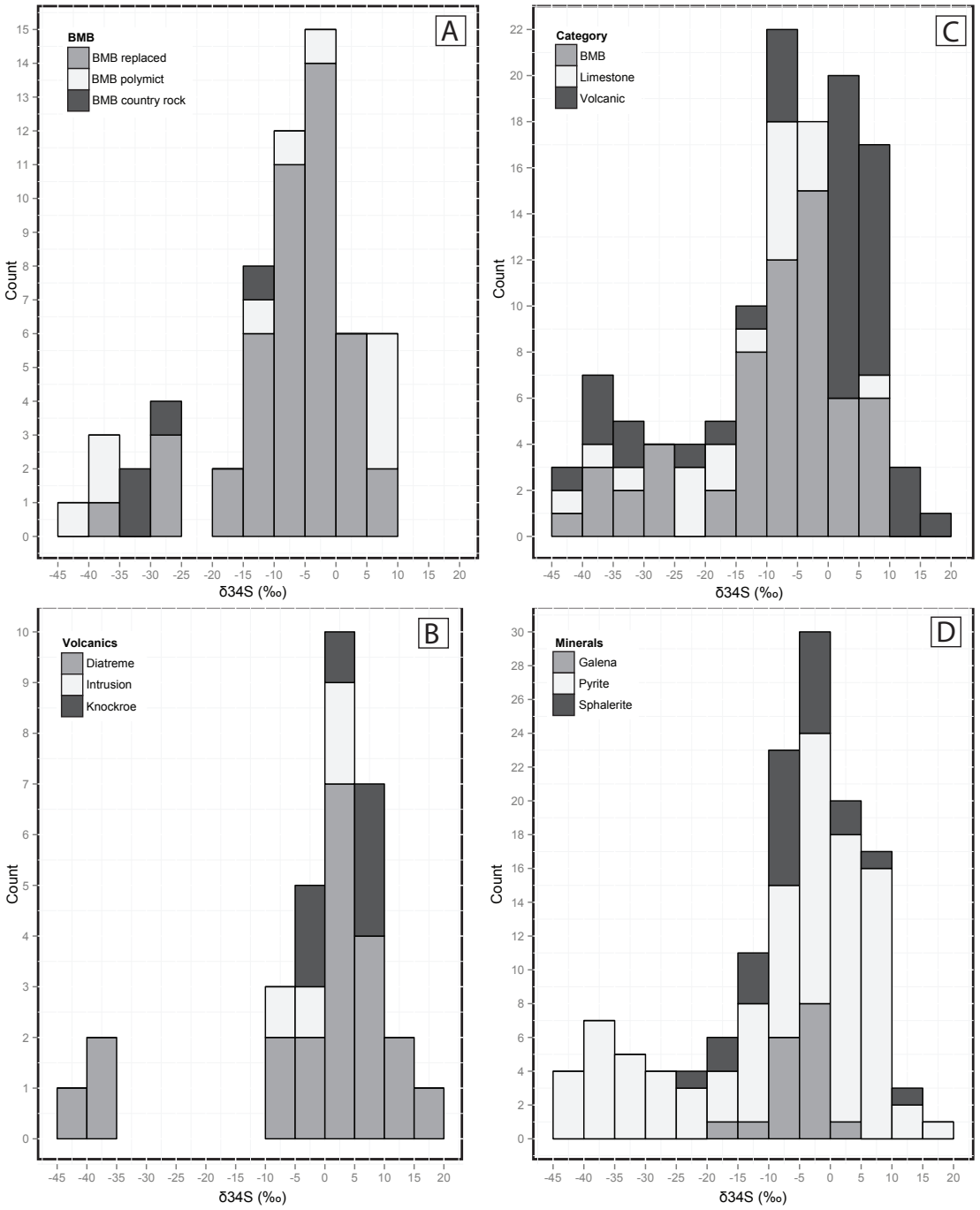

FIGURE 6.3: Graphs illustrating Limerick sulphur isotope data. **A:** BMB categories including country rock poorly mineralised breccia, polymict breccia containing volcanic and diatreme-related clasts, and breccia completely replaced by sulphides. **B:** Categories including BMB data, country rock limestone mineralisation and sulphides within volcanic material (diatreme and extra-crater Knockroe Formation deposits). **C:** Volcanic-related sulphur isotopes from diatreme, extra crater Knockroe Formation and relatively unaltered intrusion samples. **D:** Sulphur isotopes from different minerals within all environments.

replaced BMBs range from -20 to +5 ‰. However, over 70 % of the data lie between -10 and +1 ‰.

Sulphides within volcanic material show a much more restricted range, with the majority of data between -10 and +20 ‰ (Fig. 6.3B and 6.3C). Diatreme values vary greatly between -40 and +20 ‰, with a modal value of +4 ‰. Waulsortian Limestone-related mineralisation which includes veins, fractures and breccias are almost entirely negative, ranging between -45 to -1 ‰ with only one sample at +7 ‰ (Fig. 6.3C). Sulphides replacing igneous intrusions within the diatreme fill, have very similar values to that of the majority of volcanic samples, ranging from -7 to + 4 ‰. Five out of the thirteen intrusion samples lie at depths less than 100 m depth within borehole 19, above the depth of the 45 m thick intrusion at 147 m which acted as a barrier for fluid flow (see chapter 5). These five samples range between -3.6 to +4.9 ‰, averaging +0.97 ‰ and are considered to be relatively unaltered vesicular intrusions.

Ore-forming minerals, sphalerite and galena, display a different data distribution to that of the bimodal pyrite (Fig. 6.3D). Galena has a single modal value of -4.3 ‰, similar to the median for sphalerite at -5.6 ‰ (sphalerite has no modal value). Pyrite has a bimodal distribution of -37.7 and +1.0 ‰. Sphalerite and galena are predominantly

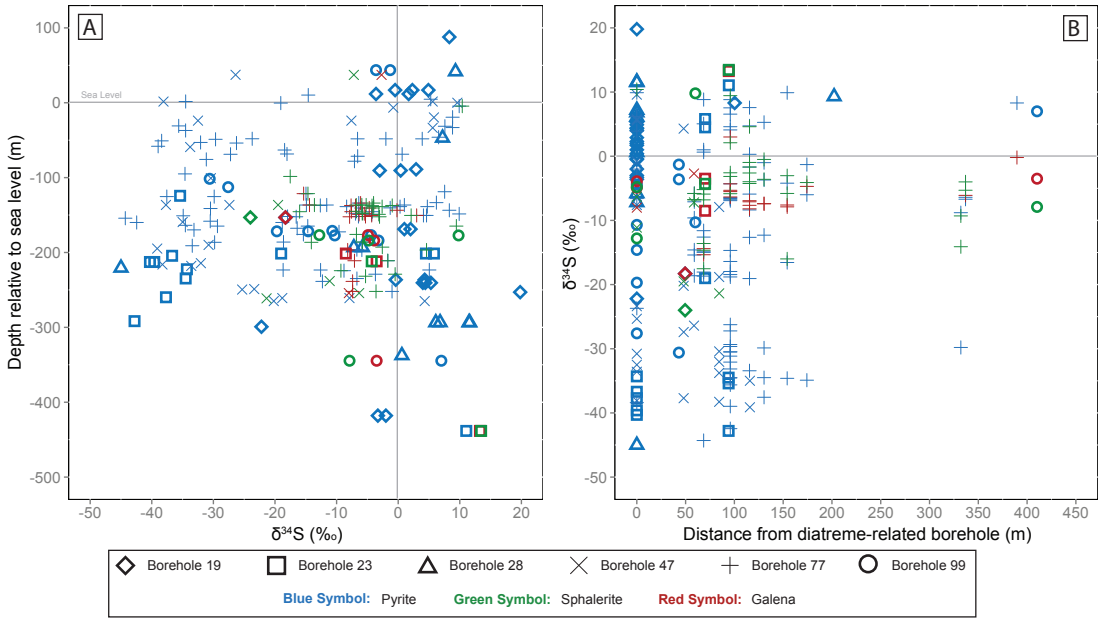

FIGURE 6.4: Graphs illustrating variations of sulphur isotope composition based upon mineralogy. Data set is a combination of values obtained by the author and by Kerr (2014). Data are categorised based on the nearest diatreme intersecting borehole. Borehole 19 is drilled directly down the centre of a diatreme, whereas boreholes 23, 28 and 99 are drilled down diatreme margins. Boreholes 47 and 77 contain intermittent polymict BMB and layered diatreme-fill. **A:** Variation of δ^{34}S with depth relative to sea level, to avoid variations due to surface erosion. **B:** Variation of δ^{34}S with distance from a diatreme intersecting borehole.

observed between 100-350 mbsl, whereas pyrite occurs from 100 masl to 427 mbsl (Fig. 6.4A). Sulphur isotope values at 100 mbsl range between -32 and +3 ‰, whereas values at depths of 200 mbsl have a narrower range between -9 and +9 ‰ (Fig. 6.4A). Diatreme sulphide samples are recorded at 0 m distance on Fig. 6.4B. Borehole 23, drilled down the margin of diatreme 19 (see Fig. 3.2), appears to contain predominantly negative δ^{34}S values between -34 and -40 ‰. The centre of the diatreme (borehole 19) tends to contain heavier sulphur isotopes, predominantly >-7 ‰. This trend is reversed within diatreme 28, the margin of which contains predominantly heavier sulphur isotopes (Fig. 6.4B).

6.5.1 Comparison with Irish Orefield deposits

Irish Orefield deposits are thought to comprise massive sulphides precipitated as a result of the mixing of two fluids (Wilkinson et al., 2005*b*; Davidheiser-Kroll et al., 2014). The seawater-derived low temperature brine is thought to contain high concentrations of bacteriogenic sulphur (negative δ^{34}S values; see Rollinson, 1993), and the deep-sourced metal-rich fluid is thought to be a source of hydrothermal sulphur (positive δ^{34}S values; see Rollinson, 1993) (Everett et al., 1999; Banks et al., 2002; McKillen and Tyler, 2003).

Ore-forming minerals (sphalerite and galena) at Navan show a bimodal sulphur isotope distribution with peaks at -10 and +7 ‰ (Fig. 6.5B). However the pyrite data range is much more negative than that of the galena and sphalerite. Pyrite ranges between -39 and -9 ‰, with a mode of -29.2, sphalerite has a range of -22 to +10 ‰, with a mode of -11.4 and galena has a range of -26 to +16, with a similar mode of -9.5. Deposits adjacent to faults at Navan and Lisheen contain more positive sulphur (Blakeman et al., 2002; Wilkinson et al., 2005*b*). This phenomenon is not observed at Limerick, with a range of positive and negative values existing adjacent to, and at distance from the diatremes (Fig. 6.4B). Limerick data distributions are more similar to the unimodal Lisheen dataset (see Fig. 6.5C), however the Lisheen mode is more negative at -10 ‰, compared to Limerick at -3 ‰.

The bimodal sulphur isotope distribution at Navan (Fig. 6.5B) is thought to reflect the mixing of the two sulphur sources (bacteriogenic and hydrothermal) (Blakeman et al., 2002), with >90 % of the sulphide ore minerals attributed to the bacteriogenic contribution (Fallick et al., 2001). Positive isotopic signatures adjacent to faults at Navan

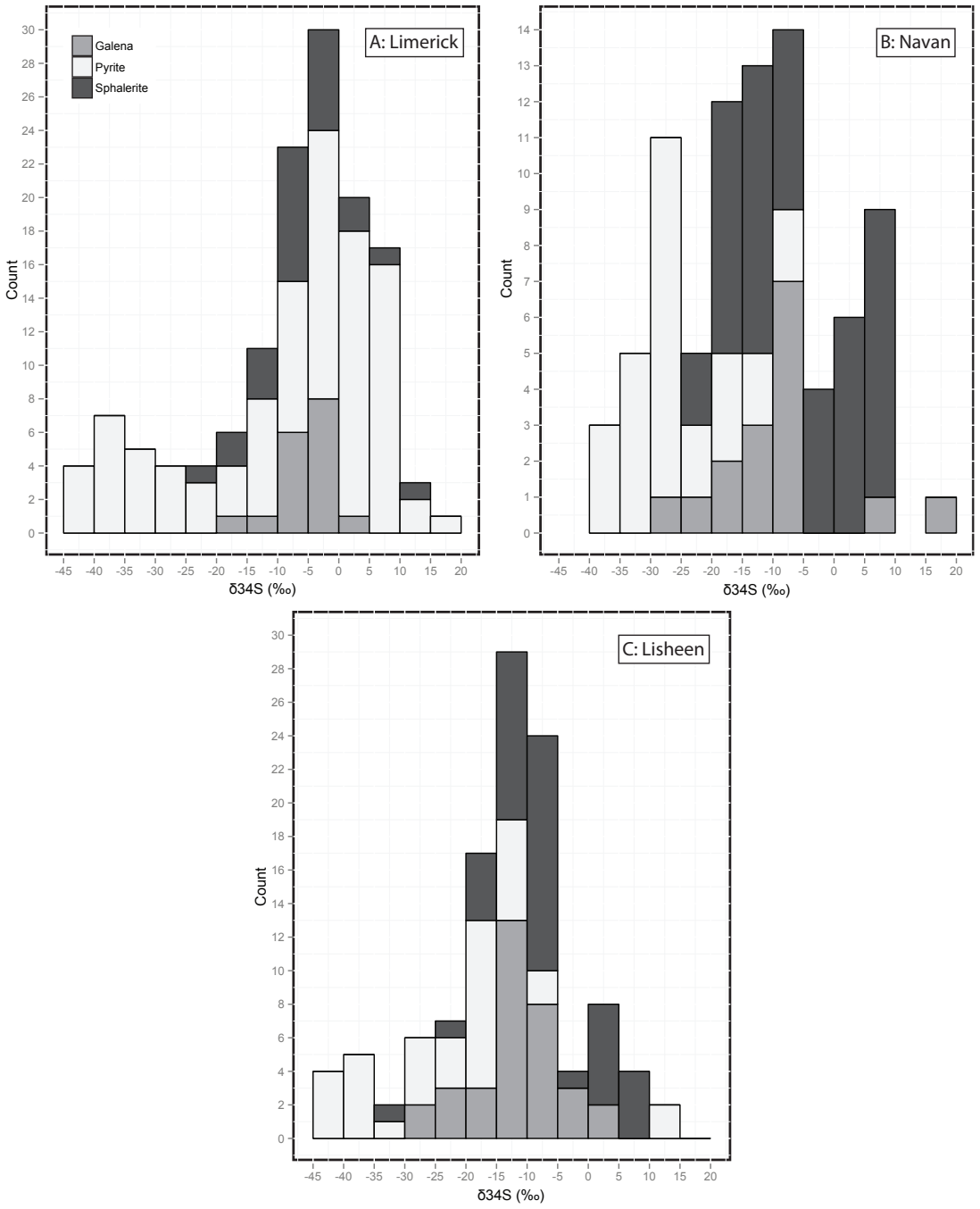

FIGURE 6.5: Sulphur isotope data from Limerick **(A)** compared to data from other Irish deposits including Navan **(B)** (Blakeman et al., 2002) and Lisheen **(C)** (Wilkinson et al., 2005*b*).

and Lisheen, suggest that they acted as fluid pathways for the deeply sourced, metal-rich fluid (Blakeman et al., 2002; Wilkinson et al., 2005*b*). This pattern is not observed at Limerick, which may be due to the diatremes acting as pathways for multiple pulses of the two fluids containing bacteriogenic and hydrothermal sulphur. This is analogous to pulses of bacteriogenic sulphur between mineralisation pulses at Navan (Blakeman et al.,

2002), and may explain the very light sulphur isotope signatures of the pyrite seen in all deposits within Fig. 6.5. The lack of massive sulphide deposition within the diatremes, suggests that pulses of these two fluids occurred at different times and did not mix to any great degree within the diatremes.

Limerick data are more similar to later stages of Lisheen ore formation, when hydrothermal components became more important (Wilkinson et al., 2005*b*). The more positive ore values at Limerick most likely reflect differences in the mineralising system not present at other ore deposits, for example the extensive Carboniferous volcanic system. The diatremes present a more permeable pathway down to depths >600 m and potentially >2.5 km (Lorenz, 2003; Valentine, 2012), allowing greater hydrothermal fluid flow from the basement and greater concentrations of more positive sulphur isotopes. The large volumes of highly alterable volcaniclastic material may have provided a third sulphur reservoir with a value of ∼0 ‰, which may have also skewed the data to more positive values. Blakeman et al. (2002) states that bacteriogenic sulphur was able to remain in solution due to a negligible presence of iron in the host rock. However, at Limerick substantial quantities of iron would have been present in the volcanic material, scavenging bacteriogenic sulphur during the passage of fluid pulses and reducing its impact on the isotopic values and ability to precipitate massive sulphides. Different morphologies at Lisheen have been attributed to different ore-forming stages, and therefore exhibit different ranges of sulphur isotope values (Wilkinson et al., 2005*b*). However, no significant differences in isotopic value have been found between mineral morphologies at Limerick, this may indicate that morphology is dependent on factors other than ore-formation phase at Limerick. Sphalerite and galena at Lisheen exhibit increasingly heavy sulphur isotope values with depth (Wilkinson et al., 2005*b*). This trend is also visible at Limerick, with the majority of sphalerite and galena only occurring at or below 100 mbsl (Fig. 6.A).

6.6 Limerick interpretation: Diatremes as conduits?

The large range in sulphur isotope values observed at Limerick suggests that there must be at least two sources of sulphide, one bacteriogenic and the other hydrothermal in origin. The relatively unmineralised country rock BMBs have been interpreted as solely containing bacteriogenic sulphur, suggesting possible syngenetic precipitation

from BMB-forming fluids or precipitation from later brines that did not interact with a second hydrothermal fluid. Mineralisation within polymict BMBs varies from bacteriogenic (-45 ‰) to hydrothermal (+10 ‰) (Fig. 6.3A), most likely resulting from sulphide precipitation from either of the two fluids. Both the brine and metal-rich hydrothermal fluid are therefore likely to have utilised the relatively high permeability of the diatremes. Sulphur isotope values of the completely replaced BMBs predominantly lie between -10 and +1 ‰. This large range of values reflects the mixing of the two fluids and therefore mixing of the two sulphur sources, required for large-scale ore precipitation.

The higher modal value of +4 indicates a greater proportion of hydrothermal sulphur within volcanic samples (Fig. 6.3C). This positive diatreme mode (Fig. 6.3B) and unaltered intrusion average of +0.93 ‰ is likely to also reflect a magmatic sulphur source, usually considered to be 0 ‰ (see Rollinson, 1993). However the large range of sulphur isotope values for diatreme samples also indicates that both the brine and hydrothermal fluids interacted with the diatremes. The different isotopic signatures for the centres and margins of the diatremes (Fig. 6.4B), suggests that the different fluids utilised different pathways within the diatremes. However, it does not seem to be consistent that fluids containing one sulphur type utilise the diatreme margin. This is because sulphides along the margin of diatreme 19 contains predominantly bacteriogenic sulphur, whereas those on the margin of diatreme 28 contain predominantly hydrothermal sulphur. Limestone sulphide veins are almost entirely negative, suggesting that hydrothermal metal-rich fluid pathways are restricted to the diatreme rather than the fractured country rock.

Sphalerite and galena are the two main stage ore-forming minerals within the replaced BMB deposits. These two minerals predominantly occur between 100–350 mbsl (Fig. 6.4A), which corresponds to the upper and lower limits of BMB horizons adjacent to the diatremes (see Fig. 6.2). At depths greater than 350 mbsl, the sulphur isotope range becomes much smaller and more positive, reflecting a greater proportion of hydrothermal sulphur at depth. Pyrite exhibits two modal values of -37.7 and +1.0 ‰, the first of which is a much lower δ^{34}S value than the ore-forming sphalerite and galena (Fig. 6.3D). These lower sulphur isotope pyrite signatures are analogous to those observed at Navan by Blakeman et al. (2002), which are suggested to precipitate from bacteriogenic sulphur-bearing brines in between pulses of the metal-bearing hydrothermal fluid. The two modal values of pyrite may therefore reflect a pre-ore and post-ore precipitation of pyrite. The presence of magmatic activity in a shallow marine environment (see chapter

3) would have created a source of heat and water, fuelling an early hydrothermal system. Passing fluids may have scavenged iron from volcanic material (see chapter 5) allowing the precipitation of early stage pyrite. This is supported by the presence of hydrothermal sulphur precipitated as pyrite in the extra-crater Knockroe Formation (Fig. 6.3B).

6.7 Discussion: Limerick mineralisation

Diatremes utilise pre-existing faults as planes of weakness during magma ascent (Kurszlaukis and Barnett, 2003; Jelsma et al., 2009). Faults are the typical fluid conduits for Irish-type mineralisation, acting as fluid pathways for metal-rich hydrothermal fluids (Wilkinson et al., 2005*b*). Diatremes at Limerick offer similar access to fluids, as evidenced by dolomite, a key BMB mineral, overprinting the lower diatremes. This is also suggested by the presence of volcanic clasts, inferred to have been sourced from the diatremes (see chapter 4), within polymict BMB horizons. The inclusion of volcanic clasts within BMB horizons and small concentrations of ore-forming minerals in the lower diatremes (Fig. 5.4C), suggests mineralisation post-dates magmatic activity. This evidence suggests that the diatremes acted as conduits for pulses of both BMB-forming and mineralising fluids.

Country rock breccias contain solely negative sulphur isotopes suggesting that sulphides have precipitated entirely from reduced bacteriogenic sulphur sourced from brines (see Fig. 6.6). Polymict BMBs contain both a positive and negative isotopic signature, suggesting they have experienced the passage of fluids containing both bacteriogenic and hydrothermal sulphur. This suggests that both fluids utilised the adjoining diatremes, however the lack of massive sulphide within the diatremes, suggest that the two did not mix to any great degree. BMBs completely replaced by sulphides show the full range of sulphur values, clearly indicating a mix between the two sulphur sources (see Fig. 6.6).

Diatremes at Limerick appear to have acted as pathways for both the brine-derived, sulphur-rich fluid and the deep-sourced metal-rich fluid, much the same as an extensional fault in the classic Irish-type mineralisation model (Wilkinson et al., 2005*b*). It appears as though the two fluids have utilised different sections of the diatremes, most likely as pulses similar to those inferred for Navan (Blakeman et al., 2002). Repeated pulses of fluid flow by both BMB and mineralising fluids have filled the initial pore

spaces of the diatreme with secondary alteration products such as clays, dolomite and silica. The initial porosity and permeability of these samples are therefore unable to be quantified, however volcaniclastic deposits within diatremes tend to be characterised by initial porosities of 20–30 % (Stripp et al., 2006). The high diatreme fill porosity and the high permeability of zones such as the diatreme and intrusion margins, small-scale faults and conduits acting as aquaducts (McCusker and Reed, 2013), provide a greater capacity for fluid flow within the diatremes compared to a fault. Additionally, country rock fragmented by explosive diatreme activity, allowed greater fluid flow both into and out of the diatreme to form greater concentrations of adjacent BMB horizons. These BMB horizons are key hosts for mineralisation. High Zn grades occur proximal to the diatremes and BMB horizons are more concentrated adjacent to the diatremes, pinching out with distance (Fig. 6.2). Igneous intrusions within the diatremes (described in chapters 3 and 5) are late-stage features, as subsequent post-emplacement eruptions would cause them to disintegrate (Kurszlaukis and Barnett, 2003; Lorenz and Kurszlaukis, 2007; Valentine, 2012). The similar values between intrusion and diatreme sulphides suggests that fluid flow occurred after the late magmatic stage described in section 3.6.5. The presence of these thick intrusions would effectively have provided a barrier to fluid flow, focusing flow out of the diatremes and into the country rock.

Volcanic sulphide samples such as those liberated from diatreme, intrusion and Knockroe Formation material, average at -0.6 to +4 ‰ (see Fig. 6.6). Relatively fresh intrusion samples above the level of hydrothermal alteration within diatreme 19 average at +0.92 ‰ and is thought to represent the original sulphur isotope composition of the magma. Volcanic and intrusion isotope values are very similar to the accepted MORB and primitive mantle δ^{34}S value of 0 ± 3 ‰ (Rollinson, 1993), and are thought to represent a third magmatic sulphur source. The large volumes of highly alterable volcanic material present within the diatremes, would most likely have been leached of sulphur by the passage of hydrothermal fluids.

The age of mineralisation in the Irish Midlands has not been determined precisely, however many deposits, including Navan, Lisheen and Galmoy, contain features that indicate a maximum mineralisation age of Chadian-Arundian (345–339 Ma) (Hitzman and Beaty, 1996). Based on the widespread development of macro-styolites, sulphide formation at Silvermines is considered to be post-Arundian (<339 Ma) (Reed and Wallace, 2004). The diatremes at Limerick are thought to be emplaced during the Viséan (345–339 Ma),

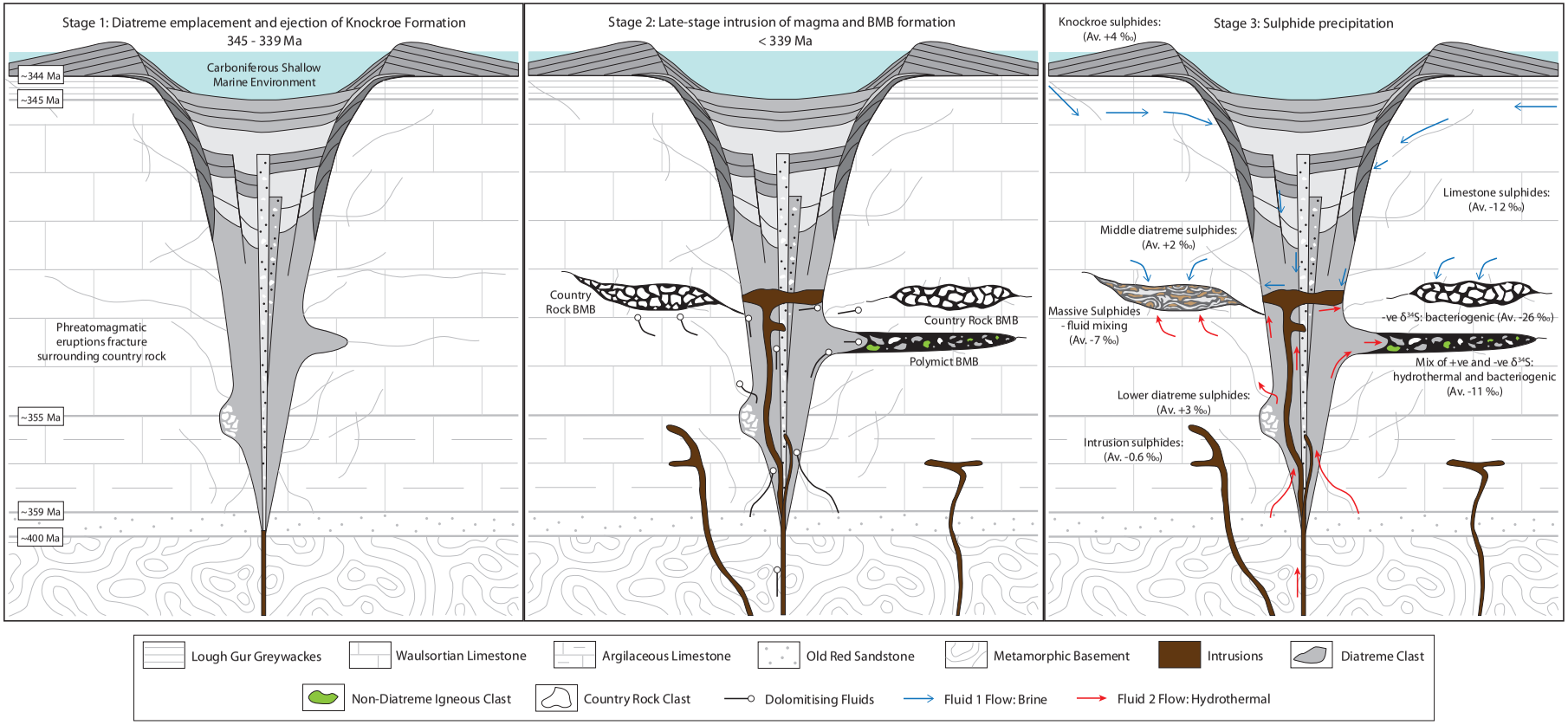

FIGURE 6.6: Illustration depicting relationship between diatremes, fluid flow and different BMB types. Intrusion within diatreme depicted, is in relation to multiple thick intrusions within diatreme 19 (see Fig. 3.3). **Stage 1:** Diatreme emplacement into the carbonate sequence during the Viséan. Phreatomagmatic eruptions fracture the surrounding country rock and eject volcaniclastic material to form the extra-crater Knockroe Formation. Boxes indicate approximate ages of Formation deposition. **Stage 2:** Late-stage intrusion of magma forming thick sills and dykes within the diatremes and surrounding country rock. Dolomitising hydrothermal fluids utilised the diatremes as flow pathways during the waning stages of eruption or soon after eruptions cease. These are channeled into the highly fractured country rock forming dissolution breccias called BMBs. **Stage 3:** The hydrothermal metal-rich fluid and brine-derived reduced sulphur-rich fluid utilise different parts of the porous and permeable diatreme system as fluid pathways. Pyritised country rock BMBs solely contain bacteriogenic sulphur from the brine-derived fluid, polymict BMBs predominantly contain hydrothermal sulphur, whereas BMBs replaced by massive sulphides display a mix of bacteriogenic and hydrothermal sulphur. δ^{34}S values are averages for each environment.

based on conodont dating of the Knockroe Formation by Somerville et al. (1992). Features within diatremes 47 and 77, such as elongation and compression of diatreme clasts within polymict BMB (see Fig. 5.2B and 5.2D), and the presence of tuffisitic dykes intruding into these BMB (Fig. 5.2D), suggests hydrothermal brecciation occurred in the waning stages of the Limerick volcanic system, prior to full diatreme-fill lithification. This is consistent with the model proposed by Davidheiser-Kroll et al. (2014), that suggests that hydrothermal fluid flow was driven by thinning of the continental crust and enhanced mantle heat flow, the same processes that caused large scale volcanism during the Carboniferous (see sections 1.2 and 1.5).

Mineralisation in the Limerick Basin has not yet been discovered using any conventional geophysical methods. However, establishing a clear genetic association between the diatremes and mineralised BMB horizons, is a potentially powerful regional prospecting tool, as these diatremes are discernible on both magnetic and seismic surveys.

6.8 Conclusions

Although the diatremes at Limerick have facilitated fluid flow, they have not solely acted as inert conduits for fluid flow. I propose that volcanic activity has provided an additional magmatic sulphur reservoir, potentially heat for hydrothermal fluid flow as well as access to large volumes of fresh volcanic material containing ore-related elements such as magnesium and iron. Diatreme formation in Limerick had a significant impact on mineralisation in this sector of the Irish Orefield, allowing more efficient fluid flow by virtue of increased porosity and permeability. High concentrations of BMB horizons formed adjacent to the diatremes as a result, providing greater hosts for mineralisation. The increased fluid pathway to the basement has enhanced the flow of hydrothermal fluid and therefore concentration of hydrothermal sulphur, compared to the traditional fault-based Irish-type model.

Chapter 7

Conclusions and Future Work

7.1 Conclusions

The primary objective of this thesis is to investigate the relationship between diatremes and adjacent Pb-Zn mineralisation in Stonepark, Limerick. The study has also provided a unique opportunity to study both the extra-crater and below-surface deposits of a maar-diatreme that erupted into a shallow marine environment. The results and conclusions of this study have important implications for diatreme evolution in sub-marine environments, as well as genetic models proposed to explain the characteristics of mineralisation within the Irish Orefield. The main conclusions of this research are summarised below:

7.1.1 Physical volcanological processes

- Samples of juvenile material from the Knockroe Formation are texturally and mineralogically very similar to the rocks of the upper diatremes (i.e. top 100 m). The paucity of vesicles in both the diatremes and extra-crater pyroclastic deposits, in addition to the presence of limestone lithic clasts in the latter, suggests they were formed during explosive magma-water interaction. Immobile trace element distributions also show many similarities between the Knockroe Formation and diatreme deposits, including the same magnitude of anomalies and gradient of REEs. The physical properties and geochemistry of both deposits suggests that

lithofacies of the Knockroe Formation were deposited from density currents sourced from the diatremes.

- Samples of the Knockroe Formation and upper diatreme comprise lapilli displaying chilled margins and thin beds of ash, analogous with deposits formed by Surtseyan volcanism. The Knockroe Formation pyroclastic deposits are also interbedded with crinoidal debris-rich Lough Gur wackestones, known to have been deposited in a shallow marine environment. The diatremes therefore appear to have initially erupted in a submarine environment, with periods of inactivity recorded as interludes of lapilli-poor greywacke beds.

- The blocky, fracture bound and incipiently vesicular clasts observed in both diatreme and Knockroe Formation deposits, indicate an origin from magma-water interactions rather than magma fragmentation by intense vesiculation. In addition, the presence of high concentrations of lithic clasts sourced from deeper in the sequence and the evidence for a shallow marine environment, strongly suggests that the diatremes were excavated by an extended period of phreatomagmatic activity.

- The massive lapilli tuffs of the middle and lower diatremes exhibit elutriated fines-rich pockets and pipes as well as the alignment of small lapilli around large clasts. These form as a result of the conversion of water to steam during phreatomagmatic eruptions, homogenising the deposits via the action of debris jets and localised fluidisation of the diatreme-fill.

- The lower diatreme deposits contain evidence for heat retention, including highly vesicular 'frothy' clasts and fluid plastically deformed lapilli such as large 'raggy' and partially sintered globular lapilli. This late magmatic stage is associated with emergence and subsequent drying out of the maar-diatreme system. Emergence of the system is also evidenced by the lack of submarine fossils in the upper Knockroe Formation as well as an overlying lava flow that does not exhibit features such as pillow lavas, hyaloclastites, intense fracturing or an extensive chilled margin that might otherwise suggest eruption into a submarine environment.

7.1.2 Deposit geochemistry

- Parent magma classification using immobile trace element geochemistry indicates that the diatreme and Knockroe Formation deposits are alkali basaltic, and are consistent with a within-plate continental rift environment. Juvenile material at Limerick is highly enriched in LREE, indicating the magma formed from partial melting of an enriched mantle. The degree of enrichment at Limerick is very similar to that produced by melting of the Carboniferous-Permian aged mantle beneath Scotland. Therefore an enriched and metasomatised mantle may also have existed below the Irish Midlands during the Lower Carboniferous.

- The majority of dark clasts within the Knockroe Formation follow similar elemental trends to that of the diatreme samples. These clasts display a greater degree of LREE enrichment, suggesting they may have formed from an earlier melt. However, a small proportion of dark clasts appear to have a more tholeiitic chemistry, indicating that they are more fractionated and may not have originated from diatreme eruptions. These are most likely accidental clasts, entrained by debris currents or sourced from more distal eruptions.

7.1.3 Diatreme-BMB-mineralisation relationship

- Immobile trace element trends for volcanic BMB samples exhibit many similarities with middle and lower diatreme samples. These include very similar magnitudes of positive Nb and Zr, and negative Sm anomalies as well as similar gradients of immobile REEs. Additionally, volcanic BMB clasts are texturally and mineralogically similar to lapilli in the lower diatreme, both exhibiting the same alteration assemblages. The evidence therefore indicates that volcanic BMB clasts originated from within the diatremes, and were most likely entrained by hydrothermal fluids before entering the country rock.

- The lower diatreme has been overprinted by a greenschist metamorphic mineral assemblage and dolomitised by the passage of BMB-forming fluids. The presence of small concentrations of ore-forming minerals also suggests that mineralising fluids utilised the diatremes as conduits. Impermeable (and therefore impassable) intrusions within the diatremes may have served to channel fluids into the country rock, exploiting what was likely to have been an extensive network of fractures

radiating out from the diatreme (formed by initial explosive activity). This yielded a concentration of BMB horizons adjacent to the diatremes, the majority of which lie below the upper limit of diatreme dolomitisation.

- Diatreme-filling deposits have an initial high porosity, and contain permeable pathways such as intrusion margins and small-scale faults that act as aquaducts. The diatremes at Limerick therefore had a greater capacity for fluid flow than the traditional fault fluid pathways in the Irish-type model. These diatremes formed a more efficient fluid pathway to the basement, increasing the amount of hydrothermal fluid that could flow through the system into mineralised horizons. This is also evidenced from the more positive sulphur isotope ore values at Limerick compared to other Irish-type ore deposits. Explosive volcanic processes would have brecciated the country rock surrounding the diatremes, allowing greater fluid flow out of the diatremes. This would have facilitated greater formation of BMB horizons (i.e. as hosts to mineralisation), immediately adjacent to the diatremes. However, the diatremes did not merely act as inert conduits for fluid flow, the presence of large volumes of highly alterable volcanic material provided a third magmatic sulphur source to the mineralising system as well as heat and important ore-forming constituents.

- Intrusion of tuffisitc dykes (thought to have been emplaced during the waning stages of diatreme eruption) into the polymict BMB lithofacies, in addition to textures indicating volcanic material had not yet fully lithified, suggests that BMB formation occurred during the late stages, or shortly after, diatreme eruptions. Magmatic activity and basin formation at Limerick is therefore the most likely heat source for hydrothermal convection cells within the basin.

- Sulphur isotope analysis indicates three sulphur sources, a bacteriogenic, hydrothermal and minor magmatic sulphur reservoir. Relatively unmineralised country rock breccias contain sulphides precipitated entirely from bacteriogenic sulphur sources (see Fig. 6.6), most likely seawater-derived brines. Polymict BMBs contain both bacteriogenic and hydrothermal sulphur, suggesting sulphides originated from both brine-derived and metal-rich fluids, and that both utilised the diatremes. The lack of massive sulphide deposits with the diatremes indicates that the two did not mix to any great degree within the conduit. Mineralised BMB horizons show a

large range in sulphur isotope values, indicating sulphur was contributed from all sources.

"I may not have gone where I intended to go, but I think I have ended up where I needed to be."

Douglas Adams (1952–2001)

7.2 Future work

Although a detailed analytical study was undertaken on the Limerick maar-diatreme system and associated mineralisation, there are many potential interesting topics that merit further investigation, as follows:

- Many ore deposits, including Navan (see Ashton et al., 2015), are considered to have several stages of ore formation related to hydrothermal fluid supply. Categorising the sulphide phases at Limerick into pre-, syn- and post-ore deposition stages using trace element analysis could answer many questions. For example, why are Knockroe Formation sulphides predominantly positive–i.e. were they precipitated by hydrothermal fluids within the diatremes and ejected by later eruptions, or precipitated by hydrothermal fluids that breached the seafloor? Are ore mineral phases such as sphalerite and galena within the diatreme part of the syn-ore phase associated with widespread BMB replacement by sulphides or are they associated with a pre- or post-ore hydrothermal system? Is it possible to identify which sulphides were precipitated from the brine or metal-rich hydrothermal from their composition?

- Although the Knockroe Formation within the 2638 license area has been thoroughly logged, thick volcanic accumulations within the graben structure to the west remain unstudied. Geochemical analysis of these deposits could be undertaken to determine whether they are sourced from diatreme eruptions or from other nearby volcanic centres. A small proportion of the dark clasts within the lower Knockroe Formation appear to have a slightly different chemical composition than the majority of other juvenile clasts. Study of the graben volcanics may provide a potential source for these clasts. The diatremes could then be fitted into a timescale of regional volcanic activity to provide a greater understanding of tectonic and volcanic processes occurring in the Irish Midlands during the Lower Carboniferous.

- A more detailed investigation into the geochemistry of both the diatremes and BMB horizons may provide a key geochemical signature or mineral assemblage unique to both. This unique signature could then be used either in the field, soil sample analysis or by analysis of core samples to carry out exploration for further diatremes and associated mineralisation.

- This project has focused predominantly on the physical processes and geochemistry of the diatreme-BMB-mineralisation system at Limerick. However an entirely new aspect of this system could be studied using geophysical techniques. Localised magnetic and seismic surveys carried out by Teck Ireland Ltd show clear evidence for sub-surface diatremes, and can therefore potentially be used to discover more diatremes and any associated mineralisation.

- $^{40}Ar/^{39}Ar$ of sanidine was initially considered to be a viable method of dating diatreme emplacement. However, no pristine sanidine crystals were observed in close proximity to the diatremes. Methods of dating, such as K-Ar dating of illite (see Clauer et al., 1997) or $^{40}Ar/^{39}Ar$ dating using incremental heating (see Koppers et al., 2000), may be feasible on the volcanic material. The high level of alteration would make this study challenging, therefore any dating techniques would have to be cross-calibrated. However, this would usefully provide a timing for fluid flow (post-diatreme and pre-mineralisation) rather than a primary volcanic signal, in turn providing relative ages for these events.

Appendix A

Supplementary Material File List

Chapter 2:

- 2.1: Core logging interval clast size test
- 2.2: Laboratory procedures
- 2.3: Accuracy and precision data
- 2.4: Errors
- 2.5: Loss on ignition
- 2.6 Borehole and sample type analysis technique

Chapter 3:

- 3.1: Borehole 19 core log
- 3.2: Borehole 19 clast size and composition graph
- 3.3: Borehole 23 core log
- 3.4: Borehole 28 core log
- 3.5: Borehole 28 clast size and composition graph
- 3.6: Vesicle data

Chapter 4:

- 4.1: Continental basalts geochemistry data
- 4.2: Microprobe geochemistry data
- 4.3: XRF geochemistry data
- 4.4: ICP-MS geochemistry data

Chapter 5:

- 5.1: SEM geochemistry data
- 5.2: XRD geochemistry data

Chapter 6:

- 6.1: Sulphur isotope geochemistry data

Bibliography

Afanasyev, A. A., Melnik, O., Porritt, L., Schumacher, J. C. and Sparks, R. S. J. (2014), 'Hydrothermal alteration of kimberlite by convective flows of external water', *Contributions to Mineralogy and Petrology* **168**, 1038–1055.

Aiuppa, A., Allard, P., D'Alessandro, W., Michel, A., Parello, F., Treuil, M. and Valenza, M. (2000), 'Mobility and fluxes of major, minor and trace metals during basalt weathering and groundwater transport at Mt. Etna volcano (Sicily)', *Geochimica et Cosmochimica Acta* **64**, 1827–1841.

Anderson, I. K., Ashton, J. H., Boyce, A. J., Fallick, Anthony, E. and Russell, M. J. (1997), 'Ore depositional processes in the Navan Zn-Pb deposit, Ireland', *Economic Geology* **93**, 535–563.

Aranda-Gómez, J. and Luhr, J. F. (1996), 'Origin of the Joya Honda maar, San Luis Potosi, Mexico', *Journal of Volcanology and Geothermal Research* **74**, 1–18.

Ashby, D. F. (1939), 'The geological succession and petrology of the Lower Carboniferous volcanic area of Co. Limerick', *Proceedings of the Geological Association* **50**, 324–330.

Ashton, J. H., Blakeman, R. J., Geraghty, J. F., Beach, A., Coller, D., Philcox, M. E., Boyce, A. J. and Wilkinson, J. J. (2015), The giant Navan carbonate-hosted Zn-Pb deposit - a review, *in* S. M. Archibald, ed., 'Current perspective on zinc deposits', Irish Association for Economic Geology, 85–122.

Banks, D. A. (1985), 'A fossil hydrothermal worm in assemblage from the Tynagh lead-zinc deposit in Ireland', *Nature* **313**, 128–131.

Banks, D. A., Boyce, A. J. and Samson, I. M. (2002), 'Constraints on the origins of fluids forming Irish Zn-Pb-Ba deposits: Evidence from the composition of fluid inclusions', *Economic Geology* **97**, 471–480.

Barnett, W. and Lorig, L. (2007), 'A model for stress-controlled pipe growth', *Journal of Volcanology and Geothermal Research* **159**, 108–125.

Barton, M. D. and Johnson, D. A. (2000), Alternative brine sources for Fe-oxide(-Cu-Au) systems: Implications for hydrothermal alteration and metals, *in* T. M. Porter, ed., 'Hydrothermal iron oxide copper-gold and related deposits: A global perspective', Australian Mineral Foundation, Adelaide, 43–60.

Bednarz, U., Gotte, P. and Schmincke, H. U. (1991), The petrography of altered submarine lavas and major element mobility in drillholes CY-1 and CY-1a, Cyprus, *in* I. L. Gibson, J. Mapas, P. Robinson and C. Xenophontos, eds, 'Cyprus crustal study project: Initial report, holes CY-1 and 1a', Vol. 90-20, Geological Survey of Canada, pp. 95–117.

Best, M. G. (2003), *Igneous and Metamorphic Petrology*, 2nd edn, Blackwell Publishing.

Blakeman, R. J., Ashton, J. H., Boyce, A. J., Fallick, Anthony, E. and Russell, M. J. (2002), 'Timing of interplay between hydrothermal and surface fluids in the Navan Zn + Pb orebody, Ireland: evidence from metal distribution trends, mineral textures, and δ^{34}S analyses', *Economic Geology* **97**, 73–91.

Blundy, J. D. and Wood, B. J. (1990), 'Crystal-chemical controls on the partitioning of Sr and Ba between plagioclase feldspar, silicate melts, and hydrothermal solutions', *Geochimica et Cosmochimica Acta* **55**, 193–209.

Bouvier, A.-S., Deloule, E. and Metrich, N. (2010), 'Fluid inputs to magma sources of St. Vincent and Grenada (Lesser Antilles): New insights from trace elements in olivine-hosted melt inclusions', *Journal of Petrology* **51**, 1597–1615.

Boyce, A. J. (1983), 'Formation of fossil hydrothermal chimneys and mounds from Silvermines, Ireland', *Nature* **306**, 545–550.

Boyce, A. J., Little, C. T. S. and Russell, M. J. (2003), 'A new fossil vent biota in the Ballynoe barite deposit, Silvermines, Ireland: evidence for intracratonic sea-floor hydrothermal activity about 352 Ma', *Economic Geology* **98**, 649–656.

Brand, B. D. and Clarke, A. B. (2009), 'The architecture, eruptive history, and evolution of the Table Rock Complex, Oregon: from a Surtseyan to an energetic maar eruption', *Journal of Volcanology and Geothermal Research* **180**, 203–224.

Branney, M. J. and Kokelaar, P. (2002), 'Pyroclastic density currents and the sedimentation of ignimbrites', *Geological Society, London, Special Publications* **No. 27**.

Brown, R. J., Gernon, T., Stiefenhofer, J. and Field, M. (2008a), 'Geological constraints on the eruption of the Jwaneng Centre kimberlite pipe, Botswana', *Journal of Volcanology and Geothermal Research* **174**, 195–208.

Brown, R. J., Field, M., Gernon, T. M., Gilbertson, M. and Sparks, R. S. J. (2008b), 'Problems with an in-vent column collapse model for the emplacement of massive volcaniclastic kimberlite. A discussion of 'In-vent column collapse as an alternative model for massive volcaniclastic kimberlite emplacement: An example from the Fox kimberlite, Ekati Diamond Mine, NWT, Canada' by Porritt et al. [J. Volcanol. Geotherm. Res. 174, 90-102]', *Journal of Volcanology and Geothermal Research* **178**, 847–850.

Cabanis, B. and Lecolle, M. (1989), 'Le diagramma La/10-Y/15-Nb/8: un outil processus de mélange et/ou de contamination crustale: Paris', *Academie des Sciences Comptes Rendus* **309**, 2023–2029.

Calvari, S. and Tanner, L. H. (2011), 'The Miocene Costa Giardini diatreme, Iblean Mountains, southern Italy: model for maar-diatreme formation on a submerged carbonate platform', *Bulletin of Volcanology* **73**, 557–576.

Campbell, I. H. and Gorton, M. P. (1980), 'Accessory phases and the generation of LREE-enriched basalts - a test for disequilibrium melting', *Contributions to Mineralogy and Petrology* **72**, 157–163.

Carracedo Sánchez, M., Sarrionandia, F., Arostegui, J., Larrondo, E. and Ibarguchi, J. I. G. (2009), 'Development of spheroidal composite bombs by welding of juvenile spinning and isotropic droplets inside a mafic eruption column', *Journal of Volcanology and Geothermal Research* **186**, 265–279.

Cas, R. A. F. and Wright, J. V. (1988), *Volcanic Successions: Modern and Ancient*, 2 edn, Unwin Hyman Ltd, London.

Cas, R. A. F. and Wright, J. V. (1991), 'Subaqueous pyroclastic flows and ignimbrites: an assessment', *Bulletin of Volcanology* **53**, 357–380.

Cas, R. A. F., Porrit, L., Pittari, A. and Hayman, P. (2008), 'A new approach to kimberlite facies terminology using a revised general approach to the nomenclature

of all volcanic rocks and deposits: Descriptive to genetic', *Journal of Volcanology and Geothermal Research* **174**, 226–240.

Clauer, N., Srodon, J., Francu, J. and Sucha, V. (1997), 'K-Ar dating of illite fundamental particles separated from illite-smectite', *Clay Minerals* **32**, 181–196.

Davidheiser-Kroll, B., Stuart, F. M. and Boyce, A. J. (2014), 'Mantle heat drives hydrothermal fluids responsible for carbonate-hosted base metal deposits: evidence from 3he/4he of ore fluids in the Irish Pb-Zn ore district', *Mineralium Deposita* **49**, 547–553.

Davies, A. G. S., Cooke, D. R., Gemmell, J. B. and Simpson, K. A. (2008), 'Diatreme breccias at the Kelian gold mine, Kalimantan, Indonesia: Precursors to epithermal gold mineralization', *Economic Geology* **103**, 689–716.

Deer, W. A., Howie, R. A. and Zussman, J. (1996), *An Introduction to the Rock-Forming Minerals*, 2nd edn, Prentice Hall.

Delpit, S., Ross, P.-S. and Hearn Jr, B. C. (2014), 'Deep-bedded ultramafic diatremes in the Missouri River Breaks volcanic field, Montana, USA: 1 km of syn-eruptive subsidence', *Bulletin of Volcanology* **76**, 832–854.

Elliott, H. A. L., Gernon, T. M., Roberts, S. and Hewson, C. (2015), 'Basaltic maar-diatreme volcanism in the Lower Carboniferous of the Limerick Basin (SW Ireland)', *Bulletin of Volcanology* **77**, 37–59.

Everett, C. E., Wilkinson, J. J. and Rye, D. M. (1999), Fracture-controlled fluid flow in the Lower Palaeozoic basement rocks of Ireland: implications for the genesis of Irish-type Zn-Pb deposits, *in* K. J. W. McCaffrey, L. Lonergan and J. J. Wilkinson, eds, 'Fractures, fluid flow and mineralization', Vol. 155, Geological Society, London, pp. 247–276.

Fagan, T. J. and Day, H. W. (1997), 'Formation of amphibole after clinopyroxene by dehydration reactions: Implications for pseudomorphic replacement and mass fluxes', *Geology* **25**, 395–398.

Fallick, Anthony, E., McConville, P., Boyce, A. J., Burgess, R. and Kelley, S. P. (1992), 'Laser microprobe stable isotope measurements on geological materials: Some experimental considerations (with special reference to δ34S in sulphides)', *Chemical Geology (Isotope Geoscience Section)* **101**, 53–61.

Fallick, Anthony, E., Ashton, J. H., Boyce, A. J., Ellam, R. M. and Russell, M. J. (2001), 'Bacteria were responsible for the magnitude of the world-class hydrothermal base metal sulfide orebody at Navan, Ireland', *Economic Geology* **96**, 885–890.

Field, M. and Scott Smith, B. (1999), Contrasting geology and near-surface emplacement of kimberlite pipes in Southern Africa and Canada, *in* J. J. Gurney, M. L. Gurney, M. D. Pascoe and S. H. Richardson, eds, 'Proceedings of the VII th International Kimberlite Conference', Vol. 1, pp. 214–237.

Finkel, R. C., D., M. J. and Chung, Y. C. (1980), 'Sulfide precipitates at 21 ^{o}N on the East Pacific Rise: ^{226}Ra, ^{210}Pb and ^{210}Po', *Geophysical Research Letters* **7**, 685–688.

Fisher, R. V. (1961), 'Proposed classification of volcaniclastic sediments and rocks', *Geological Society of America Bulletin* **72**, 1409–1414.

Fisher, R. V. and Waters, A. C. (1970), 'Base surge bed forms in maar volcanoes', *American Journal of Science* **268**, 157–180.

Fisher, R. V. and Schmincke, H. U. (1984), *Pyroclastic rocks*, Springer-Verlag.

Fiske, R. S., Cashman, K. V., Shibata, A. and Watanabe, K. (1998), 'Tephra dispersal from Myojinsho, Japan, during its shallow submarine eruption of 1952-1953', *Bulletin of Volcanology* **59**, 262–275.

Fitton, J. and Dunlop, H. M. (1985), 'The Cameroon line, West Africa, and its bearing on the origin of oceanic and continental alkali basalt', *Earth and Planetary Science Letters* **72**, 23–38.

Fontana, G., Niocaill, C. M., Brown, R. J., Sparks, R. S. J. and Field, M. (2011), 'Emplacement temperature of pyroclastic and volcaniclastic deposits in kimberlite pipes in southern africa', *Bulletin of Volcanology* **73**, 1063–1083.

Francis, E. H. (1970), Bedding in Scottish (Fifeshire) tuff-pipes and its relevance to maars and calderas, *in* 'Volcanoes and their roots', Institute of Geological Sciences.

Gainsford, A. R., Sisley, M. J., Swaddle, T. W. and Bayliss, P. (1975), 'Hydrothermal formation of ferrite spinels', *Canadian Journal of Chemistry* **53**, 12–19.

Gallagher, S. J. and Somerville, I. D. (2003), 'Lower Carboniferous (Late Viséan) platform development and cyclicity in southern Ireland: foraminiferal biofacies and lithofacies evidence', *Rivista Italiana di Paleontologia e Stratigrafia* **109**, 159–171.

Ganguly, J. (2005), 'Adiabatic decompression and melting of mantle rocks: An irreversible thermodynamic analysis', *Geophysical Research Letters* **32**, 1–4.

Geikie, A. (1897), *The ancient volcanoes of Great Britain*, Vol. 1 and 2, McMilland & Co.

Gernon, T. M., Gilbertson, M. A., Sparks, R. S. J. and Field, M. (2008), 'Gas-fluidisation in an experimental tapered bed: Insights into processes in diverging volcanic conduits', *Journal of Volcanology and Geothermal Research* **174**, 49–56.

Gernon, T. M., Field, M. and Sparks, R. S. J. (2009*a*), 'Depositional processes in a kimberlite crater: the Upper Cretaceous Orapa South Pipe Botswana', *Sedimentology* **56**, 623–643.

Gernon, T. M., Gilbertson, M. A., Sparks, R. S. J. and Field, M. (2009*b*), 'The role of gas-fluidisation in the formation of massive volcaniclastic kimberlite', *Lithos* **112, Supplement 1**, 439–451.

Gernon, T., Brown, R. J., Tait, M. A. and Hincks, T. K. (2012), 'The origin of pelletal lapilli in explosive kimberlite eruptions', *Nature Communications* **3**, 1–7.

Gernon, T. M., Upton, B. G. J. and Hincks, T. K. (2013), 'Eruptive history of an alkali basaltic diatreme from Elie Ness, Fife, Scotland', *Bulletin of Volcanology* **75**, 704–724.

Gibson, I. L. (1991), *Diagenesis, heat flow, and rifting at Broken Ridge, Indian Ocean*, Vol. 121 of *Proceedings of the Ocean Drilling Program, Scientific Results.*

Gifkins, C. C., Herrmann, W. and Large, R. R. (2005), *Altered volcanic rocks: a guide to description and interpretation*, Centre for Ore Deposit Research, University of Tasmania.

Graettinger, A. H., Valentine, G. A., Sonder, I., Ross, P.-S., White, J. D. L. and Taddeucci, J. (2014), 'Maar-diatreme geometry and deposits: Subsurface blast experiments with variable explosion depth', *Geochemistry, Geophysics, Geosystems* **15**, 740–764.

Gregg, T. K. P. and Fink, J. H. (1995), 'Quantification of submarine lava-flow morphology through analog experiments', *Geology* **23**, 73–76.

Griffiths, R. W. (1992), 'Solidification and morphology of submarine lavas: A dependence on extrusion rate', *Journal of Geophysical Research* **97**, 729–737.

Hart, W. K., WoldeGabriel, G., Walter, R. C. and Mertzman, S. A. (1989), 'Basaltic volcanism in Ethiopia: constraints on continental rifting and mantle interactions', *Journal of Geophysical Research* **94**, 7731–7748.

Hawthorne, J. B. (1975), 'Model of a kimberlite pipe', *Physics and Chemistry of The Earth* **9**, 1–15.

Head III, J. W. and Wilson, L. (2003), 'Deep submarine pyroclastic eruptions: theory and predicted landforms and deposits', *Journal of Volcanology and Geothermal Research* **121**, 155–193.

Heeremans, M., Timmerman, M. J., Kirstein, L. A. and Faleide, J. I. (2004), 'New constraints on the timing of late Carboniferous-early Permian volcanism in the central North Sea', *Geological Society, London, Special Publications* **223**, 177–193.

Heiken, G. (1972), 'An atlas of volcanic ash', *Smithsonian contributions to the Earth Sciences* **12**.

Hitzman, M. W. (1995), Geological setting of the Irish Zn-Pb-(Ba-Ag) Orefield, *in* K. Anderson, J. Ashton, G. Earls, M. Hitzman and S. Tear, eds, 'Irish Carbonate-hosted Zn-Pb Deposits', Vol. 21 of *Guidebook Series*, Society of Economic Geologists, pp. 3–24.

Hitzman, M. W. and Beaty, D. W. (1996), 'The Irish Zn-Pb-(Ba) Orefield', *Society of Economic Geologists* **Special Publication no. 4**, 112–143.

Hitzman, M. W., Allan, J. R. and Beaty, D. W. (1998), 'Regional dolomitization of the Waulsortian Limestone in southeastern Ireland: Evidence of large-scale fluid flow driven by the Hercynian orogeny', *Geology* **26**, 547–550.

Hitzman, M. W., Redmond, P. B. and Beaty, D. W. (2002), 'The carbonate-hosted Lisheen Zn-Pb-Ag deposit, County Tipperary, Ireland', *Economic Geology* **97**, 1627–1655.

Hnatyshin, D., Creaser, R. A., Wilkinson, J. J. and Gleeson, S. A. (2015), 'Re-Os dating of pyrite cofirms an early diagenetic onset and extended duration of mineralization in the Irish Zn-Pb ore field', *Geology* **43**, 143–146.

Holland, C. H. and Sanders, I. S. (2009), *The Geology of Ireland*, 2nd revised edn, Dunedin Academic Press.

Hollis, S. P. (2013), Evolution and mineralization of volcanic arc sequences: Tyrone Igneous Complex, Northern Ireland, PhD thesis, University of Southampton.

Houghton, B. F. and Wilson, C. J. N. (1989), 'A vesicularity index for pyroclastic deposits', *Bulletin of Volcanology* **51**, 451–462.

Houghton, B. F. and Smith, R. T. (1993), 'Recycling of magmatic clasts during explosive eruptions: estimating the true juvenile content of phreatomagmatic volcanic deposits', *Bulletin of Volcanology* **55**, 414–420.

Houghton, B. F., Wilson, C. J. N. and Smith, I. E. M. (1999), 'Shallow-seated controls on styles of explosive basaltic volcanism: a case study from New Zealand', *Journal of Volcanology and Geothermal Research* **91**, 97–120.

Humphris, S. E. and Thompson, G. (1978), 'Hydrothermal alteration of oceanic basalts by seawater', *Geochimica et Cosmochimica Acta* **42**, 107–125.

Ingram, R. L. (1964), 'Terminology for the thickness of stratification and parting units in sedimentary units', *Bulletin of the Geological Society of America* **86**, 937–938.

Ishikawa, Y., Sawaguchi, T., Iwaya, S. and Horiuchi, M. (1976), 'Delineation of prospecting targets for Kuroko deposits based on modes of volcanism of underlying dacite and alteration halos', *Mining Geology* **26**, 105–117.

Jacobsen, S. B. and Wasserburg, G. J. (1979), 'Nd and Sr isotopic study of the Bay of Islands Ophiolitic Complex and the evolution of the source of midocean ridge basalts', *Journal of Geophysical Research* **84**, 7429–7445.

Jarosewich, E., Nelen, J. A. and Norberg, J. A. (1980), 'Reference samples for electron microprobe analysis', *Geostandards Newsletter* **4**, 43–47.

Jelsma, H., Barnett, W., Richards, S. and Lister, G. (2009), 'Tectonic setting of kimberlites', *Lithos* **112S**, 155–165.

Jenner, G. A. (1996), Trace element geochemistry of igneous rocks: geochemical nomenclature and analytical geochemistry, *in* 'Trace element geochemistry of volcanic rocks: applications for massive sulphide exploration', Vol. 12, Geological Association of Canada, Short course notes, pp. 51–77.

Jensen, E. P. (2003), Magmatic and hydrothermal evolution of the Cripple Creek gold deposit, Colorado, and comparisons with regional and global magmatic-hydrothermal systems associated with alkaline magmatism, PhD thesis, The University of Arizona.

Jensen, L. S. (1976), 'A new cation plot for classifying subalkalic volcanic rocks', *Ministry of Natural Resouces Papers* **66**.

Karato, S. and Jung, H. (1998), 'Water, partial melting ad the origin of the seismic low velocity and high attenuation zone in the upper mantle', *Earth and Planetary Science Letters* **157**, 193–207.

Kaur, P., Chaudhri, N., Hofmann, A. W., Raczek, I., Okrusch, M., Skora, S. and Baumgartner, L. P. (2012), 'Two-stage, extreme albitization of A-type granites from Rajasthan, NW India', *Journal of Petrology* **53**, 919–948.

Kerr, N. (2014), Geology of the Stonepark Zn-Pb prospects, Master's thesis, Colorado School of Mines.

King, A. J., Waggoner, D. G. and Garcia, M. O. (1993), 'Geochemistry and petrology of basalts from LEG 136, Central Pacific Ocean', *Proceedings of the Ocean Drilling Program, Scientific Results* **136**, 107–118.

Kirton, S. R. (1984), 'Carboniferous volcanicity in England with special reference to the Westphalian of the E and W Midlands', *Journal of the Geological Society* **141**, 161–170.

Kneller, B. and Branney, M. J. (1995), 'Sustained high-density turbdity currents and the deposition of thick massive sands', *Sedimentology* **42**, 607–616.

Kokelaar, B. P. (1983), 'The mechanism of Surtseyan volcanism', *Journal of the Geological Society of London* **140**, 939–944.

Kokelaar, B. P. (1986), 'Magma-water interactions in subaqueous and emergent basaltic volcanism', *Bulletin of Volcanology* **48**, 275–289.

Koppers, A. A. P., Staudigel, H. and Wijbrans, J. R. (2000), 'Dating crystalline groundmass separates of altered Cretaceous seamount basalts by the $^{40}Ar/^{39}Ar$ incremental heating technique', *Chemical Geology* **166**, 139–158.

Kurszlaukis, S. and Lorenz, V. (1997), 'Volcanological features of a low-viscosity melt: the carbonatitic Gross Brukkaros volcanic field, Namibia', *Bulletin of Volcanology* **58**, 421–431.

Kurszlaukis, S., Franz, L. and Lorenz, V. (1998), 'On the volcanology of the Gibeon kimberlite field, Namibia', *Journal of Volcanology and Geothermal Research* **84**, 257–272.

Kurszlaukis, S. and Barnett, W. (2003), 'Volcanological and structural aspects of the Venetia kimberlite cluster - as case study of South African kimberlite maar-diatreme volcanoes', *South African Journal of Geology* **106**, 145–172.

Lagat, J. (2009), Hydrothermal alteration mineralogy in geothermal fields with case examples from Olkaria Domes geothermal field, Kenya, *in* 'Short Course IV on Exploration for Geothermal Resources', KenGen, UNU-GTP, GDC.

Large, R. R., Gemmell, J. B. and Holger, P. (2001), 'The alteration box plot: A simple approach to understanding the relationship between alteration mineralogy and lithogeochemistry associated with volcanic-hosted massive sulfide deposits', *Economic Geology* **96**, 957–971.

Leahy, K. (1997), 'Discrimination of reworked pyroclastics from primary tephra-fall tuffs: a case study using kimberlites of Fort a la Corne, Saskatchewan, Canada', *Bulletin of Volcanology* **59**, 65–71.

Lees, A. and Miller, J. (1985), 'Facies variation in Waulsortian buildups. part 2; Mid-Dinantian buildups from Europe and North America', *Geological Journal* **20**, 159–180.

Lefebvre, N. S., White, J. D. L. and Kjarsgaard, B. A. (2013), 'Unbedded diatreme deposits reveal maar-diatreme-forming eruptive processes: Standing Rocks West, Hopi Buttes, Navajo Nation, USA', *Bulletin of Volcanology* **75**, 739–756.

LeHuray, A. P., Caulfield, J. B. D., Rye, D. M. and Dixon, P. R. (1987), 'Basement controls on sediment-hosted Zn-Pb deposits: a Pb isotope study of Carboniferous mineralization in Central Ireland', *Economic Geology* **82**, 1695–1709.

Li, X., Li, Z., Zhou, H., Liu, Y. and Kinny, P. D. (2002), 'U-Pb zircon geochronology, geochemistry and Nd isotopic study of Neoproterozoic bimodal volcanic rocks

in the Kangdian Rift of South China: implications for the initial rifting of Rodinia', *Precambrian Research* **113**, 135–154.

Lloyd, F. E. and Stoppa, F. (2003), 'Pelletal lapilli in diatremes - some inspiration from the old masters', *GeoLines* **15**, 65–71.

Lorenz, V. (1975), 'Formation of phreatomagmatic maar-diatreme volcanoes and its relevance to kimberlite diatremes', *Physics and Chemistry of The Earth* **9**, 17–27.

Lorenz, V. (1985), 'Maars and diatremes of phreatomagmatic origin: A review', *Transactions of the Geological Society of South Africa* **88**, 459–470.

Lorenz, V. (1986), 'On the growth of maars and diatremes and its relevance to the formation of tuff rings', *Bulletin of Volcanology* **48**, 265–274.

Lorenz, V., Zimanowski, B. and Buettner, R. (2002), 'On the formation of deep-seated subterranean peperite-like magma-sediment mixtures', *Journal of Volcanology and Geothermal Research* **114**, 107–118.

Lorenz, V. (2003), 'Maar-diatreme volcanoes, their formation, and their setting in hard-rock or soft-rock environments', *Geolines* **15**, 72–83.

Lorenz, V. (2007), 'Syn- and posteruptive hazards of maar-diatreme volcanoes', *Journal of Volcanology and Geothermal Research* **159**, 285–312.

Lorenz, V. and Kurszlaukis, S. (2007), 'Root zone processes in the phreatomagmatic pipe emplacement model and consequences for the evolution of maar–diatreme volcanoes', *Journal of Volcanology and Geothermal Research* **159**, 4–32.

Macdonald, R. and Walker, B. H. (1985), 'Geochemistry and tectonic significance of the Lower Carboniferous Cockermouth lavas, Cumbria', *Proceedings of the Yorkshire Geological Society* **45**, 141–146.

MacKenzie, W. S. and Adams, A. E. (2011), *A colour atlas of rocks and minerals in thin section*, 11 edn, Manson Publishing, London.

MacLean, W. H. (1980), 'Mass change calculations in altered rock series', *Mineralium Deposita* **25**, 44–49.

Mahood, G. A. and Stimac, J. A. (1990), 'Trace-element partitioning in pantellerites and trachytes', *Geochimica et Cosmochimica Acta* **54**, 2257–2276.

Mangan, M. T. and Cashman, K. V. (1996), 'The structure of basaltic scoria and reticulite and inferences for vesiculation, foam formation, and fragmentation in lava fountains', *Journal of Volcanology and Geothermal Research* **73**, 1–18.

Marsh, J. S. (1987), 'Basalt geochemistry and tectonic discrimination within continental flood basalt provinces', *Journal of Volcanology and Geothermal Research* **32**, 35–49.

Mattsson, H. B. (2010), 'Textural variation in juvenile pyroclasts from an emergent, Surtseyan-type, volcani eruption: The Capelas tuff cone, Sao Miguel (Azores)', *Journal of Volcanology and Geothermal Research* **189**, 81–91.

Mattsson, H. B., Hoskuldsson, A. and Hand, S. (2005), 'Crustal xenoliths in the 6220 BP Saefell tuff-cone, south Iceland: Evidence for a deep, diatreme-forming, Surtseyan eruption', *Journal of Volcanology and Geothermal Research* **145**, 234–248.

McClintock, M. and White, J. D. L. (2006), 'Large phreatomagmatic vent complex at Coombs Hills, Antarctica: wet, explosive initiation of flood basalt volcanism in the Ferrar-Karoo LIP', *Bulletin of Volcanology* **68**, 215–239.

McCusker, J. and Reed, C. (2013), 'The role of intrusions in the formation of Irish-type mineralisation', *Mineralium Deposita* **48**, 687–695.

McDonough, W. F. and Sun, S. S. (1995), 'The composition of the Earth', *Chemical Geology* **120**, 223–253.

McGetchin, T. R., Nikhanj, Y. S. and Chodos, A. A. (1973), 'Carbonatite-kimberlite relations in the Cane Valley diatreme, San Juan County, Utah', *J. Geophys. Res.* **78**, 1854–1869.

McKenzie, D. (1984), 'The generation and compaction of partially molten rock', *Journal of Petrology* **25**, 713–765.

McKenzie, D. (1985), 'The extraction of magma from the crust and mantle', *Earth and Planetary Science Letters* **74**, 81–91.

McKillen, T. N. and Tyler, P. A. (2003), The Shinrone Property Moratorium report 2003, Technical report, Minco Ireland Limited.

Meldrum, S. J., Aquino, R. S., Gonzales, R. I., Burke, R. J., Suyadi, A., Irianto, B. and Clarke, D. S. (1994), 'The Batu Hijau porphyry copper-gold deposit, Sumbawa Island, Indonesia', *Journal of Geochemical Exploration* **50**, 203–220.

Meschede, M. (1986), 'A method of discriminating between different types of mid-ocean ridge basalts and continental tholeiites with the Nb-Zr-Y diagram', *Chemical Geology* **56**, 207–218.

Mitchell, R. H. (1990), 'Kimberlites and lamproites: Primary sources of diamond', *Geoscience Canada* **18**, 1–16.

Miyashiro, A., Shido, F. and Ewing, M. (1971), 'Metamorphism in the Mid-Atlantic Ridge near 24 and 30 N', *Philosophical Transactions of the Royal Society of London. Series A, Mathematical and Physical Sciences* **268**, 589–603.

Monaghan, A. A. and Pringle, M. S. (2004), $^{40}Ar/^{39}Ar$ geochronology of Carboniferous-Permian volcanism in the Midland Valley, Scotland, *in* M. Wilson, E. R. Neumann, G. R. Davies, M. J. Timmerman, M. Heeremans and B. T. Larsen, eds, 'Permo-Carboniferous Magmatism And Rifting in Europe', Vol. 223, Geological Society of London, pp. 219–242.

Moore, J. G. (1985), 'Structure and eruptive mechanisms at Surtsey Volcano, Iceland', *Geological Magazine* **122**, 649–661.

Mottl, M. J., Holland, H. D. and Corr, R. F. (1979), 'Chemical exchange during hydrothermal alteration of basalt by seawateräîii. experimental results for Fe, Mn, and sulfur species', *Geochimica et Cosmochimica Acta* **43**, 869–884.

Mueller, W. and White, J. D. L. (1992), 'Felsic fire-fountaining beneath Archean seas: pyroclastic deposits of the 2730 Ma Hunter Mine Group, Quebec, Canada', *Journal of Volcanology and Geothermal Research* **54**, 117–134.

Mundula, F., Cioni, R. and Funedda, A. Leone, F. (2013), 'Lithofacies characteristics of diatreme deposits: Examples from a basaltic volcanic field of SW Sardinia (Italy)', *Journal of Volcanology and Geothermal Research* **255**, 1–14.

Nemec, W. and Steel, R. J. (1984), Alluvial and coastal conglomerates: their significant features and some comments on gravelly mass-flow deposits, *in* 'Sedimentology of Gravels and Conglomerates', Vol. 10, Canadian Society of Petroleum Geology Memoirs, pp. 1–31.

Nemeth, K., Martin, U. and Harangi, S. (2001), 'Miocene phreatomagmatic volcanism at Tihany (Pannonian Basin, Hungary)', *Journal of Volcanology and Geothermal Research* **111**, 111–135.

Neumann, E. R., Wilson, M., Heeremans, M., Spencer, E. A., Obst, K., Timmerman, M. J. and Kirstein, L. (2004), Carboniferous-Permian rifting and magmatism in southern Scandinavia, the North Sea and northern Germany: a review, *in* M. Wilson, E. R. Neumann, G. R. Davies, M. J. Timmerman, M. Heeremans and B. T. Larsen, eds, 'Permo-Carboniferous Magmatism And Rifting in Europe', Vol. 223, Geological Society, London, pp. 41–74.

Nicolas, A. (1986), 'A melt extraction model based in structural studies in mantle peridotites', *Journal of Petrology* **27**, 999–1022.

Norry, M. J. and Fitton, J. (1983), Compositional differences between oceanic and continental basic lavas and their significance, *in* C. J. Hawkesworth and M. J. Norry, eds, 'Continental basalts and mantle xenoliths', Shiva Publications, pp. 5–19.

Parry, W. T. and Downey, L. M. (1982), 'Geochemistry of hydrothermal chlorite replacing igneous biotite', *Clays and Clay Minerals* **30**, 81–90.

Pearce, J. A. (1979), 'Geochemical evidence for the genesis and eruptive setting of lavas from Tethyan ophiolites', *Proceedings of the International Ophiolite Symposium, Cyprus 1979* pp. 261–272.

Pearce, J. A. (1982), Trace element characteristics of lavas from destructive plate boundaries, *in* R. S. Thorpe, ed., 'Orogenic andesites and related rocks', John Wiley and Sons, pp. 528–548.

Pearce, J. A. (1983), Role of the sub-continental lithosphere in magma genesis at active continental margins, *in* C. J. Hawkesworth and M. J. Norry, eds, 'Continental basalts and mantle xenoliths', Shiva Publications, pp. 230–249.

Pearce, J. A. (1996), 'Sources and settings of granitic rocks', *Episodes* **19**, 120–125.

Perry, F. V., Baldridge, W. S. and DePaolo, D. J. (1987), 'Role of asthenosphere and lithosphere in the genesis of Late Cenozoic basaltic rocks from the Rio Grande Rift and adjacent regions of the southwestern United States', *Journal of Geophysical Research* **92**, 9193–9213.

Peterson, D. W. and Moore, R. B. (1987), Geologic history and evolution of geologic concepts, Island of Hawaii, *in* R. W. Decker, T. L. Wright and P. H. Stauffer, eds, 'Volcanism in Hawaii', Vol. 1 of *U.S. Geological Survey Professional Paper 1350*, United States Goverment Printing Office, Washington.

Piercey, S. J. (2014), 'A review of quality assurance and quality control (QA/QC) procedures for lithogeochemical data', *Geoscience Canada* **41**, 75–88.

Pittari, A., Cas, R. A. F., Lefebvre, N. S., Robey, J., Kurszlaukis, S. and Webb, K. (2008), 'Eruption processes and facies architecture of the Orion Central kimberlite volcanic complex, Fort á la Corne, Saskatchewan; kimberlite mass flow deposits in a sedimentary basin', *Journal of Volcanology and Geothermal Research* **174**, 152–170.

Porritt, L. A., Cas, R. A. F. and Crawford, B. B. (2008), 'In-vent column collapse as an alternative model for massive volcaniclastic kimberlite emplacement: An example from the Fox kimberlite, Ekati Diamond Mine, NWT, Canada', *Journal of Volcanology and Geothermal Research* **174**, 90–102.

Pracht, M. and Kinnaird, J. A. (1997), 'Carboniferous subvolcanic activity on the Beara Peninsula, SW Ireland', *Geological Journal* **32**, 297–312.

Pracht, M. and Timmerman, M. J. (2004), 'A late Namurian (318Ma) $^{40}Ar/^{39}Ar$ age for kaersutite megacrysts from the Black Ball Head diatreme: an age limit for the Variscan deformation in south-west Ireland', *Irish Journal of Earth Sciences* **22**, 33–43.

Praeg, D. (2004), Diachronous Variscan late-orogenic collapse in response to multiple detachments: a view from the internides in France to the foreland in the Irish Sea, *in* M. Wilson, E. R. Neumann, G. R. Davies, M. J. Timmerman, M. Heeremans and B. T. Larsen, eds, 'Permo-Carboniferous Magmatism And Rifting in Europe', Vol. 223, Geological Society of London, pp. 89–138.

Redmond, P. B. (2010), 'The Limerick Basin: An important emerging subdistrict of the Irish Zn-Pb orefield', *Society of Economic Geologists Newsletter* **82**, 1, 21–25.

Reed, C. P. and Wallace, M. W. (2004), 'Zn-Pb mineralisation in the Silvermines district, Ireland: a product of burial diagenesis', *Mineralium Deposita* **39**, 87–102.

Requia, K. and Fontbote, K. (1999), Hydrothermal alkali metasomatism in the Salobo iron oxide Cu (-Au) deposit, Carajas mineral province, northern Brazil, *in* C. Stanley, ed., 'Mineral deposits: processes to processing', Balkema, Amsterdam, pp. 1025–1028.

Riding, R. (1975), '*Girvanella* and other algae as depth indicators', *Lethaia* **8**, 173–179.

Roaldset, E., He, W. and Grimstad, S. (1998), 'Smectite to illite conversion by hydrous pyrolysis', *Clay Minerals* **33**, 147–158.

Robb, L. (2005), *Introduction to ore-forming processes*, Blackwell Publishing, Oxford.

Robinson, B. W. and Kusakabe, M. (1975), 'Quantitative preparation of sulfur dioxide, for $^{34}S/^{32}S$ analyses, from sulfides by combustion with cuprous oxide', *Analytical Chemistry* **47**, 1179–1181.

Roex, A. P., Spath, A. and Zartman, R. E. (2001), 'Lithospheric thickness beneath the southern Kenya Rift: implications from basalt geochemistry', *Contributions to Mineralogy and Petrology* **142**, 89–106.

Rollinson, H. (1993), *Using geochemical data: evaluation, presentation, interpretation*, Pearson Education Limited.

Ross, P.-S. and White, J. D. L. (2006), 'Debris jets in continental phreatomagmatic volcanoes: A field study of their subterranean deposits in the Coombs Hills vent complex, Antarctica', *Journal of Volcanology and Geothermal Research* **149**, 62–84.

Ross, P.-S., White, J. D. L., Zimanowski, B. and Büttner, R. (2008*a*), 'Multiphase flow above explosion sites in debris-filled volcanic vents: Insights from analogue experiments', *Journal of Volcanology and Geothermal Research* **178**, 104–112.

Ross, P.-S., White, J., Zimanowski, B. and Büttner, R. (2008*b*), 'Rapid injection of particles and gas into non-fluidized granular material, and some volcanological implications', *Bulletin of Volcanology* **70**, 1151–1168.

Ross, P.-S. and Bédard, J. H. (2009), 'Magmatic affinity of modern and ancient subalkaline volcanic rocks determined from trace element discriminant diagrams', *Canadian Journal of Earth Sciences* **46**, 823–839.

Ross, P.-S. and White, J. D. L. (2012), 'Quantification of vesicle characteristics in some diatreme-filling deposits, and the explosivity levels of magma-water interactions within diatremes', *Journal of Volcanology and Geothermal Research* **245**, 55–67.

Sahagian, D. L. and Proussevitch, A. A. (1998), '3D particle size distributions form 2D observations: stereology for natural applications', *Journal of Volcanology and Geothermal Research* **84**, 173–196.

Schoen, R. and White, D. (1967), 'Hydrothermal alteration of basaltic andesite and other rocks in drill hole GS-6, Steamboat Springs, Nevada', *Geological Survey Research* **575**, 110–119.

Sevastopulo, G. D. and Redmond, P. B. (1999), Age of mineralization of carbonate-hosted, base metal deposits in the Rathdowney Trend, Ireland, *in* K. J. W. McCaffrey, L. Lonergan and J. J. Wilkinson, eds, 'Fractures, fluid flow and mineralisation', Vol. 151 of *Special Publications*, Geological Society, London, pp. 303–311.

Seyfried Jr, W. E. and Bischoff, J. L. (1979), 'Low temperature basalt alteration by seawater: an experimental study at 70 °C and 150 °C', *Geochimica et Cosmochimica Acta* **43**, 1937–1947.

Seyfried Jr, W. E. and Mottl, M. J. (1982), 'Hydrothermal alteration of basalt by seawater under seawater-dominated conditions', *Geochimica et Cosmochimica Acta* **46**, 958–1002.

Sharp, Z. (2006), *Principles of Stable Isotope Geochemistry*, 1 edn, Prentice Hall.

Shea, T., Houghton, B. F., Gurioli, L., Cashman, K. V., Hammer, J. E. and Hobden, B. J. (2010), 'Textural studies of vesicles in volcanic rocks: An integrated methodology', *Journal of Volcanology and Geothermal Research* **190**, 271–289.

Shearer, C. K. and Papike, J. J. (1989), 'Is plagioclase removal responsible for the negative Eu anomaly in the source regions of mare basalts?', *Geochimica et Cosmochimica Acta* **53**, 3331–3336.

Shimano, T. and Nakada, S. (2006), 'Vesiculation path of ascending magma in the 1983 and the 2000 eruptions of Miyakejima volcano, Japan', *Bulletin of Volcanology* **68**, 549–566.

Skinner, E. M. W. and Marsh, J. S. (2004), 'Distinct kimberlite pipe classes with contrasting eruption processes', *Lithos* **76**, 183–200.

Smedley, P. L. (1986), Petrochemistry of Dinantian volcanism in northern Britain, PhD thesis, University of Edinburgh.

Smith, R. A., Stephenson, D. and Monro, S. K. (1994), 'The geological setting of the southern Bathgate Hills, West Lothian, Scotland', *Transactions of the Royal Society of Edinburgh: Earth Sciences* **84**, 189–196.

Sobolev, A. V. and Shimizu, N. (1993), 'Ultra-depleted primary melt included in an olivine from the Mid-Atlantic Ridge', *Letters to Nature* **363**, 151–154.

Sohn, Y. K. (1996), 'Hydrovolcanic processes forming basaltic tuff rings and cones on Cheju Island, Korea', *Geological Society of America Bulletin* **108**, 1199–1211.

Somerville, I. D., Strogen, P. and Jones, G. L. (1992), 'Biostratigraphy of Dinantian limestones and associated volcanic rocks in the Limerick Syncline, Ireland', *Geological Journal* **27**, 201–220.

Sottili, G., Taddeucci, J., Palladino, D. M., Gaeta, M., Scarlato, P. and Ventura, G. (2009), 'Sub-surface dynamics and eruptive styles of maars in the Colli Albani Volcanic District, Central Italy', *Journal of Volcanology and Geothermal Research* **180**, 189–202.

Sparks, R. S. J., Baker, L., Brown, R. J., Field, M., Schumacher, J., Stripp, G. and Walters, A. (2006), 'Dynamical constraints on kimberlite volcanism', *Journal of Volcanology and Geothermal Research* **155**, 18–48.

Sruoga, P. and Rubinstein, N. (2007), 'Processes controlling porosity and permeability in volcanic reservoirs from the Austral and Neuquen basins, Argentina', *AAPG Bulletin* **91**, 115–129.

Stripp, G. R., Field, M., Schumacher, J. C., Sparks, R. S. J. and Cressy, G. (2006), 'Post-emplacement serpentinization and related hydrothermal metamorphism in a kimberlite from Venetia, South Africa', *Journal of Metamorphic Geology* **24**, 515–534.

Strogen, P. (1983), The geology of the volcanic rocks of southeast County Limerick, PhD thesis, University College Dublin.

Strogen, P. (1988), 'The Carboniferous lithostratigraphy of southeast County Limerick, Ireland, and the origin of the Shannon Trough', *Geological Journal* **23**, 121–137.

Strogen, P., Somerville, I. D., Pickard, N. A. H., Jones, G. L. and Fleming, M. (1996), 'Controls on ramp, platform and basinal sedimentation in the Dinantian of the Dublin

Basin and Shannon Trough, Ireland', *Geological Society, London. Special Publications* **107**, 263–279.

Stroncik, N. A. and Schminke, H.-U. (2001), 'Evolution of palagonite: Crystallization, chemical changes, and element budget', *Geochemistry, Geophysics, Geosystems* **2**.

Sturesson, U. (1992), 'Volcanic ash; the source material for Ordovician chamosite ooids in Sweden', *Journal of Sedimentary Research* **62**, 1084–1094.

Sturesson, U., Heikoop, J. M. and Risk, M. J. (2000), 'Modern and Palaeozoic iron ooids a similar volcanic origin', *Sedimentary Geology* **136**, 137–146.

Sun, S. S. and McDonough, W. F. (1989), 'Chemical and isotopic systematics of oceanic basalts: implications for mantle composition and processes', *Geological Society, London. Special Publications* **42**, 313–345.

Taylor, S. R. and McLennan, S. M. (1985), *The continental crust: its composition and evolution*, Blackwell Publishing, Oxford.

Thirlwall, M. F. and Walder, A. J. (1995), 'In situ hafnium isotope ratio analysis of zircon by inductively coupled plasma multiple collector mass spectrometry', *Chemical Geology* **122**, 241–247.

Thompson, T. B., Trippel, A. D. and Dwelley, P. C. (1985), 'Mineralized veins and breccias of the Cripple Creek District, Colorado', *Economic Geology* **80**, 1669–1688.

Thorseth, I. H., Furnes, H. and Tumyr, O. (1991), 'A textural and chemical study of icelandic palagonite of varied composition and its bearing on the mechanism of the glass-palagonite transformation', *Geochimica et Cosmochimica Acta* **55**, 731–749.

Thy, P. (1983), 'Spinel minerals in transitional and alkali basaltic glasses from Iceland', *Contributions to Mineralogy and Petrology* **83**, 141–149.

Thyne, G., Boudreau, B. P., Ramm, M. and Midtbo, R. E. (2001), 'Simulation of potassium feldspar dissolution and illitization in the Statfjord Formation, North Sea', *AAPG Bulletin* **85**, 621–635.

Timmerman, M. J. (2004), Timing, geodynamic setting and character of Permo-Carboniferous magmatism in the foreland of the Variscan Orogen, NW Europe, *in* M. Wilson, E. R. Neumann, G. R. Davies, M. J. Timmerman, M. Heeremans and

B. T. Larsen, eds, 'Permo-Carboniferous Magmatism And Rifting in Europe', Vol. 223, Geological Society, London, pp. 41–74.

Tracy, R. J. (1980), 'Petrology and genetic significance of an ultramafic xenolith suite from Tahiti', *Earth and Planetary Science Letters* **48**, 80–96.

Tsukui, M. and Suzuki, Y. (1995), 'Vesiculation of basaltic magma: Magmatic versus phreatomagmatic eruption in 1983 eruption of Miyakejima', *Volcanological Society of Japan* **40**, 395–399.

Tyler, P. A. (2007), The Pallas Green alteration trend and comparison with the Lisheen trend, Technical report, Xstrata.

Upton, B. G. J., Hinton, R. W., Aspen, P., Finch, A. and Valley, J. W. (1999), 'Megacrysts and associated xenoliths: Evidence for migration of geochemically enriched melts in the upper mantle beneath Scotland', *Journal of Petrology* **40**, 935–956.

Upton, B. G. J., Stephenson, D., Smedley, P. M., Wallis, S. M. and Fitton, J. G. (2004), Carboniferous and Permian magmatism in Scotland, *in* M. Wilson, E. R. Neumann, G. R. Davies, M. J. Timmerman, M. Heeremans and B. T. Larsen, eds, 'Permo-Carboniferous Magmatism And Rifting in Europe', Vol. 223, Geological Society of London, pp. 195–218.

Utzmann, A. U., Hansteen, T. H. and Schmincke, H. U. S. (2002), 'Trace element mobility during sub-seafloor alteration of basaltic glass from Ocean Drilling Program site 953 (off Gran Canaria)', *International Journal of Earth Sciences* **91**, 661–679.

Valentine, G. A. (2012), 'Shallow plumbing systems for small-volume basaltic volcanoes, 2: Evidence from crustal xenoliths at scoria cones and maars', *Journal of Volcanology and Geothermal Research* **223**, 47–63.

Valentine, G. A. and White, J. D. (2012), 'Revised conceptual model for maar-diatremes: Subsurface processes, energetics, and eruptive products', *Geology* .

Vernieres, J., Godard, M. and Bodinier, J.-L. (1997), 'A plate model for the simulation of trace element fractionation during partial melting and magma transport in the Earth's upper mantle', *Journal of Geophysical Research* **102**, 24771–24784.

Wagner, T., Boyce, A. J. and Fallick, Anthony, E. (2002), 'Laser combustion analysis of δ^{34}S of sulfosalt minerals: Determination of the fractionation systematics and some crystal-chemical considerations', *Geochimica et Cosmochimica Acta* **66**, 2855–2863.

Walters, A. L., Phillips, J. C., Brown, R. J., Field, M., Gernon, T., Stripp, G. and Sparks, R. S. J. (2006), 'The role of fluidisation in the formation of volcaniclastic kimberlite: Grain size observations and experimental investigation', *Journal of Volcanology and Geothermal Research* **155**, 119–137.

Wang, Y., Han, B., Griffin, W., Zhang, L. and Shu, G. (2012), 'Post-entrainment mineral-magma interaction in mantle xenoliths from inner Mongolia, western North China craton', *Journal of Earth Science* **23**, 54–76.

White, J. D. L. (1991), 'Maar-diatreme phreatomagmatism at Hopi Buttes, Navajo Nation (Arizona), USA', *Bulletin of Volcanology* **53**, 239–258.

White, J. D. L. (1996), 'Pre-emergent construction of a lacustrine basaltic volcano, Pahvant Butte, Utah USA', *Bulletin of Volcanology* **58**, 249–262.

White, J. D. L. (2000), 'Subaqueous eruption-fed density currents and their deposits', *Precambrian Research* **101**, 87–109.

White, J. D. L. and Houghton, B. F. (2006), 'Primary volcaniclastic rocks', *Geology* **34**, 677.

White, J. D. L. and Ross, P.-S. (2011), 'Maar-diatreme volcanoes: a review', *Journal of Volcanology and Geothermal Research* **201**, 1–29.

Wilkinson, J. J., Boyce, A. J., Everett, C. E. and Lee, M. J. (2003), Timing and depth of mineralization in the Irish Zn-Pb Orefield, *in* G. Kelly, J. Andrew, H. Ashton, B. Boland, G. Earls, L. Fusciardi and G. Stanley, eds, 'Europe's major base metal deposits', Irish Association for Economic Geology, pp. 483–497.

Wilkinson, J. J., Everett, C. E., Boyce, A. J., Gleeson, S. A. and Rye, D. M. (2005*a*), 'Intracratonic crustal seawater circulation and the genesis of subseafloor zinc-lead mineralization in the Irish orefield', *Geology* **33**, 805–808.

Wilkinson, J. J., Eyre, S. L. and Boyce, A. J. (2005*b*), 'Ore-forming processes in Irish-Type carbonate-hosted Zn-Pb deposits: Evidence from mineralogy, chemistry, and isotopic composition of sulfides at the Lisheen Mine', *Economic Geology* **100**, 63–86.

Wilson, B., Neumann, E. R., Davies, G. R., Timmerman, M. J., Heeremans, M. and Larsen, B. T. (2004), *Permo-Carboniferous Magmatism And Rifting in Europe*, Special Publications, Geological Society of London, London.

Wilson, L. and Head III, J. W. (2007), 'An integrated model of kimberlite ascent and eruption', *Nature* **447**, 53–57.

Winchester, J. A. and Floyd, P. A. (1976), 'Geochemical magma type discrimination application to altered and metamorphosed basic igneous rocks', *Earth and Planetary Science Letters* **28**, 459–469.

Winchester, J. A. and Floyd, P. A. (1977), 'Geochemical discrimination of different magma series and their differentiation products using immobile elements', *Chemical Geology* **20**, 325–343.

Wohletz, K. H. and McQueen, R. C. (1984), Experimental studies of hydromagmatic volcanism, *in* F. R. Boyd, A. L. Boettcher and Company, eds, 'Explosive volcanism: inception, evolution, and hazards', National Academy Press, pp. 158–170.

Wood, A. (1957), 'The type-species of the genus *Girvanella* (calcareous algae)', *Palaeontology* **1**, 22–28.

Wood, B. J. and Graham, C. M. (1986), 'Infiltration of aqueous fluid and high fluid: Rock ratios during greenschist facies metamorphism: A discussion', *Journal of Petrology* **27**, 751–761.

Woodcock, N. H. and Strachan, R. (2000), *Geological history of Britain and Ireland*, Oxford: Blackwell Science.

Xu, Y., Chung, S.-L., Jahn, B. and Wu, G. (2001), 'Petrologic and geochemical constraints on the petrogenesis of Permian-Triassic Emeishan floor basalts in southwestern China', *Lithos* **58**, 145–168.

Yasui, M. and Koyaguchi, T. (2004), 'Sequence and eruptive style of the 1783 eruption of Asama Volcano, central Japan: a case study of an andesitic explosive eruption generating fountain-fed lava flow, pumice fall, scoria flow and forming a cone', *Bulletin of Volcanology* **66**, 243–262.

Young, G. and Caldwell, W. (2011), 'Stratigraphy and geochemistry of the Early Carboniferous Clyde Plateau Lavas in south Bute, Midland Valley of Scotland', *Geological Magazine* **148**, 597–618.

Zhou, Y., Bohor, B. F. and Ren, Y. (2000), 'Trace element geochemistry of altered volcanic ash layers (tonsteins) in Late Permian coal-bearing formations of eastern Yunnan and western Guizhou Provinces, China', *International Journal of Coal Geology* **44**, 305–324.